# THERMODYNAMIC AND KINETIC MODELING OF MIXED LIPID MEMBRANES AND THEIR INTERACTION WITH MACROMOLECULES

A Dissertation
Submitted to the Graduate Faculty
of the
North Dakota State University
of Agriculture and Applied Science

By

Stephan Loew

In Partial Fulfillment of the Requirements
for the Degree of
DOCTOR OF PHILOSOPHY

Major Department:
Physics

August 2013

Fargo, North Dakota

North Dakota State University
Graduate School

**Title**

# THERMODYNAMIC AND KINETIC MODELING OF MIXED LIPID MEMBRANES AND THEIR INTERACTION WITH MACROMOLECULES

**By**

Stephan Loew

The Supervisory Committee certifies that this ***disquisition*** complies with North Dakota State University's regulations and meets the accepted standards for the degree of

**DOCTOR OF PHILOSOPHY**

SUPERVISORY COMMITTEE:

Sylvio May
*Chair*

Alexander Wagner

Daniel Kroll

Eugene Berry

Approved:

January 7, 2015
*Date*

Sylvio May
*Department Chair*

# ABSTRACT

Mixed lipid membranes play a crucial role in numerous cellular processes and pharmaceutical applications. Fully understanding the interactions between membranes and biomacromolecules is not possible without gaining insight into underlying physical concepts. In this thesis we develop theoretical models that aim to rationalize a number of experimental findings, all involving lipid layers and their interaction with macromolecules. Our models are phenomenological and employ a minimal set of order parameters, thus focusing on essential physical interactions. We address four major subjects:

First, certain mixed model membranes containing cholesterol are able to undergo macroscopic phase separation. Based on a previously suggested thermodynamic model we demonstrate that peripherally adsorbed membrane proteins tend to further facilitate phase separation, especially when they exhibit attractive interactions.

Second, we show that the coupling between the two leaflets of a mixed lipid bilayer can influence its phase behavior. To this end, we calculate detailed phase diagrams and argue that their predictions are in principal agreement with experimental observations. Specifically, the coupling can trigger or inhibit phase separation, depending on lipid compositions in each leaflet and coupling strength.

Third, we investigate the fundamental question if physiological pH-changes are sufficient — and can this be employed by cellular processes — to trigger the adsorption of peripheral proteins. Proposing a model for the previously suggested electrostatic-hydrogen bond switch mechanism, we show that protein adsorption based on electrostatic interactions alone has a weak pH dependence but is rendered pH sensitive by the electrostatic-hydrogen bond switch.

Finally, the transfer of hydrophobic drug molecules in model systems from donor liposomes to a target carrier is known from experimental work to typically exhibit a first-order kinetics, sometimes also sigmoidal behavior. We develop a detailed kinetic model for drug transfer that is based on a statistical description of drug occupation numbers in liposomes and includes both drug diffusion and liposome collision mechanisms.

# ACKNOWLEDGMENTS

Many years of graduate school at North Dakota State University culminated in this dissertation. I am deeply indebted to my advisor, Sylvio May, whose incredible support, enthusiasm and patience throughout the entire time has been crucial to this work. He introduced me to the field of membrane biophysics and is a constant source of inspiration and knowledge ever since, especially in the interdisciplinary aspects; his dedication of time and work made this research possible.

I want to thank Alexander Wagner for the countless times I could rely on his instant help. He became — next to Sylvio May — my go-to person, no matter the nature of the problem. Daniel Kroll deserves gratitude for his engagement as department head and support of my work as instructor. I thank Gene Berry for all his insights and perspective. Of course I am grateful to Sylvio May, Alexander Wagner, Anne Hinderliter, Alfred Fahr, Hossam Hefesha and Edgar Kooijman for their work as co-authors and illuminating discussions.

Special thanks to Patty Hartsoch, especially for all the work I do not even know about. I also am grateful to Goetz Kähler and Eric Foard, who went through most of the courses and all the ups and downs of life as a grad student with me.

I owe a dept of gratitude to my family for their continuous encouragement, support and concern during these years. Finally, I am thankful to all the friends who made this time unforgettable, notably Ted Nelson, Igor Svidersky, Gene Olson, Max Anders and the whole Jensen family.

# DEDICATION

To my parents.

—

Meinen Eltern.

# TABLE OF CONTENTS

# LIST OF TABLES

# LIST OF FIGURES

# LIST OF ABBREVIATIONS

| | |
|---|---|
| [$^{14}$C]mTHPC | Meta-tetrahydroxyphenylchlorin |
| Chol | Cholesterol |
| CM | Carboxymethyl |
| Cryo-TEM | Cryo-Transmission Electron Microscopy |
| DBHPC | 1,2-Dibehenyl-sn-glycero-3-phosphocholine |
| DCP | Dicetylphosphate |
| DEAE | Diethylaminoethyl |
| diPhyPC | 1,2-diphytanoyl-sn-glycero-3-phosphocholine |
| DMPC | 1,2-Dimyristoyl-sn-glycero-3-phosphocholine |
| DOPC | 1,2-Dioleoyl-sn-glycero-3-phosphocholine |
| DOTAP | 1,2-Dioleoy-3-trimethylammonium-propane sodium salt |
| DPPC | 1,2-Dipalmitoyl-sn-glycero-3-phosphocholine |
| DSPC | 1,2-Distearoyl-sn-glycero-3-phosphocholine |
| ER | Endoplasmic reticulum |
| EPR | Enhanced permeation and retention |
| LSC | Liquid scintillation counting |
| mTHPC | Temoporfin |
| PA | Phosphatidic acid |
| PC | Phosphatidylcholine |
| PCS | Photon correlation spectroscopy |
| POPC | 1-Palmitoyl-2-oleoyl-3-sn-glycero-3-phosphocholine |
| PS | Phosphatidylserine |
| SOPC | 1-Stearoyl-2-oleoyl-sn-glycero-3-phosphocholine |

# 1. INTRODUCTION

Lipid membranes are amongst the most fascinating multi-molecular structures known at present [193, 278]. This fascination results perhaps not so much from only one single membrane property but from its many facets and inter-disciplinary nature that intrigue scientists of very different backgrounds.

Biologists have recognized long ago that life, as we know it, does not exist without lipid membranes [2]. Every living cell is surrounded by a biomembrane that is composed of lipids and hosts numerous proteins. Biomembranes also enclose the nucleus and other cell organelles of eukaryotic cells. Although biomembranes typically contain tens, often hundreds, of different lipid species, their composition is tightly regulated [56]. Even more, biomembranes in different cells – say a mitochondrial membrane [200] or a bacterial membrane [45] (for example a thermophile, which is an archaea that can withstand large temperatures [46]) – are composed of vastly different lipids. And yet, most of these lipids share the same basic structural motif, a hydrophilic headgroup that is linked to one, two, or even more hydrocarbon tails. Molecules with two spatially separated hydrophilic (water-loving) and hydrophobic (water-hating) parts are known as amphiphiles [60]. All lipids are amphiphiles.

Amphiphilicity can be the result of many different chemical structures; this not only forms the basis behind the vast richness of naturally occurring lipid structures, it also has provided a playground for chemists to synthesize a plethora of new lipids for medical and technological applications such as the design of lipid-based drug carriers [64]. Chemists have also coined the term self-assembly, which describes the ability of amphiphilic molecules (such as lipids) to form complex ordered structures. In order to prevent their exposure to the aqueous phase, the hydrophobic lipid tails arrange themselves into close proximity, forming a hydrocarbon core that is shielded

by the headgroups from direct contact to water molecules. This process occurs spontaneously and is driven by the hydrophobic effect [266]. Unlike in an oil-water mixture, where the oil completely segregates into a macroscopic and homogeneous bulk phase, a pure lipid-water mixture must always form structures that are "thin" along at least one spatial direction. Here, the notion "thin" refers roughly to twice the molecular length of a lipid. Despite this constraint, lipids are able to form a large variety of structures [241], including globular and worm-like micelles, inverse phases, bicontinuous structures, sponge phase, and membranes [137, 138, 248]. Lipid membranes can interact with each other to form multilamellar membrane stacks, or they can interact with a flat or curved substrate to form a supported bilayer [35]. Most frequently, however, membrane-forming lipids arrange – or are made to arrange – into vesicles, which range from small (starting with a diameter of about 30nm) unilamellar vesicles to large (up to micrometer sizes) uni- or multilamellar vesicles.

Pharmaceutical scientists refer to vesicles as liposomes [145] and use them routinely as delivery vehicles for drug molecules [247]. For example, a water-soluble drug that is captured inside the inner aqueous region of a liposome would travel together with its host after injection into the blood stream [204]. A prominent example is small interfering RNA (siRNA), a 20–25 base pairs long double-stranded RNA molecule that can be used to silence gene expression in a specific manner [257]. However, most drug molecules are poorly water-soluble. They tend to self-aggregate in an aqueous solution, which limits their bioavailability [153]. If these drugs are sufficiently small, they will spontaneously partition into the hydrocarbon region of a liposome's lipid bilayer [110]. Liposomes as carriers for poorly water-soluble drugs are of great promise, with about a dozen clinically approved systems currently [37]. Examples include doxorubicin, paclitaxel, and amphotericin B. Significant progress has been made in designing specific targeting devices, in triggering the release of the

drug [8, 284, 150], and in protecting liposomes during their journey through the blood by a polymeric coat (stealth liposomes [187]).

Physicists too have embraced the unique properties of lipid membranes [242, 26]. On sufficiently large length scales, an extended lipid bilayer can be viewed as a two-dimensional system with correspondingly interesting physics. Moreover, lipid membranes, when in their fluid state, can undergo bending deformations of very low energy cost, implying an important role of curvature fluctuations [154]. For example, membrane-inserted inclusions interact through Casimir forces, which arise from the confinement on the membrane's fluctuation spectrum [86, 124, 55, 165]. The shapes of lipid vesicles are determined by the membrane's bending energy [101], subject to the conservations of the vesicle's volume and lateral membrane area (in fact, the lateral areas of both monolayers individually); this leads to a surprisingly rich catalog of shapes and transitions between them [53]. Also composite structures or phases of membranes with polymers and colloids have attracted considerable attention among physicists [198, 20].

One of the major conceptual ideas in molecular cell biology is related to the lateral organization of biomembranes. Instead of merely forming a permeability barrier and passively hosting integral proteins (which is what the "fluid-mosaic" model of Singer and Nicolson had postulated in 1972 [254]), the lipids in a biomembrane are thought to be actively involved in the formation of dynamic patches, called "rafts" [251], that are of some tens or even hundreds of nanometers in size and serve as platforms for signaling events and trafficking [252, 211]. Until now, some controversy remains about the nature of rafts [194, 253] and the mechanisms that stabilize and regulate their finite size [74, 28, 69]. However, it is known from numerous studies on model membranes that certain lipid mixtures tend to form domains or even undergo lateral phase separation [51, 279, 57, 252]. More specifically, certain ternary mixtures of lipids with two saturated hydrocarbon chains (especially sphingolipids [75]), at

least one unsaturated chain, and cholesterol have been found to phase separate into two coexisting phases, referred to as liquid ordered ($L_o$) and liquid-disordered ($L_d$) [216, 105]. The $L_o$ phase is enriched with both cholesterol and the saturated lipid whereas the $L_d$ phase contains mainly the unsaturated lipid. What underlies the phase separation on a molecular level is the favorable interaction of saturated hydrocarbon chains with the rigid backbone of cholesterol [252]. In contrast, the double bond of an unsaturated chain introduces a kink that appears to render the interaction with cholesterol more unfavorable. Lipid mixtures containing significant fractions of sphingolipids, cholesterol, and unsaturated phosphatidylcholine are present, for example, in the extracellular leaflet of a plasma membrane, where they could form domains similar to the $L_o$ and $L_d$ phases. Despite the appeal of this model, basic questions remain: What role do proteins play in the formation of rafts [58]? Why do rafts not coalesce into macroscopically large domains as seen for model membranes [74, 28, 69]? Do rafts form in both membrane leaves, and if so how do they interact with each other across the membrane [215]? Each of these questions is important from a biological perspective. Yet our ability to answer them will likely require some physical understanding of these lipid mixtures as well.

Model membranes are an important research subject not only in their role as a simple model for biomembranes but also because they are employed in numerous pharmaceutical and biotechnological applications. Besides their above-mentioned use as liposomes for drug delivery they serve as host systems for the reconstitution and crystallization of membrane proteins [240, 30], as supported membranes for surface patterning and functionalization [255], as monolayers at the air-water interface to study phase transitions and adsorption processes [122], or in composite phases to induce the condensation of polymers [305]. Many of these applications involve interactions of lipid membranes with various other molecules such as drugs, peptides, proteins, polymers, or colloids. Because lipid membranes are self-assembled [112] and flexible structures,

with additional compositional degrees of freedom for mixed membranes, they are able to respond when interacting with other molecules. For example, increasing the concentration of the peptide gramicidin A (gA) in a planar lipid membrane composed of a long-chain phosphatidylcholine ultimately induces the formation of an inverse hexagonal phase [126]. In this specific case, the planer membrane is only to a certain extent able to accommodate gA. Of course, any practical application that involves high concentrations of gA in a model membrane may face this instability. To gain control over this process requires insights into the physical mechanisms that determine the structures of membrane-peptide complexes.

Much of our current understanding about lipid membranes and their interactions with biomacromolecules results not exclusively from experimental studies but has been arrived at in conjunction with modeling work, either phenomenological mathematical models [17] or computer simulation studies [271, 283, 171]. Indeed, the lipid membranes can be considered as a prime example for the mutual inspiration between experiment and theory [242]. Theoretical models have often introduced new conceptual ideas, suggested new experiments, or rationalized experimental findings [175]. This is one reason for the abundance of phenomenological modeling studies that involve lipid membranes. A key contribution to the modeling of membranes was introduced in 1973 by Helfrich [101], who realized the importance of membrane bending and proposed a corresponding free energy expression. This curvature elastic free energy has entered into the modeling of many specific systems [229], sometimes even systems where the bending of a lipid layer is not immediately apparent. A prominent example is the deformation of a membrane by an integral membrane protein or peptide that does not match the hydrophobic thickness of the host bilayer [192, 163, 127]. This "hydrophobic mismatch" gives rise to a deformation of the membrane in the vicinity of the protein, which can be described reasonably well by accounting for curvature and compression contributions to the free energy of the membrane [9, 162]. For the particular case of the

hydrophobic mismatch, phenomenological models have rationalized many experimental findings [7].

Some naturally occurring lipids such as phosphatidylserine (PS), phosphatidic acid (PA), or phosphatidylglycerol (PG), carry a negative excess charge (PA in fact can carry one to up to four charges), whereas others, like phosphatidylcholine (PC) or phosphatidylethanolamine (PE), are zwitterionic. A number of cationic lipids have been synthesized for specific purposes, especially for the design of cationic lipid-DNA complexes that are used as delivery vehicles in non-viral gene transfer [29, 305]. Charged lipids are abundant in each biomembrane and many model bilayers. However, membranes where all lipids are charged are rare because the electrostatic headgroup-headgroup repulsion tends to render the membrane unstable with respect to the formation of micellar structures [113]. Hence, charged membranes usually consist of a mixture of zwitterionic and charged lipids. The adsorption of many peripheral membrane proteins is mediated, at least partially, by electrostatic interactions [99, 18], examples also include certain cationic antibacterial peptides [220] such as mellitin [190] or magainin [172]. Modeling of electrostatics is challenging because salt ions in the aqueous phase tend to screen electric charges and thus modify electrostatic interactions between macroions [94, 89, 25]. A convenient approach to model electrostatic interactions in electrolytes that contain macroions is the mean-field Poisson-Boltzmann theory [73]. This approach has also been used frequently for charged lipid membranes [6, 176].

To summarize this introduction, the study of lipid membranes represents an inter-disciplinary research field that targets biotechnological/pharmaceutical applications and aims at elucidating cellular processes on biomembranes. Lipid membranes and their interactions with biomacromolecules are a supreme example for a soft matter system, where physical concepts are indispensable to fully understand the system

behavior. Lipid membranes also exemplify the beneficial relationship between experiment-driven research and concomitant modeling. Indeed, phenomenological modeling and computer simulations have frequently played a central role in understanding experimental results. The present thesis follows up on this approach. It develops theoretical models that aim to rationalize specific experimental findings, relating to phase behavior of a lipid bilayer, to the electrostatic adsorption of proteins, and to the kinetics of drug release from liposomes.

# 2. IMPORTANCE AND ROLE OF THE PRESENT WORK

## 2.1. Modeling approaches: Methods and strategies

As outlined in the Introduction, the interplay of experiment and modeling has played an important role in understanding the behavior of lipid membranes and their interactions. From a physical point of view, lipid membranes constitute complex fluids (often multicomponent) that are immersed in water. In contrast to simple fluids, where rigorous theoretical approaches are available [95], complex fluids have to rely on phenomenological modeling, mean-field theories, and computer simulations. Each method has its own scope and limits of applicability.

Phenomenological models start with order parameters. These are scalar or vectorial (occasionally tensorial) quantities that determine the behavior of a system. For a lipid membrane, this can be the curvature at a given point in space, the local cross-sectional area per lipid, the average direction into which the lipid tails point, the local lipid composition, the concentration of ions in the vicinity of charged lipids, or a tensorial dielectric constant. Which ones to chose is often a non-trivial question and depends on the problem. Herbert Callen's textbook "Thermodynamics and an Introduction to Thermostatistics" provides an excellent discussion on how a small number of order parameters emerges from a very large number of degrees of freedom of a macroscopic system [33]. Once a set of order parameters $\lambda_i$ is identified, a set of relations is needed that describes the equilibrium values or the dynamic behavior of the order parameters. For systems in thermodynamic equilibrium, it is often most convenient to find an expression for the relevant free energy $F$ of the system. For phenomenological models, free energy expressions are typically obtained based on symmetry considerations. The free energy generally depends on the order parameters

$\lambda_i$, which are free to adjust, and on a number of fixed parameters $\tilde{\lambda}_i$ (for example, the temperature $T$). The presence of two types of variables, unconstrained ($\lambda_i$) and constrained ($\tilde{\lambda}_i$), is the defining feature of equilibrium thermodynamics. Clearly, in thermal equilibrium $F(\lambda_i, \tilde{\lambda}_i)$ adopts a minimum with respect to all unconstrained variables. The minimization typically leads to algebraic or differential equations that can be solved either analytically or numerically. Inserting the solutions $\lambda_i = \lambda_i(\tilde{\lambda}_j)$ for the $\lambda_i$'s back into the free energy expression $F = F(\lambda_i(\tilde{\lambda}_j), \tilde{\lambda}_i)$ provides access to the free energy as function of all constrained parameters $\tilde{\lambda}_i$. This then yields all thermodynamic information; i.e., all equations of state follow from the derivatives $\partial F/\partial\tilde{\lambda}_i$. For systems not too far away from thermal equilibrium, derivatives of the free energy can be used according to Onsager's reciprocity relations to set up equations of motion [33]. For example, the Cahn-Hilliard [31] equation $\partial\phi/\partial t = M\nabla^2\mu(\phi)$ for a constant mobility $M$ relates the time derivative of the local composition $\phi$ to the Laplacian $\nabla^2$ applied to the chemical potential $\mu = \mu(\phi)$. The chemical potential $\mu = \partial F/\partial\phi$ follows from a phenomenological Landau-Ginzburg expression of the free energy $F = F(\phi)$.

Mean-field models work along similar lines as phenomenological models. The difference is that the free energy is obtained from a mean-field approximation of a statistical mechanics model of the system, instead of being obtained from symmetry considerations. An example is the mean-field chain packing model developed by Ben-Shaul [17]. This approach starts from a molecular lipid chain model and adopts a mean-field approximation to derive a self-consistency relation that yields statistical properties of a lipid chain in a fluid membrane. The signature of a mean-field model is the neglect of correlations – this is often a reasonable approach, especially when far away from second order phase transitions. Mean-field approaches generally give rise to self-consistency relations; these are often algebraic or differential equations. The present thesis makes use of the Poisson-Boltzmann model, which is a mean-field

description of electrostatic interactions in aqueous solutions. Here, the self-consistency relations appear as the Poisson-Boltzmann equation [6, 176].

Computer simulation methods are widely used for complex fluids and soft matter systems, including lipid membranes. They range from atomistic molecular dynamics simulations with classical interaction potentials [271] to various levels of coarse grained models [202, 283], including molecular dynamics [169, 170, 70, 27, 41], Monte Carlo [83], and dissipative particle dynamics [282]. Atomistic simulations can typically be performed in boxes of several tens of nanometers in size. This is certainly sufficient to study the local structure of a single lipid bilayer, which is about 5 nm thick, but insufficient for extended membranes, ensembles of vesicles, protein adsorption equilibria, and charged bilayers at low salt content. The objective of simulations is often (but not always) different from that of phenomenological models. While phenomenological models aim to describe a system's behavior on the basis of its most essential interactions (described in terms of only a few order parameters), simulations typically include many degrees of freedom. Model simplifications are intentional in phenomenological modeling, in simulations they are only implemented because of computers speed restrictions. This different scope makes computer simulations a hybrid approach between theory and experiment, sometimes referred to as "in-silico" experiment. Computer simulations can also be useful to test theoretical concepts or to calculate material parameters. An example are elastic membrane properties such as the bending stiffness or the Gaussian modulus that are difficult to measure [292, 107, 108]. Here, simulations provide tools to understand the molecular origin of these quantities.

We finally recall some of the fundamental interactions that determine the energetics of lipid membranes and their interactions with other molecules. The driving force for the self assembly of a lipid membrane is the hydrophobic effect [266]. This effect is of entropic nature and results from the unfavorable perturbation of the water

structure close to a hydrophobic surface, especially the disruption of the water's hydrogen bond network. This disruption leads to an ordered water layer that bridges between the bulk water and the hydrophobic surface. The entropy loss is caused by the ordered water molecules. From a fundamental point of view, also the surface tension of water with air ($\gamma = 0.072\mathrm{N/m}^2$ at room temperature) is a result of the hydrophobic effect. There are a number of theoretical models for the hydrophobic effect [214, 36]; particularly simple and instructive is the two-dimensional Mercedes-Benz model from Dill and coworkers [276, 256]. Another important contribution to the free energy of a lipid membrane is related to the packing of the lipid tails [17]. In the fluid-like state the hydrocarbon tails change their conformation about $10^{10}$ times per second, where different conformations correspond to different trans ($t$) and gauge ($g^+$ and $g^-$) isomers along the chain [72]. The packing of the lipids in a bilayer or other aggregation geometries affects the probabilities with which certain chain conformations are adopted. The packing properties are important for the structural morphology of lipids [16, 241] and for the partitioning of hydrophobic molecules into a lipid bilayer [304]. A third interaction that is relevant for lipid membranes is the electrostatic interaction between charges. All important classes of biomolecules – lipids, proteins, and nucleic acids – are (or can be) charged. If charges are present, their spatial arrangement follows the same fundamental pattern: A biomacromolecule (lipid membrane, DNA, or protein) has an interior part of low dielectric constant, and the charges are attached exclusively to the surface, where they are in contact with water [2]. This pattern suggests that it is generally too costly to place charges inside a medium of low dielectric constant [19]. We point out that electrostatic interactions include higher moments; i.e. charged-dipole, dipole-dipole etc. For example, van der Waals interactions, which originate from permanent or induced dipolar forces are essentially of electrostatic nature.

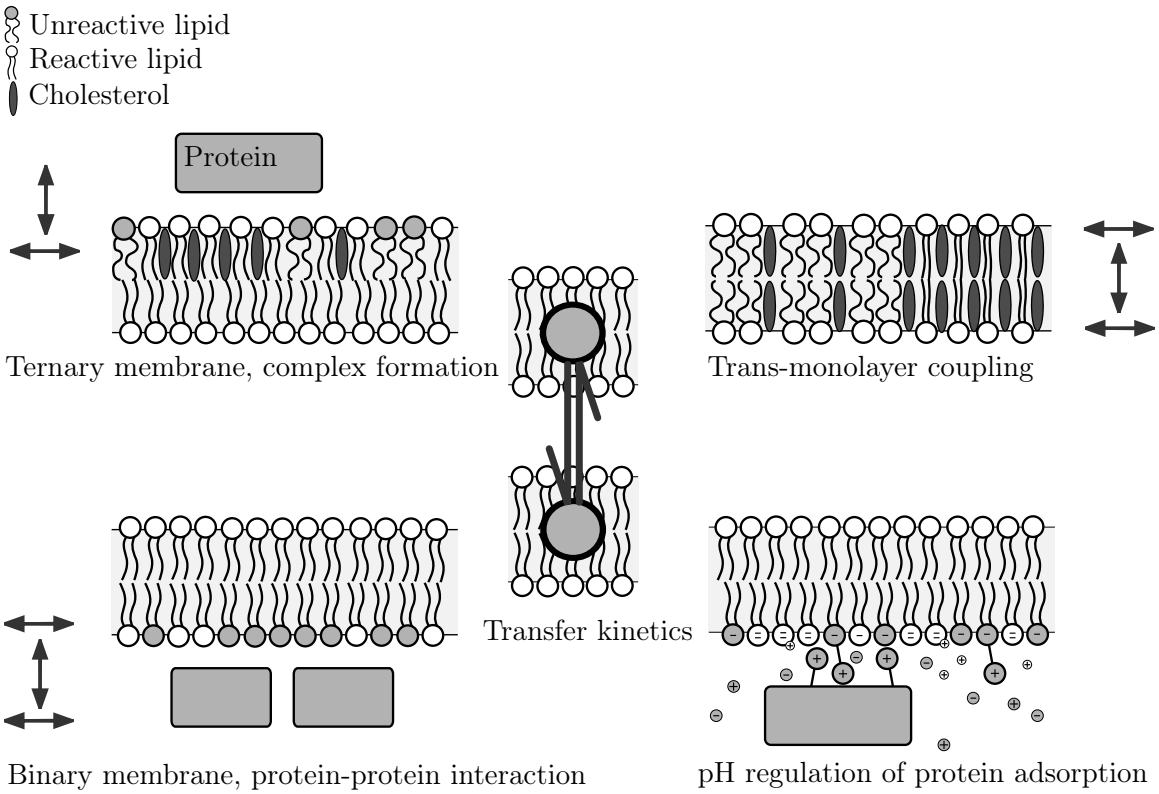


Figure 2.1. Aspects of lipid membranes and their interactions with other molecules. All illustrated systems are modeled in the present thesis. Top left: Ternary lipid membranes containing cholesterol, and interactions with peripheral proteins. Top right: The phase behavior of a bare binary bilayer is influenced by the coupling between the two membrane leaflets. Bottom left: A phase separating binary membrane interacts with peripherally adsorbed proteins allowing for the coupling between local protein and lipid compositions. Lipid-lipid, lipid-protein, and protein-protein interactions will influence the onset of instability with respect to lateral phase separation. Bottom right: Electrostatic macromolecule adsorption onto a binary membrane consisting of zwitterionic lipids and lipids with the ability to deprotonate. Middle: Transfer kinetics of hydrophobic macromolecules from one liposomal membrane to another.

## 2.2. Specific systems addressed in this thesis

Motivated by recent experimental findings, we investigated five specific systems, all containing bare mixed lipid membranes or mixed lipid membranes interacting with macromolecules; see the schematic illustration in Fig. 2.1.

First, in Chapter 4, we consider ternary model membranes consisting of unsaturated lipids, saturated lipids and cholesterol, where macroscopic separation

into a lipid-ordered ($L_o$) and lipid-disordered ($L_d$) phase has been reported [280]. We employ a simple generic thermodynamic model that rationalizes the two critical points of the closed loop phase behavior observed in experiments [281] and predict changes in stability due to membrane-adsorbed macromolecules.

The second subject (see Chapter 5) of this thesis is the influence of trans-monolayer interactions on the stability of lipid membranes with respect to lateral phase separation. We develop a thermodynamic model accounting for lateral lipid interactions and the coupling between the two apposed monolayers to predict the phase behavior of the lipid bilayer.

In the third part of this work (see Chapter 6), we investigate the influence of peripherally adsorbed model proteins on the thermodynamic stability of binary mixed membranes. Proteins and other macromolecules often interact specifically with only one of several lipid species. Yet, this specific interaction competes with other unspecific interactions. Our focus is to explicitly include into a thermodynamic model the presence lipid-lipid, lipid-protein, and protein-protein interactions, to investigate protein-induced local lipid sequestration, and predict the thermal stability of this model [104].

While the developed models alluded to so far incorporate the interplay of proteins and lipids with generic interaction parameters, we investigate in the fourth part of this thesis (see Chapter 9) the influence of hydrogen bond formation and pH value of the aqueous solution surrounding the membrane on the adsorption of proteins onto mixed lipid membranes by modeling electrostatic interactions. These are incorporated in a mean field thermodynamic approach which explicitly accounts for electrostatic effects, deprotonation of a specific phospholipids, conformational freedom of dipolar lipid headgroups, and protein binding domains under presence of a monovalent electrolyte.

The fifth and final part of the thesis (see Chapters 7 and 8) leaves the equilibrium approach behind and investigates the time evolution toward thermal equilibrium. The transfer kinetics of poorly water soluble macromolecules between liposomes, specifically the interior of the liposomal lipid membranes, are modeled based on a detailed distribution function of drug molecules among the individual liposomes, accounting for both diffusion and collision transfer mechanisms.

In the following we briefly introduce each of the five specific projects.

### *2.2.1. Modeling the phase behavior of protein-decorated ternary lipid layers*

Membrane rafts in biomembranes are dynamic, short lived and on sub-micron level in size. Although the raft model can be related to a multitude of cellular processes from cell signaling to viral entry entry, the discussion of rafts has been controversial. Rafts have never been observed directly; in fact the measurement itself can create raft-like heterogeneities [149]. Macroscopic phase separation into two lipid phases, liquid-ordered ($L_o$) and liquid-disordered ($L_d$), is observed for model membranes of appropriate ternary lipid mixtures [280]. In terms of composition, cholesterol-enriched ($L_o$) domains are reminiscent of membrane rafts in biomembranes [152]. When saturated lipid chains are in extended (all-trans) conformation their affinity to reside next to the tetracyclic ring of cholesterol is enhanced as compared to unsaturated hydrocarbon chains. Consequently, instead of being randomly mixed, such a membrane can adopt an energetically more favorable configuration by phase separating into one phase dominated by cholesterol and highly ordered saturated lipids the other phase being enriched with unsaturated lipids.

Because of the favorable interaction of saturated lipids with cholesterol, it has been suggested that these two molecules bind each other as in a chemical reaction [179]. In this context, saturated and unsaturated lipids are therefore sometimes referred

to as “reactive” and “unreactive” lipids. Ternary mixtures of reactive (saturated) lipids, unreactive (unsaturated) lipids, and cholesterol can exhibit closed loop phase coexistence region with an upper and lower critical point [281]. This means multiple phases coexist only in the presence of all three components and the depletion of one component below a critical value or an increase above it (thereby depleting another component) results in a system that does not show phase separation. Examples of such systems are model membranes consisting of unsaturated 1,2-diphytanoyl-sn-glycero-3-phosphocholine(diPhyPC), saturated 1,2-Dipalmitoyl-sn-glycero-3-phosphocholine (DPPC) , and cholesterol [281].

McConnell and co-workers [179, 217] proposed a model for the interaction of cholesterol in lipid membranes. It is based on the formation of complexes between cholesterol and the reactive lipid, where either all cholesterol or all saturated lipids will be engaged in complex formation. The ternary mixture can be viewed as consisting of unreactive lipids and complexes as well as the excess of either cholesterol or reactive lipids. We consider the free energy of such a ternary mixture within the mean-field framework of a lattice gas, with only one additional parameter accounting for non-ideal interactions between (and amongst) complexes and unreactive lipids, thereby allowing for multiple phases. Numerical analysis reveals similarities in compositional differences of the two coexisting phases, for various initial compositions. We employ these symmetries and introduce them as an additional thermodynamic constraint. This enables us to specify the two critical points of the closed-loop phase boundary analytically.

Typically, proteins bind preferentially to one lipid species. This introduces a mechanism to accumulate these lipids in the vicinity of the protein binding site [42], leading to a tendency to enhance domain formation [128]. Hence, specific lipid-protein interactions in conjunction with interactions among adsorbed proteins can be expected to influence the phase behavior of the membrane. We describe protein adsorption

onto such a ternary membrane by introducing an appropriate composition-dependent incentive into the free energy. This model, which is detailed in Chapter 4, was presented at the 51st Annual Meeting of the Biophysical Society in Baltimore in March 2007.

### *2.2.2. Trans-monolayer coupling in binary bilayers*

As described above, each leaflet of a bilayer can individually exhibit separation into phases with different composition. Experimental results demonstrate the matching of macroscopically large domains [280, 136] across the upper and lower monolayer. That is, in a symmetric bilayer the domains of the apposed leaflets are observed to be in perfect registration. This effect implies some sort of inter-leaflet coupling which is sensitive to the compositional differences.

Biomembranes are typically asymmetric. For example the plasma membrane contains predominantly phosphatidylcholine, sphingomyelin, cholesterol and glycolipids in the outer leaflet and phosphatidylethanolamine, phosphatidylserine, cholesterol and other charged lipids in the inner leaf [143]. It is known that the composition of the outer monolayer favors phase-separation, whereas the composition of the inner leaflet does not exhibit a tendency for domain formation when investigated in similar model membranes [290, 125]. Without a coupling mechanism, only the outer leaflet would form domains whereas the inner monolayer would remain homogeneous. Transmonolayer coupling can explain processes – including phase separation – that mitigate though the bilayer.

Experimental studies of ternary cholesterol-containing membranes show close-loop phase behavior of only two distinct phases under certain conditions (concentration of cholesterol and temperature range [280]), and are supported by theoretical models, including our model of ternary membranes. This gives rise to approximate three-component mixtures as pseudo-binary mixtures [217]. Existing theoretical models

consider several order parameters, for instance compositional and curvature degrees of freedom [96], or composition and monolayer thickness [3].

We have developed a thermodynamic model of a bilayer consisting of two binary monolayers, composed of the same lipid species, but not necessarily the same composition. It accounts for lateral lipid interactions in each monolayer and the coupling between the apposed monolayers, and only uses one single-order parameter, the composition of the binary monolayer. Each of the two monolayers is treated as a lattice gas on the mean field level that can phase-separate individually in the absence of monolayer-monolayer coupling. The local coupling between the two monolayers is introduced by an energy penalty proportional to the square of the compositional differences, which is accurate in the limit of small compositional differences. A coupling constant accounts for the strength of this energy penalty. The use of only one order parameter allows us to perform a simple complete thermodynamical analysis of this model as function of the coupling strength. Our model predicts that phase separation in one monolayer can induce or suppress domain formation in the apposed monolayer. Paper 1 (see Chapter 5) reproduces this work. It was published December 15, 2007 in the Biophysical Journal 93 [286].

### *2.2.3. Protein decorated mixed lipid membranes and protein-protein interactions*

In Section 2.2.1 we considered the influence of protein adsorption onto ternary membranes, where proteins did not interact directly with each other. In the present section we focus on a system of a binary lipid layer with peripherally adsorbed proteins, including not only lipid-lipid and lipid-protein but also protein-protein interactions.

Peripheral adsorption of proteins onto mixed lipid membranes generally influences the lateral stability of the membrane. Among a large number of examples is the ability of cytochrome P450 2B1 to induce lateral demixing in ionic phospholipids [128].

If proteins bind preferentially to one lipid species, it will lead to a local sequestration of that membrane species close to the protein adsorption sites [104]. That is, in the vicinity of each individual protein the membrane composition differs from the average. This difference depends on the difference in affinity of the protein with the high-affinity lipid and has been observed experimentally in certain cases [103, 104, 289, 82]. Molecular simulations support these findings [160]. Local segregation of lipids is distinct from macroscopic phase separation. Yet, attractive protein-protein interactions can trigger phase behavior [5]. Experimental results suggest proteins colocalize within membrane domains or at the domain interface [185, 106, 102, 201, 167] and cause phase separation in biomembranes [151] and model membranes [93, 208]. Several theoretical research efforts aim to explain the influence of proteins on domain sizes, for instance by limiting domain sizes due to protein immobilization [300], or through induced elastic membrane deformations [236].

A previous model suggested a combination of lipid-lipid and lipid-protein interactions can suffice to cause not only local lipid sequestration but also macroscopic phase separation [174]. The driving force for phase separation originates in the energy associated with local compositional differences. This leads to a line tension that tends to merge smaller domains into larger ones, resulting ultimately in macroscopic phase separation. We extend this preceding thermodynamic model to include direct protein-protein interactions. Our goal was to explore to what extent additional attractions between proteins further enhance the tendency to phase separate. This modified tendency is manifested in phase diagrams. We have thus calculated phase diagrams of binary membrane-protein systems with and without direct protein-protein interactions. These diagrams demonstrate an enhanced tendency to phase separate, including cooperative behavior between membrane mediated phase separations (due to lipid-protein interactions) and direct protein-protein attraction. Clearly, the interplay between lipid-protein and protein-protein interactions facilitates the membrane to

regulate its limits of stability. Chapter 6 presents this work as paper 2. It was originally published in The Journal of Chemical Physics on January 23, 2009 [157].

### *2.2.4. Modeling pH regulation of protein adsorption onto lipid membranes*

Interactions between proteins and lipids at the interface between the lipid head-groups and the electrolyte are often of electrostatic nature. This effect can be emphasized by specific structural characteristics of proteins which let the protein match the membrane surface structure [140, 148]. Phosphatidic acid (PA) is a signaling lipid located in the inner leaf of the plasma membrane, coexisting with phosphatidylethanolamine (PE), phosphatidylserine (PS), phosphatidylcholine (PC), and other lipids. The monoester headgroup of PA can carry one or two negative charges at physiological conditions. The dissociation state of PA is governed by the competition between proton binding and formation of a hydrogen bond through the so-called *electrostatic-hydrogen bond switch* [132]. The physiological significance of the electrostatic-hydrogen bond switch has been discussed in detail [134]. This mechanism may form the basis for the specific recognition of PA by membrane-binding proteins.

Charged proteins are electrostatically attracted to the membrane. Their binding regions, mainly consisting of cationic amino acids, bind transiently to anionic phospholipids. Tight docking, however, only occurs when the PA binding domain locates the phosphomonoester of PA and creates a specific and strong electrostatic interaction based on two negative charges that is further strengthened by hydrogen bond interactions. A dependence of protein binding to PA on the intracellular pH and the protonation state of PA has recently been shown [302]. In yeast, the protein Opi1 binds to the endoplasmic reticulum at neutral pH values and is released due to a drastic pH decrease (by about two units) caused by glucose starvation. A theoretical model of the electrostatic-hydrogen bond switch on bare membranes has been developed

previously [184]. It is based on the classical Gouy-Chapman theory which describes the electric potential of charged surfaces in salt-containing solutions on a mean field level. This model focuses on the dissociation state of PA and how this state is influenced by the membrane composition.

Following a similar approach, we develop an extended theoretical model of the influence of the pH value in the electrolyte on the energetics of macroion adsorption onto membranes containing PA. The electrostatic interactions between lipid charges, solvent, and macroion binding sites are treated on a mean-field level, incorporating a modified Poisson-Boltzmann model. The membrane is represented as a three-component lattice gas (PC, $PA^-$, and $PA^{2-}$). To account for the conformational freedom of PC headgroups we model the zwitterionic headgroups as dipoles of fixed length. The negative charge of the dipole is located at the membrane interface, allowing the positive charge to move freely on a hemisphere inside the electrolyte. Proteins are modeled as extended bodies of small inner dielectric constant with flexible charges attached to their surface; see the schematic illustration in Fig. 2.2. Our model allows for the sequestration of PA under the proteins, which changes the local pH value. So does the presence of binding sites of membrane adsorbed proteins. This change in local pH will affect the formation of hydrogen bonds. The short range attraction caused by the hydrogen bond has been modeled as a non-electrostatic square-well potential. Besides the rather crude approximations of the structure of involved molecules, we further assume all charges are point-like, all lipids occupy the same cross-sectional area of the membrane interface, changes in dielectric properties are laterally uniform, and drop instantly at the edge of the headgroup-region. These approximations, among others, do not allow this model to be quantitatively predictive, but demonstrate qualitative effects of changes in pH value of the electrolyte. We show that the combination of such non-electrostatic attractions and electrostatic interactions can greatly enhance the pH-sensitivity of protein adsorption and can

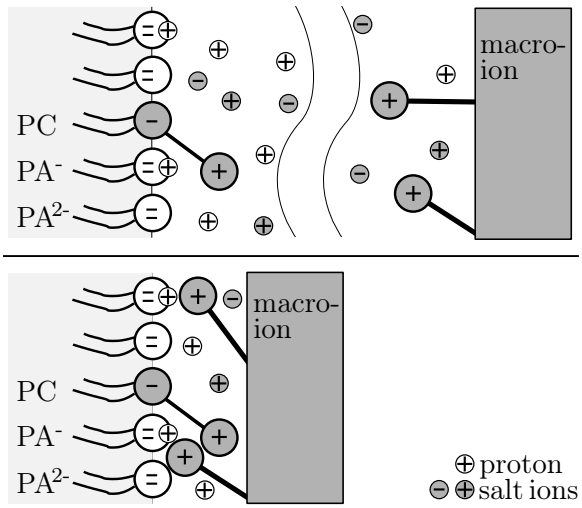


Figure 2.2. Schematic illustration of a bare membrane and isolated macroion (top), and adsorbed macroion (bottom). The membrane consists of PC and PA. PA can be found in two dissociation states, $PA^{-}$ and $PA^{2-}$. The negative lipid charges of the membrane reside in a interface plane. The electrolyte consists of positive and negative salt ions and protons. Positive poles of PC can move freely on a hemisphere around the negative pole which resides on the polar-apolar interface. Charged amino-acids of macromolecules form the PA-binding sites and can also move on a hemisphere around their anchor on the macromolecule surface.

render the regulation of protein adsorption processes under physiological conditions feasible. Chapter 9 reproduces the original paper which appeared in April 2013 in the journal Chemistry and Physics of Lipids [159].

### *2.2.5. Kinetic modeling of macromolecule transfer between liposomes*

Thus far we have considered interactions of macromolecules with lipid membranes in thermodynamic equilibrium. Yet, the time evolution toward the equilibrium state – that is, the kinetic behavior – is of fundamental importance, including numerous pharmaceutical applications. In example, for poorly water soluble drugs, liposomes are a widely used means of delivery to the target site [65]. An "good" drug delivery vehicle should keep the drug load on the way to the target and release it only after arrival at the target. Understanding the kinetics and mechanisms of drug release from

liposomal (and other) nanocarriers is thus a prerequisite to systematically improving drug delivery systems.

In recent experimental work on the transfer of the poorly water soluble drug temoporfin between two different types of liposomes (i.e. from donor liposomes to acceptor liposomes), subsequent separation of donor and acceptor liposomes allowed for observation of the time dependence of the drug transfer. The work revealed that the time dependence of the transfer kinetics is typically a simple exponential with a characteristic time of several hours [98]. Due to the hydrophobic nature of temoporfin it preferably resides in the hydrophobic compartment formed by the hydrocarbon tails of the liposomal lipids. Transfer can occur via collisions between acceptors and donors as well as directly through diffusion across the aqueous phase. Despite a large number of experimental studies addressing the kinetics of lipid and drug transfer between liposomes and other nanocarriers, there is little theoretical work available that targets the physical nature of the transfer kinetics. During collisions between liposomes, drug molecules can transfer directly, avoiding the unfavored aqueous solution and allow for a partial equilibration of drug content. This process has been used to explain lipid transfer between vesicles [117]. Drugs can also transfer by diffusion through the aqueous solution [180]. Both transfer processes can be utilized in lipid-transfer between vesicles [298].

We introduce a detailed kinetic model for the release kinetics of poorly water-soluble drug molecules from liposomal carriers, based on a detailed distribution function of drug molecules among the individual liposomes, accounting for both transfer mechanisms. This model is generic and is, in principle, applicable to a number of different carrier systems, including liposomes, micelles [272], colloids [186], and nanoparticles [32]. Our model predicts the experimentally observed simple exponential behavior and shows collision-dominated transfer for small liposome concentrations and diffusion dominating the drug exchange for higher liposome concentrations.

Furthermore, we extend this model to explain transfer curves that show a sigmoidal time-dependence of drug concentration in acceptor liposomes, which also have been reported in experiments [98]. Our studies on the transfer kinetics of macromolecules between liposomes were published in March 30, 2011 in the Journal of Controlled Release [98]; see Chapter 7. A detailed version of the model is reproduced and extended in Chapter 8. It was originally published on March 22, 2011 in the Journal of Drug Delivery [158].

### 2.3. Summary of the main results of this thesis

The results of this thesis are theoretical models that help to rationalize a multitude of experimental findings. All models relate to lipid membranes and their interactions with macromolecules such as proteins and drug molecules. Highlights among our results include:

- Protein adsorption onto binary lipid membranes tends to facilitate domain formation, even more so in the presence of attractive protein-protein interactions. The facilitation is a result of protein-induced compositional differences and the ensuing line tension. That is, domain formation can become favorable due to the reduction of compositional gradients within the membrane.

- The coupling between the two monolayers in a bilayer affects the tendency of the bilayer to phase separate. It can trigger or inhibit phase separation, depending on the lipid compositions in the monolayers and the coupling strength.

- pH-induced adsorption of proteins onto charged lipid membranes cannot be rationalized by electrostatic interactions alone. Yet, the interplay between lipid dissociation and hydrogen bond formation – the so-called electrostatic-hydrogen bond switch – renders the adsorption strength of charged proteins more sensitive

and allows for the regulation of protein adsorption under physiologically occurring pH changes.

- Transfer kinetics of poorly water soluble drug molecules such as temoporfin typically follows a simple exponential behavior. This behavior can be rationalized on the basis of a detailed kinetic model with drug exchange rates that are proportional to concentration differences of drugs in liposomes. Interactions between drug molecules can give rise to sigmoidal instead of exponential behavior.

# 3. MODELING METHODS

This section introduces the major modeling methods the present thesis employs. We focus on providing a background and framework that helps to understand Chapters 4–9.

## 3.1. Thermodynamic modeling

The present work contains multiple applications of thermodynamics, including the use of various thermodynamic potentials and their transformation, the calculation of elastic moduli, and the computation of phase diagrams and critical points. All calculations are carried out on the mean field level, and a central role is played by the lattice gas model [228]. We therefore introduce the lattice gas model and analyze its thermodynamic behavior.

### *3.1.1. Mean field lattice gas*

For lipid species of roughly the same cross-sectional area, a planar binary lipid layer can be treated as a two-dimensional incompressible fluid and described, as a first order approximation, as a lattice gas on the mean field level [228]. The corresponding free energy per lattice site, measured in units of the thermal energy $k_{\mathrm{B}}$ can be expressed as function of the lipid mole fractions $\phi_A = \phi$ and $\phi_B = 1 - \phi$ via

$$\frac{f}{k_{\mathrm{B}}T} = \phi \ln \phi + (1-\phi) \ln(1-\phi) \; . \tag{3.1}$$

Note that Eq. (3.1) follows from counting the $\Omega = M!/(N!(M-N)!)$ distinguishable states of $N$ particles on a lattice of size $M$ using Stirling's approximation

$\ln x! = x \ln x - x$ and the free energy $Mf = F = -k_{\mathrm{B}}T \ln \Omega$. We also note that Eq. (3.1) can be generalized to $n$ components with compositions $\phi_i$

$$\frac{f}{k_{\mathrm{B}}T} = \sum_{i=1}^{n} \phi_i \ln \phi_i \ . \tag{3.2}$$

The free energy in Eq. (3.1) does not account for interactions and thus cannot predict phase separation. We assume that interactions only occur between nearest neighbors, and (on the mean field level) neglect correlations, meaning the number of nearest neighbors is determined solely by the average composition and not by the exact occupancy of neighboring sites [228]. This leads to the non-ideal mixing free energy [228]

$$\frac{f}{k_{\mathrm{B}}T} = \phi \ln \phi + (1-\phi) \ln(1-\phi) + \chi\phi(1-\phi) \tag{3.3}$$

with the non-ideality parameter

$$\chi = z \left( \omega_{AB} - \frac{\omega_{AA} + \omega_{BB}}{2} \right) \ , \tag{3.4}$$

where $\omega_{AA}$, $\omega_{AB}$, $\omega_{BB}$ denote, respectively, the A-A, A-B, and B-B pair interaction strengths (measures in units of $k_{\mathrm{B}}T$), and $z$ is the coordination number of the lattice. Positive $\chi$ means that energy penalties between different lipid species are larger than between lipids of the same kind; this models net attractive interactions between alike lipids. The total free energy F can be found by summing over all $A/a$ lipids of the lipid layer,

$$F = \frac{1}{a} \int_A f \, \mathrm{d}A \ , \tag{3.5}$$

where $A$ is the total area of the layer and where each lipid occupies a lattice site of size $a$, the cross-sectional area per lipid. We assume this area to be the same for all considered lipid types as well as for membrane-embedded cholesterol. In Chapters 5 and 6 we use this free energy to describe the energetics for each individual monolayer when examining transmonolayer coupling of membrane leaflets (Chapter 5), and for modeling a protein-decorated membrane (Chapter 6) in our study of the effects of direct protein-protein interactions on membrane stability.

### *3.1.2. Equilibrium thermodynamics and stability*

In equilibrium, a thermodynamic system will reside in a state in which the free energy adopts a minimum. We consider our binary lattice gas system with a total number of $N = N_{A0} + N_{B0}$ lipids distributed into two subsystems 1 and 2 with respective energies $F_1(N_{A1}, N_{B1})$ and $F_2(N_{A2}, N_{B2})$. The overall free energy of such a system of two phases would be

$$F(N_A, N_B) = F_1(N_{A1}, N_{B1}) + F_2(N_{A2}, N_{B2}) \; . \tag{3.6}$$

The numbers of particles in the individual phases are not freely adjustable, they are constrained by the conservation relations $N_{A0} = N_{A1} + N_{A2}$ and $N_{B0} = N_{B1} + N_{B2}$. Denoting the size of the first phase relative to the system size as $\theta$, it follows that the second phase covers a relative area of $\theta_2 = (1 - \theta)$. We can express the free energy per lipid of the whole system, $f_0$, as the coexistence equation, a weighted sum of the per-lipid energies of the individual phases,

$$f(\phi_0) = \theta f(\phi_1) + (1 - \theta) f(\phi_2) \; . \tag{3.7}$$

The thermodynamic constraint of conservation of lipids has to be fulfilled and can be expressed as the lever rule

$$\phi = \theta\phi_1 + (1-\theta)\phi_2 \ . \tag{3.8}$$

To determine when a system separates into distinguishable phases, we can analyze the shape of the free energy. Fig. 3.1 shows a graph of the free energy per lipid of a certain system (in fact, it is the accessible free energy of a ternary mixture of cholesterol, saturated and unsaturated lipids under the assumption that the membrane separates along parallel tie lines, see Eq. (4.20)).

Let us look in the graph at a membrane with average composition $\varphi_0 = \varphi_0^u$, where, as we will see shortly, the membrane is unstable. Eq. (3.8) tells us that

$$\theta = \frac{\varphi_2 - \varphi_0}{\varphi_2 - \varphi_1} \ , \tag{3.9}$$

which we will use to rewrite the coexistence equation Eq. (3.7). For clarity we shall use $f_1 = f(\phi_1)$ and $f_2 = f(\phi_2)$, and find the free energy of the separated system to be

$$f(\phi_0) = \frac{f_2 - f_1}{\varphi_2 - \varphi_1}\,(\varphi_0 - \varphi_1) + f_1 \ , \tag{3.10}$$

which is the equation of a line connecting the points $(\varphi_1, f_1)$ and $(\varphi_2, f_2)$. As evident in Fig. 3.1 this energy is below $f(\varphi_0)$ at $\varphi_0 = \varphi_0^u$ and will reach a minimum if the connecting line becomes tangent to $f$. This graphical method of finding the equilibrium state of a system is known as the common tangent construction and can be expressed by the two equations

$$\left.\frac{\mathrm{d}f}{\mathrm{d}\varphi}\right|_{\varphi_1} = \left.\frac{\mathrm{d}f}{\mathrm{d}\varphi}\right|_{\varphi_2} = \frac{f(\varphi_2) - f(\varphi_1)}{\varphi_2 - \varphi_1} \ . \tag{3.11}$$

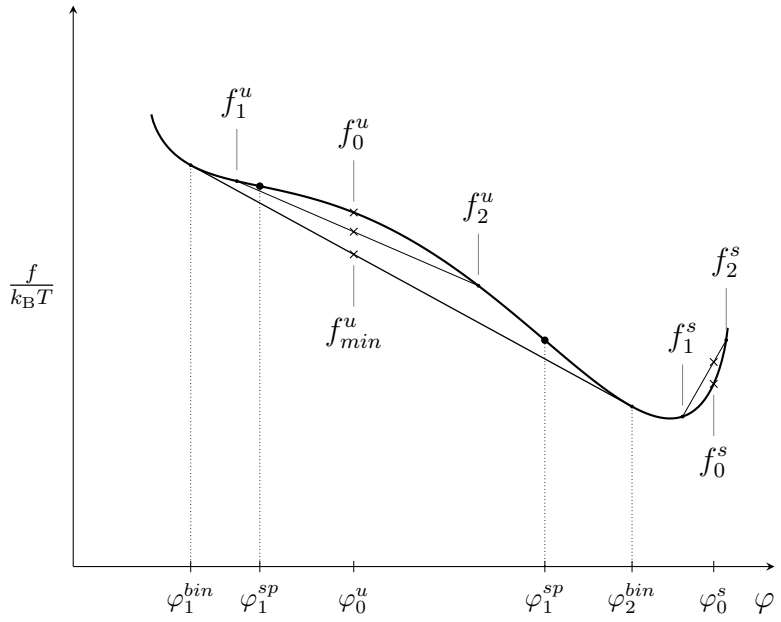


Figure 3.1. Illustration of thermodynamic stability and common tangent construction using a free energy function (thick curve) of one variable. A system with composition $\varphi_0^u$ in the unstable region has the shown free energy $f_0^u = f(\varphi_0^u)$ when homogeneous. If this system separates into two phases with compositions $\varphi_1^u$ and $\varphi_2^u$, respectively, its free energy (denoted by$_\times$) will be along the common tangent between the points connecting the free energies of the individual phases $(\varphi_1^u, f_1^u)$ and $(\varphi_2^u, f_2^u)$. In thermodynamic equilibrium a minimal free energy is achieved when the compositions of the phases are at the binodal points $\varphi^{bin}$. This minimal energy is lower than the energy of the homogeneous system if the free energy is convex. The inflection points where the curvature changes from negative to positive are the spinodal points $\varphi^{sp}$ denoted by $_\bullet$. If the total composition $\varphi_0$ is between the spinodal points (the spinodal region), any slight change from homogeneity will result in a lower free energy. A composition outside the binodal region is stable. Shown for $f_0^s = f(\varphi_0^s)$, separation into phases with different composition will result in an energy increase and in equilibrium the system will be homogeneous. For the free energy function plotted in this graph see Eq. (4.20) with $\chi = 5.25$ and $o = -.74$.

The first equation states that the lipid's chemical potential is the same in both phases. The second equation expresses the common tangent. The compositions of the two phases at which this occurs are known as the binodal points $\varphi^{bin}$.

We see that when $f$ is convex at $\varphi_0$ the system is unstable, any infinitesimal local fluctuation in composition will result in a lower free energy which will result in two distinct phases in equilibrium. On the other side, at a composition $\varphi_0 = \varphi_0^s$ the

free energy is concave and the energy of a separated system is larger than that in the homogeneous state. Here the system is stable. Convexity is ensured between the two inflection points of $f$, known as the spinodal points $\varphi^{sp}$ and shown as large circles in Fig. 3.1. These points span the spinodal region and are defined by the spinodal condition

$$\frac{\partial^2 f}{\partial \phi^2} = 0 \; . \tag{3.12}$$

For an average composition of a system outside the spinodal region phase separation can still occur if $\varphi_o$ is inside the binodal region spanned by the binodal points. Here $f$ is concave and the homogeneous system would represent a local minimum. Local fluctuations in composition can overcome the energy increase and drive the system into a separated state. A composition outside the binodal region is stable. Shown for $f_0^s = f(\varphi_0^s)$, separation into phases with any composition will always result in an energy increase and in equilibrium the system will be homogeneous.

For a system with two free variables $\varphi$ and $\psi$ the condition for convexity is

$$\frac{\partial^2 f}{\partial \phi^2}\frac{\partial^2 f}{\partial \psi^2} - \left(\frac{\partial^2 f}{\partial \phi \partial \psi}\right) \geq 0 \; . \tag{3.13}$$

The second term here ensures that besides the derivatives along the $\varphi$ and $\psi$ axis the free energy also curves downward along the diagonals. The spinodal line enclosing the region where $f$ is convex hence is found by solving the spinodal condition

$$\frac{\partial^2 f}{\partial \phi^2}\frac{\partial^2 f}{\partial \psi^2} - \left(\frac{\partial^2 f}{\partial \phi \partial \psi}\right) = 0 \; . \tag{3.14}$$

Here, three physically distinct phases are possible. Mathematically, these points lie on a surface tangential to the surface described by $f$. The number of possible different phases is predicted by the Gibbs phase rule[33]. In general, the free energy of any system consisting of $r$ components will be a function of the $r+2$ variables, temperature,

pressure and $r$ numbers of particles. A system separated in $m$ phases is fully described by $2 + m(r-1)$ variables. The composition of the last phase is determined by the total amount of particles per species. The common tangent condition states that the chemical potentials must be the same in all phases, resulting in $r(m-1)$ additional equations. The number of variables which can be arbitrarily chosen is thus

$$f = r - m + 2 \,, \tag{3.15}$$

where $f$ is the thermodynamic degree of freedom. The system is completely determined for $f = 0$. A binary mixture at fixed temperature and pressure is over-determined with more than two phases, a ternary mixture or system with two independent compositions such as a binary bilayer where upper and lower leaflet have independent compositions, can exhibit three-phase coexistence under fixed temperature and pressure. We consider all our models as incompressible systems and at constant temperature.

For the binary mixture with composition $\varphi$ and non-ideality parameter $\chi$ as described by Eq. (3.3) we find the spinodal region by solving Eq. (3.12),

$$\chi = \frac{1}{2\varphi^{sp}(1-\varphi^{sp})} \,, \tag{3.16}$$

which predicts a minimal $\chi$. This means above a critical non-ideality parameter $\chi_{crit} = 2$ the free energy has a convex region and the spinodal points are

$$\varphi^{sp}_{1/2} = \frac{1}{2} \pm \frac{1}{2}\sqrt{\frac{\chi-2}{\chi}} \,. \tag{3.17}$$

Fig. 3.2 shows the free energy for several interaction parameters $\chi$ as well as the spinodal region. We see that a common tangent exists and connects the binodal points which *coincide* with the two minima of $f$. The relevant definition of the binodal points stems from Eqs. (3.11). Finding the binodal points can be done by minimizing

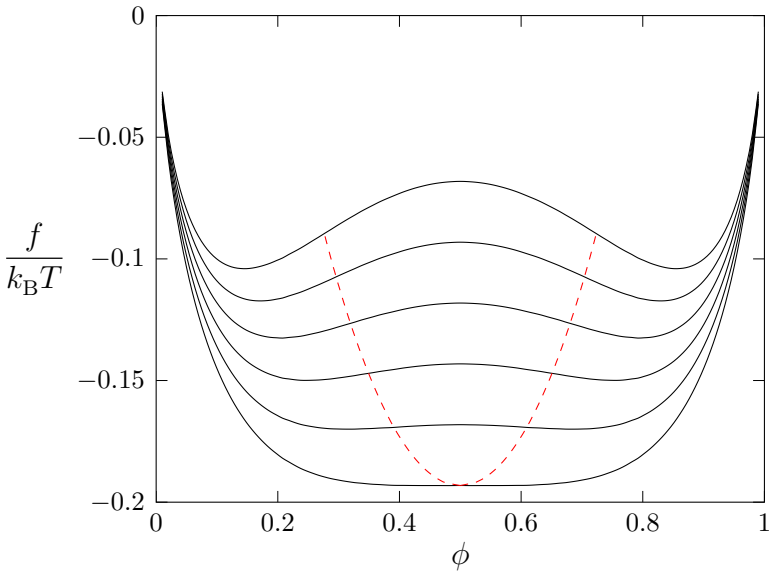


Figure 3.2. Free energy of a binary mixture according to Eq. (3.3). From bottom to top $\chi = 2$, $\chi = 2.1$, $\chi = 2.2$, $\chi = 2.3$, $\chi = 2.4$, and $\chi = 2.5$. The red dashed line encloses the spinodal region.

the coexistence equation Eq. (3.7) for an average composition $\varphi_0$ within the spinodal region, a function of the three variables $\varphi_1, \varphi_2, \theta$. Only two of these are independent, the third is fixed by the lever rule Eq. (3.8), yet introduces limitations since

$$0 \leq \varphi_1 \leq 1 \,, \tag{3.18}$$

$$0 \leq \varphi_2 \leq 1 \,, \tag{3.19}$$

$$0 \leq \theta \leq 1 \,. \tag{3.20}$$

Effectively this is a constraint global minimization with respect to two variables which can be carried out only numerically for most of the systems we consider in the present work.

Information about stability is usually visualized in a phase diagram as seen in Fig. 3.3. A system with composition $\phi$ and interaction parameter $\chi$ on a tie line will separate into two phases with compositions corresponding to the ends of that tie-line. The relative sizes of the phases can be calculated from the lever rule (Eq. (3.8)). The

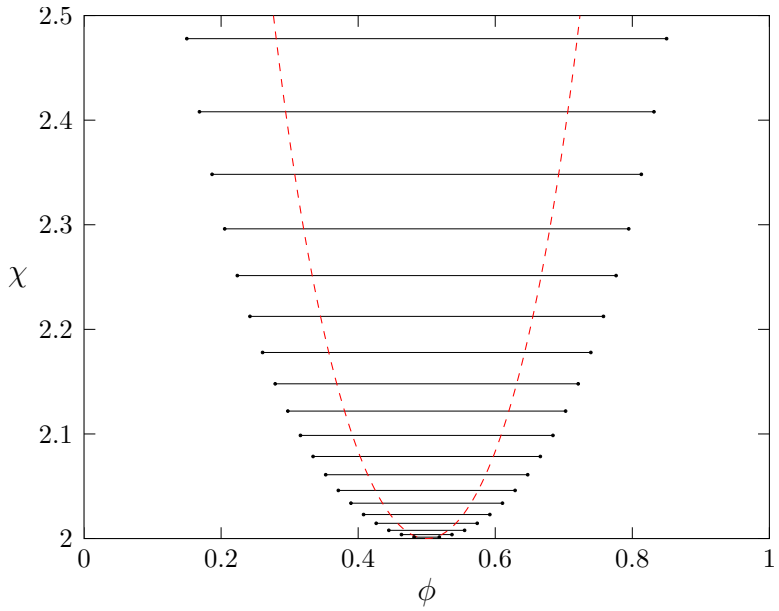


Figure 3.3. Phase diagram for the free energy $f$ of a binary mixture in Eq. (3.3). The red dashed line represents the spinodal line, tie-lines (black) connect the two states in which a system on a corresponding tie-line separates. All dots form the binodal line outside the spinodal line.

tie lines cover the binodal region, their end points describe the binodal line. Outside of this area the system is stable, that is it shows no phase separation. The point where binodal and spinodal meet is referred to as a critical point. In case of binary mixture coexistence, at the critical point the third derivative of $f$ with respect to $\varphi$ is also zero.

### 3.2. Mean-field electrostatics

In this work we model electrostatic interactions between membrane lipids, proteins, and the solvent. Specifically we calculate the adsorption free energy of a protein onto a lipid bilayer by comparing free energies of the adsorbed and desorbed states. We account for the presence of mobile salt ions in the aqueous solution, mobility of the charges on the lipids and protein, dielectric discontinuities, lipid dissociation equilibria, and compositional changes within the lipid layer as a consequence of protein

adsorption. The complexity of the system demands significant simplifications. We shall therefore employ here the mean field Poisson-Boltzmann model [6]. In the present section we present some details of Poisson-Boltzmann theory for the case of one (or more) macroions immersed in a symmetric 1:1 electrolyte, each macroion with fixed surface charge density $\sigma$. Additional levels of complexity, including mobile charges on the surface, surface-surface interactions, and dissociation equilibria, are taken into account in Chapter 9.

The electrostatic energy of a distribution of charges with charge density $\rho$ can be expressed as

$$U = \int \frac{\rho\Phi}{2}\,\mathrm{d}V\ , \tag{3.21}$$

where $\Phi$ denotes the electrostatic potential, from which one can compute the local electrical field via $\vec{E} = -\nabla\Phi$. The integration in Eq. (3.21) extends over all space. The fundamental equation of electrostatics is Poisson's equation

$$\rho = -\varepsilon\varepsilon_o\Delta\Phi\ , \tag{3.22}$$

here written for a dielectric medium of uniform dielectric constant $\varepsilon$ and vacuum permittivity $\varepsilon_o$. Note that the Poisson equation is a local representation of the $1/r$-Coulomb potential [114]. It is convenient to work with the dimensionless potential $\Psi = e\Phi/k_{\mathrm{B}}T$, where $e$ denotes the elementary charge. Note that that $\Psi = 1$ corresponds to a potential of about 25 mV at room temperature. The dielectric constant of the medium is commonly expressed by the Bjerrum length $\ell_{\mathrm{B}} = e^2/4\pi\varepsilon\varepsilon_o k_{\mathrm{B}}T$, namely the distance at which the electrostatic interaction energy of two elementary charges equals $k_{\mathrm{B}}T$. The Bjerrum length in water is approximately $\ell_{\mathrm{B}} = 0.7\,\mathrm{nm}$, and for air it

is $\ell_\mathrm{B} = 56\,\mathrm{mm}$. We can express the electrostatic energy as

$$\frac{U}{k_\mathrm{B}T} = -\frac{1}{8\pi\ell_\mathrm{B}} \int \Psi \Delta\Psi \,\mathrm{d}V = \frac{1}{8\pi\ell_\mathrm{B}} \int (\nabla\Psi)^2 \,\mathrm{d}V \;, \tag{3.23}$$

where we have used the relation $\Psi\Delta\Psi = \nabla(\Psi\nabla\Psi) - \nabla\Psi\nabla\Psi$ and Gauss' law with the assumption of a vanishing electric field at infinity.

The Poisson-Boltzmann model treats the solution of mobile co- and counter-ions as a mixture of two ideal solutions that each are in contact with a reservoir of given concentration $n_0$. Note that electroneutrality for a symmetric 1:1 electrolyte requires $n_0$ to be the same for the co- and counter-ions. Close to the charged surface, the local concentrations, $n_+$ and $n_-$ of of salt cations and anions, respectively will vary. This implies the entropy of mixing $S$ to be the sum of the mixing entropies for cations (index "+") and anions (index "−")

$$\begin{aligned} S &= S_+ + S_- \\ &= -k_\mathrm{B} \int \left[ n_+ \ln \frac{n_+}{n_0} - n_+ + n_0 \right] \mathrm{d}V - k_\mathrm{B} \int \left[ n_- \ln \frac{n_-}{n_0} - n_- + n_0 \right] \mathrm{d}V \;. \end{aligned} \tag{3.24}$$

The constant $n_0$ in each integral is added to set the reference state such that $S = 0$ for $n_+ = n_- = n_0$. The free energy $F = U - TS$ of the system is thus

$$\frac{F}{k_\mathrm{B}T} = \frac{1}{8\pi\ell_\mathrm{B}} \int (\nabla\Psi)^2 \,\mathrm{d}V + \int \left[ n_+ \ln \frac{n_+}{n_0} - n_+ + n_- \ln \frac{n_-}{n_0} - n_+ + 2n_0 \right] \mathrm{d}V \;. \tag{3.25}$$

The free energy $F$ still depends on the unconstrained variables $n_+$ and $n_-$. We thus find the equilibrium state by minimizing $F(n_+, n_-)$. Because $n_+$ and $n_-$ are functions of space, we determine the extremum of $F$ by carrying out the first variation

$$\frac{\delta F}{k_\mathrm{B}T} = \int \left[ \frac{\nabla\Psi\delta\nabla\Psi}{4\pi\ell_\mathrm{B}} + \delta n_+ \ln \frac{n_+}{n_0} + \delta n_- \ln \frac{n_-}{n_0} \right] \mathrm{d}V \;. \tag{3.26}$$

Recall the Poisson equation $\Delta\Psi = -4\pi\ell_{\mathrm{B}}\rho/e$, here written in terms of the scaled potential $\Psi$ and Bjerrum length $\ell_{\mathrm{B}}$, and note the volume charge density $\rho = e(n_+ - n_-)$ in the electrolyte. Thus, the variation of Poisson's equation is $\Delta\delta\Psi = -4\pi\ell_{\mathrm{B}}(\delta n_+ - \delta n_-)$. With this and using Gauss' law, Eq. (3.26) reads

$$\frac{\delta F}{k_{\mathrm{B}}T} = -\oint \frac{\Psi}{4\pi\ell_{\mathrm{B}}}\delta\frac{\partial\Psi}{\partial\vec{n}}\,\mathrm{d}A + \int\left[\delta n_+\left(\ln\frac{n_+}{n_0} + \Psi\right) + \delta n_-\left(\ln\frac{n_-}{n_0} - \Psi\right)\right]\mathrm{d}V\ , \quad (3.27)$$

where the integration in the first integral runs over all involved macroion surfaces and $\vec{n}$ denotes the surface normal (pointing into the electrolyte). Poisson's equation applied to the surfaces of the involved macroions yields the boundary condition

$$\frac{\partial\Psi}{\partial\vec{n}} = -4\pi\ell_{\mathrm{B}}\sigma/e\ , \quad (3.28)$$

where $\sigma$ is the local surface charge density. We point out that Eq. (3.28) assumes the macroions to have a dielectric constant much smaller than that of water. For biologically relevant macroions such as membranes, DNA, or proteins this assumption is generally fulfilled. We thus find $\Psi\delta\sigma/e$ for the integrand of the first integral in Eq. (3.27). In fact, if $\sigma$ is fixed everywhere on the macroion surfaces, that integral vanishes. Vanishing of the first variation in Eq. (3.27) then implies the Boltzmann distributions

$$n_\pm = n_o\,\mathrm{e}^{\mp\Psi}\ . \quad (3.29)$$

Combining the Boltzmann distributions with Poisson's equations yields the nonlinear Poisson-Boltzmann equation

$$\Delta\Psi = \kappa^2\sinh\Psi\ , \quad (3.30)$$

where we have defined the inverse Debye screening length $\kappa = 1/\ell_{\mathrm{D}} = 1/\sqrt{8\pi n_0 \ell_{\mathrm{B}}}$. Indeed the Debye screening length $\ell_{\mathrm{D}} = 1/\kappa$ appears as the characteristic length in the solutions of the linearized Poisson-Boltzmann equation $\Delta\Psi = \kappa^2\Psi$. For example, in the one-dimensional case $\Psi''(x) = \kappa\Psi(x)$ with $\Psi(0) = \Psi_0$ and $\Psi(x \to \infty)$ we find $\Psi(x) = \Psi_0 e^{-x\kappa}$.

In the model we develop in Chapter 9 we treat the lipid layer as a flat surface and utilize the corresponding free energy. Here, we derive the free energy for a single charged surface. The corresponding calculation forms the basis for the more complex situation (involving mobile macroion charges and dissociation equilibria) in Chapter 9. The one-dimensional Poisson-Boltzmann equation $\Psi''(x) = \kappa^2 \sinh\Psi(x)$ adopts the boundary conditions $\Psi'(0) = -4\pi\ell_{\mathrm{B}}\sigma/e$ and $\Psi(\infty) = 0$ for a single flat surface with surface charge density $\sigma$. A first integration of the Poisson-Boltzmann equation yields $\Psi'(x) = -2\kappa \sinh[\Psi(x)/2]$. At $x = 0$ this can be combined with the corresponding boundary condition, resulting in the relation

$$\Psi_0 = 2\,\mathrm{asinh}(2\pi\ell_{\mathrm{B}}\ell_{\mathrm{D}}\sigma/e) \tag{3.31}$$

between the surface potential $\Psi_0 = \Psi(x = 0)$ and surface charge density $\sigma$. Note that a second integration of the Poisson-Boltzmann equation yields an explicit expression, expressed in terms of the surface potential $\Psi_0$,

$$\Psi(x) = -2\ln\frac{\mathrm{e}^{\kappa x} - \tanh\frac{\Psi_o}{4}}{\mathrm{e}^{\kappa x} + \tanh\frac{\Psi_o}{4}}\,. \tag{3.32}$$

In order to calculate the free energy $F$ we note that if the ion concentrations $n_+$ and $n_-$ fulfill the Boltzmann distributions in Eq. (3.29), the variation of the free energy in

Eq. (3.27) reads

$$\frac{\delta F}{k_{\mathrm{B}}T} = \int \Psi \, \frac{\delta\sigma}{e} \, \mathrm{d}A \, . \tag{3.33}$$

Note that the free energy in Eq. (3.25) is defined such that $F = 0$ for $\Psi \equiv 0$ and thus $n_{\pm} = n_0$. Hence, integrating Eq. (3.33) yields an expression for the free energy

$$\frac{F}{k_{\mathrm{B}}T} = \int \mathrm{d}A \int_0^{\sigma} \Psi_0(\bar{\sigma}) \, \frac{\mathrm{d}\bar{\sigma}}{e} \, , \tag{3.34}$$

which only requires to know the relation $\Psi_0 = \Psi_0(\sigma)$ at the macroion surface. The free energy in Eq. (3.34) can be interpreted as a charging process, starting with $\bar{\sigma} = 0$ (implying $F = 0$) and then increasing the surface charge density $\bar{\sigma}$ to the final value $\sigma$. For our example of a single charged surface we have already determined the relation $\Psi_0 = \Psi_0(\sigma)$; see Eq. (3.31). Inserting it into Eq. (3.34) yields the charging free energy of a single planar surface

$$\frac{F}{Ak_{\mathrm{B}}T} = \frac{1}{\pi\ell_{\mathrm{B}}\ell_{\mathrm{D}}} \int_0^{2\pi\ell_{\mathrm{B}}\ell_{\mathrm{D}}\sigma/e} \mathrm{d}p \, \operatorname{asinh} p \, . \tag{3.35}$$

In the limit of the linearized Poisson-Boltzmann model (the Debye-Hückel model) Eq. (3.35) reads $F/(Ak_{\mathrm{B}}T) = 2\pi\ell_{\mathrm{B}}\ell_{\mathrm{D}}\sigma^2/e$. At physiological conditions $n_0 = 0.1\,\mathrm{M} = 0.06/\mathrm{nm}^3$; this implies a Debye screening length of about $\ell_{\mathrm{D}} = 1$ nm. Then, the linearized free energy is a reasonable approximation of the nonlinear expression in Eq. (3.35) for $|\sigma| \leq 0.1\, e/\mathrm{nm}^2$. Typical charge densities in lipid membranes can easily exceed this value. For example, a fully charged anionic membrane with lipids of cross-sectional value $a = 0.65\,\mathrm{nm}^2$ has a charge density $\sigma = -e/a = -1.5\, e/\mathrm{nm}^2$. Other biomacroions such as DNA and proteins can have similarly hight local surface charge densities. Clearly then, the nonlinear Poisson-Boltzmann equation should be used

when modeling typical charged biomacromolecules. If the system contains additional degrees of freedom their corresponding free energy contribution is added to $F$ and the resulting total free energy is again minimized with respect to all unconstrained degrees of freedom. Chapter 9 details that approach for three additional degrees of freedom: conformationally flexible lipid headgroups, variable lipid composition, and charge regulation of the anionic lipid phosphatidic acid.

### 3.3. Kinetics of solute transfer between carrier systems

Interactions between biomembranes and macromolecules are of great importance in pharmaceutical applications. Liposomal carrier systems are routinely used to deliver hydrophobic substances to the target site (and ideally only to the target site) [13, 187, 64]. Optimizing drug administration requires understanding of the kinetics of such processes. The transfer of drugs from drug-donating liposomes into accepting target sites can be formally viewed [117] as a chemical reaction of donor drugs D to acceptor drugs A, $D \rightleftharpoons A$. The experimental studies described in Chapter 7 employ liposomes not only as donors but also as acceptors.

The kinetics of chemical reactions are commonly studied by expressing the reaction rates as function of reactant concentrations. The rate of change of concentration $\mathrm{d}[D]/\,\mathrm{d}t$ can depend in various ways on the concentration $[D]$ of substance D. The exponents with which the concentrations enter the rate equation describing this dependence is the order of reaction and is used to classify reactions [11].

In first-order reactions the reaction rate shows a linear relationship to the substance concentration. For example, during the decomposition $2\mathrm{N_2O_5} \rightarrow 2\mathrm{NO_2} + \mathrm{O_2}$ of dinitrogen pentoxide into nitrogen dioxide and oxygen, its concentration change is proportional to the concentration, $\mathrm{d}[\mathrm{N_2O_5}]/\,\mathrm{d}t = -k[\mathrm{N_2O_5}]$. Here, $k$ is a time-independent rate constant. This differential equation determines the time dependence of the

reactant concentration as an exponentially decaying function $[N_2O_5] = [N_2O_5]_0\, e^{-kt}$, with $[N_2O_5]_0$ expressing the initial concentration. Radioactive decay can also be viewed as a first-order reaction.

A reaction that requires two freely moving particles to collide is often of second order. The dimerization of iodine $2I \rightarrow I_2$ takes place with highest probability when two atoms are in close vicinity to each other. The rate of change is thus proportional to the square of the iodine concentration, $d[I]/\,dt = -k[I]^2$. The concentration in this reaction, $[I] = [I]_0/(1 + kt)$, is proportional to $1/t$ in the long time limit. This is much slower that the exponential behavior for first order reactions.

We have observed in experiments that transfer of hydrophobic drugs between donor and acceptor liposomes often exhibit first-order kinetics with a simple exponential behavior, in some cases they show sigmoidal time dependence. Considering the fact that poorly water soluble drugs are unlikely to diffuse through the aqueous solution, the transfer mechanism likely involves collisions between donor and acceptor liposomes. It is therefore not obvious why the observed kinetics is exponential. The model we present in Chapters 7 and 8 accounts for collision and diffusion, and starts with a detailed distribution of drug molecules among the individual liposomes.

Let us focus on the transfer by the collision mechanism only, exclude any attractive or repulsive interactions among the drug molecules inside the liposomes and develop a kinetic model. We consider an aqueous solution (of fixed volume $V$) that contains a number of $N$ liposomes. Each liposome can hold maximally $m$ drug molecules. Since each of the $N$ vesicles can carry any number $i < m$ of drug molecules, there will be at any time a certain number of vesicles $a_i = a(i)$ that hold $i$ drugs, $a(i)$ can be interpreted as a discrete distribution function. We assume only one drug molecule at a time could be exchanged at a collision of two vesicles, and for now consider only exchanges from a higher loaded to lower loaded vesicle. The probability for this exchange is proportional to the difference in drug load of two colliding vesicles.

The probability for a collision between two vesicles with loads $i_1$ and $i_2$ is proportional to the product of the two vesicle concentrations, hence proportional to $a(i_1)a(i_2)/V$. The rate of change in the number of vesicles with drug $i$ can proceed in four distinct ways:

- Decrease
    1. a vesicle of load $i$ collides with a vesicle of load $j < i - 1$ and donates a drug molecule, with probability proportional to $(i - j)$
    2. a vesicle of load $i$ collides with a vesicle of load $j > i + 1$ and accepts a drug molecule, with probability proportional to $(j - i)$
- Increase
    1. a vesicle of load $i - 1$ collides with a vesicle of load $j > i$ and accepts a drug molecule, with probability proportional to $(j - i + 1)$
    2. a vesicle of load $i + 1$ collides with a vesicle of load $j < i$ and donates a drug molecule, with probability proportional to $(i - j - 1)$

The amount of liposomes holding $i$ drugs does not change in a collision with a liposome that has either one more or one less drug, since either of the resulting liposomes will carry $i$ drugs in the end. In a collision between a liposome with $i - 1$ drugs and one with $i + 1$ drugs both resulting partners carry $i$ drugs, so it seems intuitive to count these twice, and in fact we do as we consider for this collision an increase of types 1 *and* 2.

We assign a rate constant $K_c$ of drug transfer through collisions between two chemically equivalent liposomes and can find the rate of change of the amount of liposomes holding $i$ drugs, $\mathrm{d}a_i/\,\mathrm{d}t$, by performing a sum over all collision partners,

distinguishing these four scenarios.

$$\frac{V}{K_c}\frac{\mathrm{d}a_i}{\mathrm{d}t} = -\sum_{j=0}^{i-2} a_i a_j (i-j) - \sum_{j=i+2}^{m} a_i a_j (i-j) \tag{3.36}$$

$$+\sum_{j=0}^{i-1} a_{i+1} a_j (i+1-j) \; + \sum_{j=i+1}^{m} a_{i-1} a_j (j-(i-1)) \; . \tag{3.37}$$

The elements needed (or in excess) to synchronize the limits of these sums cancel each other out. If we formally allow non-physical elements, namely liposomes holding less than zero or more than $m$ drugs, we can rewrite these sums to

$$\frac{V}{K_c}\frac{\mathrm{d}a_i}{\mathrm{d}t} = \sum_{j=0}^{i} a_j [a_{i+1}(j-i+1) - a_i(i-j)] + \sum_{j=i}^{m} a_j [a_{i-1}(i+1-j) - a_i(i-j)] \; . \tag{3.38}$$

The distributions $a_i$ are not an experimentally accessible quantity. As described in Chapter 7, acceptor vesicles are chemically labeled to be separable from donors (for instance by charge) and then the total amount of drug molecules in the separated population is measured. To match the results and to be able to extend this model, we introduce a second distribution, Analogous to the amount of acceptor liposomes holding $i$ drugs, $a_i$, the amount of donor liposomes holding $i$ drugs is denoted by $d_i$. The sums in the above equations can easily be extended to consider the "$j$" collision partners to be either donors or acceptors by replacing $a_j \to a_j + d_j$. We assume the rate constants for acceptor-acceptor, donor-donor, and donor-acceptor collisions are equal. To allow for chemically distinct liposome donor and acceptor species, we adjust the transfer probability from $|i-j|$ to $|i-j+k|$, where the integer $k$ generically models a difference in drug affinity in acceptors or donors. A donor holding $i+k$ drugs is in equilibrium with an acceptor holding $i$ drugs. Mathematically, $k$ is merely an index shift which we account for by adjusting the sum limits. This leads to two

equations

$$\frac{V}{K_c}\frac{\mathrm{d}a_i}{\mathrm{d}t} = \sum_{j=0}^{i} a_j[a_{i+1}(j-i+1) - a_i(i-j)] + \sum_{j=i}^{m} a_j[a_{i-1}(i+1-j) - a_i(i-j)]$$
$$\sum_{j=-k}^{i} d_{j+k}[a_{i+1}(j-i+1) - a_i(i-j)] + \sum_{j=i}^{m-k} d_j[a_{i-1}(i+1-j) - a_i(i-j)] \ , \quad (3.39)$$

$$\frac{V}{K_c}\frac{\mathrm{d}d_i}{\mathrm{d}t} = \sum_{j=0}^{i} d_j[d_{i+1}(j-i+1) - d_i(i-j)] + \sum_{j=i}^{m} d_j[d_{i-1}(i+1-j) - d_i(i-j)]$$
$$\sum_{j=k}^{i} a_{j-k}[d_{i+1}(j-i+1) - d_i(i-j)] + \sum_{j=i}^{m+k} a_j[d_{i-1}(i+1-j) - d_i(i-j)] \ . \quad (3.40)$$

We note the experimentally observable quantities are the total number of donor liposomes $N_d = \sum_{j=0}^{m} d_j$ and the total number of acceptor liposomes $N_a = \sum_{j=0}^{m} a_j$ (both of which are conserved) and the total numbers $M_d = \sum_{j=0}^{m} j d_j$ and $M_a = \sum_{j=0}^{m} j a_j$ of drugs residing in donor and acceptor liposomes, respectively. The latter two are not conserved, but the total amount of drugs in the system $M = M_d + M_a$ is. By carrying out the summations we find the differential equations we present and solve in Chapter 8

$$\dot{M}_d = \frac{K}{N}\left(M_a\, N_d - M_d\, N_a + k N_a N_d\right) \ , \quad (3.41)$$
$$\dot{M}_a = \frac{K}{N}\left(M_d\, N_a - M_a\, N_d - k N_a N_d\right) \ . \quad (3.42)$$

It is worth noting that introducing different rate constants for acceptor-acceptor or donor-donor transfer does not affect these equations, thus the kinetics of the transfer are independent of these. We further extend this model in Chapter 8 by incorporating diffusion transfer and attractive interactions between the drug molecules when residing in a liposome.

# 4. MODELING THE PHASE BEHAVIOR OF PROTEIN-DECORATED TERNARY LIPID LAYERS

## 4.1. Introduction

The existence of inhomogeneities in lipid membranes is known for more than five decades but a truly remarkable increase in research efforts has occurred since the formulation of the membrane raft hypothesis [251]. Macroscopic phase separation into two lipid phases (liquid-ordered $L_o$ and liquid-disordered $L_d$) is observed for appropriate ternary lipid mixtures [280]. The saturated hydrocarbon chains of lipids such as dipalmitoylphosphatidylcholine (DPPC) can, when in its extended all-trans conformation, interact favorably with the rigid backbone of cholesterol. They are commonly referred to as reactive or saturated lipids. On the other hand, unsaturated or unreactive lipids, i.e. diphytanoylphosphatidylcholine (DiPhyPC), are not able to interact in such a way with cholesterol due to a kink in the chain introduced by one or more double-bonds between the carbon atoms. As a consequence there exist two energetically favorable states, one for highly ordered saturated lipids in contact with cholesterol, and the other for a disordered mixture of unsaturated and saturated lipids. This results in the formation of macroscopically observable domains, liquid-ordered phases enriched with cholesterol and reactive lipids, and liquid-disordered with a higher than average concentration of unreactive lipids. While probing rafts in *in vivo* membranes is difficult, domains are observed in model membranes [280].

Ternary mixtures of reactive lipids, unreactive lipids, and cholesterol can exhibit a closed-loop phase coexistence region with an upper and lower critical point [281]. That means only a ternary system, not a binary mixture can be unstable. A remarkably simple theoretical model for the interactions of cholesterol in lipid membranes has

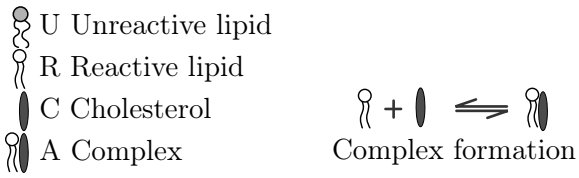


Figure 4.1. Formation of complexes (A) between cholesterol (C) and reactive lipid(R). Unreactive lipids (U) do not form complexes. We assume the complex formation to be complete, so that the membrane is a mixture of unreactive lipids, complexes, and either excess cholesterol or excess reactive lipids.

been proposed by McConnell and co-workers [179, 217]; it suggests the formation of a condensed complex between cholesterol and a reactive lipid. This complex is treated as an individual species in a lattice gas model.

If we assume that the complex formation is complete, either all cholesterol or all saturated lipids will be bound in complexes. The ternary mixture therefore consists of unsaturated lipids, complexes and the excess of either cholesterol or saturated lipids. The free energy $f$ per lipid cross-sectional area in the limit of complete reaction, written in terms of the compositions of unreactive lipid ($\varphi_U$), reactive lipid ($\varphi_R$), cholesterol ($\varphi_C$), and complex ($\varphi_A$), entails the mixing free energies of the three components according to Eq. (3.2) as well as a non-ideal energy contribution as derived in Eq. (3.3).

$$\frac{f}{k_{\mathrm{B}}T} = \varphi_U \ln \varphi_U + |\varphi_R - \varphi_C| \ln |\varphi_R - \varphi_C| + \varphi_A \ln \varphi_A + \chi \varphi_U \varphi_A \tag{4.1}$$

$$\text{with a } \varphi_A = \begin{cases} \varphi_C & \text{for} \quad \varphi_C < \varphi_R \\ \varphi_R & \text{for} \quad \varphi_R < \varphi_C \, . \end{cases} \tag{4.2}$$

The constant $\chi$ accounts for nonideal interactions between the complexes (A) and the unreactive lipid (U). This only contributes in the presence of all three species and is effectively a three-body interaction, which is necessary to model a closed-loop phase behavior.

### 4.2. Phase behavior and critical points

The Gibbs phase rule (Eq. (3.15)) predicts the coexistence of three phases. We find the binodal region by minimizing the corresponding coexistence equation

$$\begin{aligned} f_3(\varphi_{R1}, \varphi_{C1}, \varphi_{R2}, \varphi_{C2}, \theta_1, \theta_2) = \theta_1 f(\varphi_{R1}\varphi_{C1}, \varphi_{U1}) \\ + \theta_2 f(\varphi_{R2}\varphi_{C2}, \varphi_{U2}) \\ + \theta_3 f(\varphi_{R1}\varphi_{C3}, \varphi_{U3}) \end{aligned} \tag{4.3}$$

as a function of four variables with the constraints

$$1 = \theta_1 + \theta_2 + \theta_3 \,, \tag{4.4}$$

$$1 = \varphi_{R1} + \varphi_{C1} + \varphi_{U1} \,, \tag{4.5}$$

$$1 = \varphi_{R2} + \varphi_{C2} + \varphi_{U2} \,, \tag{4.6}$$

$$1 = \varphi_{R1} + \varphi_{C3} + \varphi_{U3} \,, \tag{4.7}$$

$$\varphi_U = \theta_1\varphi_{U1} + \theta_2\varphi_{U2} + \theta_3\varphi_{U3} \,, \tag{4.8}$$

$$\varphi_R = \theta_1\varphi_{R1} + \theta_2\varphi_{R2} + \theta_3\varphi_{R3} \,, \tag{4.9}$$

$$\varphi_C = \theta_1\varphi_{C1} + \theta_2\varphi_{C2} + \theta_3\varphi_{C3} \,, \tag{4.10}$$

and ensure that all variables are between 0 and 1. These constraints are actually over-determined and one equation is redundant. The numerically calculated phase diagram as shown in Fig. 4.2 is obtained by performing a constrained global minimization of Eq. (4.3) for $\chi = 4$ for many points of average compositions $\varphi_R$ and $\varphi_C$. The phase diagram exhibits no three-phase coexistence and the tie-lines connecting the two existing phases are almost parallel. We see a closed loop phase behavior. This unstable region grows with increasing $\chi$, and vanishes if $\chi$ is smaller that a certain critical $\chi_{crit}$. We will determine this critical value analytically.

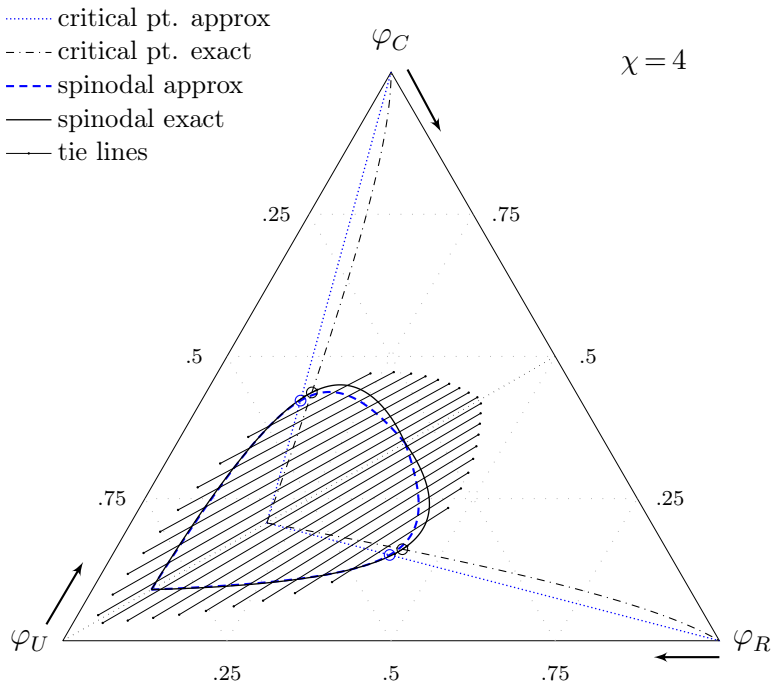


Figure 4.2. Phase diagram for ternary mixture of cholesterol (C), reactive (R) and unreactive(U) lipids, according to Eq. (4.1) with $\chi = 4$. The model is based on complete complex formation between reactive lipid and cholesterol as introduced by McConnell. The blue dotted straight lines represent the approximate location of the upper and lower critical points, comparable to the exact values (black dash dotted). Phase separation occurs above $\chi_{crit} = 2.91$.

The symmetry of $f$ along the line $\varphi_R = \varphi_C$ suggests we can limit our analysis to the case $\varphi_R < \varphi_C$, the other case follows from simple variable substitution. Together with the constraint

$$\varphi_U + \varphi_R + \varphi_C = 1 \tag{4.11}$$

we can write $f$ as a function of two variables

$$\begin{aligned}\frac{f(\varphi_R, \varphi_C)}{k_\mathrm{B}T} =& (1 - \varphi_R - \varphi_C)\ln(1 - \varphi_R - \varphi_C) + (\varphi_C - \varphi_R)\ln(\varphi_C - \varphi_R) \\ &+ \varphi_C \ln \varphi_C + \chi\varphi_R(1 - \varphi_C - \varphi_R)\end{aligned} \tag{4.12}$$

with domain limitations $0 \leq \varphi_R \leq 1/2$ and $\varphi_R \leq \varphi_C \leq 1 - \varphi_R$. This means we are restricted to the upper half of the phase diagram. The exact spinodal line follows from solving the spinodal condition, Eq. (3.14), to

$$\varphi_C^{sp\pm}(\varphi_R) = \frac{(\chi - 4)}{2\chi} \pm \frac{\sqrt{\varphi_R(2\varphi_R - 1)(\chi^2\varphi_R(2r - 1) - 8\chi\varphi_R + 4)}}{2\chi\varphi_R} \,. \tag{4.13}$$

Only parts of these solutions are above $\varphi_C \geq \varphi_R$ and the upper critical point lies on the $\varphi_C^{sp-}$ solution. To find the minimal $\chi_{crit}$ we note that the two intersections of the spinodal line and $\varphi_C = \varphi_R$ converge. We can solve $\varphi_C^{sp-} = \varphi_R$ to

$$\chi = \frac{2\varphi_R + 1}{2\varphi_R - 8\varphi_R^2} \tag{4.14}$$

and minimize this expression with respect to $\varphi_R$. This leads to the composition $\varphi_{R,crit}$ at which phase separation first occurs. $\varphi_{C,crit}$ will have the same value. Eq. (4.13) now defines to the $\chi_{crit}$ and we see that phase separation starts to occur at the minimal critical values

$$\chi_{crit} = \frac{3}{2} + \sqrt{2} = 2.91 \,, \tag{4.15}$$

$$\varphi_{R,crit} = \frac{\sqrt{2} - 1}{2} = 0.207 \,, \tag{4.16}$$

$$\varphi_{C,crit} = \varphi_{R,crit} \,. \tag{4.17}$$

This point is apparent in Fig. 4.2 at the intersections of the lines describing the upper and lower critical points, which we will derive next.

We find the upper and lower critical points for any given $\chi$ by noting that a tie-line at this point is tangential to the spinodal line and the inflection points of $f$ along the tie-line converge here. This leads to two more conditions which can be solved numerically. The second derivative of $f$ along the tangential to the spinodal

has to be zero *and* minimal. Denoting with prime derivatives with respect to $\varphi_R$ this reads

$$\frac{\partial^2 f(\varphi_R+\delta,\varphi_C^{sp}+\delta\varphi_C^{sp'})}{\partial\delta^2}=0\ , \tag{4.18}$$

$$\frac{\partial^3 f(\varphi_R+\delta,\varphi_C^{sp}+\delta\varphi_C^{sp'})}{\partial\delta^3}=0\ , \tag{4.19}$$

and while the derivatives can be found analytically, the roots of these equations leading to $\varphi_{R,crit}$ can only be found numerically. The position of this exact upper critical point is also shown in Fig. 4.2.

Noting that all tie-lines are nearly parallel, we can approximate them to be perfectly parallel to $\varphi_C = \varphi_R$. We can restrict the system to only be capable of changing compositions along a line described by $\varphi_C = \varphi_R + o + 1$, where $o$ is a negative fixed offset. This reduces the free energy to a function of only one variable.

$$\begin{aligned}\frac{f(\varphi_R)}{k_\mathrm{B}T} =&(1+o)\ln(1+o)+\varphi_R\ln\varphi_R+(-2\varphi_R-o)\ln(-2\varphi_R-o)\\ &-\chi\varphi_R(2\varphi_R+o)\ .\end{aligned} \tag{4.20}$$

This function is plotted for $\chi = 5.25$ and $o = -.74$ in Fig. 3.1. The spinodal condition Eq. (3.12) and its solution are

$$0=\frac{1}{\varphi_R}-\frac{4}{2\varphi_R+o}-4\chi\ , \tag{4.21}$$

$$\varphi_R^{sp\pm}(\varphi_R)=\frac{-(2\chi o+1)\pm\sqrt{(3+2\chi o)^2-8}}{8\chi}\ . \tag{4.22}$$

These two spinodal points have to degenerate into one at the critical point, which determines $o$ at this point. Inserting this expression back into the spinodal equation

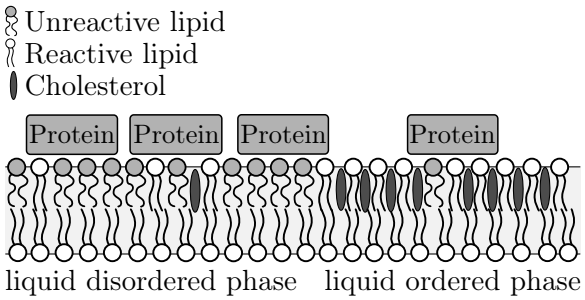


Figure 4.3. Proteins adsorb on a ternary membrane, interacting differently with unreactive lipids, complexes, and uncomplexed lipids. This leads to different protein decorations in phases with different composition.

we determine the upper critical point to

$$\varphi_R = \frac{1}{4\chi}\,(1+\sqrt{2}) \qquad = \frac{0.603}{\chi}\,, \tag{4.23}$$

$$\varphi_C = 1 - \frac{1}{4\chi}\,(5+3\sqrt{2}) = 1 - \frac{2.31}{\chi}\,. \tag{4.24}$$

Fig. 4.2 shows this approximation in comparison to the numerically calculated exact behavior of the critical points as well as the approximated spinodal line.

### 4.3. Protein adsorption

The influence of proteins adsorbing on such a ternary membrane is illustrated in Fig. 4.3. Proteins interact differently with the individual lipid species and their binding affinity will depend on the local compositions, changing the energetics of the different phases. This can influence the phase behavior. The effect of proteins can be described in an analytical way by adding a term that accounts for the free energy of adsorbed proteins onto the membrane to Eq. (4.1).

We accomplish this by modeling the energy contribution on the mean field level to $f$ that accounts for the presence of membrane-adsorbed proteins

$$\begin{aligned}\frac{f_p}{k_\mathrm{B}T} = \frac{1}{\sigma}\left[\vartheta\ln\vartheta + (1-\vartheta)\ln(1-\vartheta) + \vartheta\ln c\right] \\ - \vartheta(\alpha_U\varphi_U + 2\alpha_A\varphi_A + \alpha_{RC}|\varphi_R - \varphi_C|)\ .\end{aligned} \tag{4.25}$$

The first line describes the ideal gas entropic contribution of the protein layer to the system, where $\vartheta$ is the area fraction of the membrane covered by proteins. A scaled bulk concentration $c$ of proteins in the surrounding solution relates to the chemical potential of the proteins. $\sigma$ is the protein-to-lipid cross-sectional area ratio, scaling the protein contribution on a per-lipid site level. The interaction of adsorbed proteins with the unreactive lipids ($\varphi_U$), lipid-cholesterol complexes ($\varphi_A$), and uncomplexed lipids ($|\varphi_R - \varphi_C|$) is characterized by the parameters $\alpha_U$, $\alpha_A$ and $\alpha_{RC}$, respectively. Complexes cover twice the area of lipids, which is accounted for by the factor 2.

The optimal protein coverage can be found by minimizing the free energy per lipid area $f_T = f + f_P$ with respect to $\vartheta$ as

$$\vartheta_{eq} = \frac{1}{1 + c\ \mathrm{e}^{-\sigma[\alpha_{RC}|\varphi_R-\varphi_C| + \alpha_U\varphi_U+2\alpha_A\varphi_A]}}\ . \tag{4.26}$$

For analysis of stability criteria we can fix $\vartheta$ to this value. Numerically minimizing the coexistence equation however becomes more involved because the local protein coverage at the individual phases can deviate from the equilibrium value. This introduces three new variables (two of which are independent), the coverage of the three individual phases and an additional constraint in form of the lever rule

$$\vartheta_{eq} = \theta_1\vartheta_1 + \theta_2\vartheta_2 + \theta_3\vartheta_3\ . \tag{4.27}$$

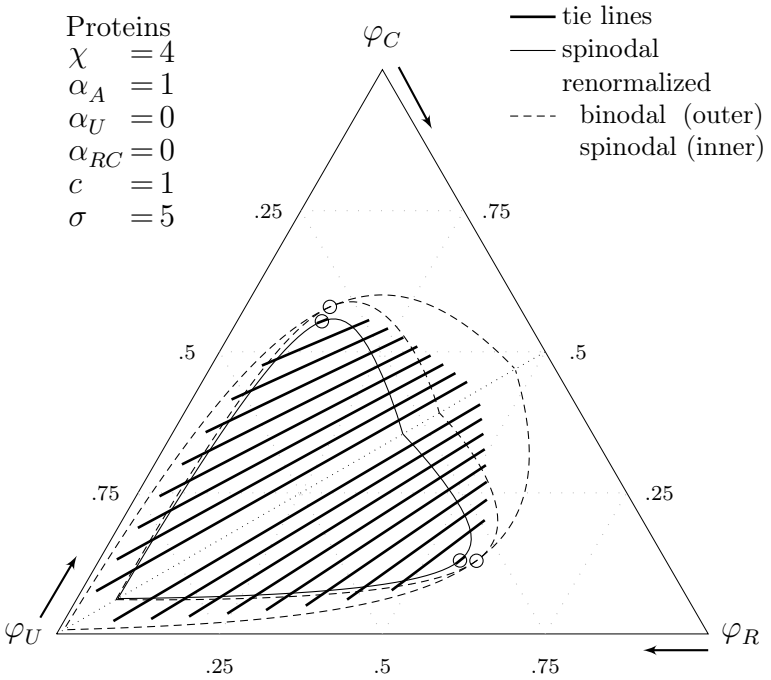


Figure 4.4. Phase diagram for a protein-decorated ternary membrane. The exact spinodal (solid curve) is shown as well as the exact spinodal of a renormalized membrane (with $\chi_{eff} = 5.25$, inner dashed curve). The exact binodal line of the renormalized system is represented by the outer dashed curve and the upper and lower critical points of both actual and renormalized system are circled.

The free energy of a three-phase system now has to be minimized with respect to eight variables.

$$\begin{aligned} f_{T3}(\varphi_{R1}, \varphi_{C1}, \vartheta_1, \varphi_{R2}, \varphi_{C2}, \vartheta_2, \theta_1, \theta_2) = f_3(\varphi_{R1}, \varphi_{C1}, \varphi_{R2}, \varphi_{C2}, \theta_1, \theta_2) \\ + \theta_1 f_p(\varphi_{R1}, \varphi_{C1}, \vartheta_1) \\ + \theta_2 f_p(\varphi_{R2}, \varphi_{C2}, \vartheta_2) \\ + \theta_3 f_p(\varphi_{R1}, \varphi_{C3}, \vartheta_3) \end{aligned} \tag{4.28}$$

The phase diagram showing the obtained tie-lines for $\chi = 4$ is shown in Fig. 4.4. Clearly, protein adsorption has a destabilizing effect on the membrane. Determination of the critical points follows the same procedure as above.

Assuming again parallel tie-lines in a manner as described above, we obtain the spinodal line analytically, using $\vartheta = \vartheta_{eq}$. For weak protein-lipid interaction, that is small $\alpha$'s, we can express these parameters as

$$\alpha_U \to \delta\alpha_U \ , \tag{4.29}$$

$$\alpha_A \to \delta\alpha_A \ , \tag{4.30}$$

$$\alpha_{RC} \to \delta\alpha_{RC} \ , \tag{4.31}$$

and approximate $f_T$ by a Taylor expansion up to second order around $\delta = 0$. The spinodal condition reveals

$$0 = \frac{1}{\varphi_R} - \frac{4}{2\varphi_R + o} - 4\chi + 4\sigma \frac{c}{(1+c)^2}(\alpha_A - \alpha_U)^2 \ , \tag{4.32}$$

which we can compare with the spinodal condition for the bare membrane, Eq. (4.21). We see that that proteins effectively rescale the interaction parameter

$$\chi_{eff} = \chi + \sigma \, \frac{c}{(1+c)^2} \, (\alpha_A - \alpha_U)^2 \ . \tag{4.33}$$

This effective increase in $\chi$ corresponds to a destabilization of the membrane, as seen in Fig. 4.4.

## 4.4. Conclusion

The model from McConnell and co-workers [179, 217] predicts the observed closed-loop phase behavior of ternary lipid-cholesterol mixtures. We note that this model is minimal; it employs a single compositional order parameter. The critical value for the interaction strength $\chi$ can be specified analytically. Below $\chi_{crit}$ domain formation does not occur. We have predicted an approximative analytical expression

for $\chi_{crit}$ which compares well with the numerically derived values. Fig. 4.2 shows a comparison between the exact and approximate locations. The closed-loop behavior of the coexistence region as well as the near-parallel orientation of the tie-lines in the phase diagram agree with experimental findings [281]. Only two-phase coexistence is predicted by the theoretical model, in concurrence with experimental results. This is the basis for approximating a ternary membrane as a pseudo-binary mixture. The major result of this chapter is the demonstration that proteins merely need to interact differently with the unsaturated lipid and the saturated lipid-cholesterol complexes in order to substantially lower the stability of the ternary membrane. In fact, proteins simply shift the spinodal surface $\chi(\varphi_R, \varphi_C)$ to larger values.

Experimentally gathered evidence of the phase behavior suggests more complexity. Most notable is the existence of a gel phase in the lower part of the phase diagram [84]. Our model is not designed to predict non-fluid phases. After this work was developed and presented, Michael Schick and his group presented an especially noteworthy approach utilizing chain order and composition as order parameters [78]. Closed loop behavior as well as the transition to the gel state are predicted.

# 5. PAPER 1 : INFLUENCE OF MONOLAYER-MONOLAYER COUPLING ON THE PHASE BEHAVIOR OF A FLUID LIPID BILAYER[1]

ABSTRACT: We suggest a minimal model for the coupling of the lateral phase behavior in an asymmetric lipid membrane across its two monolayers. Our model employs one single order parameter for each monolayer leaflet, namely its composition. Regular solution theory on the mean-field level is used to describe the free energy in each individual leaflet. Coupling between monolayers entails an energy penalty for any local compositional differences across the membrane. We calculate and analyze the phase behavior of this model. It predicts a range of possible scenarios. A monolayer with a propensity for phase separation is able to induce phase separation in the apposed monolayer. Conversely, a monolayer without this propensity is able to prevent phase separation in the apposed monolayer. If there is phase separation in the membrane, it may lead to either complete or partial registration of the monolayer domains across the membrane. The latter case which corresponds to a three-phase coexistence is only found below a critical coupling strength. We calculate that critical coupling strength. Above the critical coupling strength, the membrane adopts a uniform compositional difference between its two monolayers everywhere in the membrane, implying phase coexistence between only two phases and thus perfect spatial registration of all domains on the apposed membrane leafs. We use the lattice Boltzmann simulation method to also study the morphologies that form during phase separation within the three-phase

[1] Sylvio May (S.M.) provided the initial plan for the research presented in this paper. The free energy model development and Landau expansion was done jointly by S.M. and Alexander Wagner (A.W.). Theoretical analysis of the model and determination of critical points were done jointly by S.M. and Stephan Loew (S.L.). Phase diagrams for three-phase coexistence were developed by S.L. Lattice Boltzmann simulation and morphologies were executed by A.W. This paper is published in [286].

coexistence region. Generally, domains in one monolayer diffuse but remain fully enclosed within domains in the other monolayer.

## 5.1. Introduction

One of the most challenging problems in membrane bio-physics is to understand the influence of lipids on the lateral organization of biomembranes. Numerous experimental results point at the existence of lateral domains–membrane rafts–and their various functional roles [252, 57]. Yet, size, stability, and dynamic behavior of domains in biomembranes remain poorly characterized. This is in contrast to model membranes, consisting of only a few lipid species at well-characterized conditions, for which a wealth of detailed information on structural and phase behavior exists. Especially the ability of cholesterol to induce phase coexistence between two fluidlike lateral phases, the more condensed liquid-ordered ($l_o$) and the less condensed liquid-disordered ($l_d$) phase, has been well-characterized experimentally and through various subsequent modeling attempts [109, 179, 130].

An interesting problem concerns the coupling of coexisting liquid-like domains between the two leaflets of a lipid bilayer [50]. Current evidence suggests matching of like-phase domains across a symmetric bilayer [136, 14, 123, 280]. That is, domains are observed to be in perfect registration, implying that some degree of composition-sensitive structural coupling must exist between the two apposed monolayers. The strength of this coupling could possibly be of importance for biomembranes. This is because the plasma membrane generally has an asymmetric lipid distribution, with domain-forming lipids enriched in the extracellular monolayer but depleted from the cytoplasmic monolayer [290]. Indirect evidence (the colocalization of raft proteins with inner leaflet proteins [215] and the presence of inner leaflet proteins in detergent-resistant membranes [12]) could suggest the presence of domains in the cytoplasmic

monolayer [215]. The question arises whether domains in one monolayer can be imposed (imprinted) by the presence of domains in the other monolayer.

An experimental method to produce asymmetric membranes and to study their phase behavior is provided by combining the Langmuir-Blodgett/Schäfer method with fluorescence-based imaging. As the domains within the monolayer facing the solid support are immobile, they do not register with domains in the apposed monolayer [262, 44]. Yet, complete registration can be recovered by introducing a polymer cushion that sufficiently increases the substrate-membrane distance [79, 125]. The study by Garg et al.[79] clearly shows that domains in one monolayer can induce registered domains in the other monolayer, even if the latter monolayer has an insufficient tendency to phase-separate on its own. Kiessling et al. [125] also report cases where the domain-forming monolayer was unable to induce formation of registered domains in the apposed monolayer. In summary, present experimental evidence points to a composition dependence of a monolayer's ability to imprint its phase structure onto the apposed monolayer.

A number of recent theoretical studies have addressed consequences of a coupling between the two monolayers in a membrane [287, 144]. Two studies directly address the coupling of thermodynamic phase formation across the two membrane leaflets [96, 3]. Hansen et al. [96] have considered the coupling of two monolayers where each individual monolayer was modeled as having both a compositional and curvature degree of freedom. Based on Landau theory, the formation of a number of different phases, some of them flat and others with shape modulations, are predicted. In another study, Allender and Schick [3] also used Landau theory with two order parameters; again one was a compositional order parameter (an effective cholesterol concentration) but the other one described the thickness of a monolayer. The choice of this second-order parameter is common [233, 288] and is well-motivated by the different chain ordering in the $l_o$ and $l_d$ phases [209]. Monolayer-monolayer coupling

was assumed to emerge only from a coupling between the thickness order parameters in each leaflet. Allender and Schick have specifically analyzed a situation where, without coupling, the outer leaflet of a membrane is unstable, whereas the inner one is stable. The coupling between the two monolayers then leads to a transition (though a weaker one) in the inner monolayer as well.

In this work, we analyze a minimal model of the coupling between monolayers and its influences on the phase behavior of a lipid bilayer. To this end, we shall employ only one single-order parameter, the composition of a binary monolayer. (Note that by merging two lipid species into a single effective one, we may, in principle, apply our results to a ternary lipid mixture that contains cholesterol; similar to Allender and Schick [3].) Each of the two individual monolayers will be described by the familiar regular solution model on the mean-field level [228, 47]. Without coupling between the two monolayers, each leaflet can independently undergo a lateral phase transition. We may, somewhat arbitrarily, refer to the two phases as condensed and uncondensed. Monolayer-monolayer coupling acts on the difference between the local compositions across the membrane. To suggest a physical mechanism we consider Figure 5.1. It schematically displays two (initially symmetric) membranes that have undergone phase separation in both monolayers. Only in the lower membrane are the phases of the same type in registration. Despite being entropically unfavorable and creating a thickness mismatch (and corresponding line tension [141]) between the condensed and uncondensed regions, this is the experimentally observed scenario in a symmetric membrane [136, 14, 123, 280]. Various mechanisms such as van der Waals interactions or cholesterol flip-flop might contribute to the coupling [3]. However, we speculate the main contribution has entropic origin and results from the conformational confinement of the lipid chains in the uncondensed phase when being opposite to a condensed monolayer. This confinement would concern predominantly the terminal segments of the lipid chains in the uncondensed monolayer. Facing a more condensed (i.e.,

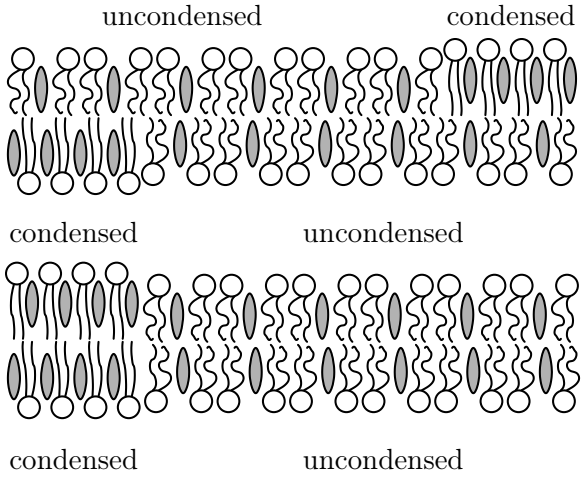


Figure 5.1. Schematic illustration of two mixed bilayer membranes. The two membranes have the same average composition in both monolayers. Each monolayer separates into two fluidlike phases, a condensed and an uncondensed one. A practical realization of this scenario could contain cholesterol and additional lipid species (in this case the phases would correspond to the $l_o$ and $l_d$ phases). In the upper membrane the condensed domains in one monolayer face the uncondensed ones in the apposed monolayer. We argue that this mismatch entails an energy penalty that is proportional to the square of the local compositional difference across the bilayer. The coupling between the two monolayers leads to complete registration of domains of the same kind, as illustrated for the lower membrane. Note that domain registration can be incomplete if the membrane is asymmetric; i.e., if there is a mismatch in composition between the two monolayers (this case is not shown but is part of our analysis).

more rigid) monolayer makes it more difficult for these segments to explore their conformational degrees of freedom by dynamically interpenetrating into the apposed monolayer. Note that the strength of this type of coupling would increase with the local compositional difference between the monolayers. This consideration motivates the simple expression for the coupling (see below in Eq. (5.2)) that we use in this work.

We shall provide a complete thermodynamic analysis of our model as a function of the coupling strength. The results will be presented in phase diagrams. In addition, we analyze our model in terms of a Landau expansion which connects the present with previous work [96]. The Landau expansion allows us to express the phase behavior in the limiting cases of small and large coupling analytically. Our model, despite being

simple, would explain a range of possible observations, including the induction or suppression of phase separation due to the presence of monolayer-monolayer coupling and the formation of three-phase regions; i.e., incomplete spatial registration of domains between the monolayers. We finally use the lattice Boltzmann method to simulate possible morphologies during the process of phase separation in the three-phase region.

### 5.2. Free energy model

Consider a planar, binary lipid membrane with the same lipid species but possibly different compositions in each of its two apposing monolayers. Assume the two lipid species exhibit non-ideal mixing, with a tendency toward phase separation.

We model this tendency using regular solution theory on the mean-field level which is also referred to as the Bragg-Williams or random mixing approximation [228, 47]. The free energy per lipid $f_{BW}$ of a single two-component lipid monolayer can then be written as a function of its composition $\phi$,

$$f_{BW}(\phi) = \phi \ln \phi + (1-\phi)\ln(1-\phi) + \chi\phi(1-\phi)\ . \tag{5.1}$$

Note that here and in the following, all energies are expressed in units of $k_{\mathrm{B}}T$ (Boltzmann's constant $\times$ absolute temperature). The nonideality parameter *chi* describes the effective strength of nearest-neighbor interactions. For $chi > 0$ this interaction is attractive, and for $\chi > \chi_c$ it is able to induce phase separation. Mean-field theory predicts the critical point$\chi_c = 2$. We note that in a more general approach each monolayer would have its own nonideality parameter. In view of our objective to formulate a minimal model, we assume that both monolayers have the same underlying energetics (namely, the same $\chi$). What may be different are the average compositions of the two monolayers.

The main focus of this work is to investigate the consequences of the energetic coupling between the two apposed monolayers of a lipid bilayer. The coupling is local and likely reflects the dependence on composition of interactions between lipid tails across the bilayer midplane, such as interdigitation or, more accurately, dynamic interpenetration, as outlined in the Introduction. That is, any local compositional differences across the bilayer give rise to an extra energy penalty. If the compositional difference is sufficiently small this energy penalty must be proportional to $(\phi - \psi)^2$ where $\phi$ and $\psi$ denote the local compositions in the upper and lower monolayers, respectively. (Note that invariance of the free energy with respect to exchanging the upper and lower monolayer excludes the presence of the linear term $\phi - \psi$.) Denoting the coupling strength by $\Lambda$ (with $\Lambda > 0$), we can write for the local free energy of a lipid bilayer

$$f(\phi, \psi) = f_{BW}(\phi) + f_{BW}(\psi) + \Lambda(\phi - \psi)^2 \, . \tag{5.2}$$

The first two terms describe the free energies of each monolayer leaflet individually, and the last term accounts for the coupling between the apposed monolayers. To obtain the overall free energy $F$ of a lipid bilayer we integrate $f(\phi, \psi)$ over the total lateral area $A$ of the membrane,

$$F = \frac{1}{a} \int_A \mathrm{d}a f(\phi, \psi) \, , \tag{5.3}$$

where $a$ denotes the cross-sectional area per lipid (which we assume to be the same for both species). Equations (5.1)–(5.3) form the basis of the present work. In the following, we theoretically analyze and discuss the implications of a nonvanishing coupling strength $\Lambda$.

### 5.3. Phase behavior

We characterize the phase behavior as a function of the two membrane compositions, $\phi$ and $\psi$, in the upper and lower monolayers, respectively. Let us first calculate the spinodal line that separates locally stable and unstable regions in the phase diagram. At the spinodal line, the determinant

$$\frac{\partial^2 f}{\partial \phi^2}\frac{\partial^2 f}{\partial \psi^2} - \left(\frac{\partial^2 f}{\partial \phi \partial \psi}\right)^2 = 0 \tag{5.4}$$

of the stability matrix corresponding to $f(\phi, \psi)$ vanishes. Carrying out the derivatives using Eqs.(5.1) and (5.2) gives rise to the relation

$$\begin{aligned} 0 = &\left(\frac{1}{2\phi(1-\phi)} - \chi\right)\left(\frac{1}{2\psi(1-\psi)} - \chi\right) \\ &+ \Lambda\left[\frac{1}{2\phi(1-\phi)} + \frac{1}{2\psi(1-\psi)} - 2\chi\right] . \end{aligned} \tag{5.5}$$

Solutions of that equation specify the spinodal lines for any given $\chi$ and $\Lambda$. Fig. 5.2 displays a number of representative examples of spinodals, derived for $\chi = 2.2$ and different choices of the coupling parameter $\Lambda$. We note that sets of spinodals for values of $\chi$ different to $\chi = 2.2$ (but with $\chi > 2$) appear qualitatively equivalent to those shown in Fig. 5.2. Let us discuss the behavior of the spinodal lines: First, all spinodal lines exhibit fourfold symmetry about the two axes $\phi = \psi$ and $\phi = 1 - \psi$. Second, the smallest $\chi$ for which Eq. (5.5) can be fulfilled is $\chi = \chi_c = 2$ with the corresponding compositions $\phi = \psi = 1/2$. Hence, the coupling parameter does not affect the critical point. Also, close to the critical point, the behavior of the spinodals is independent of $\Lambda$. This becomes evident from an expansion of the spinodal up to quadratic order in

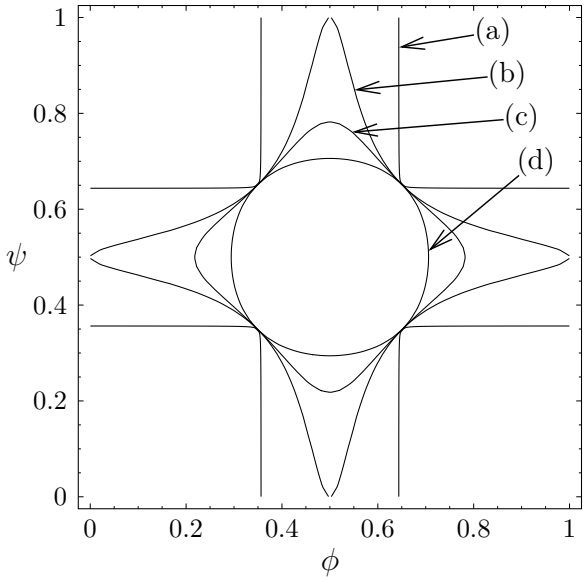


Figure 5.2. Spinodal lines for $\chi = 2.2$ and $\Lambda = 0.02$ (a), $\Lambda = 0.2$ (b), $\Lambda = 0.275$ (c), and $\Lambda = 5$ (d). The spinodals represent solutions of Eq. (5.5).

$\phi$ and $\psi$ in the vicinity of the critical point, leading to

$$\left(\sqrt{\frac{\chi-2}{4}}\right)^2 = \left(\phi - \frac{1}{2}\right)^2 + \left(\psi - \frac{1}{2}\right)^2 , \tag{5.6}$$

which describes a circle of radius $\sqrt{\chi-2}/2$, independent of $\Lambda$. Third, for vanishing coupling parameter, $\Lambda = 0$, the spinodals consist of the two sets of straight lines,

$$\phi = \frac{1}{2}\left(1 \pm \sqrt{\frac{\chi-2}{\chi}}\right) , \qquad \psi = \frac{1}{2}\left(1 \pm \sqrt{\frac{\chi-2}{\chi}}\right) . \tag{5.7}$$

The four points where these lines cross each other are part of the entire set of spinodals for fixed $\chi$ but variable $\Lambda$ (see Fig. 5.2). What changes at these four points as a function of $\Lambda$ (but fixed $\chi$) is the curvature of the spinodal. For small $\Lambda$ the spinodal is convex, and for large $\Lambda$ it is concave. For the discussion below we note that the curvature vanishes at $\Lambda = \Lambda_V$ with

$$\Lambda_V = \chi \frac{\chi-2}{2\chi-3} . \tag{5.8}$$

For example, for $\chi = 2.2$ this is the case at $\Lambda \approx 0.31$ (a spinodal close to that, namely for $\Lambda = 0.275$, is shown in Fig. 5.2. And finally, note that for small $\Lambda$ each spinodal (for fixed $\chi$ and $\Lambda$) consists of four individual segments. For sufficiently large $\Lambda$, the spinodal is described by a single closed curve in the $\phi, \psi$-plane. The smallest $\Lambda$ for which this appears to be the case is

$$\Lambda = \chi - 2 \; . \tag{5.9}$$

For example, $\chi = 2.2$ leads to $\Lambda = 0.2$; shown in Fig. 5.2. To summarize, a growing coupling parameter $\Lambda$ restricts the regions of local instability of the bilayer but does not affect the critical point.

Let us now calculate the binodal phase behavior, with all multiphase regions and representative tie-lines included. To this end, we need to minimize the overall free energy $F$ of the bilayer, defined in Eq. (5.3). Because the local free energy $f(\phi, \psi)$ depends on a single compositional degree of freedom in each of the two monolayers, the membrane can for any nonvanishing coupling $\Lambda > 0$, at most, separate laterally into three phases. (Of course, in each individual phase, the compositions of the upper and lower monolayer need not be the same.) Allowing for the coexistence of three homogeneous phases we may rewrite Eq. (5.3) as

$$\frac{aF}{A} = \theta_1 f(\phi_1, \psi_1) + \theta_2 f(\phi_2, \psi_2) + \theta_3 f(\phi_3, \psi_3) \; , \tag{5.10}$$

where $\theta_1$, $\theta_2$, $\theta_3$ are the area fractions of the three phases, $\phi_1$, $\phi_1$, $\phi_1$ are the corresponding compositions of the upper monolayer, and $\psi_1$, $\psi_2$, $\psi_3$ are the corresponding compositions of the lower monolayer. Area fractions and compositions must fulfill the three conservation conditions $\theta_1 + \theta_2 + \theta_3 = 1$, $\phi_1 + \phi_2 + \phi_3 = \phi$, and $\psi_1 + \psi_2 + \psi_3 = \psi$ where $\phi$ and $\psi$ are the fixed average compositions in the upper and lower monolayer,

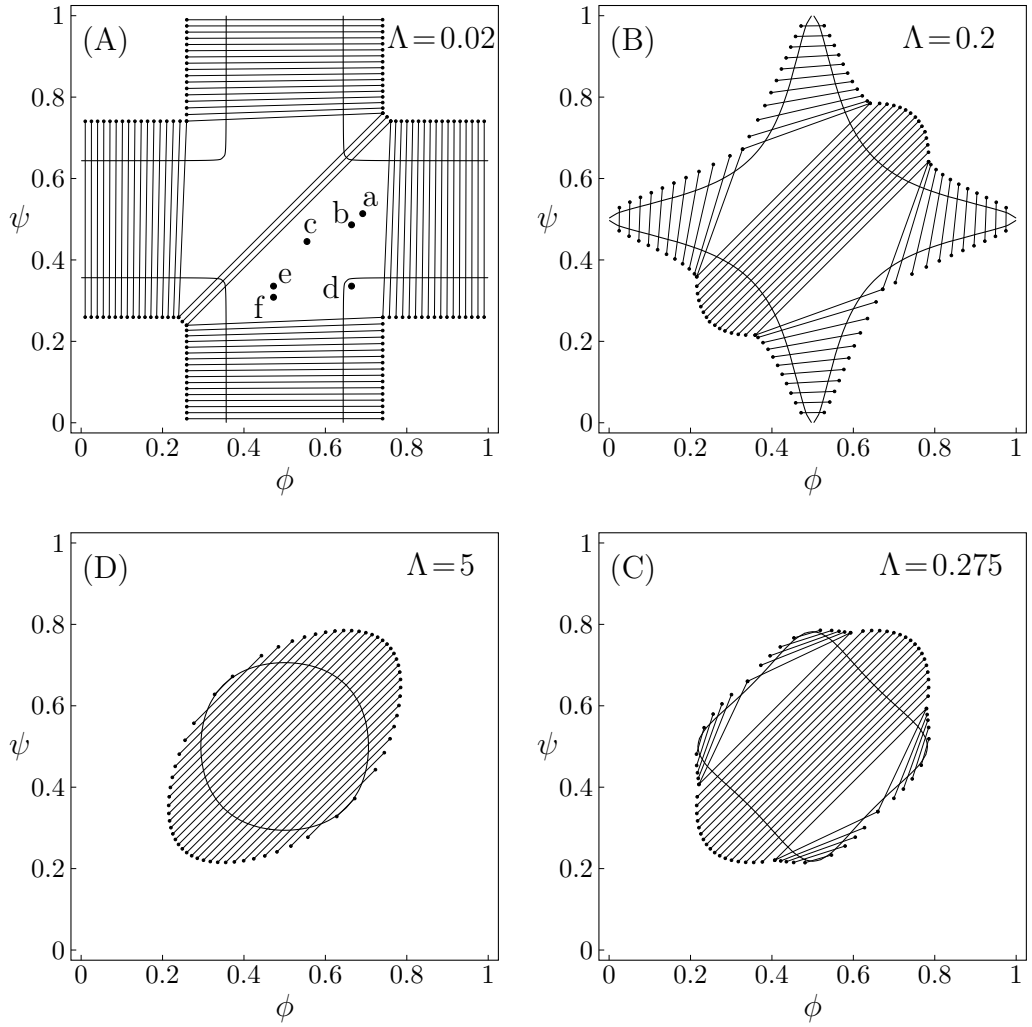


Figure 5.3. Phase diagrams for $\Lambda = 0.02$ (top, left), $\Lambda = 0.2$ (top, right), $\Lambda = 0.275$ (bottom, left), and $\Lambda = 5$ (bottom, right). Three-phase regions are indicated by triangles. Representative tie-lines are displayed in regions of two-phase coexistence. Also shown are the spinodal lines (see also Fig. 5.2). Note that $\chi = 2.2$ in all four diagrams. The points marked $a - f$ in diagram $A$ indicate systems for which we have carried out simulations of their morphological phase structure; see below in Fig. 5.4, $A - F$.

respectively, thus specifying a point $\{\phi, \psi\}$ in the phase diagram (see Fig. 5.3). (For brevity, we shall use the same symbols $\phi$ and $\psi$ to denote local and average compositions; everywhere below the concrete meaning of $\phi$ and $\psi$ is uniquely determined by its context).

Owing to the three conservation conditions, only six variables in Eq. (5.10) are independent. In thermal equilibrium, the free energy $F$ adopts its global minimum with respect to these six variables. The minimization can be carried out numerically; results of phase diagrams as functions of the fixed average compositions $\phi$ and $\psi$ are shown in Fig. 5.3, derived for $\chi = 2.2$ and various choices of $\Lambda$. Again, changing $\chi$ does not affect the qualitative features of the phase diagrams. Let us discuss the influence of the coupling parameter $\Lambda$.

In the absence of coupling, $\Lambda = 0$, the two monolayers, if unstable, phase-separate independently from each other. For example, if only the upper monolayer is unstable, then a tie-line parallel to the $\phi$-axis of the phase diagram indicates the two coexisting compositions $\phi_1$ and $\phi_2 = 1 - \phi_1$, which solve the equation $\ln[\phi/(1-\phi)] = \chi(2\phi - 1)$. This last equation corresponds to the familiar common tangent construction. Instability of both monolayers would lead to a phase coexistence with compositions $\phi_1$, $\phi_2 = 1 - \phi_1$ and $\psi_1 = \phi_1$,$\psi_2 = \phi_2$ in the upper and lower monolayer, respectively. Morphological phase structure and dynamic evolution toward the equilibrium structure in one monolayer is entirely independent from that in the apposed monolayer. Therefore phase morphologies in both monolayers are spatially uncorrelated in the limit $\Lambda \to 0$.

For nonvanishing but still sufficiently small coupling parameter, $\Lambda$, we find both two-phase and three-phase coexistence regions. Let us first discuss two-phase coexistence. Consider, for example, $\Lambda = 0.02$ which is shown in Fig. 5.3 A. If only the upper monolayer is unstable, say at $\phi = 0.5$ and $\psi = 0.1$, it will split into two phases. Yet, the corresponding tie-line is tilted with respect to the $\phi$-axis, implying that a compositional difference is also induced in the lower monolayer. (The tilt of the tie-lines grows with the coupling parameter $\Lambda$.) Hence, if without coupling one monolayer is unstable and the other monolayer is stable, the coupling between them

may induce phase-separation in both monolayers. In this scenario, the phases in both monolayers are in complete registration.

The phase diagrams in Fig. 5.3 also predict another possibility. A membrane with its two monolayers–one being stable and the other unstable without coupling–may not phase separate at all if coupling is present. This is evident from the decrease in size of the four symmetric two-phase regions with increasing $\Lambda$ (see Fig. 5.3 B) for $\Lambda = 0.2$ and, even more pronounced, for $\Lambda = 0.275$ (see Fig. 5.3 C).

Three-phase coexistence is equivalent to incomplete phase registration across the bilayer. Yet, regions of three-phase coexistence only exist below a certain coupling strength $\Lambda^\star$. Above this maximal coupling strength, the membrane no longer exhibits three-phase coexistence. We can calculate $\Lambda^\star$ by noting that along the spinodal $\psi(\phi)$ two critical points merge at position $\phi = \phi_m$ with $\phi_m = (1 + \sqrt{(\chi - 2)\chi})/2$ (see Eq. (5.7)). This can be written as

$$\left( \frac{\mathrm{d}}{\mathrm{d}\phi} \left( \frac{\mathrm{d}^3 f(\phi + \delta, \psi(\phi) + \delta\psi'(\phi))}{\mathrm{d}^3 \delta} \right)_{\delta=0} \right)_{\phi=\phi_m} = 0 \,, \tag{5.11}$$

where the prime in $\psi'(\phi)$ denotes the first derivative with respect to the argument. Solving Eq. (5.11) leads to the maximal coupling strength

$$\Lambda^\star = \frac{3}{2}\,\chi\,\frac{\chi - 2}{2\chi - 3} \,, \tag{5.12}$$

above which three-phase coexistence does not exist. (It is interesting to note that $\Lambda^\star = 3\Lambda_V/2$; see Eq. (5.8).) For $\chi = 2.2$, three-phase coexistence thus ceases to exist for $\Lambda > 0.47$.

The sizes of the three-phase regions shrink with growing coupling parameter, as is evident from Fig. 5.3, A–C. In fact, the three-phase regions are replaced by an additional two-phase region (absent for $\Lambda = 0$) that has all its tie-lines parallel to the

diagonal $\phi = \psi$, implying a constant compositional difference across the monolayers everywhere in the membrane. T his is the most restrictive effect that the coupling between the monolayers can have. Hence, the additional two-phase region represents the strong coupling limit. Indeed, for large coupling parameter, $\Lambda \geq \Lambda^{\star}$, the phase diagram has all its tie-lines with slope of 1 in the $\phi, \psi$-diagram. Fig. 5.3 D displays this limiting case of large coupling.

Our final comment concerns the phase behavior of a membrane that has one of its two monolayers being a binary mixture whereas the other one contains only a single component. Assume the mixed monolayer is unstable for $\Lambda = 0$. Our phase diagrams show that with increasing coupling parameter the region of instability of the bilayer decreases until, eventually, a phase transition is completely absent. The strength of the coupling parameter beyond which phase separation ceases is $\Lambda = \chi - 2$, corresponding to Eq. (5.9), for which the spinodal line starts forming a single closed curve in the phase diagram. With $\chi = 2.2$, this happens for $\Lambda = 0.2$; shown in Fig. 5.3 B.

### 5.4. Landau expansion

Close to the critical point it is convenient to expand the free energy into a series up to fourth-order in the order parameters. This often provides a means to characterize the phase behavior in terms of analytical expressions. Here, we shall also demonstrate the use of such a Landau expansion. The order parameter of the binary lipid membrane is the composition, $\phi$ in the lower monolayer and $\psi$ in the upper monolayer. The critical point is adopted at $\phi = \psi = 1/2$. It will be convenient to define the two new scaled compositions,

$$\bar{\phi} = \frac{\phi - 1/2}{\sqrt{(3/8)(\chi - 2)}} \,, \qquad \bar{\psi} = \frac{\psi - 1/2}{\sqrt{(3/8)(\chi - 2)}} \,. \tag{5.13}$$

We then expand the free energy $f_L = (4/3)f(\phi,\psi)/(\chi-2)^2$ up to fourth-order in $\bar{\phi}$ and $\bar{\psi}$ at position $\bar{\phi} = \bar{\psi} = 0$. The result can be written up to an irrelevant constant term as

$$f_L(\bar{\phi},\bar{\psi}) = \frac{1}{4}(\bar{\phi}^4 + \bar{\psi}^4) - \frac{1}{2}(\bar{\phi}^2 + \bar{\psi}^2) + \frac{\Lambda'}{2}(\bar{\phi} - \bar{\psi})^2 \,, \tag{5.14}$$

where we have defined the normalized coupling strength $\Lambda' = \Lambda/(\chi-2)$. The reason for introducing scaled compositions is now evident: $f_L(\bar{\phi},\bar{\psi})$ depends on $\Lambda$ and $\chi$ only through the normalized coupling strength $\Lambda'$. Hence, close to the critical point (where the Landau expansion is valid), the phase behavior only depends on one single parameter. This justifies presenting a sequence of phase diagrams in Fig. 5.3 as function of $\Lambda$ for only one single value $\chi$. Different choices of $\chi$ do not lead to qualitatively different behavior in the phase diagrams.

It is obvious that for $\Lambda' = 0$ the free energy $f_L(\bar{\phi},\bar{\psi})$ decouples into two additive contributions. In this case, the binodal lines (representing solutions of the common tangent construction) are located at $\bar{\phi} = \pm 1$ f and $\bar{\psi} = \pm 1$ with constant $\bar{\psi}$ and constant $\bar{\phi}$, respectively. The corresponding spinodal lines are $\bar{\phi} = \pm 1/\sqrt{3}$ and $\bar{\psi} = \pm 1/\sqrt{3}$, which agrees with Eq. (5.7) for small $\chi - 2$.

Let us first investigate the limit of small coupling $\Lambda'$. Here, the phase diagram contains both three-phase and two-phase regions. Using the case $\Lambda' = 0$ as a reference state, we can perform an expansion of the phase coexistence equations with respect to small $\Lambda'$. For the three-phase region we then obtain the triangle, $\{\bar{\phi}_1,\bar{\psi}_1\}, \{\bar{\phi}_2,\bar{\psi}_2\}, \{\bar{\phi}_3,\bar{\psi}_3\}$ of coexisting (scaled) compositions in the upper and lower monolayer. Our calculation yields $\bar{\phi}_1 = -\bar{\psi}_3 = 1 + \Lambda'/2$, and $\bar{\phi}_2 = \bar{\psi}_1 = -\bar{\phi}_3 = -\bar{\psi}_2 = 1 - \Lambda'/2$. This indeed describes the shift in the lower phase triangle ($\psi > \phi$ in Fig. 5.3) as a function of $\Lambda$. Analogous expressions are valid for the upper phase triangle (where $\psi < \phi$).

A similar expansion of the coexistence equations with respect to the coupling parameter can be performed to obtain the tie-lines of the two-phase region in the limit of small $\Lambda'$. More specifically, we calculate the lower set of almost horizontal tie-lines in the phase diagram (see Fig. 5.3 A). Here the resulting two coexisting bilayer compositions $\{\bar{\phi}_1, \bar{\psi}_1\}$ and $\{\bar{\phi}_2, \bar{\psi}_2\}$ define an almost horizontal tie-line ($\bar{\phi}_1 \approx \bar{\phi}_2$) that crosses through the point $\{\bar{\phi}, \bar{\psi}\}$ of given (scaled) average compositions of the two monolayers. Our calculation leads to $\bar{\phi}_2 = -\bar{\phi}_1 = 1 - \Lambda'/2$ and

$$\bar{\phi}_1 = \bar{\phi} - \Lambda' \frac{1+\bar{\phi}}{3\bar{\psi}^2 - 1} \; ; \qquad \bar{\phi}_2 = \bar{\phi} + \Lambda' \frac{1-\bar{\phi}}{3\bar{\psi}^2 - 1} \; . \tag{5.15}$$

Analogous expressions can be derived for the other almost horizontal and two almost vertical sets of tie-lines (see next paragraph for the remaining set of tie-lines that are parallel to the $\psi = \phi$-diagonal of the phase diagram).

Let us now investigate the limit of large coupling parameter. (This analysis is valid for all tie-lines at $\Lambda > \Lambda^\star$, and also applies to the set of tie-lines parallel to the $\psi = \phi$-diagonal of the phase diagram for $0 < \Lambda < \Lambda^\star$.) As argued above, no three-phase coexistence region exists in this regime. Hence, the membrane can only exhibit two-phase coexistence. Whenever this is the case, the two monolayers have the same compositional difference between their respective phases. This fact can be used to solve the coexistence equations for any point of given (scaled) average compositions $\{\bar{\phi}, \bar{\psi}\}$ within the two-phase region. The result for the two coexisting

bilayer compositions $\{\bar{\phi}_1, \bar{\psi}_1\}$ and $\{\bar{\phi}_2, \bar{\psi}_2\}$ is

$$\begin{aligned}
\bar{\phi}_1 &= \frac{\bar{\phi}-\bar{\psi}}{2} - \sqrt{1-\frac{3}{4}\left(\bar{\phi}-\bar{\psi}\right)^2} \\
\bar{\phi}_2 &= \frac{\bar{\phi}-\bar{\psi}}{2} + \sqrt{1-\frac{3}{4}\left(\bar{\phi}-\bar{\psi}\right)^2} \\
\bar{\psi}_1 &= -\frac{\bar{\phi}-\bar{\psi}}{2} - \sqrt{1-\frac{3}{4}\left(\bar{\phi}-\bar{\psi}\right)^2} \\
\bar{\psi}_2 &= -\frac{\bar{\phi}-\bar{\psi}}{2} + \sqrt{1-\frac{3}{4}\left(\bar{\phi}-\bar{\psi}\right)^2} \,.
\end{aligned} \tag{5.16}$$

Again, it can be verified that the corresponding tie-lines cross the point $\{\bar{\phi}, \bar{\psi}\}$. The tie-lines described by Eq. (5.16) are indeed parallel to the diagonal $\psi = \phi$ of the phase diagram. In the $\phi, \psi$-phase diagram, there are two critical points where the binodal and spinodal lines merge (see Fig. 5.3 D). These points are $\{\bar{\phi}, \bar{\psi}\} = \{1, -1\}/\sqrt{3}$ and $\{\bar{\phi}, \bar{\psi}\} = \{-1, 1\}/\sqrt{3}$. The longest tie-line, extending along the $\bar{\psi} = \bar{\phi}$-diagonal, connects the two points $\{\bar{\phi}, \bar{\psi}\} = \{1, 1\}$ and $\{\bar{\phi}, \bar{\psi}\} = \{-1, -1\}$. We thus see that the binodal region in the regime $\Lambda > \Lambda^\star$ corresponds to an ellipse with ratio $\sqrt{3}$ between its long and short axis (see Fig. 5.3).

### 5.5. Morphologies

We also simulated the dynamic phase-separation process using a lattice Boltzmann method (see Appendix (Section 5.8) for details) based on the Landau expansion of the free energy, Eq. (5.14). We simulated the following equations of motion. For the total density $\rho$ we have the continuity equation

$$\partial_t \rho + \nabla(\rho \mathbf{u}) = 0 \,, \tag{5.17}$$

where $\mathbf{u}$ denotes the mean fluid velocity, and the Navier-Stokes equation for the total momentum

$$\partial_t(\rho\mathbf{u}) + \nabla(\rho\mathbf{u}\mathbf{u}) = \nabla P + \nabla\{\eta[\nabla\mathbf{u} + (\nabla\mathbf{u})^T]\} \; . \tag{5.18}$$

Here $P$ is the pressure tensor given by Eq. (5.24) and $\eta$ is the viscosity. For the order parameters $\bar{\phi}$ and $\bar{\psi}$ the drift diffusion equation reads

$$\partial_t\bar{\phi} + \nabla(\bar{\phi}\mathbf{u}) = \nabla(M^{\bar{\phi}}\nabla\mu^{\bar{\phi}}) \; , \tag{5.19}$$

$$\partial_t\bar{\psi} + \nabla(\bar{\psi}\mathbf{u}) = \nabla(M^{\bar{\psi}}\nabla\mu^{\bar{\psi}}) \; , \tag{5.20}$$

where $M^{\bar{\phi}}$ and $M^{\bar{\psi}}$ are Onsager coefficients. The chemical potentials, $\mu^{\bar{\phi}}$ and $\mu^{\bar{\psi}}$ ; are derived from the Landau free energy, Eq. (5.14), with the additional interfacial energy term, $(\kappa/2)[(\nabla\bar{\phi})^2 + (\nabla\bar{\psi})^2]$, given by Eq. (5.28) and Eq. (5.29).

Simulations for parameters leading to a two-phase region give rise to the usual morphologies seen for coarsening of two-phase systems [285]. More interesting are the three-phase regions on which we focus here. In the following, it is sufficient to consider the case where the initial value of $\bar{\phi}$ (that is, the scaled average composition of the upper monolayer) is larger than the corresponding initial value of $\bar{\psi}$ (the scaled average composition of the lower monolayer). The three equilibrium phases are then $\bar{\phi}$-rich and $\bar{\psi}$-rich domains (condensed-condensed), $\bar{\phi}$-rich and $\bar{\psi}$-poor domains (condensed-uncondensed), and $\bar{\phi}$-poor and $\bar{\psi}$-poor domains (uncondensed-uncondensed). In Fig. 5.4 these domains are shown as bright, gray, and dark domains, respectively. We initialized our simulations with homogeneous compositions $\bar{\phi}$ and $\bar{\psi}$; modulated with small spatial disturbances to initiate spinodal decomposition.

Six examples of typical morphologies are shown in Fig. 5.4 for $\Lambda' = 0.1$. Note that for $\chi = 2.2$ the choice $\Lambda' = 0.1$ corresponds to $\Lambda = \Lambda'(\chi - 2) = 0.02$. We thus simulate morphologies in the three-phase region of Fig. 5.3 A. The corresponding

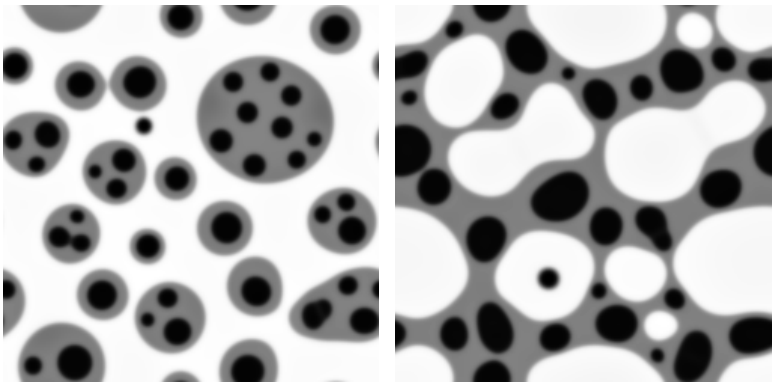

**(A)** $\bar{\phi} = 0.7, \bar{\psi} = 0.05$ **(B)** $\bar{\phi} = 0.6, \bar{\psi} = -0.05$

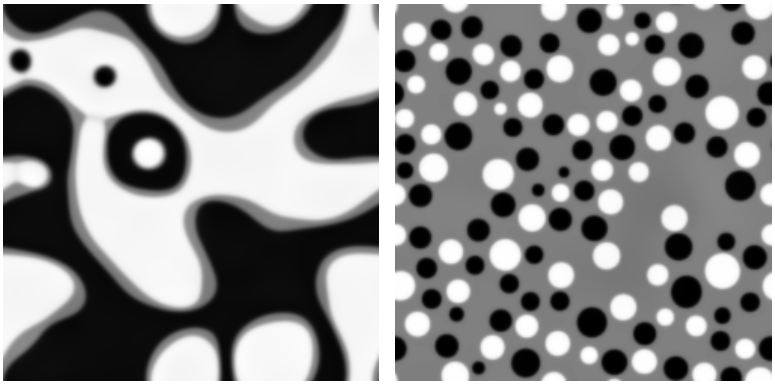

**(C)** $\bar{\phi} = 0.2, \bar{\psi} = -0.2$ **(D)** $\bar{\phi} = 0.6, \bar{\psi} = -0.6$

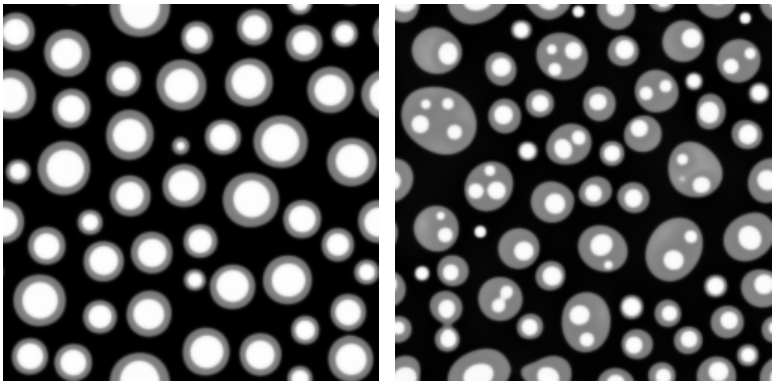

**(E)** $\bar{\phi} = -0.1, \bar{\psi} = -0.6$ **(F)** $\bar{\phi} = -0.1, \bar{\psi} = -0.7$

Figure 5.4. Dynamically formed membrane domain morphologies for different compositions of the upper and lower monolayers for parameters in the three-phase region of the phase-diagram. The three equilibrium phases are $\bar{\phi}$-rich and $\bar{\psi}$-rich domains (bright, condensed-condensed), $\bar{\phi}$-rich and $\bar{\psi}$-poor domains (gray, condensed-uncondensed) and $\bar{\phi}$-poor and $\bar{\psi}$-poor domains (dark, uncondensed-uncondensed). Generally, domains are in complete registration. That is, domains in one monolayer are fully contained in the domains of the other monolayer. Or, equivalently expressed, domain boundaries never cut each other. Simulations $A$–$F$ correspond to the points $a$–$f$ of the phase diagram shown in Fig. 5.3 A.

points are indicated in the phase diagram of Fig. 5.3 A. That is, point $a$ in Fig. 5.3 A corresponds to the system simulated in Fig. 5.4 A, and analogously for points $b$–$f$. Note that for values of $\Lambda'$ an order-of-magnitude smaller ($\Lambda' \leq 0.01$) the domains begin to decouple dynamically, implying that domain boundaries start crossing each other. Morphologically, this is reminiscent of recent observations in solid-supported lipid bilayers where domains are not registered because domains in the substrate-facing monolayer are immobilized ([262, 44, 79]). In all simulations displayed in Fig. 5.4, the coupling parameter $\Lambda' = 0.1$ is sufficiently high so that domains of one monolayer are always fully contained within domains of the other monolayer. In other words, the domains in the apposed monolayers are in full registration. All of the displayed morphologies are time-dependent and they continue to coarsen through the coalescence of domains (viscous hydrodynamic growth) and the occasional evaporation of very small domains (Oswald ripening).

If both average (scaled) compositions are larger than zero ($\bar{\phi} > 0$ and $\bar{\psi} > 0$) the membrane will form predominantly the condensed phase in both monolayers. This is the case in Fig. 5.4 A, derived for $\bar{\phi} = 0.7, \bar{\psi} = 0.05$ where we indeed observe a large and continuous bright domain, enclosing gray domains that themselves each enclose one or more small dark domains. Recall that the upper monolayer, present with large composition, forms the uncondensed phase only within the dark domains. Decreasing both $\bar{\phi}$ and $\bar{\psi}$ (see Fig. 5.4 B) derived for $\bar{\phi} = 0.6, \bar{\psi} = -0.05$, favors formation of the gray phase; this phase then becomes the majority phase and contains distinct sets of bright and dark domains.

Symmetric systems, $\bar{\phi} = -\bar{\psi}$ are displayed in Fig. 5.4, C and D. For small absolute values of $\bar{\phi} = -\bar{\psi}$ the system resembles a familiar two-phase fluid where the gray phase decorates the interface of the dark and bright domains (see Fig. 5.4 C). For larger absolute values, the area fraction of the gray domains increases until there is a mixture of dark and bright domains suspended in a gray matrix (see Fig. 5.4 D).

If both $\bar{\phi} < 0$ and $\bar{\phi} < 0$ the membrane tends to form mostly the uncondensed phase in both monolayers (of course, more of it in the lower monolayer because we have assumed $\bar{\phi} > \bar{\psi}$). This is seen in Fig. 5.4, E and F, where we indeed observe mostly the dark phase. Because of the $\bar{\phi} \to -\bar{\phi}$ and $\bar{\psi} \to -\bar{\psi}$ symmetries this is roughly the complementary morphology to Fig. 5.4 A. Note for Fig. 5.4 E that we find only one single white domain enclosed in each gray one. The coarsening dynamics provides the reason for this observation: If the gray domains coarsen more slowly than the domains dispersed in them we will always end up with only one single domain suspended. If the gray domains coarsen faster than the domains dispersed in them we will end up with gray domains that contain an increasing number of smaller domains. Examples of the latter are shown in Fig. 5.4, A and F.

To discuss the dynamics of this simple model in relation to that observed in experiments it is important to compare several timescales. The first timescale refers to the phase-separation process which is roughly given by the time it takes to de-mix an initially homogeneous lipid layer and form small domains. The next two timescales are related to the coarsening of the domains. There are two coarsening mechanisms present: a diffusive coarsening mechanism dominating at small length scales and a hydrodynamic coarsening mechanism dominating for large domains. This is the case for all fluid mixtures.

In our special case there is an additional timescale involved. This timescale specifies the coupling of the hydrodynamics between the domains in both leafs of the membrane. If this coupling is small, or if one monolayer is prevented from hydrodynamic motion by being immobilized on a solid substrate, the domains may become spatially decoupled and registration of the domains can be lost. This is seen in experiments [262, 44] using supported membranes where the hydrodynamic motion of the support-facing monolayer is inhibited or recovered by an additional polymer cushion [79, 125].

## 5.6. Conclusions

This study investigates how the coupling between the two monolayers of a lipid membrane affects the phase behavior in each of the two membrane leaflets. Our model employs only one order parameter. In this respect it is simpler than previous theoretical studies [96, 3]. Still, it makes a number of nontrivial and experimentally verifiable predictions. First, if one monolayer leaflet is unstable it may induce phase separation in the apposed monolayer, even if this monolayer would be stable otherwise. A stable monolayer may also suppress phase separation in the apposed intrinsically unstable monolayer. If phase separation occurs, it always occurs in both monolayers, but is generally weaker in the more stable monolayer. This might be of relevance for the plasma membrane for which the extracellular leaflet typically contains a raft-forming lipid mixture whereas the cytoplasmatic one does not. Somewhat surprisingly, our simple model predicts that for low coupling strength the domains in the two monolayers are not always in registration. This is manifested by the presence of three-phase coexistence in the phase diagram. Here, each monolayer contains three phases of different compositions. The compositions of the two monolayers can be different but the three phases in each monolayer must be in perfect registration for thermodynamic reasons. Morphologically, the three-phase coexistence appears as two sets of domains, one contained in the other. Above a critical coupling strength (which we have calculated analytically; see Eq. (5.12)) three-phase coexistence is no longer possible, and the membrane can only split into two phases in each monolayer that are always in perfect registration.

As our model is based on one single order parameter it should be the simplest model to investigate intermonolayer coupling. The simplicity of the model implies a considerable number of approximations. In particular, all effects related to other degrees of freedom beyond compositional changes are neglected. This includes

curvature degrees of freedom [96], thickness changes of the membrane [3], and flip-flop (which could be particularly relevant for cholesterol [92].) In addition, we have considered a two-component system, thus neglecting the three components that are commonly used to produce fluid-phase coexistence (cholesterol and two lipid species with one of which cholesterol interacts more favorably). Note also that the coupling parameter between the two monolayers, $\Lambda$ (see Eq. (5.2)), was introduced phenomenologically; hence, it does not reveal the molecular origin of the coupling. At this point, further modeling studies might be useful to extract the source(s) of the coupling and to estimate the actual magnitude of $\Lambda$. Finally, we have assigned the same nonideality parameter, $\chi$, to both leaflets of the membrane. A more general approach would allow for different free energy functions (and thus two different $\chi$) in both monolayers. Still, the surprising variety of predicted phenomena makes us confident that our model captures some essential features of the coupling between the apposed monolayers and its thermodynamic implications.

## 5.7. Acknowledgments

S.M. thanks Sarah Keller for illuminating discussions.

This work was supported by National Institutes of Health grant No. GM077184-01.

## 5.8. Appendix: Lattice Boltzmann

The application of the lattice Boltzmann method to the coupled leaflets of a lipid bilayer is presented here for the first time. It is based on a free energy in the spirit of the original Swift model [207, 265] and consists of evolution equations for the densities $f_i^c$ for component $c$ associated with a lattice velocity $\mathbf{v}_\mathrm{i}$

$$f_i^c(\mathbf{x}+\mathbf{v}_\mathrm{i}, t+\Delta t) = f_i^c(\mathbf{x},t) + \frac{\Delta t}{\tau^c}(f_i^{c0}(n^c(\mathbf{x},t), \mathbf{u}(\mathbf{x},t)) - f_i^c(\mathbf{x},t)) \ , \qquad (5.21)$$

where the density is $n^c = \sum_i f_i^c$ and $\mathbf{u}$ denotes the mean fluid velocity. The equilibrium distribution is given by

$$f_i^{c0} = w_i(n^c\delta_{i,0} + 3\mathbf{u}.\mathbf{v}_\mathrm{i} + \frac{9}{2}\Pi^c : \mathbf{v}_\mathrm{i}\mathbf{v}_\mathrm{i} - \frac{3}{2}\mathrm{tr}\Pi^c) \ . \tag{5.22}$$

We will use a standard D2Q9 velocity set of

$$\{\mathbf{v}_\mathrm{i}\} = \left\{ \begin{pmatrix}0\\0\end{pmatrix}, \begin{pmatrix}1\\0\end{pmatrix}, \begin{pmatrix}-1\\0\end{pmatrix}, \begin{pmatrix}0\\1\end{pmatrix}, \begin{pmatrix}0\\-1\end{pmatrix}, \begin{pmatrix}1\\1\end{pmatrix}, \begin{pmatrix}-1\\1\end{pmatrix}, \begin{pmatrix}-1\\-1\end{pmatrix}, \begin{pmatrix}1\\-1\end{pmatrix} \right\} \ . \tag{5.23}$$

For this velocity set the weights are $w_0 = 1$, $w_{1-4} = 1/9$, and $w_{5-8} = 1/36$. We use three lattice Boltzmann equations to represent the total density $\rho$ and the two order parameters $\bar{\phi}$ and $\bar{\psi}$. The first density can then be used to define the mean fluid velocity through $\rho\mathbf{i} = \sum_i f_i^1\mathbf{v}_\mathrm{i}$. The pressure tensor is given by

$$\begin{aligned} P_{\alpha\beta} = & \Big\{ -\frac{1}{2}(\bar{\phi}^2 + \bar{\psi}^2) + \frac{3}{4}(\bar{\phi}^4 + \bar{\psi}^4) + \frac{\Lambda'}{2}(\bar{\phi} - \bar{\psi})^2 \\ & + \frac{\kappa}{2}[\bar{\phi}\nabla^2\bar{\phi} + \bar{\psi}\nabla^2\bar{\psi} - (\nabla\bar{\phi})^2 + (\nabla\bar{\psi})^2] \Big\}\delta_{\alpha\beta} \\ & + \kappa(\nabla_\alpha\bar{\phi}\nabla_\beta\bar{\phi} + \nabla_\alpha\bar{\psi}\nabla_\beta\bar{\psi}) \ , \end{aligned} \tag{5.24}$$

and we choose

$$\Pi^\rho = \rho\mathbf{u}\mathbf{u} + P \ . \tag{5.25}$$

For the other two $\Pi$ we choose

$$\Pi^{\bar{\phi}} = \bar{\phi}\mathbf{u}\mathbf{u} + \mu^{\bar{\phi}}\mathbf{1} \ , \tag{5.26}$$

$$\Pi^{\bar{\psi}} = \bar{\psi}\mathbf{u}\mathbf{u} + \mu^{\bar{\psi}}\mathbf{1} \ , \tag{5.27}$$

where the chemical potentials are given by

$$\mu^{\bar{\phi}} = -\bar{\phi} + \bar{\phi}^3 - \kappa\nabla^2\bar{\phi} - \Lambda'(\bar{\phi} - \bar{\psi}) \,, \tag{5.28}$$

$$\mu^{\bar{\psi}} = -\bar{\psi} + \bar{\psi}^3 - \kappa\nabla^2\bar{\psi} - \Lambda'(\bar{\psi} - \bar{\phi}) \,, \tag{5.29}$$

A Taylor expansion method can then be used to derive the hydrodynamic equations simulated by this lattice Boltzmann method [285]. The resulting equations are Eqs. (5.17)–(5.20)17 with $\eta = n^0(\tau^\rho - 1/2)/3$, $M^{\bar{\phi}} = \tau^{\bar{\phi}} - 1/2$, and $M^{\bar{\psi}} = \tau^{\bar{\psi}} - 1/2$. We performed our simulations on a $250^2$ lattice. The simulation parameters were $\kappa = 0.5$, $\tau^\rho = \tau^{\bar{\phi}} = \tau^{\bar{\psi}} = 1$, $\Delta t = 0.1$, and $\Lambda' = 0.1$.

# 6. PAPER 2: STABILITY OF PROTEIN-DECORATED MIXED LIPID MEMBRANES: THE INTERPLAY OF LIPID-LIPID, LIPID-PROTEIN, AND PROTEIN-PROTEIN INTERACTIONS[1]

ABSTRACT: Membrane-associated proteins are likely to contribute to the regulation of the phase behavior of mixed lipid membranes. To gain insight into the underlying mechanism we study a thermodynamic model for the stability of a protein-decorated binary lipid layer. Here, proteins interact preferentially with one lipid species and thus locally sequester that species. We aim to specify conditions that lead to an additional macroscopic phase separation of the protein-decorated lipid membrane. Our model is based on a standard mean-field lattice-gas description for both the lipid mixture and the adsorbed protein layer. Besides accounting for the lipid-protein binding strength, we also include attractive lipid-lipid and protein-protein interactions. Our analysis characterizes the decrease in the membrane's critical interaction parameter as a function of the lipid-protein binding strength. For small and large binding strengths we provide analytical expressions, numerical results cover the intermediate range. Our results reiterate the crucial importance of the line tension associated with protein-induced compositional gradients and the presence of attractive lipid-lipid interactions within the membrane. Direct protein-protein attraction effectively increases the line tension and thus tends to further destabilize the membrane.

[1] Sylvio May (S.M.) and Anne Hinderliter provided the initial plan for the research presented in this paper. The free energy model development and analytical analysis was done by S.M. and verified by Stephan Loew (S.L.) Phase diagrams were developed by S.L. This paper is published in [157].

## 6.1. Introduction

Peripheral adsorption of proteins (as well as for peptides) onto mixed lipid membranes is an ubiquitous phenomenon in cellular biology. Typically, proteins bind preferentially to one (or more) lipid species while there is no preferential interaction with other lipids. Among a plethora of examples for the dependence of protein binding on membrane composition are phospholipase A2 [295, 147], lysozyme [85], $\alpha$-synuclein [261], cytochrome c [99], various cytoskeletal proteins [203], and antimicrobial peptides [199]. A direct consequence of preferential binding is the sequestration of the favored lipid species by the proteins. That is, in the vicinity of each individual protein the membrane composition is shifted from the average value towards that preferred by the protein. The degree of sequestration depends on the differences in affinity of the protein for the various lipid species. In some cases the sequestration may be small so that it is difficult to detect [82]; yet, in other cases it has been observed experimentally [103, 104, 289, 82] and in molecular simulations [160].

Even in the absence of associated proteins, lipid membranes are able to form lateral domains or to macroscopically phase separate. Most of the current interest to study domain formation in model membranes is motivated by the discovery of lipid rafts in biological membranes and their various functional roles [252, 181]. It is well documented that many binary lipid membranes exhibit non-ideal mixing properties [146, 80, 221]. In presence of cholesterol, appropriate ternary lipid mixtures undergo lateral phase-separation [280, 123]. For a number of mixtures lipid-lipid interaction parameters have been extracted based on fluorescence resonance energy transfer, by means of cross-linking of individual lipids, and heat capacity measurements (reviewed in Ref. [5]).

An unresolved question is how proteins modulate the phase propensity of a mixed bilayer. As discussed recently, proteins may participate in the process of

domain formation actively through attractive protein-protein interactions or passively by interacting preferentially with one lipid species or with the domain interface [5, 59]. Clustering of proteins within lipid domains (or at domain boundaries) has been suggested based on experimental results for a large number of systems, including lipid monolayers [301, 224], model membranes [185, 106, 102, 212, 201, 85, 261, 167] and lipid mixtures from the plasma membrane [15], the latter at sufficiently low temperature. There is also experimental evidence that proteins are able to induce phase separation in both model [93, 208] and biological [151] membranes. Yet, the mechanisms how membrane-associated proteins influence domain formation and phase behavior of the lipid bilayer remain elusive. Current theoretical approaches suggest a role of immobile proteins in the restriction of domain sizes [300], domain formation through wetting of proteins by lipids [81, 1], and a dynamic membrane remodeling through nonequilibrium lipid transport and interactions with membrane proteins [68]. Other models are based on inclusion-induced elastic membrane deformations [245, 235, 236]. Here, proteins are described as rigid inclusions that induce elastic deformations in the host membrane. If that deformation is coupled energetically with one lipid species, an inclusion-induced macroscopic phase transition can result. Still another mechanism, based on the experimentally observed repartitioning of streptavidin protein coats from the liquid-disordered to the liquid-ordered phase upon forming an ordered structure, was suggested by Manley et al.[167]. Here, protein ordering is associated with an entropic penalty that is smaller in the liquid-ordered phase and thus may drive the repartitioning. This mechanism could contribute, quite generally, to the tendency of proteins to repartition into more ordered phases upon their oligomerization [244]. Finally, Monte-Carlo simulations [258, 81, 100, 103] have played a pivotal role in studying the ability of proteins (and also flexible polypeptides [274, 275]) to induce lipid sequestration and domain formation. We note that Monte-Carlo simulations typically employ a lattice model for the mixed membrane. For

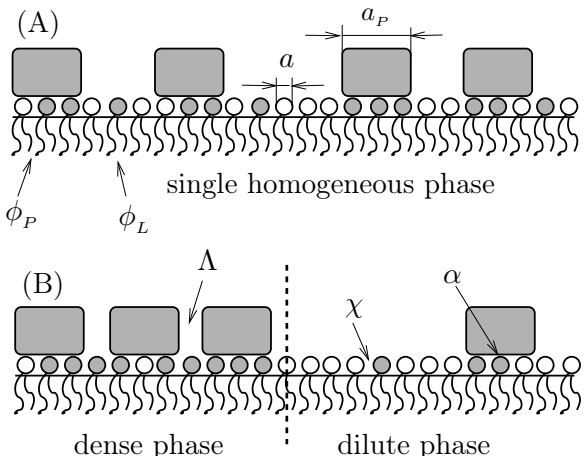


Figure 6.1. Schematic illustration of local lipid segregation (A) versus global phase separation (B). In the former case, proteins (shaded rectangles) bind to a preferred lipid species (lipids with shaded headgroups) without causing the formation of large domains. Even though the membrane compositions, $\phi_P$ and $\phi_L$, within the protein-covered regions and bare membrane, respectively, may differ from each other, the membrane remains homogeneous on a macroscopic scale. In the latter case, there is macroscopic phase separation into a protein-dense and protein-dilute phase. The ability of proteins to induce phase separation depends on the lipid-protein binding strength ($\alpha$), lipid-lipid interaction ($\chi$), and protein-protein interaction ($\Lambda$). The only structural parameter that enters our model is the protein's number of binding sites or, equivalently, protein-to-lipid size ratio $\sigma = a_P/a$ where $a_P$ and $a$ denote the cross-sectional areas per protein and lipid, respectively.

example, Almeida et al.[5] have recently reviewed the quantitative determination of lipid-lipid interaction parameters by modeling fluorescence measurements of protein-induced membrane reorganization through Monte-Carlo simulations. As we shall see below, our present work is based on a similar lattice model, analyzed through mean-field level calculations of phase boundaries.

Proteins that locally sequester lipids of one species do not necessarily induce phase separation of the host membrane. The sequestration is a *local* process that must be distinguished from macroscopic, *global*, phase separation. Fig. 6.1 displays schematically two protein-decorated lipid layers; both sequester lipids underneath the proteins but only layer (B) exhibits macroscopic phase separation whereas layer (A) does not. A theoretical study [174] has addressed the question what interactions

are needed to render a mere sequestration into macroscopic phase separation. It was shown that the presence of attractive interactions among lipids of the same species in the host membrane can be sufficient. In this case, phase separation is driven solely by the *line tension* between the two regions of different composition (that at the protein adsorption sites and that of the bare membrane). The line tension between coexisting fluid-like macroscopic phases in a lipid membrane is on the order of $\approx$ 1pN [270]. It has been suggested to result (at least partially) from the thickness mismatch between the coexisting phases [141, 273]. More generally, the line tension in a non-ideally mixed binary fluid simply results from compositional gradients [228]. Thus, if the host membrane exhibits attractive lipid-lipid interactions, then a line tension appears as a consequence of lipid sequestration at the boundary between a protein adsorption site and bare membrane. Reduction of the line tension contribution is the driving force for protein clustering and phase separation. In a related study [177] detailed electrostatic calculations were presented for a number of generic model proteins adsorbed onto a mixed membrane, corroborating the importance of the line tension for the ability of proteins to induce membrane phase separation.

We note that the above-mentioned previous modeling studies [174, 177] have focused on *indirect*, membrane-mediated, interactions between adsorbed proteins. That is, the presence of attractive interactions between membrane lipids (and the corresponding line tension) can be sufficient to induce phase separation. The influence of *direct* attraction between the adsorbed proteins on the stability of the membrane was not considered. The objective of the present work is thus to include direct protein-protein interactions into the model of Ref. [174]. Specifically, we shall employ a two-state model (see also Ref. [91]) where lipids can reside either at the protein adsorption region or within the bare (protein-free) membrane. The model is investigated on the mean-field level, thereby allowing for (i) a preferential binding of one lipid species with adsorbed proteins, (ii) lipid-lipid attraction within the host membrane, and (iii)

direct protein-protein attraction. Below, we shall characterize these interactions by the three parameters, $\alpha$ (lipid-protein), $\chi$ (lipid-lipid), and $\Lambda$ (protein-protein). In the limits of both small and large lipid-protein binding strength $\alpha$ we shall derive simple analytical expressions that show how attractive interactions among lipids and among proteins can act together to destabilize the composite membrane.

It should be noted that the model employed in the present study is a *minimal* model; it is simple enough to reveal a number of analytical results and a clear understanding of the underlying physics. At the same time it employs various approximations such as its lattice-character, mean-field treatment, and the neglect of membrane-mediated elastic forces. The latter ones act also between proteins adsorbed on a *single-component* lipid membrane and have been studied extensively in that context [87].

## 6.2. Theory

We consider a large planar lipid layer of lateral area $A = Na$ that contains $N$ lipids, each of cross-sectional area $a$. The lipid layer is composed of two different lipid species with molar compositions $\phi$ and $1 - \phi$. Let a number $M$ of proteins be peripherally adsorbed on the lipid layer. The extent of protein coverage on the lipid layer can be characterized by the fraction $\theta = M/M^{max}$ where $M^{max}$ is the maximal number of adsorbed proteins. Note that usually the cross-sectional area per adsorbed protein $a_P$ will be considerably larger than $a$, implying the size ratio $\sigma = a_P/a \gg 1$. In the following we analyze a simple two-state model that is based on a lattice gas description of an incompressible fluid. Here, both the lipid layer and the adsorbed proteins are described as two, energetically coupled, lattice gases. For simplicity, we treat the number of protein adsorption sites to be dictated by area conservation, $a_P M^{max} = aN$, implying $M^{max} = N/\sigma$. In the two-state approximation lipids can

reside in only two energetically distinct states, within either the bare lipid layer or protein-covered regions. We denote the molar compositions corresponding to these two states by $\phi_L$ and $\phi_P$, respectively. On the mean-field (Bragg-Williams) level, we write for the total free energy $f = F/N$ of the protein-decorated lipid layer, measured per lipid,

$$f = \theta f_P(\phi_P) + (1-\theta) f_L(\phi_L) + \frac{f_{pr}(\theta)}{\sigma} + \lambda(\Delta\phi)^2\theta(1-\theta) \,, \tag{6.1}$$

where here and in the following all energies are expressed in units of the thermal energy $k_{\mathrm{B}}T$. In Eq. (6.1), the functions $f_P(\phi_P)$ and $f_L(\phi_L)$ denote the free energies per lipid in protein-covered and protein-free regions of the lipid layer, respectively. The function $f_{pr}(\theta)$, appearing in the third term of Eq. (6.1), accounts for the free energy contribution of the adsorbed protein layer, measured per protein. The additional factor $1/\sigma$ converts to measuring $f$ in units of "per lipid". Finally, the last term in Eq. (6.1) describes the additional line tension between the bare lipid layer and its protein-covered regions. The presence of this term is a consequence of the compositional changes in the lipid layer [228]; within the present two-state model these changes are expressed in terms of the compositional difference $\Delta\phi = \phi_P - \phi_L$ between the protein-covered and protein-free regions. Moreover, the line tension contribution is proportional to the total length of the boundary between the two regions and thus, on the mean-field level, contains the pre-factor $\theta(1-\theta)$. Note that $\lambda$ is a material constant that is independent of $\phi$ and $\theta$.

The free energy $f = f(\phi, \theta)$ (see Eq. (6.1)) is a function of the two independent compositional variables $\phi$ and $\theta$. Note that $\Delta\phi = \Delta\phi(\phi, \theta)$ is not an independent variable but must be determined from the equilibrium condition $\partial f/\partial\Delta\phi = 0$. Hence, the equation describing breakdown of local thermodynamic stability (the spinodal

equation)

$$\frac{\partial^2 f}{\partial \phi^2}\frac{\partial^2 f}{\partial \theta^2} - \left(\frac{\partial^2 f}{\partial \phi \partial \theta}\right)^2 = 0 \,, \tag{6.2}$$

depends on the second derivatives of $f$ with respect to the two degrees of freedom $\phi$ and $\theta$. Even without specifying the structure of the functions $f_P(\phi_P)$, $f_L(\phi_L)$, and $f_{pr}(\theta)$ one may transform Eq. (6.2) into the equivalent expression

$$\begin{aligned} 0 = &\left[f_L''(\phi_L) + 2\lambda\right]\left[f_P''(\phi_P) + 2\lambda\right]\left[\frac{\sigma(\Delta\phi)^2}{f_{pr}''(\theta)} - \frac{1}{2\lambda}\right] \\ &+ 2\lambda + (1-\theta) f_P''(\phi_P) + \theta f_L''(\phi_L) \,. \end{aligned} \tag{6.3}$$

The derivation of Eq. (6.3) is sketched in the appendix (Section 6.6). Note that this form of the spinodal equation is expressed entirely in terms of the second derivatives of the unspecified functions $f_P(\phi_P)$, $f_L(\phi_L)$, $f_{pr}(\theta)$ and as a function of $\Delta\phi$. That is, no derivative of $\Delta\phi$ is involved which will prove valuable for a numerical determination of the spinodal (see below). We also remark that in the limit of vanishing line tension, $\lambda \to 0$, Eq. (6.3) is fulfilled if $f_L''(\phi_L) = 0$ or $f_P''(\phi_P) = 0$. Here, the stability of the lipid and adsorbed protein layers is independent of each other. In the opposite limit, that of large line tension ($\lambda \to \infty$), all compositional changes are suppressed implying $\Delta\phi = 0$ in Eq. (6.3). Hence, in this case the lipid layer remains laterally homogeneous on a microscopic scale.

We note that the free energy in Eq. (6.1) has been considered in a previous study [174] subject to the condition of *fixed* chemical potential $\mu_P = \partial f/\partial\theta$ of the membrane-adsorbed proteins. Clearly, by appropriately choosing $\mu_P$ we may adjust the protein coverage $\theta = \theta(\phi, \mu_P)$ to any desired value. The relevant thermodynamic potential is then $\bar{f} = f - \mu_P\theta$. The corresponding spinodal can be written in the form

$$\frac{d\theta}{d\phi} = \frac{2\sigma\lambda\Delta\phi}{f_{pr}''(\theta)} \,, \tag{6.4}$$

as previously presented in reference [174]. The appendix (Section 6.6) of the present work outlines the derivation of Eq. (6.4).

Let us specify the functions $f_P(\phi_P)$, $f_L(\phi_L)$, and $f_{pr}(\theta)$. In order to include, on the mean-field level, interactions within the lipid layer, between the proteins, and between lipids and proteins, we chose

$$\begin{aligned} f_L(\phi_L) &= f_{mix}(\phi_L) + \chi\phi_L(1-\phi_L) \ , \\ f_P(\phi_P) &= f_L(\phi_P) - \alpha\phi_P \ , \\ f_{pr}(\theta) &= f_{mix}(\theta) + \Lambda\theta(1-\theta) \ , \end{aligned} \tag{6.5}$$

where $f_{mix}(x) = x\ln x + (1-x)\ln(1-x)$ is the free energy (per site of a lattice gas) of ideal mixing. The free energy of the bare, protein-free, lipid layer, $f_L(\phi_L)$, is given by the familiar Bragg-Williams expression for an incompressible binary lattice gas with nearest-neighbor interactions where the effective interaction strength is characterized by the parameter $\chi$. Note that $\chi$ depends on the mutual molecular interactions $\omega_{11}$, $\omega_{22}$, and $\omega_{12}$, among and between the two lipid species, through $\chi = z[\omega_{12} - (\omega_{11}+\omega_{22})/2]$ where $z$ is the coordination number of the lattice. The spinodal of a bare lipid layer is $\chi = 1/[2\phi(1-\phi)]$, implying the critical interaction parameter $\chi_c = 2$ and the corresponding critical composition $\phi_c = 1/2$. That is, for $\chi > \chi_c$ there is a compositional range where the membrane is unstable with respect to macroscopic phase separation.

The second equation, that for $f_P(\phi_P)$, is identical to the one for $f_L(\phi_P)$ apart from an additional favorable interaction of the protein with one lipid species. Assuming that each bound high-affinity lipid contributes the same amount to the protein binding energy renders the interaction term in this equation proportional to $\phi_P$, the composition at the protein adsorption site. The prefactor $\alpha > 0$ (the binding strength per high-affinity lipid, measured in units of $k_{\mathrm{B}}T$) thus provides the driving force for the

adsorption. We note that our model treats the protein-to-lipid size ratio $\sigma$ to be equal to the number of lipid-protein binding sites thus rendering $B = \alpha\sigma$ the maximal protein adsorption strength (which becomes equal to the actual protein adsorption strength in the limit of complete lipid sequestration, $\phi_P \to 1$).

Finally, the free energy, $f_{pr}(\theta)$, of the adsorbed proteins is again given by the Bragg-Williams expression for a binary lattice gas. (Alternative expressions based on the van der Waals gas or scaled particle theory yield more involved expressions for the mixing entropy of membrane-adsorbed proteins [38, 99] – using them would not alter the physical mechanism of protein-induced phase separation studied in the present work.) The interaction strength $\Lambda$ that appears in $f_{pr}(\theta)$ accounts for *direct* interactions between the adsorbed proteins. We shall assume that these interactions alone are insufficient to induce phase separation of the adsorbed protein layer, implying $\Lambda < 2$. This assumption focuses our attention on the influence of the lipid layer in inducing lateral phase separation. We note that the present study extends previous work [174] by including the protein-protein interaction constant $\Lambda$.

We also note that our assumption of a constant $\Lambda$ will not be fulfilled if protein conformation changes as function of coverage $\theta$. Yet, even with constant $\Lambda$ the *total* interaction between proteins includes not only a direct but also an indirect, membrane-mediated, contribution which depends on membrane composition and protein coverage as shown below in Eq. (6.11).

To sum up, we have introduced in Eqs. (6.5) mean-field expressions for the functions $f_L(\phi_L)$, $f_P(\phi_P)$, and $f_{pr}(\theta)$. They involve the three material constants $\chi$, $\alpha$, and $\Lambda$, describing the strengths of lipid-lipid, lipid-protein, and protein-protein interactions, respectively.

The line tension term in Eq. (6.1) represents the excess free energy penalty due to the presence of compositional changes within the lipid layer. Our two-state model involves compositional changes (of magnitude $|\Delta\phi|$) only at the boundaries between

the bare lipid layer and the protein covered regions. The total length of all boundaries is $L = \sqrt{a_P}\theta(1-\theta)M^{max}$ on the mean-field level (where $\sqrt{a_P}$ is the spatial extension of a single protein). On the other hand, the lipid's excess free energy per unit length of the boundary – the line tension – can be written as $F_t/L = b\chi(\Delta\phi)^2/\sqrt{a}$ where $b$ is a numerical prefactor and $\sqrt{a}$ is the spatial extension of a single lattice site (which represents a lipid). Note that the line tension depends on the compositions of the two phases through $\Delta\phi$; it vanishes for $\Delta\phi \to 0$ as would be the case when approaching a critical point. The line tension contribution to the total free energy per lipid is thus $f_t = F_t/N = (b\chi/\sqrt{\sigma})\,(\Delta\phi)^2\theta(1-\theta)$. Comparing this expression with the last term in Eq. (6.1) yields

$$\lambda = b\frac{\chi}{\sqrt{\sigma}}\ . \tag{6.6}$$

We note that the numerical prefactor is generally $b \approx 1$; its exact magnitude depends on the geometry of the protein species or, equivalently, on the curvature of the domain boundary. More specifically, it is $b = 1$ for a perfectly straight boundary. That value would somewhat increase for a curved boundary (as will be the case for finite-sized proteins) and would decrease if the constraint of a sharp, step-like, compositional change between bare lipid layer and protein-covered region was relaxed. In the present work it is convenient and sufficient to simply use $b = 1$.

Let us finally verify consistency of the expression for the line tension, $F_t/L = b\chi(\Delta\phi)^2/\sqrt{a}$, with experiment. For example, Tian et al.[270] obtained $F_t/L \leq 3.3$pN, inside the fluid-fluid coexistence region of a ternary lipid mixture containing cholesterol. That value was observed to decrease towards zero when approaching the critical point. Using reasonable values such as $a = 0.65\,\mathrm{nm}^2$, $\chi = 1$, $b = 1$, our present model predicts $F_t/L = 4(\Delta\phi)^2$pN, in agreement with both the magnitude and pronounced composition dependence measured by Tian et al.[270].

### 6.3. Results and discussion

Eq. (6.1) together with Eqs. (6.5) and (6.6) define the free energy $f = f(\phi, \theta; \chi, \alpha, \Lambda)$ as functions of the two degrees of freedom, $\phi$ and $\theta$, and in terms of the molecular interaction constants $\chi$, $\alpha$, and $\Lambda$. The region of spinodal stability within the $\phi, \theta$-phase diagram is determined by Eq. (6.2) (or, equivalently, by Eq. (6.3) or Eq. (6.4)). A spinodal curve will only exist for $\chi < \chi_c$. Any choice $\chi > \chi_c$ corresponds to a membrane that is stable with respect to lateral phase separation. For the specific choice $\chi = \chi_c$ the spinodal degenerates to a point $\phi_c, \theta_c$ in the $\phi, \theta$-phase diagram. The corresponding *critical* interaction parameter $\chi_c = \chi_c(\alpha, \Lambda)$ can thus be expressed in terms of $\alpha$, and $\Lambda$. Recall, that for a bare (protein-free) membrane $\chi_c = 2$. An interesting question is thus to what extent protein adsorption ($\alpha > 0$) is able to reduce $\chi_c$ below the value of 2. For $\Lambda = 0$ this question has been addressed in previous work [174]. The main objective of the present study is to study the influence of direct protein-protein interactions as expressed through $\Lambda$. The full relation $\chi_c = \chi_c(\alpha, \Lambda)$ can only be calculated numerically (see below). However, in the limits of small and large lipid-protein binding strengths $\alpha$ analytical solutions are available.

In the limit of small binding strength ($\alpha \ll 1$) the solution of the equilibrium condition $\partial f / \partial \Delta\phi = 0$ for the compositional difference $\Delta\phi = \Delta\phi(\phi, \theta)$ can be calculated, yielding

$$\Delta\phi = \frac{\alpha}{\frac{1}{(1-\phi)\phi} - 2(\chi - \lambda)} \ . \tag{6.7}$$

Using this expression in the spinodal equation, we obtain for the critical interaction parameter

$$\chi_c = 2 - \frac{\alpha^2}{8}\, \sigma \, \left[ \frac{1}{1 - \Lambda/2} - 1 \right] \ . \tag{6.8}$$

The corresponding critical compositions are $\phi_c = \theta_c = 1/2$. Eq. (6.8) shows that adsorbed proteins are able to reduce the critical interaction parameter $\chi_c$ of the lipid layer even in the limit of small $\alpha$ if direct protein-protein attraction ($\Lambda > 0$) is present.

The other limit, that of large interaction strength $\alpha \gg 1$, is most conveniently analyzed for fixed chemical potential $\mu_P$ of the membrane-adsorbed proteins; see Eq. (6.4). In this case, the coverage $\theta$ adjusts until all lipids that interact favorably with the proteins are localized within the protein-covered regions. This implies $\phi_L = 0$ and $\theta\phi_P = \phi$. Hence, $d\theta/d\phi = 1/\phi_P$ and $\Delta\phi = \phi_P$. Eq. (6.4) now is equivalent to

$$\chi = \frac{1}{2\sqrt{\sigma}} \frac{1}{\phi_P^2} \left( \frac{1}{\theta(1-\theta)} - 2\Lambda \right) , \tag{6.9}$$

and adopts its minimum for $\phi_P = 1$ and $\theta = 1/2$. Thus, for $\alpha \to \infty$ the critical point is specified by $\phi_c = \theta_c = 1/2$ and

$$\chi_c = \frac{2}{\sqrt{\sigma}} \left( 1 - \frac{\Lambda}{2} \right) . \tag{6.10}$$

In the special case of vanishing protein-protein interactions, $\Lambda = 0$, this coincides with the previously derived result $\chi_c = 2/\sqrt{\sigma}$ [174]. The presence of direct protein-protein attraction further destabilizes the membrane.

For intermediate $\alpha$ the critical interaction parameter $\chi_c$ must be determined numerically. This is most conveniently accomplished using Eq. (6.3) because no derivatives of $\Delta\phi(\phi, \theta)$ appear in that equation. Specifically, we first determine $\Delta\phi$ from solving the equilibrium condition $\partial f/\partial\Delta\phi = 0$. With that, we minimize the spinodal, $\chi = \chi(\phi, \theta)$, in Eq. (6.3) with respect to $\phi$ and $\theta$ . The minimum specifies the critical interaction parameter, $\chi_c$, and the corresponding critical compositions, $\theta_c$ and $\phi_c$, for any given $\alpha$ and $\Lambda$.

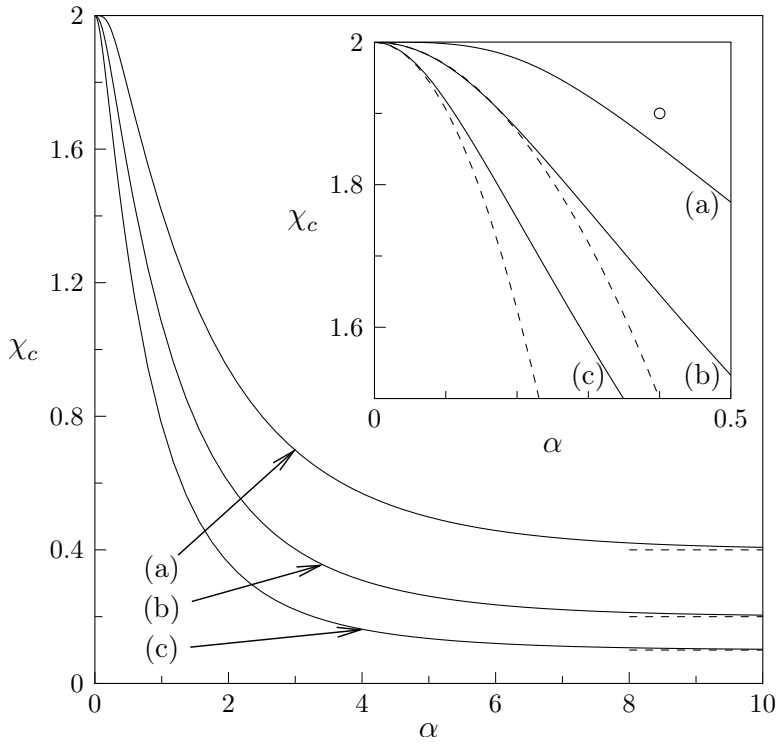


Figure 6.2. The critical interaction parameter $\chi_c$ plotted as a function of $\alpha$. The different curves correspond to $\Lambda = 0$ (a), $\Lambda = 1.0$ (b), and $\Lambda = 1.5$ (c). In all cases $\sigma = 25$. Dashed lines indicate the approximation for large $\alpha$ in Eq. (6.10). The inset shows the same graphs for small $\alpha$. Here the dashed lines correspond to the limiting behavior for small $\alpha$ according to Eq. (6.8). The circle corresponds to the parameters used to calculate the phase diagrams in Fig. 6.4.

Fig. 6.2 shows numerical results for $\chi_c$ as a function of $\alpha$; the three different curves correspond to different choices of $\Lambda$. All curves are calculated for $\sigma = 25$. The prediction for large $\alpha$ according to Eq. (6.10) is indicated by the corresponding horizontal dashed lines. The inset of Fig. 6.2 redisplays the small-$\alpha$ region and shows (dashed lines for curves (b) and (c)) $\chi_c(\alpha)$ according to the analytical result for small $\alpha$; see Eq. (6.8). The numerical results confirm the trend predicted by the analytical expressions in the limits of small and large $\alpha$: Direct protein-protein attraction further destabilizes the membrane.

Let us discuss Fig. 6.2. As reported previously [174] protein-induced phase separation of the lipid bilayer does not require the presence of direct protein-protein

interaction. Indeed, even for $\Lambda = 0$ the critical membrane interaction parameter $\chi_c$ is reduced below its bare-membrane value $\chi_c = 2$; see curve (a) in Fig. (6.2). The reason that phase separation can occur even in the absence of direct protein-protein interactions is the line tension contribution to the membrane's free energy – the last term in Eq. (6.1). That is, adsorbed proteins induce a compositional difference $\Delta\phi$ between the protein-covered and protein-free regions. The corresponding energy penalty can be diminished by protein clustering (thus reducing the total length of the boundary between protein-covered and protein-free regions). Hence, phase separation of the protein-decorated lipid layer is – for $\Lambda = 0$ – mediated entirely by the lipid's line tension. We note that the role of the line tension contribution can also be illustrated by setting $\lambda = 0$ in Eq. (6.1). The result for the critical membrane interaction parameter is then $\chi_c = 2$, irrespective of $\Lambda$ and $\alpha$. Thus, in the absence of line tension ($\lambda = 0$), protein adsorption does not affect the stability of the underlying lipid layer. The presence of direct protein-protein attraction, $0 < \Lambda < 2$, adds another energy penalty in addition to the line tension contribution of the membrane which leads to a further reduction of $\chi_c$. Indeed, both the lipid's line tension contribution in Eq. (6.1) and the protein's nonideal mixing contribution in $f_{pr}(\theta)$ (see Eqs. (6.5)) provide terms $\sim \theta(1-\theta)$. The excess free energy per unit length $L$ of the boundary between the bare lipid layer and protein-covered region is thus

$$\frac{F_t}{L} = [\Lambda\sqrt{\sigma} + b\chi(\Delta\phi)^2]\frac{1}{\sqrt{a}} \,, \tag{6.11}$$

which explicitly shows the two contributions. In particular, because of $\Delta\phi = \Delta\phi(\phi, \theta)$ the line tension depends on lipid compositions and protein coverage.

Increasing the number of binding sites $\sigma$ on the protein reduces the stability of the membrane. This can be seen from our analytical expressions, Eqs. (6.8) and (6.10), in the limits of small and large $\alpha$ respectively. Fig. 6.3, which shows $\chi_c = \chi_c(\alpha)$

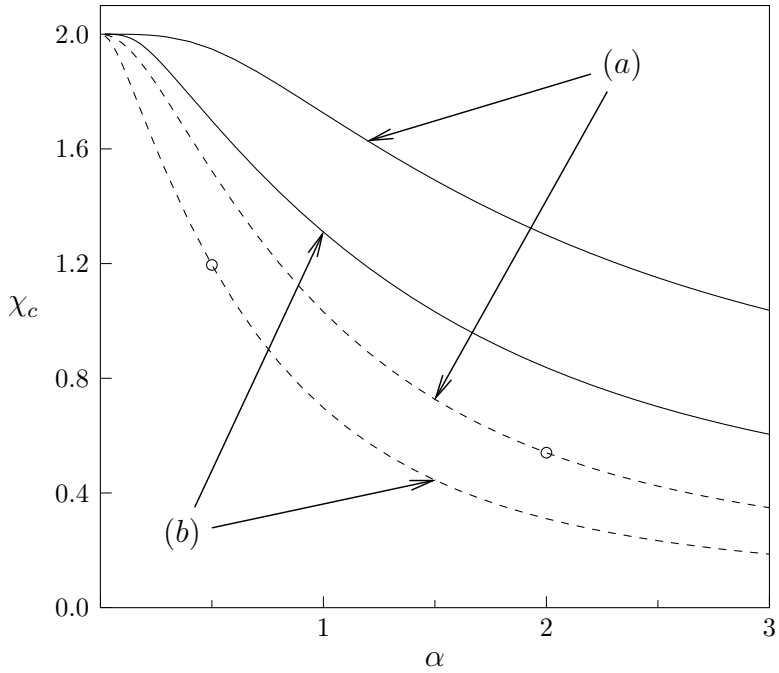


Figure 6.3. The critical interaction parameter $\chi_c$ plotted as a function of $\alpha$. Curves marked (a) and (b) correspond to $\sigma = 9$ and $\sigma = 36$, respectively. Solid curves are calculated for $\Lambda = 0$, dashed curves for $\Lambda = 1.5$. The two open circles mark the critical interaction parameters for $\Lambda = 1.5$ at fixed maximal adsorption strength $B = 18$, calculated for $\alpha = 0.5$ and $\alpha = 2$; see discussion in the text.

for different combinations of $\sigma$ and $\Lambda$, corroborates this behavior for intermediate $\alpha$. Increasing the number of binding sites $\sigma$ on the protein, while conserving the maximal adsorption strength $B = \alpha\sigma$, does not usually (unless $\alpha \gg 1$) reduce $\chi_c$, but it yields a larger slope $\chi_c'(\alpha)$. For example, compare the behavior of $\chi_c$ at the points indicated by the two open circles in Fig. 6.3. Both cases correspond to the same maximal adsorption strength $B = 18$. The larger protein species ($\sigma = 36$ and $\alpha = 0.5$) implies a more stable membrane but increased sensitivity of $\chi_c$ with respect to changes in $\alpha$. This larger sensitivity may be one advantage of having many weak (instead of a single or a few strong) binding sites of a protein with membrane lipids. Many weak binding sites increase the impact of small variations in lipid binding strength on lateral membrane organization.

So far, our analysis has only addressed the behavior of the critical interaction parameter $\chi_c$. For any $\chi > \chi_c$ the protein-decorated lipid layer is unstable in a certain region within the $\phi, \theta$-diagram. Stronger direct protein-protein attraction increases the size of that region. As an illustration Fig. 6.4 presents two phase diagrams, both calculated for $\chi = 1.9$, $\alpha = 0.4$, and $\sigma = 25$. At this particular point (marked by a circle in the inset of Fig. 6.2) it is $\chi > \chi_c$ for any choice of $\Lambda$ (with $\Lambda > 0$). The two phase diagrams in Fig. 6.4 correspond to the specific values $\Lambda = 0$ and $\Lambda = 1$. Displayed are the spinodal lines, which represent solutions of Eq. (6.2), and a number of tie-lines. The tie-lines correspond to solutions of the four familiar coexistence equations

$$\begin{aligned} \left(\frac{\partial f}{\partial \phi}\right)_A &= \left(\frac{\partial f}{\partial \phi}\right)_B , \qquad \left(\frac{\partial f}{\partial \theta}\right)_A = \left(\frac{\partial f}{\partial \theta}\right)_B , \\ f_A - f_B &= (\phi_A - \phi_B)\left(\frac{\partial f}{\partial \phi}\right)_A + (\theta_A - \theta_B)\left(\frac{\partial f}{\partial \theta}\right)_A , \\ \phi &= \frac{\phi_A(\theta - \theta_B) - \phi_B(\theta - \theta_A)}{(\theta_A - \theta_B)} , \end{aligned} \tag{6.12}$$

for the two points $\phi_A, \theta_A$ and $\phi_B, \theta_B$ (with $f_A = f(\phi_A, \theta_A)$ and $f_B = f(\phi_B, \theta_B)$ and given $\phi$ and $\theta$ for any given tie-line). Comparison of the two phase diagrams in Fig. 6.4 corroborates our notion of reduced stability of the protein-decorated lipid layer in the presence of direct protein-protein attraction.

Let us discuss the context of our present model and its possible implications for the interpretation of experimental results. As mentioned in the introduction, protein-induced elastic membrane deformations provide an alternative theoretical concept to explain lateral remodeling of lipid membranes. These models account for proteins that impose elastic deformations onto the mixed host membrane. Examples include transmembrane proteins that have a cone-like shape [39], a mismatch in hydrophobic thickness with respect to their host bilayer [48], or are incorporated into a membrane

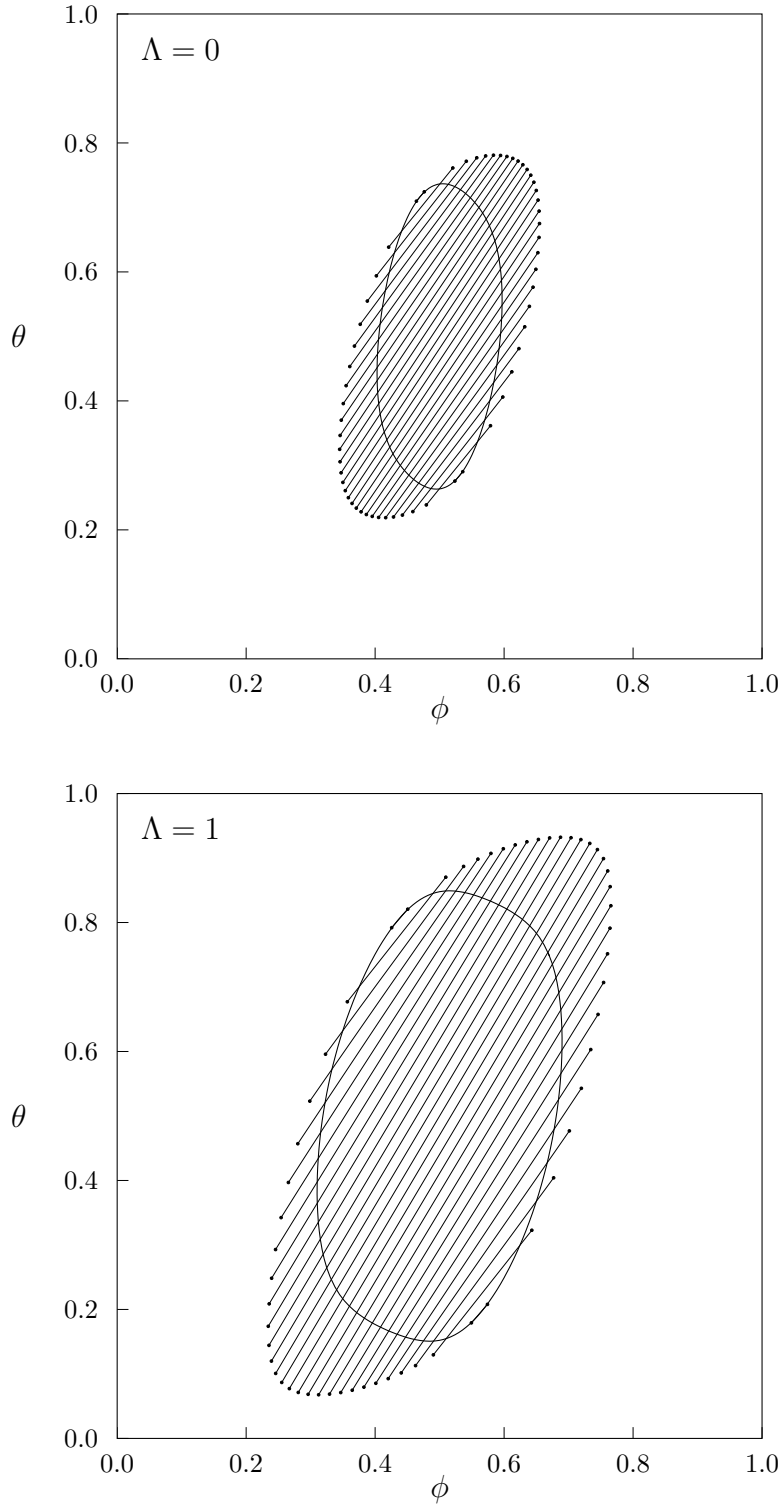


Figure 6.4. Phase diagrams for $\Lambda = 0$ (top) and $\Lambda = 1$ (bottom). In both cases $\chi = 1.9$, $\alpha = 0.4$, and $\sigma = 25$. (The point $\chi = 1.9$ and $\alpha = 0.4$ is marked in the inset of Fig. 6.2 by an open circle.) The closed loops correspond to the spinodal lines. The endpoints of the tie-lines form the binodal region.

that is subject to substantial bending deformations [246]. Similar models have also been applied to mixed membranes [245, 235, 236, 1]. Note that non-elastic interactions are usually ignored in order to extract elasticity-based physical mechanisms. Our present model adopts a complementary approach. It ignores elastic deformations but accounts for specific interactions (lipid-lipid, lipid-protein, and protein-protein). As we demonstrate in the present work, membrane-mediated protein-protein interactions may be strong enough to induce macroscopic phase separation, even in the absence of elastic membrane deformations. Of course, the presence of elastic membrane deformations may further enhance the tendency to phase separate.

Our model is likely to be relevant in a number of situations: First, membrane-matching transmembrane proteins and peripherally-adsorbed proteins are unlikely to evoke significant elastic deformations. For example, membrane reorganization induced by the C2 protein motif in various peripheral proteins has been modeled using Monte-Carlo simulations that employ the same lattice description as we use in the present study [103, 104]. Second, supported membranes and lipid monolayers have reduced capacity to undergo bending deformations. Hence, our model could be relevant for the observed ability of the peripheral protein $\alpha$-synuclein to induce macroscopic phase separation on supported phosphatidylcholine/phosphatidylglycerol membranes [208]. Similarly, it may be used to describe annexin A2-induced formation of large domains in supported bilayers composed of phosphatidylcholine/phosphatidylserine [185]. Finally, recent experiments demonstrated that cross-linking of the minor membrane component ganglioside $GM_1$ by CTB (cholera toxin subunit B) can induce macroscopic phase separation in model [93] and biological [151] membranes. Here, the membrane is primed to undergo phase separate which is initiated by the CTP-induced cross-linking. In terms of our present model the membrane resides close to the phase boundary prior to the cross-linking. Addition of CTP effectively induces *sequestration* of $GM_1$. The

fact that sequestration may give rise to macroscopic phase separation is exactly the subject of our present model.

## 6.4. Conclusions

We have studied the stability of a protein-decorated, mixed lipid layer with respect to lateral phase separation. The proteins are assumed to preferentially interact with only one species of a binary membrane. Starting with the assumption that both the isolated lipid layer and the adsorbed protein layer each on their own are stable ($\chi < 2$ and $\Lambda < 2$), we have addressed the question whether the coupled system is able to undergo phase splitting. The energetics of the protein-decorated lipid layer depends generally on three effective interaction strengths, lipid-protein ($\alpha$), lipid-lipid ($\chi$), and protein-protein ($\Lambda$). Our present model is complete in the sense that it accounts for all these interactions; it extends a previous study [174] in which only the interaction constants $\alpha$ and $\chi$ were taken into account. As in that study, we find that protein adsorption onto a stable binary membrane can induce lateral phase separation as expressed by the reduction of the critical interaction parameter $\chi_c$ even for $\Lambda = 0$. The driving force for the phase transition is the membrane line tension contribution to the free energy. Beyond that we quantify the role of direct protein-protein attraction ($\Lambda > 0$). These generally enhance the destabilization of the lipid layer. That is, both $\chi_c$ is further reduced and the region of instability in the $\phi, \theta$-phase diagram widens as a function of growing $\Lambda$.

## 6.5. Acknowledgments

This work was supported by NIH Grant GM077184. The authors would like to thank Dr. Alexander Wagner for illuminating discussions.

## 6.6. Appendix: Derivation of equations (6.3) and (6.4)

Eq. (6.2), the spinodal equation, defines the boundary between local thermodynamic stability and instability in the $\phi, \theta$-diagram. (For a numerical calculation of the spinodal see the phase diagrams in Fig. 6.4.) To calculate the spinodal based solely on Eq. (6.1) we point out that the two compositions $\phi_P$ and $\phi_L$ in, respectively, the protein-covered and protein-free regions of the lipid layer are connected through the lever rule $\phi = \theta\phi_P + (1-\theta)\phi_L$. Together with the definition of $\Delta\phi = \phi_P - \phi_L$ this implies

$$\phi_P = \phi + (1-\theta)\Delta\phi \;, \qquad \phi_L = \phi - \theta\Delta\phi \;. \tag{6.13}$$

In thermal equilibrium, the compositional difference $\Delta\phi$ adjusts so as to minimize $f$, implying the equilibrium condition $\partial f/\partial\Delta\phi = 0$ must be fulfilled. Using Eq. (6.1) this is equivalent to

$$f_P'(\phi_P) - f_L'(\phi_L) + 2\lambda\Delta\phi = 0 \;, \tag{6.14}$$

which defines the relation $\Delta\phi = \Delta\phi(\phi, \theta)$. Hence, the free energy $f = f(\phi, \theta)$ in Eq. (6.1) depends only on the two compositional degrees of freedom, $\phi$ and $\theta$. Furthermore, partially differentiating the equilibrium condition, Eq. (6.14), with respect to $\theta$ and $\phi$ leads to two equations that can be combined to yield the relation

$$\frac{\partial\phi_P}{\partial\theta}\frac{\partial\phi_L}{\partial\phi} = \frac{\partial\phi_L}{\partial\theta}\frac{\partial\phi_P}{\partial\phi} \;. \tag{6.15}$$

Together with Eq. (6.13) this becomes

$$\frac{\partial\Delta\phi}{\partial\theta} = -\Delta\phi\frac{\partial\Delta\phi}{\partial\phi} \;. \tag{6.16}$$

Using Eqs. (6.13)-(6.16) allows us to calculate the first derivatives

$$\begin{aligned}\frac{\partial f}{\partial \phi} =& f'_L(\phi_L) - 2\lambda\,\Delta\phi\,\theta\ ,\\ \frac{\partial f}{\partial \theta} =& f_P(\phi_P) - f_L(\phi_L) - \Delta\phi f'_L(\phi_L) + \lambda(\Delta\phi)^2 + \frac{f'_{pr}(\theta)}{\sigma}\ ,\end{aligned} \tag{6.17}$$

and from that the second derivatives

$$\begin{aligned}\frac{\partial^2 f}{\partial \phi^2} &= \frac{\partial \phi_L}{\partial \phi}[f''_L(\phi_L) + 2\lambda] - 2\lambda\ ,\\ \frac{\partial^2 f}{\partial \theta^2} &= (\Delta\phi)^2 \frac{\partial \phi_L}{\partial \phi}[f''_L(\phi_L) + 2\lambda] + \frac{f''_{pr}(\theta)}{\sigma}\ ,\\ \frac{\partial^2 f}{\partial \phi \partial \theta} &= -\Delta\phi \frac{\partial \phi_L}{\partial \phi}[f''_L(\phi_L) + 2\lambda]\ .\end{aligned} \tag{6.18}$$

Inserting these relations into the spinodal, Eq. (6.2), gives rise to

$$-\frac{\partial \phi_L}{\partial \phi}\left[f''_L(\phi_L) + 2\lambda\right]\left[\frac{\sigma(\Delta\phi)^2}{f''_{pr}(\theta)} - \frac{1}{2\lambda}\right] = 1\ . \tag{6.19}$$

The derivative $\partial\phi_L/\partial\phi$ can be obtained by differentiating the equilibrium condition for $\Delta\phi$, Eq. (6.14), with respect to $\phi$. The result is

$$\frac{\partial \phi_L}{\partial \phi} = \frac{2\lambda + f''_P(\phi_P)}{2\lambda + (1-\theta) f''_P(\phi_P) + \theta f''_L(\phi_L)}\ . \tag{6.20}$$

Together with Eq. (6.20), the spinodal in Eq. (6.19) yields the final result in Eq. (6.3).

Let us also outline the derivation of Eq. (6.4). The (fixed) chemical potential $\mu_P = \partial f/\partial\theta$ of the membrane-adsorbed proteins is given in Eq. (6.17). Taking the full derivative of $\mu_P$ with respect to $\theta$ results in

$$\frac{d\mu_P}{d\theta} = -\Delta\phi \frac{d\phi_L}{d\theta}\left[f''_L(\phi_L) + 2\lambda\right] + \frac{1}{\sigma} f''_{pr}(\theta) = 0\ . \tag{6.21}$$

Using Eq. (6.21) we eliminate $f_L''(\phi_L)$ from Eq. (6.19). The spinodal, Eq. (6.19), then becomes

$$\frac{\frac{d\phi_L}{d\theta}}{\frac{\partial\phi_L}{\partial\phi}} = \frac{f_{pr}''(\theta)}{2\sigma\lambda\Delta\phi} - \Delta\phi \ . \tag{6.22}$$

But $(d\phi_L/d\theta)/(\partial\phi_L/\partial\phi) = -\Delta\phi + (d\phi/d\theta)$ and we thus obtain Eq. (6.4). We note again that the calculations in this appendix are valid irrespective of the structure of the functions $f_P(\phi_P)$, $f_L(\phi_L)$, and $f_{pr}(\theta)$.

# 7. PAPER 3 : TRANSFER MECHANISM OF TEMOPORFIN BETWEEN LIPOSOMAL MEMBRANES[1]

ABSTRACT: The transfer kinetics of temoporfin, a classic photosensitizer, was analyzed by investigating the influence of total lipid content, temperature, as well as charge, acyl chain length, and saturation of the lipids in donor vesicles using a mini ion exchange column technique. The obtained results are consistent with an apparent first order kinetics in which the transfer proceeds through both liposome collisions and through the aqueous phase. We present a corresponding theoretical model that accounts for the detailed distribution of drug molecules in donor and acceptor liposomes and predicts the transfer rates as a function of drug concentration and number of donor and acceptor liposomes. The experimentally observed transfer rates depended strongly on the temperature and comply with the Arrhenius equation. Thermodynamic calculations indicate the transfer process to be entropically controlled. In terms of the charge of donor liposomes, positively charged liposomes showed transfer rates faster than negatively charged liposomes whereas the maximum amount transferred was almost the same. A more rigid structure of the donor liposomes increases the transfer rate of temoporfin, which is caused by expelling the drug from the membrane interior, as proposed in former work. In summary, our combined theoretical/experimental approach offers a systematic way to study the mechanism of drug release from liposome-based delivery systems.

[1] Experiments were planned, executed and evaluated by Hossam Hefesha, Xiangli Liu, and Alfred Fahr. The theoretical modeling was developed by Stephan Loew and Sylvio May. This paper is published in [98].

## 7.1. Introduction

Unilamellar phospholipid vesicles (liposomes) are often used as drug delivery vehicles for hydrophobic drugs such as cyclosporine A, paclitaxel, amphotericine B or photosensitizers. Poorly water soluble drugs are most likely located within the lipophilic interior of the liposomal membrane as shown e.g. for cyclosporine A [237] and paclitaxel [293]. When transported via liposomes or other nanocarriers, the drug typically accumulates after an i.v. injection at tumor sites because of the "enhanced permeation and retention" (EPR) effect [76]. To become pharmacologically active, the drug must be either endocytosed by the target cells or, as is the case for the lipophilic drugs described earlier, transferred from the liposomal membrane to the tumor cell membranes via collisional or diffusional processes (i.e. without the need to be endocytosed by the tumor cells). However, the drug – while being transported in the liposomal membrane through the blood stream – may also change binding places with blood components like albumin or erythrocytes on the way to the tumor site. Therefore, a balance between losing drug molecules prior to reaching the target site and releasing drugs at the target site must be established by designing the drug-carrier system accordingly.

Early in vitro studies have already shown [43], that porphyrins administered in liposomes to HeLa-cells are more efficient than conventionally administered porphyrin, even if serum is present in the cell culture medium. Furthermore, results from in vivo studies in tumor-bearing rats indicate [120], besides an enhanced therapeutic efficiency, that porphyrins administered in liposomes are to a large extent not complexing with serum albumin. The authors conclude, that these differences "imply a different mechanism of interaction with receptors and/or serum proteins". Clearly, an analysis of the transfer mechanism of drug molecules from liposomes to a target site is likely to help optimizing the delivery system. In addition, such transfer studies may also

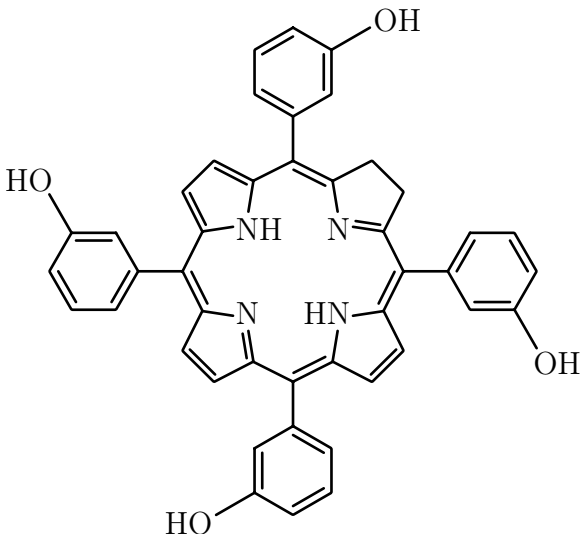


Figure 7.1. Chemical structure of temoporfin.

elucidate the pathway of the drug from the target cells to the place of action inside the cell, as liposomal membranes also serve as model systems for cell membranes. In the present study, we focused on temoporfin (mTHPC) as one of the few approved porphyrins in cancer therapy to date. Temoporfin belongs to the second generation photosensitizers clinically used under the trade name of Foscan® [24]; its structure is depicted in Fig. 7.1.

Besides being a therapeutically used drug, its high lipophilicity (X. Liu, unpublished: $\log P_{lipid\ membrane/water} = 9.25$), its fluorescence properties, and its availability as a $^{14}$C derivative predestine it for the investigations described in the present work. Specifically, using mTHPC and the radiolabeled [$^{14}$C]mTHPC as tracer, the kinetics of temoporfin transfer between unilamellar vesicles was measured by a previously optimized method [67] and analyzed. The influence of total lipid content, temperature, charge of donor vesicles, and fatty acyl chain structure of phospholipids in donor vesicles was investigated.

## 7.2. Experimental procedure

### *7.2.1. Materials*

1,2-Dipalmitoyl-sn-glycero-3-phosphocholine (DPPC) and 1,2-distearoyl-sn-glycero-3-phosphocholine (DSPC) were purchased from Sygena LTD (Switzerland). 1,2-Dimyristoyl-sn-glycero-3-phosphocholine (DMPC), 1,2-dibehenyl-sn-glycero-3-phosphocholine (DBHPC), 1,2-dioleoyl-sn-glycero-3-phosphocholine (DOPC), 1-stearoyl-2-oleoyl-sn-glycero-3-phosphocholine (SOPC) and 1,2-dioleoyl-3-trimethylammonium-propane sodium salt (DOTAP) were purchased from Avanti Polar Lipids (Alabaster, AL, USA). 1-Palmitoyl-2-oleoyl-3-sn-glycero-3-phosphocholine (POPC) was purchased from Genzyme Pharmaceuticals (Liestal, Switzerland). Meta-tetrahydroxyphenylchlorin ($^{14}$C-temoporfin; [$^{14}$C]mTHPC) was kindly provided as a gift from Biolitec AG (Jena, Germany). Cholesterol (Chol), dicetylphosphate (DCP), pre-set crystals and sodium azide were obtained from Sigma Chemical Co. (St. Louis, MO. USA). Diethylaminoethyl (DEAE) Sepharose$^{TM}$ CL-6B and Carboxymethyl (CM) Sepharose$^{TM}$ Fast Flow preserved in 20% ethanol were purchased from GE Healthcare Bio-Sciences AB (Uppsala, Sweden). Sucrose was purchased from Carl Roth GmbH (Karlsruhe, Germany). Radioactive substances $^{3}$H-cholesteryl-oleate (1 mCi/mL) and $^{14}$C-cholesteryl-oleate (100 Ci/mL) were purchased as a stock solution in the toluene solvent from GE Healthcare UK Ltd (Amersham radiochemicals) (Buckinghamshire, UK). Sodium chloride was purchased from Merck KgaA (Darmstadt, Germany).

### *7.2.2. Methods*

Preparation of donor and acceptor liposomes: Liposome preparation was carried out by a well-established thin-film hydration method. Chloroform solution of lipids and [$^{14}$C]mTHPC was dried at a temperature at least 10° above the gel-to-liquid crystalline phase transition ($T_m$) of the lipid used by using a Rotavapor® R114 (Büchi,

Essen, Germany) at 60 rpm and escalating vacuum (200 mbar for 15 min, 100 mbar for 15 min and 50 mbar for 60 min) and finally under a stream of $N_2$, till no chloroform could be detected. The dried film was hydrated by Trizma buffer saline (pH7.4; 10 mM). The resulting film was completely dispersed by vortexing for 10 min. The suspension was equilibrated for 2 h. The resulting liposome suspension was extruded through a polycarbonate membrane filter with a pore diameter of 100 nm [164]. The final donor vesicle composition was 70 mol% phospholipid, 10 mol% DCP, 20 mol% of Chol loaded with an appropriate amount of mTHPC and appropriate amounts of [$^{14}$C]mTHPC. Acceptor vesicles comprised 80 mol% POPC and 20 mol% of Chol. Particle size analysis and Zeta-potential measurements of the vesicles were determined by photon correlation spectroscopy (PCS) using a Zetasizer Nano ZS (Malvern, UK). The samples were diluted with Milli-Q water and measured at 25°C. Liposomes were routinely checked for lamellarity by Cryo-Transmission Electron Microscopy (Cryo-TEM).

Production of micro-columns and separation of vesicles and drug transfer measurements are described in [67] in great detail, therefore we refer to this publication for the description of the whole methodology. The principal method of vesicle population separation is depicted in Fig. 7.2. The samples were analyzed by liquid scintillation counting (LSC) using a Liquid Scintillation Analyzer Tri-Carb 2800TR (PerkinElmer, USA).

### *7.2.3. Method validity*

In a series of validation experiments, the recovery of the acceptor vesicles and the retention of the donor vesicles in the separation columns were investigated. An appropriate amount of donor vesicles containing $^{3}$H-cholesteryl-oleate and acceptor vesicles containing $^{14}$C-cholesteryl-oleate as non-exchangeable markers [64] and a

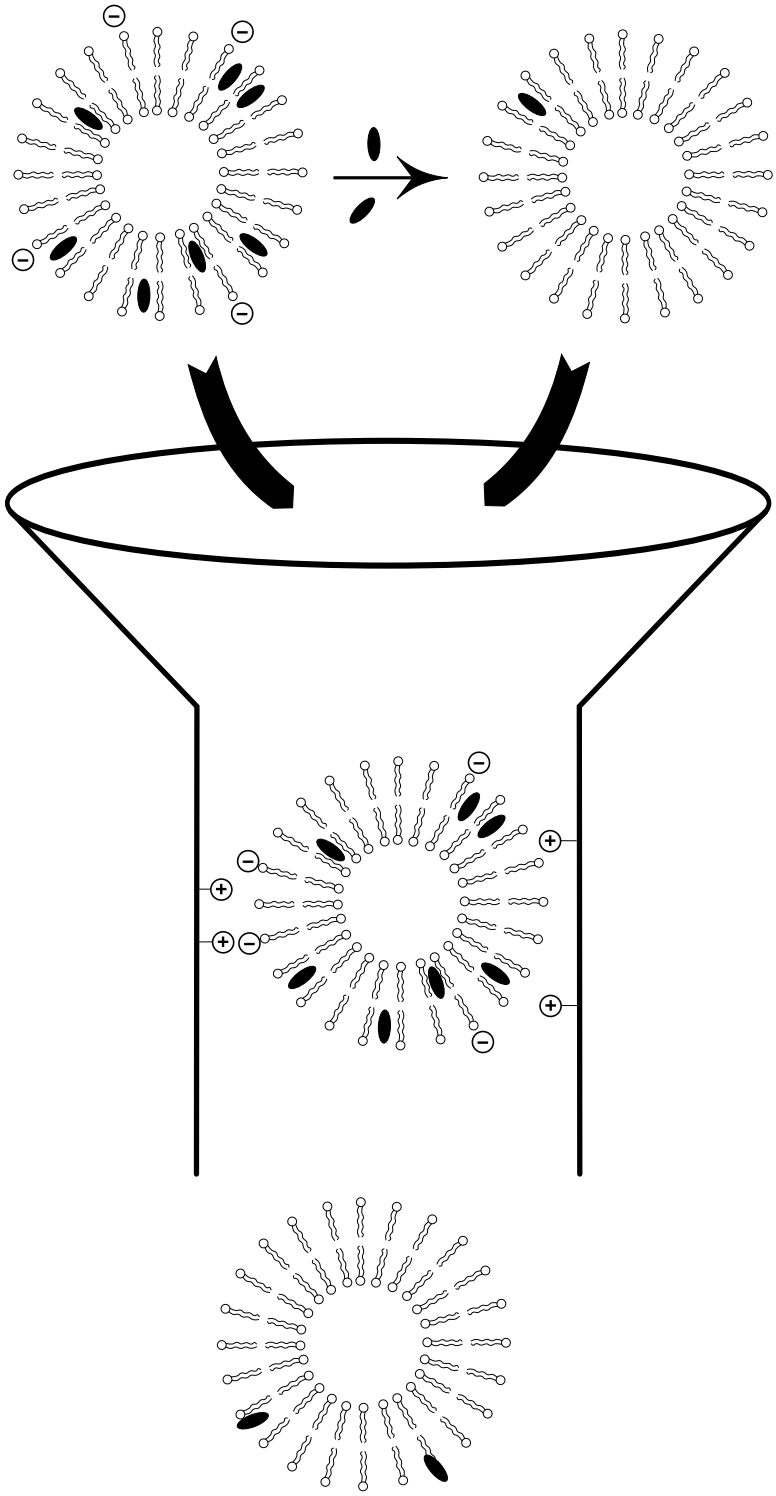

Figure 7.2. Methodology of temoporfin transfer measurement between liposomal membranes. Micro-columns made of Perspex® were filled with DEAE Sepharose™ CL-6B or CM Sepharose™ Fast Flow equilibrated in iso-osmolar sucrose (modified from [67]).

mixture of them were applied to each of the six micro-columns. The marker amount in the eluates was examined by LSC.

### *7.2.4. Effect of total lipid content on [$^{14}$C]mTHPC transfer kinetics*

For the investigation of the [$^{14}$C]mTHPC transfer mechanism regarding the total lipid concentration, the rate of the [$^{14}$C]mTHPC transfer was examined over a wide range of total lipid concentrations at 37 ± 1°C. The donor vesicle (DMPC:Chol:DCP; 7:2:1) concentrations were 0.1, 1, and 2 mg/mL, while the acceptor vesicle (POPC:Chol; 8:2) concentrations were 1, 10, and 20 mg/mL keeping the ratio between donor and acceptor lipid constant at 1:10.

### *7.2.5. Effect of temperature on [$^{14}$C]mTHPC transfer kinetics*

The temperature dependence of mTHPC transfer kinetics between large unilamellar liposomes was investigated at four different temperatures 15, 22, 30, and 37°C (±1°C). Vesicles were mixed at a concentration of 0.1 mg of donor vesicle lipid/mL (DMPC:Chol:DCP; 7:2:1) and 5.0 mg of acceptor vesicle lipid/mL (POPC:Chol; 8:2). The activation energy for this process between 15 and 37°C was calculated according to the Arrhenius equation. Enthalpy, entropy, and free energy were calculated from the van't Hoff equation.

### *7.2.6. Effect of donor liposomes charge on mTHPC transfer kinetics*

The influence of the donor liposome charge on mTHPC transfer kinetics was investigated by using positively and negatively charged vesicles as donors at 37 ±1°C. Positively charged vesicles comprised (DOPC/DOTAP/Chol; 5:3:2) while negatively charged vesicles were composed of (DOPC/DCP/Chol; 7:1:2). Acceptor vesicle composition was (POPC:Chol; 8:2). Vesicles were mixed at a concentration of 1 mg of donor vesicles (lipid/mL) and 10 mg of acceptor vesicles (lipid/mL).

### *7.2.7. Effect of donor lipid saturation on mTHPC transfer kinetics*

To further evaluate the inner bilayer structure influencing the transfer kinetics of mTHPC, the sensitivity of transfer to variation in the lipid acyl chain saturation was examined. While keeping the phosphocholine head group and chain length constant, the fatty acids for 1,2-diacyl species were varied in terms of the degree of saturation. The donor vesicle composition was 70 mol% of (DOPC or SOPC or DSPC), 20 mol% Chol, and 10 mol% DCP. Acceptor vesicles comprised 80 mol% POPC and 20 mol% Chol. The donor lipid concentration was 1 mg/mL while the acceptor lipid concentration was 10 mg/mL and the temperature was kept at 37±1°C.

### *7.2.8. Effect of acyl chain length of donor vesicles on mTHPC transfer kinetics*

This experiment was an extension to the aforementioned one in order to investigate the influence of acyl chain length (rigidity) of donor liposomes on the mTHPC transfer between liposomal membranes. The phospholipid head groups were kept constant, while the 1,2-diacyl fatty acids were varied in terms of acyl chain length. The donor vesicle composition was 70 mol% of [DMPC (14:0/14:0) or DPPC (16:0/16:0) or DSPC (18:0/18:0) or DBHPC (22:0/22:0)], 20 mol% Chol, and 10 mol% DCP. Acceptor vesicles comprised 80 mol% POPC and 20 mol% Chol. The donor lipid concentration was 1 mg/mL while the acceptor lipid concentration was 10 mg/mL at a temperature of 37±1°C.

### *7.2.9. Calculations*

The transfer curves of the percentage mTHPC transferred over time were fitted using Microcal Origin 6.0 software (OriginLab Corporation, US-Northampton) using

the exponential function:

$$y = y_\infty \left(1 - e^{-K(t-t_0)}\right) \ . \tag{7.1}$$

Here, $y$ is the percentage of mTHPC transferred to the acceptor vesicles at time $t$, and $y_\infty$ denotes the final percentage of mTHPC transferred, corresponding to the height of the plateau. Conducting the experiments involves a small time offset $t_0$ that is incorporated in Eq. (7.1). The constant $K$ is the apparent rate constant of the transfer.

In the appendix (Section 7.7) we derive Eq. (7.1) from a simple kinetic transfer model that accounts for two different transfer mechanisms, collisions between liposomes (characterized by a rate constant $K_c$) and diffusion of mTHPC through water (characterized by a rate constant $K_d$). The apparent rate constant is then $K = K_d + cK_c$ where $c$ is the total concentration of liposomes (both donor and acceptor) in the aqueous solution. For further details we refer to the appendix (Section 7.7). The dependence of the measured rate constants $K$ on the concentration of donor and acceptor liposomes suggests the transfer mechanism to be controlled either by diffusion or collisions.

Half life corresponding to Eq. (7.1) can be calculated from $K$ as

$$t_{1/2} = (\ln 2)\,/K \ . \tag{7.2}$$

The apparent transfer coefficient ($K_{D\to A}$) of mTHPC between donor vesicles and acceptor vesicles was calculated from the following equation:

$$K_{D\to A} = C_A/C_D \tag{7.3}$$

with $C_A$ being the concentration of mTHPC in the acceptor vesicles at equilibrium and $C_D$ the concentration of mTHPC in the donor vesicles at equilibrium at a given temperature. Note that $K_{D\to A}$ is simply the equilibrium constant corresponding to the reaction $D \rightleftharpoons A$ of transferring drug molecules from donors (D) to acceptors (A). The temperature dependence of $K_{D\to A}$ is given from a van't Hoff plot of $\ln(K_{D\to A})$ versus $T^{-1}$:

$$\ln K_{D\to A} = -\Delta H/RT + \Delta S/R \tag{7.4}$$

where, $-\Delta H/R$ refers to the slope of this linear dependence, and $\Delta S/R$ is the intercept. $\Delta H$ (J mol$^{-1}$) is the enthalpy of the transfer, $\Delta S$ (J mol$^{-1}$ K$^{-1}$) is the entropy of the transfer, $T$ is the absolute temperature, and $R = 8.3145$ J mol$^{-1}$ K$^{-1}$. Once $\Delta H$ and $\Delta S$ are known, the Gibbs free energy $\Delta G$ of the transfer can be calculated from the expression:

$$\Delta G = \Delta H - T\Delta S\ . \tag{7.5}$$

### 7.3. Results

The average diameter of donor and acceptor liposomes prepared by extrusion exhibited a polydispersity index less than 0.10 indicating a narrow vesicle size distribution. More than 93% of the donor liposomes were unilamellar, the remaining small fraction showing only bilamellarity. In order to evaluate the validity of the method in terms of donor retention and acceptor recovery, a control experiment was carried out using non-exchangeable markers. With pre-equilibrated columns, 99% of donor liposomes (charged vesicles) were retained. For the acceptor liposomes (neutral vesicles), $91 - 99\%$ were recovered in the eluate. The measured acceptor recovery is a significant improvement over the recoveries reported ($40\% - 70\%$) by van den

Table 7.1. Total lipid, rate constants, half-life, and maximum percent transferred of temoporfin transfer depending on total lipid content. Donor liposomes (DMPC/DCP/ Chol=7:1:2) were 110 nm (PDI 0.06), Zeta-potential -33.4 mV, and preloaded with temoporfin. Acceptor liposomes (POPC/Chol= 8:2) were 115 nm (PDI 0.04) and Zeta-potential -0.36 mV. The ratio of donor lipid to acceptor lipid was 1:10 mg/mg, the temoporfin: lipid ratio in donor liposomes was 0.01:10 mg/mg.

| Total lipid mg/mL | $K$/h$^{-1}$ | $t_{1/2}$/h | Max.% transferred |
|---|---|---|---|
| 1.1 | 0.19 ± 0.02 | 3.65 | 74.70 |
| 11 | 0.28 ± 0.03 | 2.48 | 79.39 |
| 22 | 0.40 ± 0.04 | 1.73 | 86.34 |

Besselaar et al. [277] and recoveries ($80 - 95\%$) obtained by McLean and Phillips [180].

To gain insight into the mTHPC transfer mechanism, the rate of transfer was examined over a range of total lipid concentrations. Table 7.1 and Fig. 7.3 report the results of mTHPC transfer experiments in which the donor:acceptor vesicle ratio was kept constant, while the total lipid concentration was varied. The transfer (Fig. 7.3a) can be described very well by a simple exponential function (see Eq. (7.1)). To compare with the transfer model presented in the appendix (Section 7.7) we have plotted in Fig. 7.3b the rate constant $K$ as a function of the total lipid concentration (as stated in Table 7.1). Also shown in Fig. 7.3b is a linear fit, which relates the experimental data to the theoretically predicted relation for $K$. The fit exhibits both a finite slope and a finite intercept, suggesting that transfer through both diffusion and collision mechanisms contributes to the experimentally observed data. However, the reliability of this interpretation is weakened by the small number of data points and by the simplifying assumptions of the model in the appendix (Section 7.7). In particular, the non-ideality of the mixture of drug molecules in donor and acceptor vesicles (including self-assembly and aggregation phenomena) is not accounted for by the theoretical model in the appendix (Section 7.7) or by any other previous modeling

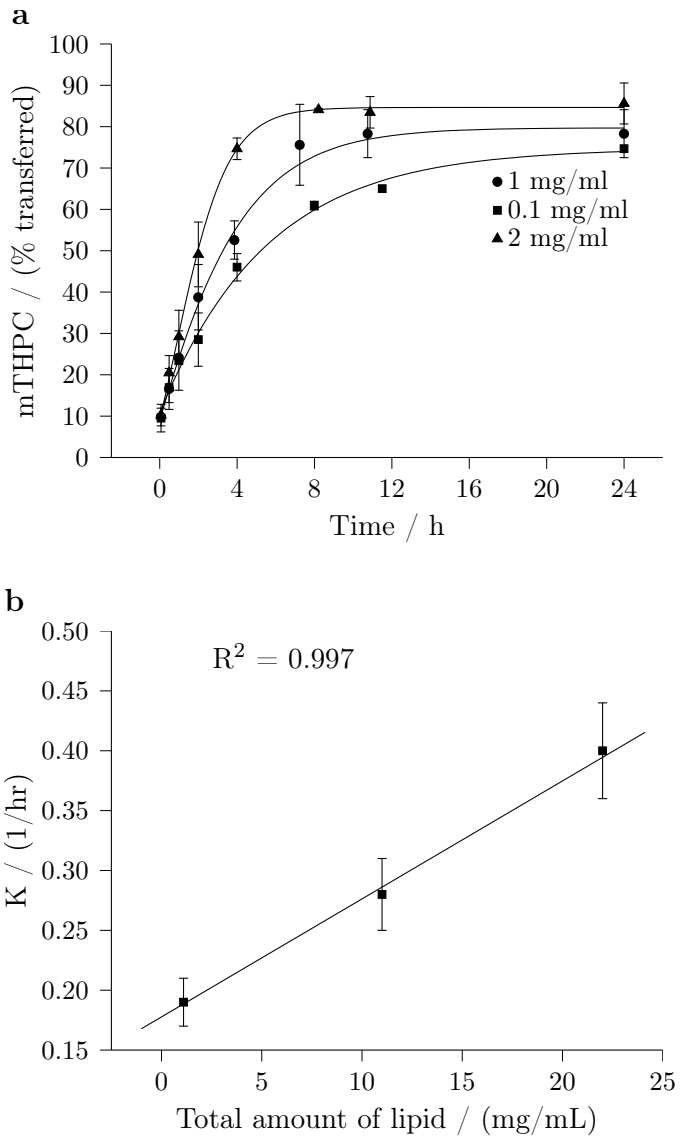


Figure 7.3. a) Temoporfin transfer between liposomes at three different lipid concentrations at 37°C (±1°C). Donor liposomes (DMPC/DCP/Chol= 7:1:2) were 110 nm (PDI 0.06), Z-potential -33.4 mV, and preloaded with temoporfin. Acceptor liposomes (POPC/ Chol= 8:2) were 115 nm (PDI 0.04) and Zeta-potential -0.36 mV. The ratio between donor and acceptor was 1:10. Error bars represent ±SEM (n= 6). The molar drug: donor lipid ratio was 1:867. b) Calculated total lipid content plotted versus transfer constants (see Table 7.1).

Table 7.2. Rate constants, half-life and maximum percent transferred of temoporfin transfer regarding temperature and donor vesicle's charge. Donor liposomes (DMPC/DCP/Chol=7:1:2) were 90 nm (PDI 0.08), Zeta-potential -33.4 mV, and preloaded with temoporfin. Acceptor liposomes (POPC/Chol= 8:2) were 115 nm (PDI 0.04) and Zeta-potential 0.36 mV. For the comparison between oppositely charged donor liposomes (at 37°C), the negatively charged ones were composed of DOPC/DCP/Chol; 7:1:2, while positively charged ones were prepared from DOPC/DOTAP/Chol 5:3:2. Acceptor liposomes (POPC/Chol= 8:2) were 115 nm with (PDI 0.04) and Zeta-potential -0.36 mV. Donor lipid concentration was 1 mg/mL while acceptor lipid concentration was 10 mg/mL. The molar drug:donor lipid ratio was 1:867. The ratio between donor and acceptor was 1:50 in order to achieve sink conditions.

| Temperature-dep. | | | | | | | Charge-dep. | | |
|---|---|---|---|---|---|---|---|---|---|
| Temp/°C | 15 | 19 | 22 | 25 | 30 | 37 | Donor charge | − | + |
| $K$/h$^{-1}$ | 0.05 | 0.07 | 0.09 | 0.12 | 0.17 | 0.24 | $K$/h$^{-1}$ | 0.26 | 0.43 |
| SDev/h$^{-1}$ | 0.01 | 0.01 | 0.06 | 0.04 | 0.04 | 0.03 | SDev/h$^{-1}$ | 0.03 | 0.06 |
| $t_{1/2}$/h | 13.9 | 9.9 | 7.7 | 5.8 | 4.1 | 2.9 | $t_{1/2}$/h | 2.67 | 1.61 |
| Max trans./% | 24.35 | 34.32 | 51.5 | 60.2 | 70.44 | 88.41 | $\text{Transf}_{24\text{ h}}$/% | 65.31 | 72.29 |

attempt [117]. There clearly is a need to develop and make available more realistic modeling approaches. Our model also does not account for the small offset at $t = 0$ (for example visible in Figs. 7.3 and 7.5). In our experience this is due to drug bound to the surface, which can be transferred fast to the acceptor liposomes.

The obtained results of the experiments designed to examine the sensitivity of transfer rate constants to temperature are presented in Table 7.2 and Fig. 7.3a. The sensitivity of the transfer rate on the phase transition temperature (22°C) for DMPC can be easily seen. In the chosen temperature range (15–37°C), an increase in the transfer rate constants and the maximum amount transferred can be easily noticed.

A plot of log K over 1/T (see the right diagram in Fig. 7.4) suggests two different linear regimes, separated by the main phase transition temperature (22°C) of DMPC which is the major lipid in the donor liposomes. The corresponding fits to the Arrhenius equation yield activation energies of 56 kJ/mol below the main transition temperature and 44 kJ/mol above the main transition temperature. The somewhat

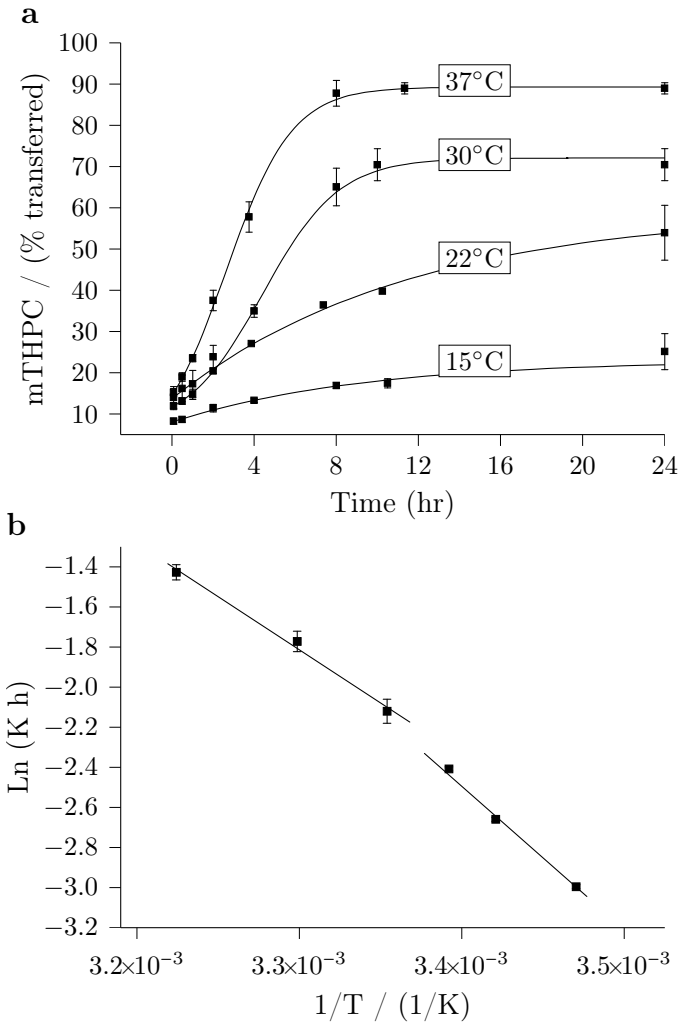


Figure 7.4. a) Temoporfin transfer between liposomes at four representative temperatures 15, 22, 30, and 37°C(±1) from Table 7.2. Donor liposomes (DMPC / DCP / Chol= 7:1:2) were 90 nm (PDI 0.08), Zeta-potential -33.4 mV, and preloaded with temoporfin. Acceptor liposomes (POPC/Chol = 8:2) were 115 nm (PDI 0.04) and Zeta-potential -0.36 mV. Error bars represent ±SEM (n = 9). The molar drug:donor lipid ratio was 1:867. b) Arrhenius plot of all temperature points from Table 7.2 and piecewise fit to the Arrhenius equation.

smaller activation energy in the fluid phase state may reflect a less severe perturbation of the lipid matrix upon transferring mTHPC from the hydrocarbon core of the lipid bilayer into the aqueous region outside the membrane.

We note, that the transfer kinetics for the higher temperatures, 30 and 37°C, exhibits a point of inflection, thus implying sigmoidal behavior. This generally is the

result of some kind of cooperativity in the transfer process. We do not know what molecular mechanism causes cooperative behavior in our experiments. A possible scenario is the presence of attractive interactions between mTHPC molecules in the liposomes. This would make the inter-liposomal transfer of mTHPC more favorable if a target liposome already contains mTHPC. Another possibility is that mTHPC molecules residing in acceptor liposomes generate defects (particularly at higher temperatures) that increase the probability of additional mTHPC molecules to be transferred from donor to acceptor liposomes. If this cooperative enhancement is sufficiently strong, it leads to an inflection point (i.e., sigmoidal behavior) in the corresponding kinetics.

To investigate the role of donor liposome charge on the mTHPC transfer rate, we used binary lipid mixtures as compiled in Table 7.2. These mixtures are composed of DOPC either with DOTAP or with DCP, yielding positively and negatively charged vesicles, respectively. From Table 7.2 and Fig. 7.5 we conclude that positively charged liposomes exhibit faster transfer rates than negatively charged liposomes. The observed transfer rate of positively charged liposomes ($0.43\pm0.06$ $h^{-1}$) was about 1.7-times larger than that of the negatively charged liposomes ($0.26\pm0.03$ $h^{-1}$). In terms of the maximum amount transferred, the measured percentages 65.3% and 72.3% for negatively and positively charged liposomes, respectively, do not indicate a significant difference. The influence of the degree of saturation of the phospholipid fatty acid chains used in donor liposomes is presented in Table 7.3. It is evident that there is no significant difference between the transfer rate constants of DOPC (18:1/18:1, $T_m = -20°C$) and SOPC (18:0/18:1, $T_m = +6°C$), whereas for DSPC (18:0/18:0, $T_m = +55°C$) about 4-fold higher value (1.0 $h^{-1}$) was observed. Since membrane rigidity is increased with the increase in hydrocarbon saturation, a potential relationship between transfer rate and rigidity is evident.

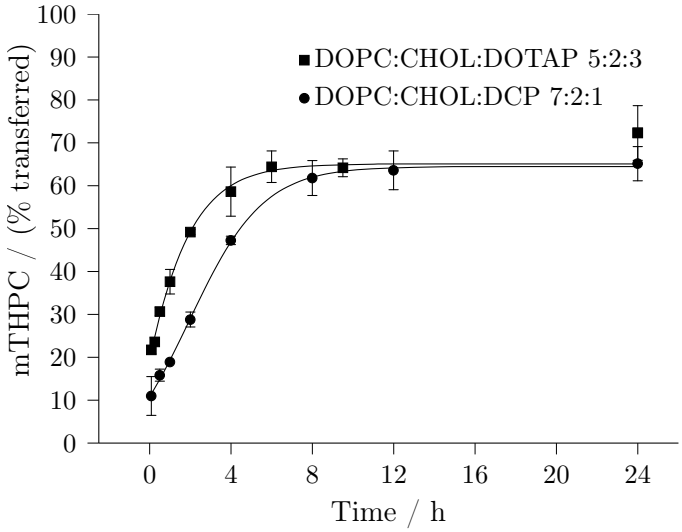


Figure 7.5. Temoporfin transfer between negatively and positively charged donor and neutral acceptor liposomes at 37°C (±1°C). Donor liposomes formulated as (DOPC/DCP/Chol = 7:1:2) and (DOPC/DOTAP/Chol = 5:3:2) loaded with temoporfin. Acceptor liposomes (POPC/Chol = 8:2) were 114.8 nm (PDI 0.04) and Zeta-potential -0.36 mV. The ratio between donor and acceptor was 1:10, being below sink conditions in order to detect additional processes easier. Error bars represent ±SEM (n = 6). The molar drug:donor lipid ratio was 1:867.

Table 7.3. Phase transition temperatures, rate constants, half-life and maximum percent transferred of temoporfin transfer regarding donor lipid saturation and donor lipid acyl chain length at 37°C. Donor liposomes (PhL/DCP/Chol = 7:1:2) preloaded with temoporfin had PDIs less than 0.10. Acceptor liposomes (POPC/Chol = 8:2) were 115 nm (PDI 0.04) and Zeta-potential -0.36 mV. The donor and acceptor lipid concentrations were 1 mg/mL and 10 mg/mL, respectively.

| Lipid type | DOPC | SOPC | DSPC | DMPC | DPPC | DBHPC |
|---|---|---|---|---|---|---|
| $T_m$/°C | -20 | +6 | +55 | +22 | +41 | +75 |
| Liposome size/nm | 88.0 | 89.0 | 100.9 | 110 | 100.8 | 168.3 |
| $K$/h$^{-1}$ | 0.26±0.03 | 0.18±0.01 | 1.00±0.11 | 0.28±0.03 | 0.35±0.03 | 1.24±0.30 |
| Max. % transf. | 65.31 | 83.63 | 82.01 | 79.39 | 86.38 | 75.51 |

As an extension of the former experiment, the influence of fatty acyl chain length was examined. With the four di-saturated phospholipids used [(DMPC 14:0/ 14:0, $T_m$ = +22°C), (DPPC 16:0/16:0, $T_m$ = +41°C), (DSPC 18:0/18:0, $T_m$ = +55°C), and (DBHPC 22:0/22:0, $T_m$ = +75°C)] the transfer rate was faster for the phospholipids having longer chains; the temperature (37°C) in these experiments was either below or above their respective phase transition temperatures (Table 7.3 and Fig. 7.6).We find that there is no significant difference between the transfer rate of DMPC(0.28±0.03 $h^{-1}$) and DPPC (0.35±0.03 $h^{-1}$). The transfer rate constants for DSPC and DBHPC increased to about 4-fold (1.00±0.11 $h^{-1}$ and 1.24±0.30 $h^{-1}$ respectively). The maximum amount transferred was almost the same as the plateaus were reached at 79%, 86%, 82%, and 75% for DMPC, DPPC, DSPC, and DBHPC respectively.

## 7.4. Discussion

The assessment of inter-membrane transfer properties yields valuable information about the use of liposomes as solubilisers or as targeting devices for lipophilic drugs. In addition, the transfer properties may be predictive to some extent for the distribution and retention kinetics of drugs in biomembranes after parenteral administration [64]. It is well known that with increasing incubation time, photosensitizers (temoporfin) can migrate from the plasma membrane to the more sensitive stores within the cell [189].

The inter-membrane transfer phenomenon was first described as part of membrane biochemistry studies with liposomes as model systems for biological membranes [64]. Previously, two different models have been suggested to explain the transfer of lipophilic or amphiphilic membrane components between two lipid domains (either inter-membrane transfer or transfer from membrane to, e.g. plasma components). The first model proposes a collision mechanism for, e.g. phosphatidylcholine [117] and

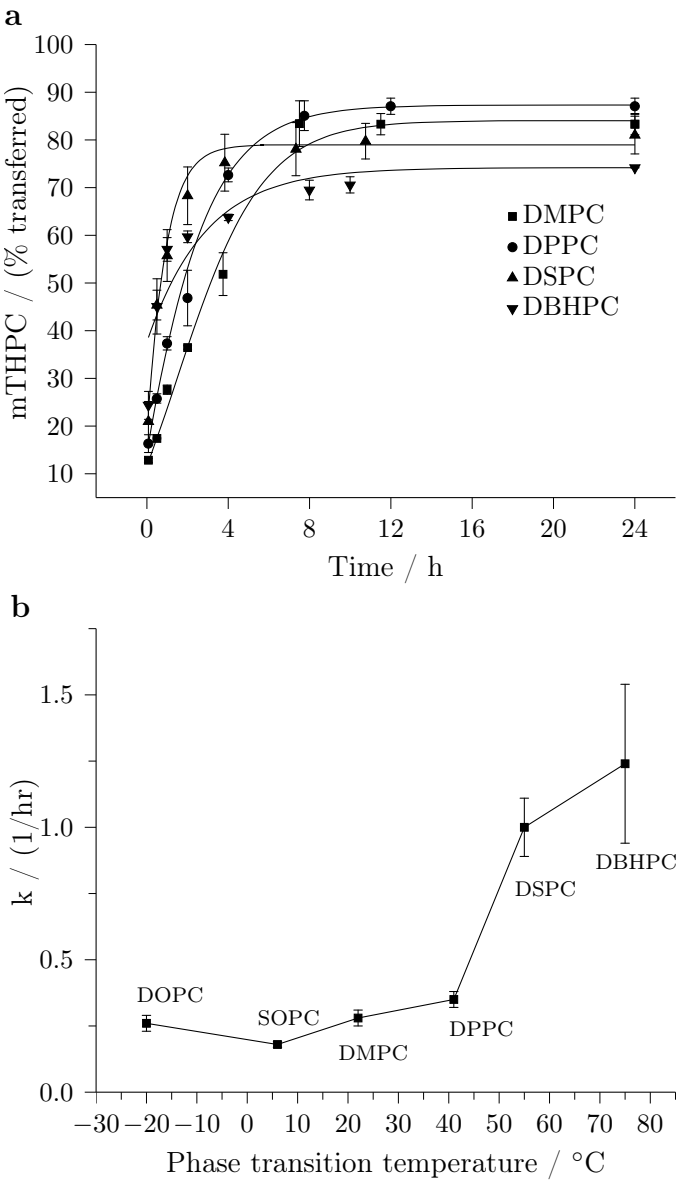


Figure 7.6. a) Temoporfin transfer between liposomal membranes regarding hydrocarbon chain length (DMPC, DPPC, DSPC, and DBHPC) at 37°C (±1). Donor liposomes were formulated as (PhL/DCP/Chol = 7:1:2) and loaded with temoporfin. Acceptor liposomes (POPC/Chol = 8:2) were 115 nm (PDI 0.04) and the Zeta-potential -0.36 mV. The ratio between donor and acceptor liposomes was 1:10. Error bars represent ±SEM (n = 6) for DMPC and DPPC; for DSPC and DBHPC ±SEM (n = 9). The molar drug:donor lipid ratio was 1:867. b) Rate constants as a function of the phase transition temperature of the donor liposome composition (data taken from Table 7.3).

cholesterol transfer [260]. The second model postulates transfer through the water phase as demonstrated by cholesterol transfer [180] and [142] and phosphatidylcholine transfer studies [180]. Other studies suggest that both mechanisms may simultaneously play a role, as indicated by the transfer of monoacylglycerols from SUV's to brush border membrane vesicles [239]. The kinetic equations describing both transfer mechanisms (through liposome collisions and through diffusion via the water phase) are derived in the appendix (Section 7.7). Our derivation is based on a detailed distribution function of drug molecules among donor and acceptor vesicles. A similar derivation, although without considering the distribution of drug molecules among donor and acceptor liposomes, was suggested previously by Jones and Thompson [117]. In both models, lipid transfer between liposomes via desorption from the bilayer and subsequent diffusion through the aqueous phase is described by a "First Order Model". In contrast, the transfer upon collisions of liposomes (donor–donor, donor–acceptor, or acceptor–acceptor) corresponds to a "Second Order Model". As we show in the appendix (Section 7.7), both lead to a simple exponential transfer kinetics with an apparent rate constant $K = K_d + cK_c$ where $K_d$ and $K_c$ are constants and $c$ is the total liposome concentration. (We note that there is an additional dependence of $K$ on the ratio between the total number of drug molecules in the system and the maximal number of drug molecules that all liposomes are able to carry; see appendix (Section 7.7) for details. This dependence is only relevant for liposomes with maximal, or near maximal, drug loading. The molar drug:donor lipid ratio was 1:867 in all experiments described, sufficiently far away from the maximal ratio 1:10 [139].) We emphasize that only the collision mechanism leads to a dependence on the total liposome concentration $c$. Fig. 7.3b shows the dependence of the apparent rate constant $K$ on the total lipid concentration. The finite slope and the finite intercept of the linear fit suggest that both the diffusion and collision mechanisms are involved in the transfer process.

Comparison of the linear fit in Fig. 7.3b with the relation $K = K_d + cK_c$ yields $K_d$=0.18/h and $K_c$=0.01 $m_L$ mL/(mg h) where $m_L$ is the mass of a single liposome. The vesicles in our experiments have a radius of approximately $R$=50 nm. Assuming a cross-sectional area $a$=0.7 nm$^2$ per lipid, this implies a number of $\frac{2 \cdot 4 \cdot \pi \cdot R^2}{a}$=90,000 lipids per liposome (where the additional factor of 2 accounts for the two leaflets of the liposomal membrane). The molar mass per lipid is roughly 700 g/mol. Hence, $m_L$=700 g/mol 90,000 = $10^{-13}$ mg. Our estimate for $K_c$ then becomes $K_c$= $10^{-3}\mu$m$^3$/h. The liposome concentration $c$ in $K = K_d + cK_c$ can be stated conveniently as "number of liposomes/$\mu$m$^3$". Our estimates for $K_d$ and $K_c$ imply that up to a liposome concentration of $c = K_d/K_c = 180/\mu$m$^3$ the transfer is dominated by the collision mechanism. In other words, once the average center-to-center distance between neighboring liposomes is larger than about 200 nm, diffusion through the aqueous phase becomes the predominant transfer mechanism. It should be noted that our final estimates $K_d$=0.18/h and $K_c = 10^{-3}\mu$m$^3$/h are subject to the assumptions of our underlying theoretical model, namely that the mixture of mTHPC in each individual liposome is ideal. This neglects other possible rate limiting physical mechanisms such as aggregation and self-assembly of mTHPC inside the liposomes. Hence, our study suggests the transfer of mTHPC via both a diffusion and collision mechanism, subject to the (yet not verified) assumption that interactions among drug molecules inside the liposomes do not limit the rate of transfer.

Molecular motion in general and acyl chain mobility in particular increase with temperature resulting in a more fluid membrane environment. Although a drug apparently favors a more fluid bilayer arrangement, the rate of transfer and the maximum amount transferred increased when the lipid membranes were heated (see Table 7.2 and Fig. 7.4). Moreover, the transfer rate constant of mTHPC at 37°C is about 5-fold higher than at 15°C which might lead to the rapid release of mTHPC at body temperature. This may be ascribed to the decrease of the hydrophobic

interaction strength between the lipid and the drug when the temperature is increased, thus resulting in a higher aqueous solubility of mTHPC. In agreement with the study of Wenk et al. [293] regarding paclitaxel (Taxol®) partitioning into lipid bilayers, the binding of paclitaxel to liposomes is four times stronger at 20°C than at 37°C. In contrast, the aqueous solubility of cyclosporine A increases with decreasing temperature. This might cause problems in stability-related issues of cyclosporine A liposomal formulations, as cyclosporine A can partition out of the liposomal membrane and form crystals in the suspending medium (Fahr, unpublished results). Another explanation for the temperature-related effects may be provided by the thermally-induced changes in the conformation of the head group. It has been suggested that the $N^+$ end of the phosphocholine headgroup of PC, which lies parallel to the bilayer surface, becomes increasingly submerged into the hydrocarbon chain region with increasing temperature, resulting in lateral head group repulsion and decreasing surface pressure. The reduction of surface pressure may be expected to favor transfer [52].

With regard to the equilibrium properties we conclude from the much larger value of entropic contribution $-T\Delta S$ as compared to the change in enthalpy $\Delta H$ (see Eq. (7.5)) that the transfer of mTHPC over the temperature range of 15–37°C is dominated by entropy. It is interesting to also discuss the prediction of our kinetic model, presented in the appendix (Section 7.7), for the Gibbs free energy of transfer $\Delta G$ (see Eq. (7.5)). To this end, we note that our model assumes all liposomes to be equivalent (i.e. mTHPC is assumed to have the same standard chemical potential in donor and acceptor vesicles). The enthalpic contribution $\Delta H$ to $\Delta G$ therefore vanishes. On the other hand, the equilibrium constant $K_{D\to A} = N_a/N_d$ is given in our model by the ratio of the numbers of acceptor to donor liposomes. Then, with Eqs. (7.4) and (7.5) and using the experimentally fixed ratio $N_a/N_d = 10$ (see Table 7.1), we find $\Delta G = -RT\ln(N_a/N_d) = -5.7\text{kJ/mol}$, which is in reasonable agreement with

the experimentally determined value $\Delta G = -4.46$kJ/mol. Although our experiments reveal the presence of a non-vanishing enthalpic contribution to $\Delta G$, the transfer is still dominated by entropy. This provides a major justification for the assumption of constant standard chemical potential in our kinetic model.

The effect of the donor liposomes charge was investigated by using negatively and positively charged donor liposomes. In the case of positively charged liposomes, the rate of transfer was faster than for negatively charged liposomes as presented in Table 7.2 and Fig. 7.5. A possible reason for this finding may be the influence of charged lipids on physical membrane properties. Binary anionic/zwitterionic and cationic/zwitterionic lipid mixtures exhibit characteristic differences in terms of their average cross-sectional area per lipid, headgroup orientation, and interaction strengths as evidenced by experiments [234], [303] and [121], molecular dynamics simulations [90], and mean-field electrostatic modeling [178] and [183]. Generally, cationic lipids are found to electrostatically interact more strongly with zwitterionic lipids due to the typically close proximity of the cationic charge to the phosphate group of the zwitterionic lipid. Hence, mixed cationic/zwitterionic membranes tend to be more condensed than their anionic counterparts, which suggests a less favorable packing environment of drug molecules inside the membrane and a larger driving force for the transfer out of the membrane interior.

The overall affinity of the porphyrin for the vesicles is largely dominated by hydrophobic interactions between the macrocycle core and the phospholipid chains. Two of the chain's characteristic structural properties are the degree of unsaturation and acyl chain length. A sharp increment in mTHPC transfer rates was observed for DSPC and DBHPC, suggesting a potential relationship between transfer rate and rigidity below the phase transition temperature. Specifically, as presented in Table 7.3 and Fig. 7.6b, there is no significant difference between transfer rate constants for DOPC ($T_m = -20$°C), SOPC ($T_m = +6$°C), DMPC ($T_m = +22$°C), and DPPC

($T_m = +41°C$), whereas for DSPC ($T_m = +55°C$) and DBHPC ($T_m = +75°C$) the transfer rate was increased by about a factor of 4. The experiments were conducted at a temperature of 37°C at which DOPC, SOPC, and DMPC reside in the fluid phase state whereas DPPC tends to form the "ripple" phase. In contrast, membranes containing DSPC and DBHPC exhibit the gel phase, where the fully stretched and tightly packed fatty acyl chains give rise to a more rigid membrane architecture. This could cause the drug molecules to be squeezed out of the bilayer interior and to accumulate near the liposome surface [64]. At the same time, this would increase the probability of being transferred to another membrane, as desorption of the drug from the liposomes becomes easier. A rapid release of a hydrophobic drug (Vitamin A) was also observed for solid lipid nanoparticles [115], the classic example of a rigid lipidic matrix. It was shown for these rigid carriers ([119], see also the review in Ref. [66]), that the mere lipophilicity of carrier and drug does not necessarily cause a retardation effect. Only if there is a structural fit between carrier assembly and drug is a retardation effect to be expected [66]. For less rigid carriers such as liposomes in their fluid state, the structural fit may be provided by the ability of the fluid-like lipid tails to adapt to the shape of the hydrophobic drug molecule. Such accommodation would be expected to be weakly dependent on chain length, as observed. However, this effect is overridden by the rigidity of the membrane, as exemplified by the case of DBHPC.

Maman and Brault [166] report, that varying the bilayer thickness by using C14-C22 unsaturated phospholipids at pH 6.5, a profound decrement in dicarboxylic porphyrin transfer rate was observed. They ascribed this influence to the length of the hydrocarbon chain since all of unsaturated lipids used in their report are liquid at their experimental temperature 25°C, thereby the degree of burying porphyrin within the bilayer will be high. In a study of anticancer teniposide partitioning into membranes using different lipids regarding unsaturation and acyl chain length at 37°C, Wright et

al. found that the partitioning coefficient was decreased when the membrane rigidity increased having the lowest partitioning coefficient recorded for DSPC [297], which is also supporting our notion.

Of course, these in vitro experiments of drug transfer presented here are not sufficient to describe the in vivo situation. However, attempts to explain e.g. mean residence time of a lipophilic drug showed for example a clear relation of lipid dose to AUC in blood after injection [61]. The used drug here, cyclosporine A, however, does not fit as well as temoporfin into the lipid bilayer, as demonstrated by the fast transfer rate (time constant about 4 min) in similar experimental setups [62] and [63].

Further work will address the localization and aggregation of mTHPC in the liposomal bilayer as well as a general kinetic model that accounts for aggregation.

## 7.5. Conclusions

In this study we have investigated the kinetics of transfer of the hydrophobic drug temoporfin from donor to acceptor liposomes. We showed that the transfer rates depend on thermodynamic parameters such as temperature and concentrations of donor and acceptor vesicles as well as on liposomal material properties. The observed transfer kinetics generally follows a simple exponential behavior with a corresponding rate constant that contains information about the mechanism of transfer. We present a theoretical model that analyzes the transfer based on a detailed distribution function of drug molecules in liposomes. The model accounts for drug transfer through liposome collisions and via diffusion through the aqueous phase. Comparison of the theoretically predicted with the measured rate constants suggests that both mechanisms contribute to the transfer. The collision mechanism dominates for large overall liposome concentration (larger than about $1/(200\text{nm})^3$). Our model gives also

reasonable agreement for the (entropy-dominated) free energy of transfer of temoporfin from the donor to the acceptor liposomes.

## 7.6. Acknowledgments

This work was supported by a grant from the Egyptian government to Hossam Hefesha. We thank Dr. Alexander Wagner for valuable discussions. We thank biolitec AG (Jena, Germany) for the generous gift of mTHPC and [$^{14}$C]mTHPC and Frank Steiniger (FSU Jena) for supporting Cryo-TEM pictures of the liposomes.

## 7.7. Appendix: Supplementary data

This appendix describes a kinetic model that predicts an exponential transfer curve and includes both a diffusion-based and a collision-based transfer mechanism. The model is microscopic in the sense that it explicitly accounts for the distribution of mTHPC in donor and acceptor liposomes. Specifically, we introduce the numbers $d_j = d_j(t)$ and $a_j = a_j(t)$ of, respectively, donor and acceptor liposomes that contain $j$ molecules of mTHPC. The index $j$ varies in the region $0 \leq j \leq m$ where $m$ is the maximal number of mTHPC that can be incorporated into a single liposome. The total number of donor liposomes $N_d = \sum_{j=0}^{m} d_j$ and the total number of acceptor liposomes $N_a = \sum_{j=0}^{m} a_j$ are both conserved. All $N = N_d + N_a$ liposomes are enclosed in a volume $V$ at fixed temperature $T$. The total numbers $M_d = \sum_{j=0}^{m} j d_j$ and $M_a = \sum_{j=0}^{m} j a_j$ of mTHPC residing in, respectively, donor and acceptor liposomes are not conserved, but the sum $M = M_d + M_a$ is. A simple kinetic model of mTHPC

transfer among all different donor and acceptor liposomes can be written as

$$\begin{aligned}
\frac{\mathrm{d}}{\mathrm{d}t}d_j =& \frac{K_c}{V}\Bigg\{ \sum_{i=0}^{j} (d_i + a_i)\left[d_{j+1}(j+1-i) - d_j(j-i)\right] \\
&+ \sum_{i=j}^{m} (d_i + a_i)\left[d_{j-1}(i-j+1) - d_j(i-j)\right] \Bigg\} \\
&+ K_d\left[(j+1)d_{j+1} - jd_j + \frac{m-(j-1)}{m(N/M)-1}d_{j-1} - \frac{m-j}{m(N/M)-1}d_j\right] \\
\frac{\mathrm{d}}{\mathrm{d}t}a_j =& \frac{K_c}{V}\Bigg\{ \sum_{i=0}^{j} (a_i + d_i)\left[a_{j+1}(j+1-i) - a_j(j-i)\right] \\
&+ \sum_{i=j}^{m} (a_i + d_i)\left[a_{j-1}(i-j+1) - a_j(i-j)\right] \Bigg\} \\
&+ K_d\left[(j+1)a_{j+1} - ja_j + \frac{m-(j-1)}{m(N/M)-1}a_{j-1} - \frac{m-j}{m(N/M)-1}a_j\right] . \qquad (7.6)
\end{aligned}$$

This model accounts for two different transfer mechanisms, transfer upon collisions between liposomes and transfer through diffusion via the aqueous phase. The collision and diffusion mechanisms are accounted for by the first and second lines, respectively, in the expressions for the time derivatives of $d_j$ and $a_j$. Specifically, the first line accounts for all possible collisions that increase (terms with positive sign) or decrease (terms with negative sign) the number $d_j$ (and analogous for $a_j$). Each term is proportional to the concentration difference of mTHPC between the colliding liposomes. The rate constant $K_c$ for transfer through collisions is assumed to be constant, irrespective of the nature of the collision (donor-donor, acceptor-acceptor, or donor-acceptor). The third line describes a diffusive transport through the aqueous phase; $K_d$ is the rate constant for the transfer of a single mTHPC from a vesicle into the aqueous phase or vice versa. Note, that the set of Eqs. (7.6) treat all liposomes to be structurally and chemically equivalent; i.e. with donor and acceptor liposomes to have the same equilibrium concentration of mTHPC. Moreover, Eq. (7.6) assume

that due to its low solubility mTHPC is present in the aqueous phase with negligible concentration.

Eq. (7.6) can be expressed as kinetic equations in terms of $M_d = M_d(t)$ and $M_a = M_a(t)$ only. Using the above definitions for $M_d$ and $M_a$ we find

$$\frac{\mathrm{d}M_d}{\mathrm{d}t} = \frac{K}{N}\,(N_d M_a - N_a M_d), \qquad \frac{\mathrm{d}M_a}{\mathrm{d}t} = \frac{K}{N}\,(N_a M_d - N_d M_a) \tag{7.7}$$

with the rate constant

$$K = \frac{K_d}{1 - \frac{M}{mN}} + K_c\,\frac{N}{V} \tag{7.8}$$

where $c = N/V$ is the total liposome concentration. Note that the factor $M/mN$ is the ratio between the total number of drug molecules in the system and the maximal number of drug molecules that all liposomes (donor+acceptor) are able to carry. It usually is $M \ll mN$ unless the loading of liposomes with drugs approaches its maximum (at a drug: lipid ratio of 1:10 for temoporfin). The set of Eqs. (7.7) effectively describes the reversible chemical reaction $D \rightleftharpoons A$ of mTHPC bound to donor (D) and acceptor (A) liposomes, with on and off rate constants $KN_d/N$ and $KN_a/N$, respectively. The kinetics of this net reaction strictly follows a first order kinetics, despite the fact that the transfer via liposome collisions is based on a bimolecular reaction, namely the collision between two liposomes. However, the number of liposomes does not change with time, leaving the rate of collisions between liposomes constant. This absence of a depletion of the reactants renders the transfer first order. The present model predicts an equilibrium constant, defined in Eq. (7.7), of $K_{D\to A} = N_a/N_d$. With the initial conditions $M_d(t=0) = M$ and $M_a(t=0) = 0$ the predicted time dependence is given by a simple exponential function

$$\frac{M_a(t)}{M} = 1 - \frac{M_d(t)}{M} = \frac{N_a}{N}\,\left(1 - e^{-Kt}\right) \tag{7.9}$$

where $N_a/N$ is the fraction of acceptor liposomes in the system. Eqs. (7.8) and (7.9) represent an exact solution of the model introduced through Eqs. (7.6). Clearly, there are two different regimes, corresponding to diffusion-dominated ($(N - M/m)/V \ll K_d/K_c$) and collision-dominated ($(N - M/m)/V \gg K_d/K_c$) transport. The observed time dependence for the mTHPC transfer from donors to acceptors does not depend on the overall concentration of liposomes in the diffusion-dominated regime. In the collision-dominated regime the transfer becomes faster with increasing liposome concentration. On the other hand, a dependence of $K$ on total number of drug molecules, $M$, is only encountered in the diffusion-dominated regime. Here, $K$ increases with $M$ until all donor liposomes initially contain their maximal amount of drug molecules $M = mN_d$.

We again point at the simplistic level of the present model. First, it does not account for the chemical specificity of the donor and acceptor liposomes. That is, the standard chemical potential of drug molecules is the same in donors and acceptors. Consequently, in equilibrium all individual liposomes (donor and acceptor liposomes) carry the same number of drug molecules (as expressed by $K_{D\to A} = N_a/N_d$), and there is no enthalpic contribution to the free energy of transfer $\Delta G$; see Eq. (7.8). Second, our model does not account for nonideal mixing of drug molecules in liposomes, including possible aggregation phenomena or self-assembly. Including the difference in affinity for drug molecules of donors and acceptors as well as aggregation of drug molecules within liposomes will be the subject of future theoretical work.

# 8. PAPER 4: MODELING THE RELEASE KINETICS OF POORLY WATER-SOLUBLE DRUG MOLECULES FROM LIPOSOMAL NANOCARRIERS[1]

ABSTRACT: Liposomes are frequently used as pharmaceutical nanocarriers to deliver poorly water soluble drugs such as temoporfin, cyclosporine A, amphotericin B, and paclitaxel to their target site. Optimal drug delivery depends on understanding the release kinetics of the drug molecules from the host liposomes during the journey to the target site and at the target site. Transfer of drugs in model systems consisting of donor liposomes and acceptor liposomes is known from experimental work to typically exhibit a first-order kinetics with a simple exponential behavior. In some cases, a fast component in the initial transfer is present, in other cases the transfer is sigmoidal. We present and analyze a theoretical model for the transfer that accounts for two physical mechanisms, collisions between liposomes and diffusion of the drug molecules through the aqueous phase. Starting with the detailed distribution of drug molecules among the individual liposomes, we specify the conditions that lead to an apparent first-order kinetic behavior. We also discuss possible implications on the transfer kinetics of (1) high drug loading of donor liposomes, (2) attractive interactions between drug molecules within the liposomes, and (3) slow transfer of drugs between the inner and outer leaflets of the liposomes.

## 8.1. Introduction

Poor solubility in water is a well-recognized obstacle for efficient oral or parenteral drug administration [153, 65]. Liposomes are among the most widely

[1] Sylvio may and Stephan Loew developed and evaluated the model in close cooperation. This paper is published in [158].

used type of pharmaceutical nanocarriers for small and poorly water-soluble drug molecules [66].These drugs preferentially partition into the hydrophobic compartment that is formed by the hydrocarbon tails of the liposomal lipids. Liposomes have been used in their first generation (conventional liposomes) predominantly as long-circulating transport vehicles [213, 247], followed by a second generation that improved the circulation time further by decorating the surface with PEG-chains (STEALTH liposomes [111]). Third generation liposomes are now being engineered to contain targeting ligands [230] and to carry out stimuli-sensitive triggering of the drug release [232].

An important property of liposome-based drug delivery is the release kinetics of the drug from the host, which has been investigated for a number of model systems [223, 168, 227, 188]. Experimental investigations of the transfer of temoporfin between two different types of liposomes (i.e. from donor liposomes to acceptor liposomes) have recently been carried out using a mini ion exchange column technique [98]. The column separates donor from acceptor liposomes and thus allows to monitor the time dependence of the drug transfer. It is observed that, typically, the transfer follows an apparent first-order behavior, characterized by a single exponential function. This is remarkable given the complexity of the system, with the drug molecules being able to migrate from the donor to the acceptor liposomes via different physical mechanisms. In fact, there are two mechanisms that, in general, act simultaneously. The first mechanism is the transfer of drugs upon collisions between two liposomes. In this case the drug molecules directly migrate from one liposome to another with minimal exposure to the aqueous phase. The second mechanism refers to the transfer of drugs via diffusion through the aqueous phase. We note that the collision mechanism has been invoked, for example, to explain the transfer of lipids [117] and cholesterol [260] between vesicles, and the transfer of fatty acids between vesicles and fatty acid binding proteins [296]. Also the diffusion mechanism was found to be consistent with the

transport of lipids [180]. In some cases, both mechanisms were suggested to contribute to the transport of lipids between vesicles [298] and to the transport of lipophilic drugs from oil-in-water emulsions to cells [49] and from plasma proteins to lipid vesicles [231]. In our preceding experimental work, where we have investigated the kinetics of temoporfin transport from donor to acceptor liposomes [98], we found that below a certain concentration (corresponding to a liposome-to-liposome distance of about 200 nm for our specific system) the transfer was dominated by collisions; for larger concentrations transport through diffusion was prevalent.

The objective of the present work is to introduce and discuss a detailed kinetic model for the release properties of poorly water-soluble drug molecules from liposomal nanocarriers. Despite a large number of experimental studies about the kinetics of lipid and drug transfer between liposomes and other nanocarriers, there is little theoretical work available that addresses the nature of the transfer kinetics. Our theoretical formalism is based on a detailed distribution function of drug molecules among the individual liposomes. Kinetic rate equations for that distribution function account for two transport mechanisms: collisions between liposomes and drug diffusion through the aqueous phase. We specify a set of conditions at which our microscopic model produces an apparent first-order kinetics with simple exponential behavior, as used in previous work [117, 49]. We point out that our kinetic model can be applied to any kind of small mobile pharmaceutical nanocarrier, including liposomes, micelles [272], colloids [186] and nanoparticles [32].

In the second part of our work we discuss conditions that lead to deviations from simple exponential behavior: First, for the diffusion mechanism, high drug loading tends to increase the transfer rate. The kinetics remains exponential only if donor and acceptor liposomes are chemically similar. Second, the presence of attractive interactions between drug molecules within the liposomes (which can result in the formation of aggregates [222]) is expected to slow down the transfer kinetics. We

note that not much molecular detail is presently known about how poorly water-soluble drug molecules inside a lipid bilayer interact. However, modeling studies of rigid membrane-embedded inclusions such as transmembrane proteins or peptides suggest a *general* tendency of the host membrane to mediate attractive interactions between inclusions that may lead to the formation of aggregates [294]. These attractive interactions may be driven by elastic deformations of the host membrane [129], by depletion of the flexible lipid chains from the region in between rigid inclusions [22], and by fluctuations via the Casimir effect [86]. Our analysis for the collision mechanism suggests that aggregate formation can give rise to sigmoidal behavior of the transfer kinetics. Third, drug molecules (even if they are poorly water-soluble) do not necessarily reside predominantly in the innermost region of the membrane's hydrocarbon region. For example, some aromatic compounds such as indole are well known for their preference of the membrane's interfacial region between the headgroups and the hydrocarbon chains [210, 206]. Other aromatic compounds such as benzene are distributed throughout the hydrocarbon chain region without a bias toward the polar/apolar interface [206]. Among the various reasons for the preferential partitioning of indole are electrostatic interactions, hydrogen bond formation, and the steric shape of the molecule. For lipid monolayers there is evidence that drug partitioning also depends on the lateral pressure [54]. Generally, whenever a drug molecule interacts more favorably with the interfacial or headgroup region than with the hydrocarbon tail region, the corresponding partitioning preference can be lumped into at least two energetically preferred states that correspond to the inner and outer leaflet of the membrane. Transfer between the two states (i.e., flip-flop) then introduces an additional characteristic time [23]. We note that two- or multiple state modeling has been invoked previously to model the partitioning of amino-acid analogues in membranes [243] and the permeation of drug molecules through membranes [34, 13].

## 8.2. Model

Consider an aqueous solution (of fixed volume $V$) that contains a number of $N_d$ donor and $N_a$ acceptor liposomes. Donor and acceptor liposomes may be either two chemically different types of liposomes (i.e., composed of different lipids), or equivalent liposomes (i.e., containing the same lipid composition). In the latter case, the distinction between donor and acceptor liposomes refers only to their initially loading; at the end of the transport process (i.e., at thermal equilibrium) both types would be indistinguishable.

The donor liposomes initially carry a total number of $M$ poorly water-soluble drug molecules. Transfer of drug molecules from donor to acceptor liposomes will take place with time until, eventually, an equilibrium partitioning is reached. We can describe the time dependence of this transfer by the number of drug molecules carried by the donor liposomes, $M_d(t)$, and by the acceptor liposomes, $M_a(t)$. It is then initially $M_d(t=0) = M$ and $M_a(t=0) = 0$, as well as in equilibrium $M_d(t \to \infty) = M_d^{eq}$ and $M_a(t \to \infty) = M_a^{eq}$, where $M_d^{eq}$ and $M_a^{eq}$ denote the equilibrium number of drug molecules carried by donor and acceptor liposomes, respectively. We point out that, although we refer to the drug carriers as liposomes, our model is more general. That is, it can be applied to different types of mobile carriers such as micelles, colloids, nanoparticles, or polymeric aggregates, given the carrier possesses some capacity to host poorly water-soluble drug molecules.

In the following we suggest a model for the time dependence of the transfer process (i.e. for $M_d(t)$ and $M_a(t)$) that leads to a first-order kinetics, characterized by a simple exponential function. We consider a "single-state model" where there is only a single energetic state available for each drug molecule in a given liposome. The single-state model excludes the presence of intra-liposomal kinetics. (The extension to a two-state model will be discussed below.) We account for two different transport

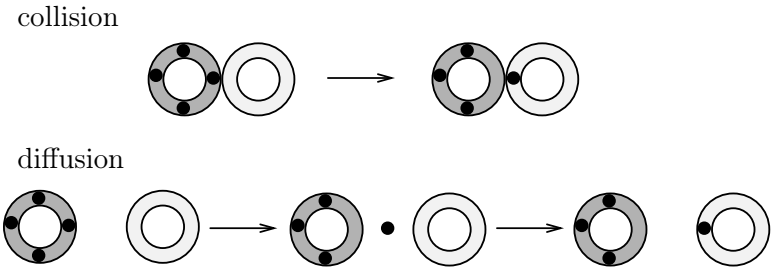


Figure 8.1. Transfer of a drug molecule (black bullets) from donor liposome (dark-shaded) to acceptor liposome (light-shaded) upon the collision of the two liposomes or upon diffusion of the drug molecule through the aqueous phase. The displayed scheme refers to the special situation of initially empty acceptor liposomes but analogous schemes apply to any other initial situation.

mechanisms, (i) transport through collisions between liposomes and (ii) transport via diffusion of drug molecules through the aqueous phase. Both mechanisms are schematically illustrated in Fig. 8.1.

Our transport model of drugs from donor to acceptor liposomes employs the framework of chemical reaction kinetics. We note that due to the generally slow release kinetics of poorly-water soluble drugs we can treat the aqueous solution as *spatially uniform* at all times. Hence, no combined diffusion-reaction kinetics [88] needs to be included in our model.

### *8.2.1. Transfer through collisions only*

Our model for the collision-mediated drug transfer between liposomes starts with the detailed distribution of drug molecules among all liposomes. We introduce the number $d_j$ of donor liposomes that carry $j$ drug molecules. An analogous definition is used for the number $a_j$ of acceptor liposomes that carry $j$ drug molecules. The index $j$ is confined to the region $0 \leq j \leq m$ where $m$ is the maximal number of drug molecules that a liposome can carry. The time-dependent distribution functions $d_j = d_j(t)$ and $a_j = a_j(t)$ represent a full microscopic knowledge of the kinetics of drug transfer. The total numbers of donor liposomes $N_d$, acceptor liposomes $N_a$, drug

molecules residing in donor liposomes $M_d$, and drug molecules residing in acceptor liposomes $M_a$, can be calculated on the basis of the distribution functions $d_j = d_j(t)$ and $a_j = a_j(t)$ according to

$$N_d = \sum_{j=0}^{m} d_j \ , \quad N_a = \sum_{j=0}^{m} a_j \ , \quad M_d = \sum_{j=0}^{m} j \, d_j \ , \quad M_a = \sum_{j=0}^{m} j \, a_j \ . \tag{8.1}$$

Mathematically, $N_d$ and $N_a$ are the zeroth-moments of the distributions functions $d_j = d_j(t)$ and $a_j = a_j(t)$, whereas $M_d$ and $M_a$ appear as the corresponding first moments. We assume that $N_d$ and $N_a$ are constant (i.e. independent of time), and so then is the total number of liposomes $N = N_d + N_a$. This is appropriate if fusion and fission between liposomes can be ignored. Due to our focus on poorly water-soluble drug molecules it is also justified to assume that the total number of drug molecules carried by all liposomes, $M = M_d + M_a$, is constant. That is, we neglect the small fraction of drug molecules that reside in the aqueous phase without being bound to a liposome. Fig. 8.2 schematically illustrates a specific exemplification of the system. Collisions require two liposomes to come to close proximity. The magnitude of drug transport between, say, donor liposomes $d_i$ and $d_j$ is thus $\sim d_i \times d_j/V$ where $V$ is the volume of the aqueous solution. The underlying transfer process is thus second-order. If a single drug molecule is transferred from a donor that carries initially $i$ drug molecules to a donor that carries initially $j$ drug molecules, the distribution function changes according to $d_i \to d_i - 1$, $d_{i-1} \to d_{i-1} + 1$, $d_j \to d_j - 1$, and $d_{j+1} \to d_{j+1} + 1$. Hence the numbers $d_i$ and $d_j$ decrease, whereas $d_{i-1}$ and $d_{j+1}$ increase. Fig. 8.3 shows an illustration of this scheme for $i = 5$ and $j = 1$. The transfer rate between the populations $d_i$ and $d_j$ will also depend on the corresponding numbers of drug molecules $i$ and $j$. We assume the drug molecules within each liposome form an ideal mixture so that the transfer rate is directly proportional to $|i - j|$. In writing a rate equation for donor population $d_j$ we have to account for all possible ways of collisions between

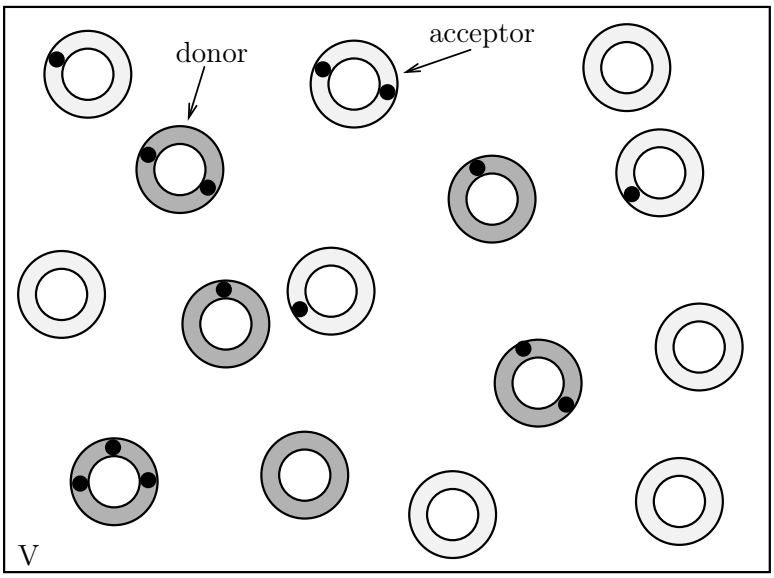


Figure 8.2. Exemplification of our system: $N_d = 6$ donor liposomes (dark shaded) and $N_a = 9$ acceptor liposomes (light shaded) reside in an aqueous space of volume $V$; each liposome can carry at most $m = 3$ drug molecules (black bullets). For the displayed hypothetical snapshot (taken at a certain time $t$) the distribution function of drug molecules among the donor liposomes is: $d_0 = 1$, $d_1 = 2$, $d_2 = 2$, $d_3 = 1$, leading to a total of $M_d = \sum_{j=0}^{m} j d_j = 9$ drug molecules residing in donor liposomes. Analogously for the acceptor liposomes, the distribution function is $a_0 = 5$, $a_1 = 3$, $a_2 = 1$, $a_3 = 0$, implying $M_a = \sum_{j=0}^{m} j a_j = 5$.

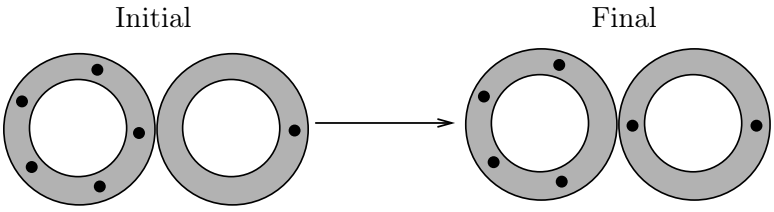


Figure 8.3. Transfer of a drug molecule (black bullets) upon the collision of two liposomes (here assumed to be two donor liposomes). The drug distribution function changes from initially $d_1 = 1$, $d_2 = 0$, $d_3 = 0$, $d_4 = 0$, $d_5 = 1$ to $d_1 = 0$, $d_2 = 1$, $d_3 = 0$, $d_4 = 1$, $d_5 = 0$. This represents an example (for $i = 5$ and $j = 1$) of the general scheme $d_i \to d_i - 1$, $d_{i-1} \to d_{i-1} + 1$, $d_j \to d_j - 1$, and $d_{j+1} \to d_{j+1} + 1$.

donor liposomes of index $j$ with other liposomes (donors and acceptors) of index $i$.

These considerations lead us to

$$\begin{aligned}\frac{V}{K_{coll}}\dot{d}_j = &\sum_{i=0}^{j} d_i \left[d_{j+1}\, g(j+1,i) - d_j\, g(j,i)\right] \\ &+ \sum_{i=j}^{m} d_i \left[d_{j-1}\, g(i,j-1) - d_j\, g(i,j)\right] \\ &+ \sum_{i=k}^{j} a_{i-k} \left[d_{j+1}\, g(j+1,i) - d_j\, g(j,i)\right] \\ &+ \sum_{i=j}^{m+k} a_{i-k} \left[d_{j-1}\, g(i,j-1) - d_j\, g(i,j)\right] , \end{aligned} \tag{8.2}$$

where we have defined the function

$$g(i,j) = i - j \ . \tag{8.3}$$

In Eq. (8.2) $K_{coll}$ is the unit rate of drug transfer through collisions between two chemically equivalent liposomes, and $\dot{x} = dx/dt$ denotes the time derivative of a physical quantity $x(t)$. The first two lines in Eq. (8.2) account for collisions of donor liposomes with other donor liposomes. The last two lines in Eq. (8.2) account for collisions of donor liposomes with acceptor liposomes.

Note that Eq. (8.2) allows for a difference in the chemical nature of donor and acceptor liposomes. This chemical mismatch is accounted for by the integer $k$ in the last two lines of Eq. (8.2), which expresses the difference in the number of drug molecules between a donor and acceptor liposomes in thermal equilibrium. (That is, for $k = 0$ each donor and acceptor liposome will contain the same number of drug molecules in thermal equilibrium). We do not attempt to calculate $k$ from a microscopic model; yet below we show how $k$ is related to the change in standard Gibbs free energy for the process of transferring drug molecules from donor to acceptor liposomes.

Due to symmetry we obtain $\dot{a}_j$ from $\dot{d}_j$ by replacing $d_i \to a_i$, $a_i \to d_i$, and $k \to -k$,

$$\begin{aligned}\frac{V}{K_{coll}}\dot{a}_j =& \sum_{i=0}^{j} a_i \left[a_{j+1}\, g(j+1,i) - a_j\, g(j,i)\right] \\ &+ \sum_{i=j}^{m} a_i \left[a_{j-1}\, g(i,j-1) - a_j\, g(i,j)\right] \\ &+ \sum_{i=-k}^{j} d_{i+k} \left[a_{j+1}\, g(j+1,i) - a_j\, g(j,i)\right] \\ &+ \sum_{i=j}^{m-k} d_{i+k} \left[a_{j-1}\, g(i,j-1) - a_j\, g(i,j)\right] . \end{aligned} \tag{8.4}$$

Eqs. (8.2) and (8.4) constitute a microscopic model for the kinetic behavior of drug transport from donor to acceptor liposomes through the collision mechanism; it can be verified that

$$\sum_{j=0}^{m} \dot{d}_j = \sum_{j=0}^{m} \dot{a}_j = \sum_{j=0}^{m} j\,(\dot{a}_j + \dot{d}_j) = 0\ , \tag{8.5}$$

implying $\dot{N}_d = \dot{N}_a = \dot{M} = 0$ and thus ensuring conservation of the number of donor and acceptor liposomes ($N_d$ and $N_a$) as well as of the total number of drug molecules ($M = M_d + M_a$). To characterize the total numbers $M_d$ and $M_a$ of drug molecules that reside in donor and acceptor liposomes, respectively, we carry out the summations $\sum_{j=0}^{m} j\dot{d}_j$ and $\sum_{j=0}^{m} j\dot{a}_j$ using Eqs. (8.2) and (8.4). The result are the two first-order differential equations

$$\begin{aligned}\dot{M}_d =& \frac{K}{N}\left(M_a\, N_d - M_d\, N_a + kN_aN_d\right)\ , \\ \dot{M}_a =& \frac{K}{N}\left(M_d\, N_a - M_a\, N_d - kN_aN_d\right)\ , \end{aligned} \tag{8.6}$$

where we have introduced the definition of the apparent rate constant

$$K = K_{coll}\,\frac{N}{V}. \tag{8.7}$$

Initially all drug molecules are incorporated in the donor liposomes, implying $M_d(t = 0) = M$ and $M_a(t = 0) = 0$. The solution of Eqs. (8.6) is then

$$M_a(t) = M - M_d(t) = \left(1 - e^{-Kt}\right)\,\frac{N_a}{N}\,(M - kN_d)\,. \tag{8.8}$$

Hence $K$ indeed appears as the inverse characteristic time for the transfer process. In contrast to previous models [117], $K$ depends only on the total concentration of liposomes $N/V$ but not on the concentrations of donor or acceptor liposomes individually. We also mention that Eqs. (8.6) (and the solution in Eq. (8.8)) are valid for any number of donor and acceptor liposomes (i.e, any choice of $N_d$ and $N_a$). This includes but is not restricted to sink conditions (where $N_a \gg N_d$).

Thermodynamic equilibrium corresponds to the long-time limit, $t \to \infty$, at which we have $M_d = M_d^{eq}$ and $M_a = M_a^{eq}$ with

$$\frac{M_d^{eq}}{M} = \frac{N_d}{N}\left(1 + k\frac{N_a}{M}\right)\,, \qquad \frac{M_a^{eq}}{M} = \frac{N_a}{N}\left(1 - k\frac{N_d}{M}\right)\,. \tag{8.9}$$

From Eqs. (8.9) we obtain the difference between the numbers of drug molecules per donor and acceptor liposome, $(M_d^{eq}/N_d) - (M_a^{eq}/N_a) = k$. This agrees with our interpretation of $k$ in Eqs. (8.2) and (8.4). We note that for chemically identical donor and acceptor liposomes it is $k = 0$ and all liposomes carry the same number of drug molecules in equilibrium, implying $M_d^{eq}/N_d = M_a^{eq}/N_a = M/N$. The largest possible value of $k$ is $k = M/N_d$ for which we obtain $M_a^{eq} = 0$ and $M_d^{eq} = M$. The smallest possible value of $k$ is $k = -M/N_a$ implying $M_a^{eq} = M$ and $M_d^{eq} = 0$. Hence $-M/N_a \leq k \leq M/N_d$.

The solution in Eq. (8.8) corresponds to a simple exponential decay of the number of drug molecules in the donor liposomes. This suggests that we can express the transfer kinetics of drug molecules from donor (D) to acceptor (A) liposomes as the chemical reaction scheme

$$\mathrm{D} \underset{K_2}{\overset{K_1}{\rightleftharpoons}} \mathrm{A} \ , \tag{8.10}$$

with rate constants $K_1$ and $K_2$. The corresponding kinetic behavior is then governed by the equations $\dot{M}_d = -K_1\, M_d + K_2\, M_a$ and $\dot{M}_a = K_1\, M_d - K_2\, M_a$ where $M_d = M_d(t)$ and $M_a = M_a(t)$ are the numbers of drug molecules carried by donor and acceptor liposomes, respectively. With $M_d(t=0) = M$ and $M_a(t=0) = 0$ we obtain

$$M_a(t) = M - M_d(t) = \left(1 - e^{-(K_1+K_2)t}\right) \left(\frac{K_1}{K_1+K_2}\right) \frac{N_a}{N}\, M \ , \tag{8.11}$$

which has indeed the same structure as Eq. (8.8). Comparison of Eq. (8.8) with Eq. (8.11) reveals $K_1 = (1 - kN_d/M)\, KN_a/N$ and $K_2 = (1 + kN_a/M)\, KN_d/N$. The equilibrium constant $K_{eq} = K_1/K_2$ of the reaction in Eq. (8.10) is thus

$$K_{eq} = \frac{N_a}{N_d}\, \frac{M - kN_d}{M + kN_a} \ . \tag{8.12}$$

Comparing this with $K_{eq} = \exp(-\Delta g^0/k_{\mathrm{B}}T)$ (where $k_{\mathrm{B}}$ is Boltzmann's constant and $T$ is the absolute temperature) allows us to compute the change in standard Gibbs free energy

$$\Delta g^0 = k_{\mathrm{B}}T \ln\left(\frac{M/N_a + k}{M/N_d - k}\right) \ , \tag{8.13}$$

for the transfer of a single drug molecule from a donor to an acceptor liposome. The enthalpic and entropic contributions to $\Delta g^0$ will be influenced by $k$, which is, generally, temperature-dependent ($k = k(T)$). Let us briefly discuss two cases. First, if donor and acceptor liposomes are chemically identical, then $k = 0$ and $\Delta g^0 = k_{\mathrm{B}}T \ln(N_d/N_a)$

has only an entropic contribution. Specifically, for $N_d > N_a$ we find $\Delta g^0 > 0$ because a given drug molecule has more donor liposomes to reside in than acceptor liposomes. Second, the limiting cases for $k$, namely $k = -M/N_a$ and $k = M/N_d$, yield $\Delta g^0 \to -\infty$ (thus with all drugs migrating to the acceptor liposomes) and $\Delta g^0 \to \infty$ (thus with all drugs remaining in the donor liposomes), respectively.

We point out that our model predicts a simple exponential time behavior despite the presence of drug transfer through a second-order two-body collision process (i.e., collisions between two liposomes). Chemical reactions that deplete the reactants through binary collisions generally display a long time tail $c(t) \sim 1/t$ in their concentration dependence. For example, the kinetic behavior of the dimerization reaction 2 *monomer* $\to$ *dimer* follows the equation $\dot{c} = -\tilde{K}c^2$ where $c(t)$ is the concentration of the reactant (i.e., the monomers) and $\tilde{K}$ the rate constant. With an initial concentration $c(t = 0) = c_0$ the time behavior becomes $c(t) = c_0/(1 + c_0\tilde{K}t)$, implying $c(t) \sim 1/t$ for long times. For our system, however, the numbers of donor and acceptor liposomes remain unchanged. Thus, collisions do not deplete the reactants, and the concentration dependencies of $M_d(t)$ and $M_a(t)$ become exponential in time.

### *8.2.2. Transfer through diffusion only*

Diffusion allows for transfer of drug molecules directly through the aqueous phase, without the need of collisions between liposomes. Denoting the additional state in the aqueous phase by W (in addition to donor (D) and acceptor (A)) the corresponding transport scheme (again, as in Eq. (8.10), formally expressed as a chemical reaction) can be written as [269, 117]

$$\mathrm{D} \underset{K_d^{upt}}{\overset{K_d^{rel}}{\rightleftharpoons}} \mathrm{W} \underset{K_a^{rel}}{\overset{K_a^{upt}}{\rightleftharpoons}} \mathrm{A} \ , \tag{8.14}$$

with rate constants $K_d^{rel}$, $K_a^{rel}$, $K_d^{upt}$ and $K_a^{upt}$ for the drug release ("rel") and uptake ("upt") in donor ("d") and acceptor ("a") liposomes. To formulate the rate equations it is useful to first consider the drug distribution function $d_j(t)$. We assume the probability of a drug molecule to leave donor liposomes of index $j$ to be proportional to the total number $jd_j$ of drug molecules in that liposome population. Similarly, the probability of a drug molecule to enter donor liposomes of index $j$ is assumed to be proportional to the total number $(m-j)d_j$ of empty binding sites in that liposome population. Because the uptake is based on collisions of liposomes with drug molecules in the aqueous solution, the rate should also be proportional to the drug concentration $M_w/V$ in the aqueous phase (here $M_w$ is the total number of drug molecules residing in the aqueous phase). This leads to the following rate equations

$$\dot{d}_j = K_d^{rel}\left[(j+1)d_{j+1} - jd_j\right] + K_d^{upt}\,\frac{M_w}{V}\,\left[(m-(j-1))d_{j-1} - (m-j)d_j\right]\ , \quad (8.15)$$

for $0 \le j \le m$ (with $d_j = a_j = 0$ for $j < 0$ or $j > m$). A similar equation can be written for the acceptor liposomes. Based on Eq. (8.15) it can be verified that $\sum_{j=0}^{m} \dot{d}_j = 0$ thus ensuring conservation of $N_d$ (and similarly for $N_a$). Carrying out the summation $\dot{M}_d = \sum_{j=0}^{m} j\dot{d}_j$ using Eqs. (8.15) leads to

$$\dot{M}_d = -K_d^{rel} M_d + K_d^{upt}\,\frac{M_w}{V}\,(mN_d - M_d)\ . \quad (8.16)$$

This equation simply expresses the proportionality of the release to the total number of bound drug molecules and the proportionality of the uptake to the total number of free binding sites. Consistent with Eq. (8.16) we complete the set of rate equations

corresponding to the scheme in Eq. (8.14)

$$\begin{aligned}\dot{M}_w = &\quad K_d^{rel} M_d - K_d^{upt} \frac{M_w}{V}(mN_d - M_d) \\ &+ K_a^{rel} M_a - K_a^{upt} \frac{M_w}{V}(mN_a - M_a) \ , \\ \dot{M}_a = &- K_a^{rel} M_a + K_a^{upt} \frac{M_w}{V}(mN_a - M_a) \ . \end{aligned} \tag{8.17}$$

To obtain first-order behavior, we make three assumptions. The first is a steady state approximation for the number of drug molecules in the aqueous phase, $\dot{M}_w = 0$. The solubility limit of poorly water-soluble drugs is small so that, effectively, any release of drugs from one liposome is accompanied by an immediate uptake by another (or the same [4]) liposome. The second assumption is weak drug loading of all liposomes; this amounts to $M_d \ll mN_d$, $M_a \ll mN_a$, and $M \ll mN$. We finally assume the same rate for the uptake of drug molecules from the aqueous phase into donor and acceptor liposomes, implying $K_d^{upt} = K_a^{upt}$. This is strictly valid only for chemically equivalent donor and acceptor liposomes but should generally be a reasonable approximation. That is, we expect the energy barrier for entering a liposome from the aqueous phase to be small (as compared to the energy barrier for the release from a liposome), irrespective of the liposome's chemical structure. Subject to our three assumptions Eqs. (8.16) and (8.17) become equivalent to

$$\begin{aligned}\dot{M}_d = &- K_d^{rel} \frac{N_a}{N} M_d + K_a^{rel} \frac{N_d}{N} M_a \ , \\ \dot{M}_a = &K_d^{rel} \frac{N_a}{N} M_d - K_a^{rel} \frac{N_d}{N} M_a \ . \end{aligned} \tag{8.18}$$

Eqs. (8.18) are now identical to Eqs. (8.6) if we identify $K_d^{rel} = K_{diff}(1 - kN_d/M)$ and $K_a^{rel} = K_{diff}(1 + kN_a/M)$ where $K_{diff} = K$ appears as the rate constant. Here again, as for Eqs. (8.6), the validity of Eqs. (8.18) is not subject to a restriction with respect to $N_d$ and $N_a$.

## 8.3. Discussion

Both transfer mechanisms, through liposome collisions and via diffusion through the aqueous phase, lead to the same first-order kinetic behavior; see Eqs. (8.6) and (8.18). The rate constant of the combined process is

$$K = K_{coll}\,\frac{N}{V} + K_{diff}\ . \tag{8.19}$$

Its dependence on the *total* liposome concentration allows the experimental determination of the transfer mechanism [98]. We note that the first order behavior predicted by Eqs. (8.6) and (8.18) requires several assumptions to be fulfilled: low liposome loading with drug molecules, rate constants that are strictly proportional to concentrations of drug molecules, and no intra-liposomal kinetics with a rate similar to $K$. In the following we discuss how the kinetic behavior is predicted to change if any of these assumptions is not fulfilled.

### *8.3.1. Extension to high drug loading*

While high drug loading obviously increases the number of available drug molecules (and thus increases the efficiency of liposomal carriers [156]) it also affects the kinetics of the drug release. Our present model predicts such a dependence for the diffusion mechanism whereas the kinetics for the collision mechanism is not affected. Recall that the transition from Eqs. (8.16) and (8.17) to Eq. (8.18) was based on the approximation of weak drug loading, $M_d \ll mN_d$, $M_a \ll mN_a$, and $M \ll mN$. Without that approximation we obtain instead of Eqs. (8.18) a nonlinear

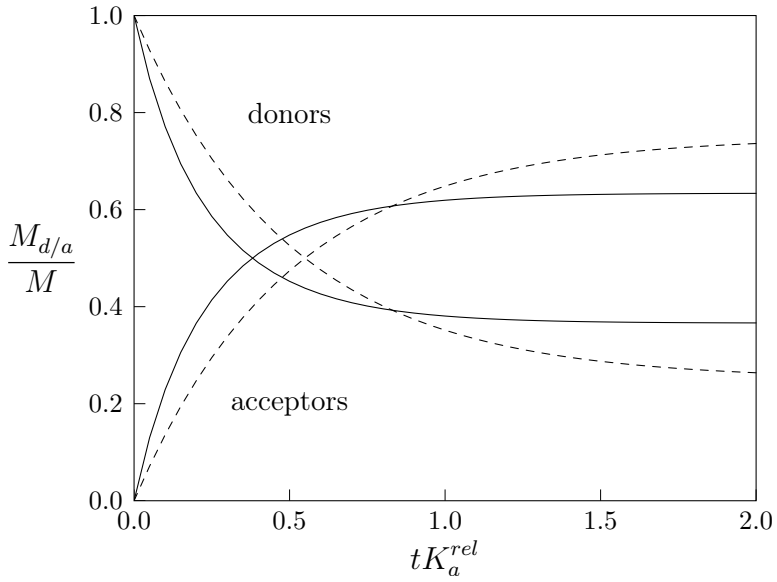


Figure 8.4. Numerical solutions of Eqs. (8.20), derived for $M/(Nm) = 0$ (broken lines) and $M/(Nm) = 0.5$ (solid lines). The remaining parameters are $K_d^{rel}/K_a^{rel} = 3$, $N_d/N = N_a/N = 0.5$. The time $t$ is plotted in units of $1/K_a^{rel}$.

set of differential equations

$$\begin{aligned}
\dot{M}_d &= -K_d^{rel}\frac{\frac{N_a}{N} - \frac{M_a}{M}\frac{M}{mN}}{1-\frac{M}{mN}}M_d + K_a^{rel}\frac{\frac{N_d}{N} - \frac{M_d}{M}\frac{M}{mN}}{1-\frac{M}{mN}}M_a \ , \\
\dot{M}_a &= \ \ K_d^{rel}\frac{\frac{N_a}{N} - \frac{M_a}{M}\frac{M}{mN}}{1-\frac{M}{mN}}M_d - K_a^{rel}\frac{\frac{N_d}{N} - \frac{M_d}{M}\frac{M}{mN}}{1-\frac{M}{mN}}M_a \ .
\end{aligned} \tag{8.20}$$

For the special case that donor and acceptor liposomes are chemically similar, $K_d^{rel} = K_a^{rel} = K_{diff}$, we obtain a simple exponential behavior

$$M_a(t) = M - M_d(t) = \left(1 - e^{-\frac{K_{diff}\,t}{1-M/(mN)}}\right)\,\frac{N_a}{N}\,M \ . \tag{8.21}$$

Here, high drug loading simply increases the rate constant for the diffusion mechanism by the factor $1/(1 - M/(mN))$. In the general case $K_d^{rel} \neq K_a^{rel}$, and no simple exponential decay is predicted for high loading of the liposomes with drug molecules. Fig. 8.4 shows a numerical example, based on Eqs. (8.20) with $K_d^{rel}/K_a^{rel} = 3$ and $N_d/N = N_a/N = 0.5$. For $M \ll mN$ (weak loading regime; broken lines in Fig. 8.4)

we observe the simple exponential behavior according to Eqs. (8.18) with equilibrium values $M_d^{eq}/M = 1/4$ and $M_a^{eq}/M = 3/4$. For $M/(mN) = 0.5$ the initial loading of the donor liposomes is maximal. This leads to both a faster decay and a shift in the equilibrium distribution, reaching $M_d^{eq}/M = (\sqrt{3}-1)/2 = 0.366$ and $M_a^{eq}/M = (3-\sqrt{3})/2 = 0.634$. The reason for the increased rate constant is the reduced ability of highly loaded liposomes to take up drug molecules. Hence, if drug molecules are released from initially highly loaded donor liposomes they will be taken up exclusively by acceptor liposomes. The increase in the transfer rate at high loading also affects the equilibrium values $M_d^{eq}/M$ and $M_a^{eq}/M$. The equilibrium is shifted toward a more uniform distribution of drug molecules between donor and acceptor liposomes (in agreement with Fig. 8.4).

### *8.3.2. Sigmoidal behavior*

Our model presented so far is unable to predict sigmoidal behavior. That is, no inflection point can be observed in $M_d(t)$ and $M_a(t)$. Behind this prediction is our assumption that the transfer rates are strictly proportional to the concentration difference of the drug molecules. For the collision mechanism this is expressed by our definition of the function $g(i,j)$ in Eq. (8.3). However, if drug molecules within a given liposome interact with each other, the simple relation $g(i,j) = i - j$ will no longer be valid. More specifically, attractive interactions between drug molecules within liposomes will increase the energy barrier to remove a drug molecule. This becomes relevant at high drug loading. Hence, in the presence of attractive interactions it will be more unlikely that a drug molecule is transferred from a highly loaded donor liposome to an empty acceptor liposome.

We discuss the consequences of attractive interactions for the collision mechanisms, which is described by Eqs. (8.2) and (8.4). To account for the decrease in the

rate constant at high loading we replace Eq. (8.3) by

$$g(i,j) = (i-j)\left(1-\frac{i}{m}\right)\left(1-\frac{j}{m}\right) . \tag{8.22}$$

Clearly, for weak loading ($i \ll m$ and $j \ll m$) the original first-order model leading to the exponential behavior in Eq. (8.8) is recovered. For large loading of either donor or acceptor liposomes, the transfer rate becomes small. We note that using Eq. (8.22) does not lead to a set of differential equations in terms of only $M_d(t)$ and $M_a(t)$. Here, we do not attempt to provide an analytical solution to the problem. Instead, we illustrate its predictions by numerically solving Eqs. (8.2) and (8.4) with $g(i,j)$ given in Eq. (8.22).

Fig. 8.5 shows the behavior of $M_d(t)$ and $M_a(t)$ as function of $tK$ (with $K = K_{coll}N/V$), derived for $m = 100$. For simplicity we have set $k = 0$ which results in a equipartitioning of drug molecules between donor and acceptor liposomes ($M_d/N_d = M_a/N_a = M/N$). We start with $N_d = N_a = 100$ liposomes. The acceptor liposomes are initially empty whereas each donor liposome contains initially $l$ drug molecules (out of a maximal number $m = 100$). Different curves in Fig. 8.5 correspond to $l = 2$ (a), $l = 10$ (b), $l = 50$ (c), $l = 90$ (d), and $l = 98$ (e). As long as the drug loading is weak (curves (a) and (b)), the solution is simply exponential, characterized by $M_a/M = 1 - M_d/M = (1-e^{-Kt})N_a/N$ (see Eq. (8.8) with $k = 0$). Here the kinetics is independent of the total number of drug molecules $M = lN_d$ (which is why curves (a) and (b) virtually overlap). If the initial loading of the donor liposomes becomes larger (curve (c)) the kinetics slows down. Eventually, once the initial loading approaches its maximal value $mN_d$, the behavior slows down even more and, in addition, becomes sigmoidal. Attractive drug-drug interactions slow down the release from initially highly loaded donor liposomes; at later times (when the donor liposomes are no longer highly loaded) the release becomes faster. This leads to sigmoidal behavior.

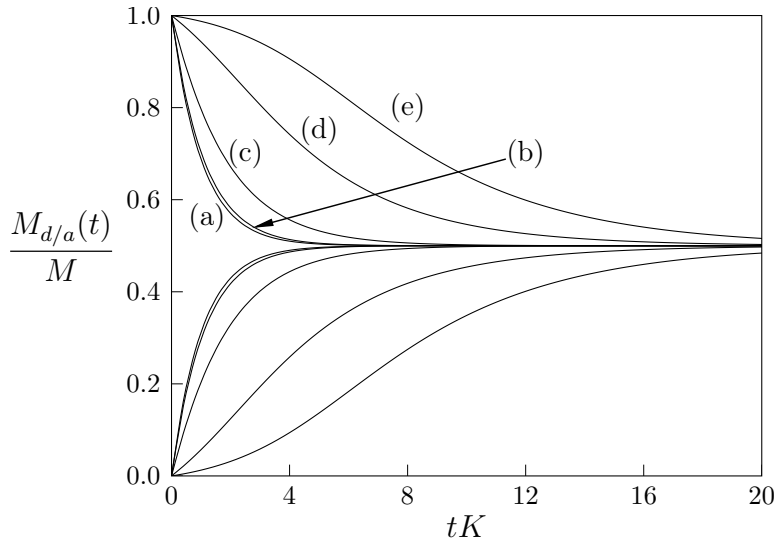


Figure 8.5. Fraction of drug molecules contained in donor liposomes ($M_d(t)/M$; upper set of curves) and acceptor liposomes ($M_a(t)/M$; lower set of curves) as function of the scaled time $Kt$. The curves represent numerical solutions of Eqs. (8.2) and (8.4) with Eq. (8.22), derived for $k = 0$ and $m = 100$ with the initial conditions $d_j(0) = 0$ for $j \neq l$, $d_l(0) = 100$, $a_j(0) = 0$ for $j > 0$, $a_0(0) = 100$. Different curves correspond to $l = 2$ (a), $l = 10$ (b), $l = 50$ (c), $l = 90$ (d), and $l = 98$ (e).

### *8.3.3. Extension to a two-state model*

In the final part of this work we briefly discuss an extension of our model to account for two distinct states of the drug molecule inside each liposome. A simple rationale for the presence of two distinct states is provided by the bilayer structure of the liposomes. That is, a drug molecule may preferentially be bound to either the inner or outer monolayer, having to flip-flop in order to change the host monolayer. The typical flip-flop time can be large if the drug has some amphiphilicity or surface activity instead of being strongly lipophilic [238]. Drug molecules residing in the inner monolayer cannot be transported directly to another liposome; they first have to migrate to the outer monolayer.

We denote by $M_d^I$ and $M_d^O$ the number of drug molecules residing in the inner ($D^I$) and outer ($D^O$) leaflets of donor liposomes, respectively. Similarly, $M_a^I$ and $M_a^O$ refer to the number of drug molecules residing in the inner ($A^I$) and outer ($A^O$) leaflets

of acceptor liposomes. The reaction scheme in Eq. (8.10) can then be generalized to account for the inter-leaflet transport in donor and acceptor liposomes

$$\mathrm{D}^I \underset{K_2^d}{\overset{K_1^d}{\rightleftharpoons}} \mathrm{D}^O \underset{K_2}{\overset{K_1}{\rightleftharpoons}} \mathrm{A}^O \underset{K_1^a}{\overset{K_2^a}{\rightleftharpoons}} \mathrm{A}^I \ . \tag{8.23}$$

Here, $K_1^d$ and $K_2^d$ are the two rate constants corresponding to the transfer of drugs between the two leaflets of the donor liposomes (and similarly for $K_1^a$ and $K_2^a$ referring to the acceptor liposomes). The rate constants $K_1 = (1 - kN_d/M)\, KN_a/N$ and $K_2 = (1 + kN_a/M)\, KN_d/N$ are identical to those for the single-state model, where $K$ is given in Eq. (8.19). Based on Eq. (8.23) the rate equations can be written as

$$\begin{aligned}
\dot{M}_d^O =& \frac{K}{N}(M_a^O N_d - M_d^O N_a + kN_a N_d) - K_2^d M_d^O + K_1^d M_d^I \ , \\
\dot{M}_d^I =& K_2^d M_d^O - K_1^d M_d^I \ , \\
\dot{M}_a^O =& \frac{K}{N}(M_d^O N_a - M_a^O N_d - kN_a N_d) - K_2^a M_a^O + K_1^a M_a^I \ , \\
\dot{M}_a^I =& K_2^a M_a^O - K_1^a M_a^I \ .
\end{aligned} \tag{8.24}$$

In the limit of a symmetric lipid bilayer the two rate constants for flip-flop of a drug molecule from the inner to the outer leaf and from the outer to the inner leaf are identical. (We note that the two leaflets of a liposomal bilayer are not strictly equivalent which, in a more refined model, would entail two different rate constants for flip-flop; this dependence on liposome curvature is neglected here.) If we assume furthermore that donor and acceptor liposomes are chemically similar, we may write

$K_1^d = K_2^d = K_1^a = K_2^a = G$ as well as $k = 0$. In this case, the rate equations

$$\begin{aligned}
\dot{M}_d^O =& \frac{K}{N}(M_a^O N_d - M_d^O N_a) - G(M_d^O - M_d^I) \,, \\
\dot{M}_d^I =& G(M_d^O - M_d^I) \,, \\
\dot{M}_a^O =& \frac{K}{N}(M_d^O N_a - M_a^O N_d) - G(M_a^O - M_a^I) \,, \\
\dot{M}_a^I =& G(M_a^O - M_a^I)
\end{aligned} \tag{8.25}$$

depend on only two parameters, the rate constants $K$ and $G$. If we assume all drug molecules initially reside in the donor liposomes, the initial conditions are $M_d^O(t=0) = M_d^I(t=0) = M/2$, and $M_a^O(t=0) = M_a^I(t=0) = 0$, where $M$ is the total number of drug molecules in the system. The solution of Eqs. (8.25) can be expressed as

$$\begin{aligned}
M_d^I(t) =& \frac{M}{2}\left[\frac{N_d}{N} + \frac{N_a}{N}\,\frac{\omega_2 e^{-\omega_1 t} - \omega_1 e^{-\omega_2 t}}{\omega_2 - \omega_1}\right] \,, \\
M_d^O(t) - M_d^I(t) =& \frac{M}{2}\,K\,\frac{N_a}{N}\,\frac{e^{-\omega_2 t} - e^{-\omega_1 t}}{\omega_2 - \omega_1} \,, \\
M_a^I(t) =& \frac{MN_a}{2N}\left[1 - \frac{\omega_2 e^{-\omega_1 t} - \omega_1 e^{-\omega_2 t}}{\omega_2 - \omega_1}\right] \,, \\
M_a^O(t) - M_a^I(t) =& \frac{M}{2}\,K\,\frac{N_a}{N}\,\frac{e^{-\omega_1 t} - e^{-\omega_2 t}}{\omega_2 - \omega_1} \,.
\end{aligned} \tag{8.26}$$

The solution is thus a combination of exponential decays with corresponding effective rate constants $\omega_1$ and $\omega_2$. Such biexponential behavior has been observed for the spontaneous transfer of certain lipids between phosphatidylcholine vesicles [118] and also for the release behavior of an imidazole derivate from liposomes [155]. The effective rate constants $\omega_1$ and $\omega_2$ can be calculated from $G$ and $K$ through

$$2G + K = \omega_1 + \omega_2 \,, \qquad 4G^2 + K^2 = (\omega_2 - \omega_1)^2 \,. \tag{8.27}$$

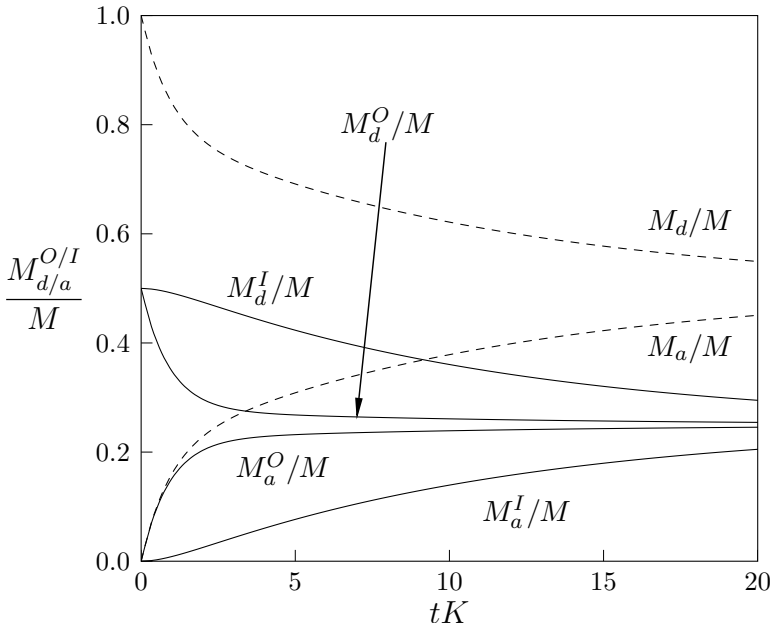


Figure 8.6. Fractions of drug molecules in inner and outer leaflets of donor and acceptor liposomes. The quantities $M_d^O(t)$, $M_d^I(t)$, $M_a^O(t)$, and $M_a^I(t)$ are plotted according to Eqs. (8.26) for $G/K = 1/10$ and $N_a/N = N_d/N = 0.5$. The broken lines show the biexponential behaviors of the sums $M_d = M_d^O + M_d^I$ and $M_a = M_a^O + M_a^I$. The time is plotted in units of the inverse rate constant $K$. Note also $\omega_1 = 1.11K$ and $\omega_2 = 0.09K$ are the effective rate constants for the decay.

Hence, a measurement of $\omega_1$ and $\omega_2$ could be used to obtain the two model parameters ($K$ and $G$). Fig. 8.6 displays a plot of $M_d^O(t)$, $M_d^I(t)$, $M_a^O(t)$, $M_a^I(t)$, $M_a(t)$, $M_d(t)$, calculated for $G/K = 1/10$ and $N_a/N = N_d/N = 0.5$. All drug molecules are initially distributed equally among the two leaflets of the donor liposomes. Release of drug molecules from the outer leaf of the donor liposomes is fast ($K = 10G$), the slow process is the flip-flop of drug molecules between the two leaflets of the liposomes. Hence, at intermediate times, say at $t = 3/K$, the outer leaflets have almost reached their equilibrium values whereas the inner layers remain still fairly close to their initial values. After reaching thermal equilibrium ($t \to \infty$), half of all drug molecules have migrated to the acceptor liposomes. Clearly, the presence of the two different rate constants ($K$ and $G$) leads to the biexponential behavior of $M_d$ and $M_a$ in Fig. 8.6.

We briefly discuss two limiting cases for Eq. (8.26). First, for $G = 0$ the flip-flop of drug molecules between the inner and outer leaves is infinitely slow, implying $M_d^I(t) = M/2$, $M_a^I(t) = 0$, $M_a^O(t) = M/2 - M_d^O(t) = (1 - e^{-Kt})\,(MN_a)/(2N)$. In this case, we recover the kinetics of Eq. (8.8), yet with only $M/2$ (instead of $M$) drug molecules participating in the transfer and identical donor and acceptor liposomes ($k = 0$). Second, for $G \to \infty$ flip-flop becomes infinitely fast and Eqs. (8.26) read $M_a^I(t) = M_a^O(t) = M/2 - M_d^I(t) = M/2 - M_d^O(t) = (1 - e^{-Kt/2})(MN_a)/(2N)$. Because 50% of the drug molecules reside in the inner leaflets, they do not contribute to the outer-leaflet-concentration-differences that drive the transfer kinetics. Hence, the apparent rate constant is reduced from $K$ to $K/2$.

## 8.4. Conclusions

In this work we have presented a detailed model for the transfer kinetics of poorly water-soluble drug molecules between liposomal carrier systems. Apart from liposomes, the scope of the model includes other types of small and mobile pharmaceutical nanocarriers, such as micelles, colloids, and nanoparticles. Starting from a microscopic distribution function of drug molecules among donor and acceptor liposomes, we have specified the conditions that lead to an apparent first order kinetic behavior. These include low drug loading of the liposomes, strict proportionality of all rate constants to drug concentrations, no aggregation phenomena of drugs within liposomes, and no overlap of the intra-liposomal flip-flop kinetics. Systems that do not fulfill these conditions do, generally, not exhibit an apparent first order kinetics. Instead the behavior may become biexponential or sigmoidal. High drug loading may preserve the first order kinetics but with increased apparent rate constant.

An optimal drug delivery system should keep the drug load on the way to the target and release it only after arrival at the target. Understanding the kinetics

and mechanisms of drug release from liposomal (and other) nanocarriers is thus a prerequisite to systematically improving drug delivery systems.

## 8.5. Acknowledgments

We thank Drs. Alexander Wagner, Martin Holzer, and Rolf Schubert for illuminating discussions. SM acknowledges support from NIH through Grant GM077184.

# 9. PAPER 5 : INCREASED PH-SENSITIVITY OF PROTEIN BINDING TO LIPID MEMBRANES THROUGH THE ELECTROSTATIC-HYDROGEN BOND SWITCH[1]

ABSTRACT: The signaling lipid phosphatidic acid (PA) is believed to interact specifically with membrane-bound globular proteins through a combination of electrostatic interactions and hydrogen bond formation known as the electrostatic-hydrogen bond switch. PA, which adjusts its protonation state according to the ambient pH, is able to regulate protein binding under physiological conditions in a pH-dependent manner. We investigate the question if the electrostatic-hydrogen bond switch contributes to the pH-sensitivity of protein binding. To this end, we propose a theoretical model for the adsorption of a basic protein on a zwitterionic membrane that contains phosphatidic acid as a minor component. Our model is based on an extended continuum Poisson-Boltzmann approach that accounts for zwitterionic lipids, the protonation/deprotonation equilibrium of PA, and the lateral mobility of the lipids in the membrane. The electrostatic-hydrogen bond switch enters as an additional non-electrostatic attractive interaction of deprotonated PA with basic protein residues. For a generic model protein we calculate the adsorption free energy and its pH-dependence. Our results suggest that the electrostatic-hydrogen bond switch not only increases the affinity between PA and the protein but also its sensitivity with respect to changes in pH. That is, the electrostatic-hydrogen bond switch helps enabling the membrane to use physiological pH changes in order to trigger protein adsorption/desorption.

[1] The model was developed in close cooperation of Sylvio May(S.M), Edgar Kooijman, and Stephan Loew (S.L.). Numerical evaluation was done independently by S.M. and S.L. This paper is published in [159].

## 9.1. Introduction

Protein-lipid interactions are crucial for a host of physiological functions as diverse as membrane transport and cell survival/cell death [191, 197, 299, 226, 40]. Peripheral membrane proteins bind to membranes which modulate protein function often through a conformational change [249]. Alternatively, the function of transmembrane proteins is regulated via the binding of specific membrane lipids [219]. Fundamental understanding of how these proteins recognize (specificity) and bind (affinity) their lipid binding partners should provide important insight into the function of these proteins, and may lead to improved drug development strategies for a variety of pathological conditions. We focus here on the signaling lipid phosphatidic acid (PA) which is not only a crucial intermediate in phospholipid and triacylglycerol synthesis but is also involved in multiple signaling processes [10]. Phosphatidic acid is a unique glycerophospholipid in that it has only a phosphomonoester headgroup, located close to the headgroup-acylchain interface, to regulate the binding of peripheral and transmembrane proteins. Despite this seemingly insignificant headgroup many proteins have evolved domains that are specific in their binding of PA [267, 268, 218, 259]. In previous work, we and others, have investigated the origin of this specificity but very little is known about how affinity of this binding is regulated. [132] have recently proposed a model for the binding specificity, namely the *electrostatic-hydrogen bond switch* model.

The electrostatic-hydrogen bond switch model describes the mode of binding of PA-binding proteins and thus the unique ionization properties of the phosphomonoester of PA. The basic principles of this model are valid for other phosphomonoester groups (singly bonded phosphate group) [133, 135, 264]. In case of protein binding the switch can be understood as follows. The initial interaction of a cytosolic PA binding protein with a biomembrane is electrostatic in nature. When the protein binds the membrane

it samples the local environment to locate PA which is present in a sea of more abundant (e.g. phosphatidylserine) anionic lipids. If the protein does not locate PA it diffuses away, but when it is able to interact with PA via hydrogen bonds between basic [or other [116]] amino acids in its binding domain, the PA binding protein switches from a loosely bound state to one where it is docked onto the membrane. During this process the ionization of PA switches from $-1$ [the most probable ionization state [131]] to $-2$, further anchoring the PA binding protein to the membrane.

In previous work we explored how this switch mechanism regulates the dissociation state of PA. We showed that the electrostatic-hydrogen bond switch regulates the pKa of PA with much greater sensitivity than would be possible based on pure electrostatics alone [184]. In addition, if divalent cations are present, electrostatic correlations appear to play a key role in regulating the electric charge of PA; this was observed experimentally and modeled by simulations and by incorporating binding equilibria into mean-field electrostatics [71, 291]. However, a fundamental question remains as to how the ionization mechanism modulates the affinity of membrane (peripheral) proteins for binding to PA. Regulation of PA binding through (local) changes of pH is one of the hypotheses of the electrostatic-hydrogen bond switch model. Recently, work by Loewen and co-workers showed how membrane biogenesis and general metabolism are linked through pH-modulated PA binding of the negative transcriptional regulator Opi1 [302]. Here we explore how hydrogen bond formation modulated pKa changes, as observed experimentally, affect the affinity of PA binding proteins.

We propose a theoretical model to study how changes of the solution's pH value affect the binding energy of a basic protein with a PA-containing lipid membrane. In our model the membrane is a binary mixture, consisting of the zwitterionic lipid phosphatidylcholine (PC) and the minority component PA (typically present with no more than a few mole percent). We model the binding as an adsorption process of

a basic protein onto the binary (PA-containing) membrane. The binding process is generally accompanied by migration of PA into the adsorption region. Within the adsorption region, the *local* concentration of PA may be increased, and the degree of deprotonation of PA may be altered. Both mechanisms act toward optimizing the adsorption free energy of the protein. For PA it has been proposed that in addition to the electrostatic interactions of the phosphomonoester with the protein's basic residues the formation of hydrogen bonds contribute to the protein-lipid interaction [132]. This obviously can lead to a more favorable adsorption free energy. Yet, it is much less obvious to what extent the additional, non-electrostatic, interaction (i.e., the ability to form hydrogen bonds) also increases the *sensitivity* of the adsorption free energy with respect to changes in pH. To demonstrate that the interplay of electrostatic and non-electrostatic interactions can, in fact, be exploited to make pH-induced protein adsorption more sensitive, is the main objective of the present work.

Mean-field electrostatics has frequently been used in the past to model protein adsorption. Some approaches employ molecular-level representations of proteins and membranes with discrete charges [195, 196, 289, 77], whereas others apply some form of continuum electrostatics [225, 99, 173, 91, 306]. Charge regulation, including the protonation/deprotonation equilibrium, has also been modeled extensively, both for isolated membranes [205, 21] and with regard to protein adsorption onto membranes [161] or solid surfaces [97]. Due to the complexity to include charge-charge correlations, almost all approaches employ the mean-field level Poisson-Boltzmann model. Our present approach too makes use of the Poisson-Boltzmann model, yet modified so as to account for the presence of zwitterionic lipids. We aim to incorporate only the dominating interactions into a generic model for the pH-regulation of protein adsorption onto PA-containing membranes. This implies to make significant approximations such as using continuum electrostatics, treating all involved charges as point-like, ignoring differences in the lateral cross-sectional area of chemically different lipids,

and assuming perfectly planar step-like dielectric boundaries at the polar/apolar interfaces of membrane and protein. With that, our goal is not to quantitatively predict adsorption free energies but to understand how the electrostatic-hydrogen bond switch facilitates protein binding onto biomembranes being regulated through pH changes.

## 9.2. Theory

We successively introduce our models and corresponding free energies of a bare lipid layer (Section 9.2.1), a bare protein (Section 9.2.2), and the complex between the two (i.e., a protein that is adsorbed onto the lipid layer, in Section 9.2.3).

### *9.2.1. Bare lipid layer*

We consider a planar lipid layer that is part of a lipid membrane and consists of a two-component mixture: a charged lipid that can adjust its dissociation state and a zwitterionic lipid. For the charged lipid we specifically have in mind phosphatidic acid (PA) with its deprotonation/protonation equilibrium $PA^{2-} + H^+ \leftrightharpoons PA^-$ (where $H^+$ denotes a proton)

close to physiological pH values. Note that only one of PA's pKa values is close to physiological conditions, allowing us to focus on only two charging states. The zwitterionic lipid may simply be phosphatidylcholine (PC), which is abundant in biomembranes. We denote the mole fractions of PA and PC by $\phi$ and $1-\phi$, respectively. Assume that of all PA lipids, a (yet unknown) fraction $\eta$ is deprotonated ($PA^{2-}$) and a fraction $1-\eta$ is protonated ($PA^-$). We can then view the lipid layer as a ternary system of $PA^{2-}$, $PA^-$, and PC, with corresponding mole fractions $\phi\eta$, $\phi(1-\eta)$, and $(1-\phi)$, respectively. Note that both $\phi$ and $\eta$ can vary within 0 and 1 (i.e., $0 \leq \phi \leq 1$ and $0 \leq \eta \leq 1$). Fig. 9.1 illustrates the lipid layer with the different lipids and corresponding mole fractions.

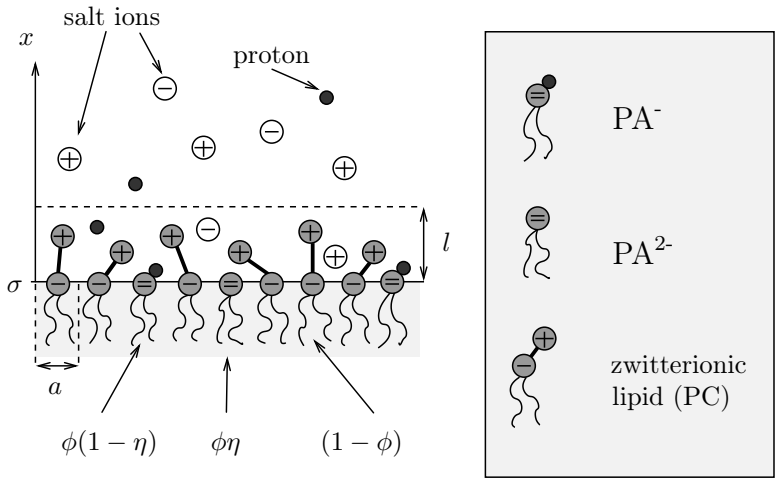


Figure 9.1. Illustration of a mixed acidic-zwitterionic lipid layer, consisting of $PA^{-}$, $PA^{2-}$, and PC with mole fractions $\phi(1-\eta)$, $\phi\eta$, and $(1-\phi)$, respectively. Each lipid occupies the same cross-sectional area $a$. The direction normal to the lipid layer is denoted by $x$. All lipid charges (apart from the positive charges of the zwitterionic lipids) reside at the (step-like) polar/apolar interface $x = 0$; the corresponding surface charge density is $\sigma$. The positive charges of the zwitterionic lipids are located within the headgroup region, $0 < x < l$, where $l$ is the headgroup thickness. The electrolyte contains monovalent salt ions and protons, with the concentration of the salt ions everywhere much larger than that of the protons. The right-hand side of the figure shows a schematic illustration of the involved lipids.

In the following we describe the electrostatic properties of the lipid layer according to a modified Poisson-Boltzmann model. A detailed discussion of the model and its application to a single lipid layer has been presented previously [184]. Assume the polar/apolar interface of the lipid layer is step-like and coincides with the $y, z$-plane of a Cartesian coordinate system. On the mean-field level, all physical properties (such as electrostatic potential, ion concentrations, etc) then depend only on the normal direction $x$ to the lipid layer. We consider the mean-field free energy *per lipid* $f_b$ of a single lipid layer. The index "b" stands for "bare" to distinguish it from a lipid layer interacting with a protein; see below in Section 9.2.3. We decompose the free energy

$f_b$ into three contributions,

$$f_b = f_{mix} + a \int_0^\infty dx\, \hat{f}_{el} + (1-\phi)\frac{k_\mathrm{B}T}{l}\int_0^l dx\, P_l \ln P_l \ . \tag{9.1}$$

They represent, respectively, the lipid's mixing free energy, the electrostatic free energy according to the classical Poisson-Boltzmann model [6], and an entropic contribution due to the conformational degrees of freedom of the zwitterionic headgroups. We discuss each contribution individually: Assuming the absence of non-electrostatic lipid-lipid interactions within the lipid layer, we can express the mixing free energy as ideal, implying for the first contribution (expressed in units of the thermal energy $k_\mathrm{B}T$, where $k_\mathrm{B}$ is Boltzmann's constant and $T$ the absolute temperature),

$$\frac{f_{mix}}{k_\mathrm{B}T} = \phi\left[\eta \ln\frac{\eta}{\eta_0} + (1-\eta)\ln\frac{1-\eta}{1-\eta_0}\right] + \phi\ln\phi + (1-\phi)\ln(1-\phi)\ . \tag{9.2}$$

Recall that $\phi$ is the mole fraction of PA and $\eta$ describes its deprotonation state. The latter is expressed subject to a conveniently chosen reference state $\eta_0$. Here $\eta_0 = 1/(1+10^{\mathrm{pK}-\mathrm{pH}})$ denotes the nominal (i.e., in the absence of external influences) probability to find PA in its deprotonated state $\mathrm{PA}^{2-}$. This probability is related to the difference of the local pH value and the lipid's intrinsic pK. Only $\eta_0$ but not the individual values of pH and pK enter into our model. Because the intrinsic pK is a constant, changes of $\eta_0$ can simply be viewed as a measure for changes of the pH in solution. This will guide our choices for $\eta_0$ as discussed below.

The second contribution to $f_b$ in Eq. (9.1) integrates the volume density $\hat{f}_{el}$ of the electrostatic free energy over the aqueous solution ($x > 0$), where $a$ denotes the

cross-sectional area per lipid (see also Fig. 9.1). According to the classical Poisson-Boltzmann model of a symmetric 1:1 electrolyte, $\hat{f}_{el}$ can be written as [6, 60]

$$\frac{\hat{f}_{el}}{k_{\mathrm{B}}T} = \frac{\Psi'^2}{8\pi\ell_{\mathrm{B}}} + n_+ \ln\frac{n_+}{n_0} - (n_+ - n_0) + n_- \ln\frac{n_-}{n_0} - (n_- - n_0)\ . \tag{9.3}$$

Here, the first term represents the electrostatic field energy, conveniently expressed in terms of the dimensionless electrostatic potential $\Psi = \Psi(x)$ (with $\Psi = e\Phi/k_{\mathrm{B}}T$, where $\Phi$ is the electrostatic potential and $e$ the elementary charge) and the Bjerrum length $\ell_{\mathrm{B}} = 0.7\,\mathrm{nm}$ in water. In the following we shall refer to $\Psi$ simply as the "potential". The prime denotes the derivative with respect to $x$, that is $\Psi' = d\Psi(x)/dx$. The remaining terms in Eq. (9.3) are ideal mixing free energies that account for the demixing penalty of the local concentrations, $n_+ = n_+(x)$ and $n_- = n_-(x)$, of positively and negatively charged salt ions, with respect to their bulk concentrations $n_0$. Hence, $n_\pm(x \to \infty) = n_0$. Note that, as we assume sufficiently small (as compared to salt) local proton concentrations everywhere, Eq. (9.3) does not need to account for an additional proton demixing penalty.

The third contribution to $f_b$ in Eq. (9.1) is related to the conformational entropy of the zwitterionic headgroups. This term is based on a previously suggested model [178], where the zwitterionic headgroup is approximated as two opposite elementary charges separated by a fixed distance $l$. The negative charge represents the phosphate group and the positive charge the choline moiety of PC (or the positively charged terminal group for similar zwitterionic phospholipids). Since the phosphate group is linked via a glycerol backbone to the two lipid tails, it is appropriate to assume the negative headgroup charge is constrained to reside at the polar/apolar interface $x = 0$. In contrast, the choline group benefits from the headgroup's conformational degrees of freedom. We represent this freedom by allowing the positive charge to move on the surface of a hemisphere with $x > 0$ about the fixed negative charge. The density of

states along the $x$-axis, corresponding to this hemisphere, is then constant within the region $0 \leq x \leq l$ (we refer to $l$ as the thickness of the headgroup region; see Fig. 9.1). This can be seen by writing the surface area of a sphere of radius $l$ in cylindrical coordinates as $2\pi \int_{-l}^{l} dx\, r(x)\sqrt{1+r'(x)^2} = 2\pi l \int_{-l}^{l} dx = 4\pi l^2$, where $r(x) = \sqrt{l^2 - x^2}$ is the distance to the $x$-axis and $r'(x)$ denotes the first derivative of $r(x)$. Alternatively expressed, if a sphere is cut into slices of equal thickness, then each slice has the same surface area of its rim. Each state is adopted with a yet unknown probability $P_l(x)$. We refer to the function $P_l(x)$ as *orientational distribution* of the zwitterionic headgroups; it is normalized according to $\int_0^l dx P_l(x) = l$. The third term in Eq. (9.1) then corresponds to the entropy-related free energy cost of changing the orientational distribution away from $P_l(x) \equiv 1$.

We point out that the free energy $f_b$ of the bare lipid layer in Eq. (9.1) contains four unconstrained quantities: $n_+(x)$, $n_-(x)$, $P_l(x)$, and $\eta$. The first three are functions of $x$ whereas $\eta$ is merely a number. In thermal equilibrium $f_b(n_+, n_-, P_l, \eta)$ adopts a minimum. To find that minimum we point out that the potential $\Psi$ too depends on some of the unconstrained variables through Poisson's equation, $\Psi''(x) = -4\pi\ell_{\rm B}\rho(x)/e$, with the local $x$-dependent volume charge density

$$\rho = e \begin{cases} n_+ - n_- + \frac{(1-\phi)}{al}\, P_l, & 0 < x < l \\ n_+ - n_-, & l \leq x < \infty\ . \end{cases} \tag{9.4}$$

This accounts for the presence of salt ions outside the headgroup region ($l \leq x < \infty$), and for the additional presence of the positively charged ends of the zwitterionic headgroups inside the headgroup region ($0 < x < l$). Strictly, one would need to also account for the local concentration of the protons. Yet, for local salt concentrations much larger than local proton concentrations (which we consider in the present work) we may ignore this additional contribution. Note that the negative lipid charges (i.e.,

the charges carried by PA and those of the zwitterionic headgroups) enter into the surface charge density $\sigma = -(1+\eta\phi)\, e/a$ at $x = 0$. The surface charge density is related to the slope of the potential $\Psi$ at $x = 0$ through $\Psi'(x=0) = -4\pi\ell_{\rm B}\sigma/e$. With this we have provided all information needed to minimize $f_b(n_+, n_-, P_l, \eta)$. To this end, it is sufficient to demand vanishing of the first variation $\delta f_b(n_+, n_-, P_l, \eta) = 0$, yielding (after some algebra) relations for the all unconstrained quantities. Specifically, we find the Boltzmann distributions $n_\pm = n_0 \exp(\mp\Psi)$ and $P_l = \exp(-\Psi)/q_l$ for, respectively, the salt ions and the orientational distribution of the zwitterionic headgroups (where the partition sum $q_l = (1/l)\int_0^l dx \exp(-\Psi)$ ensures proper normalization). In addition, we find for the degree of deprotonation

$$\eta = \frac{1}{1 + \frac{1-\eta_0}{\eta_0}\, e^{-\Psi(0)}}\ . \tag{9.5}$$

Hence, large positive surface potential $\Psi(0) \gg 1$ strongly favors deprotonation, whereas $\Psi(0) = 0$ leads to $\eta = \eta_0$ at which the solution pH matches the intrinsically preferred degree of deprotonation. To find the potential $\Psi(x)$, we insert the Boltzmann distributions into Poisson's equation, leading to a modified Poisson-Boltzmann equation

$$\Psi'' = \frac{1}{\ell_{\rm D}^2}\sinh\Psi - \begin{cases} (1-\phi)\dfrac{4\pi\ell_{\rm B}}{la}\,\dfrac{1}{q_l}\, e^{-\Psi}, & 0 < x < l \\ 0, & l \le x < \infty\ , \end{cases} \tag{9.6}$$

where $\ell_{\rm D}$ is the familiar Debye screening length, defined through $1/\ell_{\rm D}^2 = 8\pi\ell_{\rm B} n_0$. Note that Eq. (9.5) enters into the boundary condition, $\Psi'(x=0) = 4\pi\ell_{\rm B}(1+\eta\phi)$, for Eq. (9.6); the second boundary condition is $\Psi(x\to\infty) = 0$ thus ensuring $n_\pm(x\to\infty) = n_0$. We obtain $\Psi(x)$ and $\eta$ as the self-consistent numerical solutions of Eqs. (9.5) and (9.6). To compute the solution, we have employed a Newton-Raphson iteration scheme where the non-linear Eq. (9.6) was re-expressed as a sequence

of linear differential equations that can be solved using standard methods. The same method was applied throughout this work; see Eqs. (9.8) and (9.12) below. Generally, a differential equation of the form $\Psi''(x) = g(\Psi)$ (where $g$ can be a non-linear function) is expressed as an iterative sequence of linear differential equations, $\Psi''_{n+1} = g'(\Psi_n)(\Psi_{n+1} - \Psi_n) + g(\Psi_n)$, that, if converging for sufficiently large $n$ (i.e., yielding $\Psi_{n+1} = \Psi_n$ ), solves the original equation. Quantities like the partition sum and protonation fraction can be updated after each iteration step. Knowing $\Psi(x)$ enables us to calculate $n_\pm$ and $P_l$. Inserting these quantities into Eq. (9.1) finally yields the optimal free energy $f_b$.

In all of the present work we fix $l = 0.5\,\mathrm{nm}$, $a = 0.65\,\mathrm{nm}^2$, and $\ell_\mathrm{D} = 1\,\mathrm{nm}$. The former two values represent typical structural parameters of a lipid layer, whereas the latter corresponds to a physiological 0.1M salt solution. As discussed above, changes in the solution's pH value are described by choosing different values of $\eta_0$. Typical changes of the pH at physiological conditions are on the order of two units. For example, entry of protons into endosomal vesicles lowers the pH from 7 to 5. How such a change translates into different values of $\eta_0 = 1/(1 + 10^{\mathrm{pK}-\mathrm{pH}})$ depends on the lipid's intrinsic pK-value, which is typically unknown. What can be measured for PA are *apparent* pK values [134]. However, it is fully sufficient to make a generic assumption of the pK being somewhere close to pK= 7, where physiologically relevant changes of the pH impact PA's dissociation state. In the present work we find it convenient to chose pK= 6, implying that a decrease from pH= 7 to pH= 5 also decreases the nominal degree of deprotonation $\eta_0$ from $1/(1 + 10^{-1}) = 0.91$ to $1/(1 + 10^{+1}) = 0.091$. To model a pH-change of two units, it is thus appropriate to consider the two distinct values, $\eta_0 = 0.1$ and $\eta_0 = 0.9$. We will focus on these two choices throughout the present work.

We briefly discuss some basic structural properties of the bare lipid layer. A more exhaustive analysis has been provided recently [184]. The left diagram of Fig. 9.2

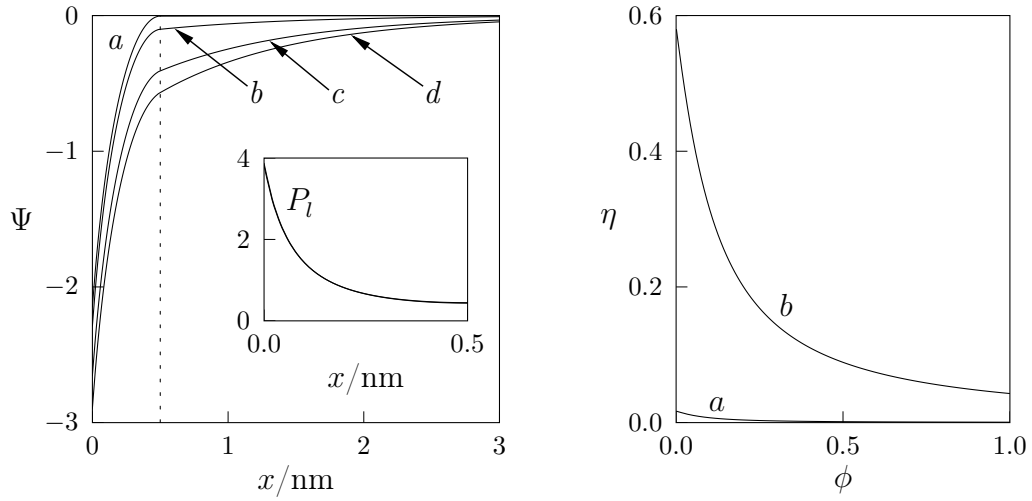


Figure 9.2. Left diagram: The potential $\Psi(x)$ for $\phi = 0.03$ and $\eta_0 = 0.1$ (curve *a*), for $\phi = 0.03$ and $\eta_0 = 0.9$ (curve *b*), for $\phi = 0.09$ and $\eta_0 = 0.1$ (curve *c*), and for $\phi = 0.09$ and $\eta_0 = 0.9$ (curve *d*). The dotted line marks the extension of the headgroup region $l = 0.5\,\mathrm{nm}$. The inset shows the corresponding orientational distributions $P_l(x)$ of the zwitterionic headgroups; here, all curves corresponding to cases *a*-*d* overlap each other. Right diagram: The degree of deprotonation $\eta(\phi)$ for $\eta_0 = 0.1$ (curve *a*) and $\eta_0 = 0.9$ (curve *b*).

shows $\Psi(x)$ for $\phi = 0.03$ and $\eta_0 = 0.1$ (curve *a*), for $\phi = 0.03$ and $\eta_0 = 0.9$ (curve *b*), for $\phi = 0.09$ and $\eta_0 = 0.1$ (curve *c*), and for $\phi = 0.09$ and $\eta_0 = 0.9$ (curve *d*).

We point out that for curve *a* the lipid layer contains only 3 mol% PA, of which almost all carry a single negative charge ($PA^-$) with very little $PA^{2-}$. Because the charge of $PA^-$ is the same as for the phosphate group of a zwitterionic lipid, the lipid layer corresponding to curve *a* is structurally similar to a purely zwitterionic one, where the potential outside the headgroup region almost vanishes. Increasing the mole fraction of PA (curves *c* and *d*) and/or its deprotonation state (curves *b* and *d*) renders the potential $\Psi(x)$ more negative. The differences of the potentials $\Psi(x)$ between the different curves *a*-*d* are notable but have negligible influence on the orientational distribution $P_l(x)$, which is displayed in the inset of Fig. 9.2 (all four curves overlap). Note that due to their electrostatic attraction it is far more likely to find the zwitterionic headgroups tilted rather than pointing in the normal direction

of the lipid layer. The right diagram of Fig. 9.2 displays the degree of deprotonation $\eta$ as function of the mole fraction of PA. Note that $\eta$ is generally smaller than $\eta_0$ because of the negative surface potential $\Psi(0)$. Increasing $\phi$ further lowers the degree of deprotonation $\eta$ because of the more negative potential associated with the presence of $PA^{2-}$ (see also Eq. (9.5)).

### *9.2.2. Bare protein*

In the present work we study a basic protein that can adsorb onto the lipid layer via electrostatic and, possibly, non-electrostatic interactions, the latter being a manifestation of the electrostatic-hydrogen bond switch mechanism. We consider two distinct states of the protein: bare (i.e., free in solution) and adsorbed (i.e., forming a complex with the lipid layer). The two states are schematically illustrated in Fig. 9.3. We assume the face of the protein that adsorbs onto the lipid layer is homogeneous, flat, and carries one single positive charge per area $a$ (recall that $a = 0.65\,\mathrm{nm}^2$ denotes the cross-sectional area per lipid). This choice is somewhat special but convenient for the interpretation of our findings below. It does not restrict the general nature of our model. In fact, any other area per charged protein residue could easily be incorporated into the present model. In addition, the adsorbing face of the protein is assumed to be sufficiently large so that finite-size effects are negligible. This renders the free energy of the protein (and similarly of the membrane-protein complex) extensive with respect to the lateral area of the protein's adsorbing face. Hence, we only need to consider the free energy per unit area, which we choose to be $a$.

We first consider the bare protein. As pointed out, its positive charges are distributed on the protein's adsorbing face with area density $1/a$. We could model the protein charge to be smeared at the protein surface. However, we choose to account in a simplified manner for the conformational flexibility that basic amino acids such as lysine typically possess [263]. Specifically, we model each protein charge to be attached

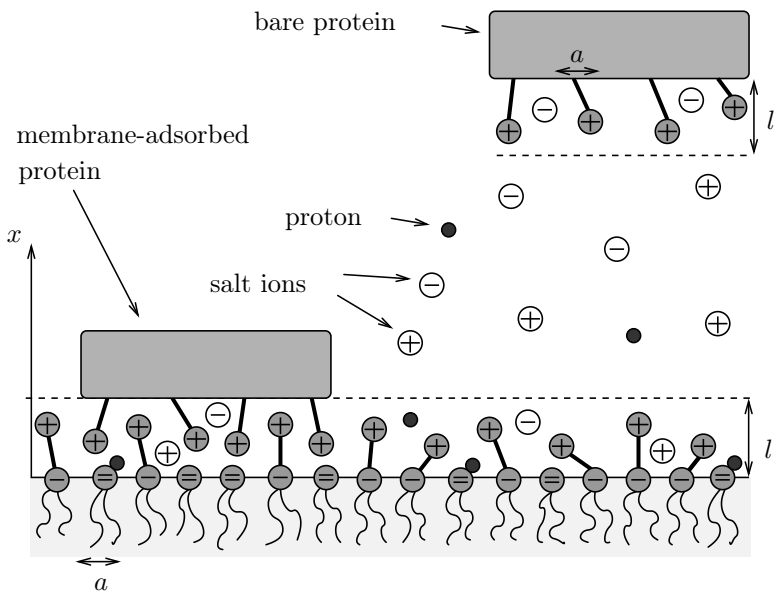


Figure 9.3. Illustration of a mixed lipid layer onto which a protein can adsorb. Displayed are the adsorbed state (left) and the desorbed state (right). The desorbed state is characterized by a bare lipid layer (as illustrated in Fig. 9.1) and a bare protein. The protein contains a flat face with attached basic residues of area density $1/a$. Each basic residue is able to move within a small region of thickness $l$ next to the protein's flat face. This models the conformational freedom of the protein's charged amino acids.

to the protein surface through a rigid rod of length $l = 0.5\,\mathrm{nm}$. The rod is free to rotate about its anchoring point so that the distance of the positive charge to the protein surface can vary between 0 and $l$. Note that this model is purposely made identical to our model for the positive charge of a zwitterionic headgroup (the difference is the presence of the negative charge at the anchoring point for the zwitterionic headgroup). As for the zwitterionic lipid layer, we denote the distance to the protein surface by $x$ and associate a function $P_p(x)$ with the probability distribution of finding the positive charges of the protein at position $x$. We normalize $P_p(x)$ according to $\int_0^l dx P_p(x) = l$. Note our use of the index "p" refers to "protein". The free energy per charge of the

bare protein can be written analogously to Eq. (9.1) as

$$f_p = a \int_0^\infty dx\, \hat{f}_{el} + \frac{k_\mathrm{B}T}{l} \int_0^l dx\, P_p \ln P_p \,, \tag{9.7}$$

where $\hat{f}_{el}$, given in Eq. (9.3), denotes the volume density of the electrostatic free energy. Note that $f_p$ is a function of the unconstrained variables $n_+$, $n_-$, and $P_p$. The local volume charge density $\rho(x)$ close to the protein is given by Eq. (9.4) with $\phi = 0$ and the replacement $P_l \to P_p$. Recall that $\rho(x)$ enters into Poisson's equation, $\Psi''(x) = -4\pi\ell_\mathrm{B}\rho(x)/e$. No charge is attached directly to the protein surface, implying $\Psi'(x = 0) = 0$. Minimization of $f_p$ then yields the familiar Boltzmann distributions $n_\pm = n_0 \exp(\mp\Psi)$ and $P_p = \exp(-\Psi)/q_p$ with the partition sum $q_p = (1/l)\int_0^l dx \exp(-\Psi)$. Inserting these distributions into Poisson's equation results in a modified Poisson-Boltzmann equation for the bare protein,

$$\Psi'' = \frac{1}{\ell_\mathrm{D}^2} \sinh\Psi - \begin{cases} \dfrac{4\pi\ell_\mathrm{B}}{la}\, \dfrac{1}{q_p}\, e^{-\Psi}, & 0 < x < l \\ 0, & l \le x < \infty \,, \end{cases} \tag{9.8}$$

to be solved subject to $\Psi'(x = 0) = 0$ and $\Psi(x \to \infty) = 0$. The solution yields $\Psi(x)$ from which we can calculate $n_+$, $n_-$, $P_p$, and thus $f_p$. Fig. 9.4 displays the potential $\Psi(x)$ and the distribution $P_p(x)$. Note that the positive potential $\Psi(x)$ saturates inside the region $0 < x < l$ within which the protein charges are distributed. The probability distribution of finding the positively charged protein residues is non-uniform due to the presence of the low dielectric interior of the protein. The corresponding image charges lead to an effective repulsion that is manifested in the small but notable shift of $P_p(x)$ away from small and toward larger $x$. We also note that the free energy of the bare protein according to Eq. (9.7) adopts the value $f_p = 2.438\, k_\mathrm{B}T$. This value refers to a single protein charge or, equivalently, to a unit area $a = 0.65\,\mathrm{nm}^2$.

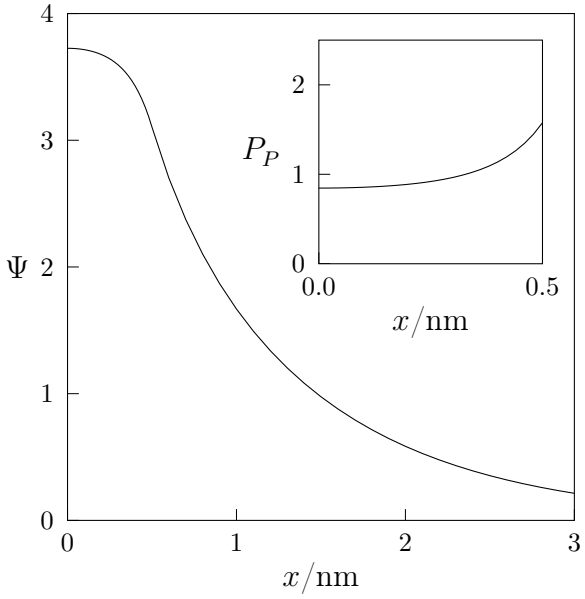


Figure 9.4. The potential $\Psi$ as function of the distance $x$ to the protein's surface for a bare protein. The inset shows the orientational distribution $P_p(x)$ of the protein charges. The parameters are $a = 0.65\,\mathrm{nm}^2$, $l = 0.5\,\mathrm{nm}$, and $\ell_\mathrm{D} = 1\,\mathrm{nm}$.

### *9.2.3. Membrane-adsorbed protein*

Next we consider the membrane-adsorbed state of the protein. The corresponding membrane-protein complex is illustrated on the left-hand side of Fig. 9.3. It is convenient and appropriate to assume the flat protein face locates on top of the headgroup region; i.e., at position $x = l$. This leaves the positive charges of both the zwitterionic lipids and the protein to reside within the headgroup region, $0 < x < l$. As for the bare membrane and bare protein, we use the functions $P_l(x)$ and $P_p(x)$ to describe the corresponding probability distributions. We also allow salt ions to partition into the headgroup region of the membrane-protein complex (see left diagram of Fig. 9.3). If the interaction between the protein and the membrane was purely of electrostatic nature, we could write the free energy as a combination of relevant terms in Eqs. (9.1) and (9.7). However, we make the additional assumption of a non-electrostatic adsorption energy between the basic protein residues and the deprotonated state of PA. This adsorption energy generally depends on the distance

between a given basic protein residue and $PA^{2-}$ along the $x$-axis. Our aim is to model a short-range attractive interaction as that arising from the formation of a hydrogen bond. Such an interaction can, roughly, be approximated by a simple square-well potential

$$U(x) = \begin{cases} -U_0, & 0 < x < \tilde{l} \\ 0, & \tilde{l} \leq x < \infty \end{cases} \tag{9.9}$$

with $\tilde{l} \approx 0.2\,\mathrm{nm}$ and a yet unspecified interaction strength $U_0$ (with $U_0 > 0$). For a discussion how the square-well potential relates to the 10-12 potential that is frequently used is molecular dynamics simulations see [184]. Below we study how the choice of the well depth, $U_0$, in Eq. (9.9) influences the pH-dependent sensitivity of protein adsorption.

With this we write for the total free energy of the membrane-protein complex, measured per lipid within the protein's adsorption region

$$\begin{aligned} f_c =& f_{mix} + a \int_0^l dx\, \hat{f}_{el} + (1-\phi)\frac{k_\mathrm{B}T}{l} \int_0^l dx\, P_l \ln P_l \\ &+ \frac{k_\mathrm{B}T}{l} \int_0^l dx\, P_p \ln P_p + \eta\phi \frac{k_\mathrm{B}T}{l} \int_0^l dx\, P_p U \ , \end{aligned} \tag{9.10}$$

where the index "c" in $f_c$ stands for "complex". Our expression for $f_c$ contains the lipid's mixing free energy ($f_{mix}$ according to Eq. (9.2)), the electrostatic free energy as in the classical Poisson-Boltzmann model ($f_{el}$ according to Eq. (9.3)), two entropic contributions due to the conformational degrees of freedom for both the zwitterionic lipids (proportional to $P_l \ln P_l$) and the basic protein residues (proportional to $P_p \ln P_p$). The final term in the last line of Eq. (9.10) describes the non-electrostatic interaction energy as discussed above. The function $U = U(x)$ is given in Eq. (9.9). The degrees of

freedom pertaining to $f_c$ are $n_\pm$, $P_l$, $P_p$, and $\eta$. To find their equilibrium values, we note that the local volume charge density $\rho(x)$ within the headgroup region can be expressed as $\rho/e = n_+ - n_- + [(1-\phi)P_l + P_p]/(al)$. This together with Poisson's equation (as specified above) allows us to minimize $f_c$. We again obtain the Boltzmann distributions $n_\pm = n_0 \exp(\mp\Psi)$, $P_l = \exp(-\Psi)/q_l$, $P_p = \exp(-\Psi - \eta\phi U)/q_p$, with the corresponding partition sums $q_l = (1/l)\int_0^l dx \exp(-\Psi)$ and $q_p = (1/l)\int_0^l dx \exp(-\Psi - \eta\phi U)$ thus ensuring the normalizations $\int_0^l dx P_l(x) = l$ and $\int_0^l dx P_p(x) = l$. In addition to that, we find for the optimal degree of deprotonation

$$\eta = \frac{1}{1 + \frac{1-\eta_0}{\eta_0}\, e^{-\Psi(0) + \frac{1}{l}\int\limits_0^l dx\, U P_p}} \,. \tag{9.11}$$

Note the presence of the non-electrostatic potential $U = U(x)$ in the expressions for $P_p$ and $\eta$; this is a manifestation of the favorable interaction between basic protein residues with $PA^{2-}$. In fact, a more favorable interaction $U$ (i.e, larger $U_0$ in Eq. (9.9)) increases both the deprotonation fraction $\eta$ and the probability of the basic protein residues to reside closer to $PA^{2-}$.

As for the bare lipid layer and bare protein, we obtain a modified Poisson-Boltzmann equation by inserting the Boltzmann distributions into Poisson's equation,

$$\Psi'' = \frac{1}{\ell_{\rm D}^2} \sinh\Psi - \frac{4\pi\ell_{\rm B}}{la}\, e^{-\Psi} \left[\frac{1-\phi}{q_l} + \frac{e^{-\eta\phi U}}{q_P}\right] . \tag{9.12}$$

This equations must be solved within the headgroup region, $0 < x < l$, subject to the boundary conditions $\Psi'(x=0) = 4\pi\ell_{\rm B}(1+\eta\phi)$ and $\Psi'(x=l) = 0$, reflecting the presence and absence of charges at $x = 0$ and $x = l$, respectively. We point out that both Eq. (9.12) as well as the boundary condition at $x = 0$ depend on $\eta$ according to Eq. (9.11). Hence, the solutions for $\Psi(x)$ and $\eta$ must be found self-consistently.

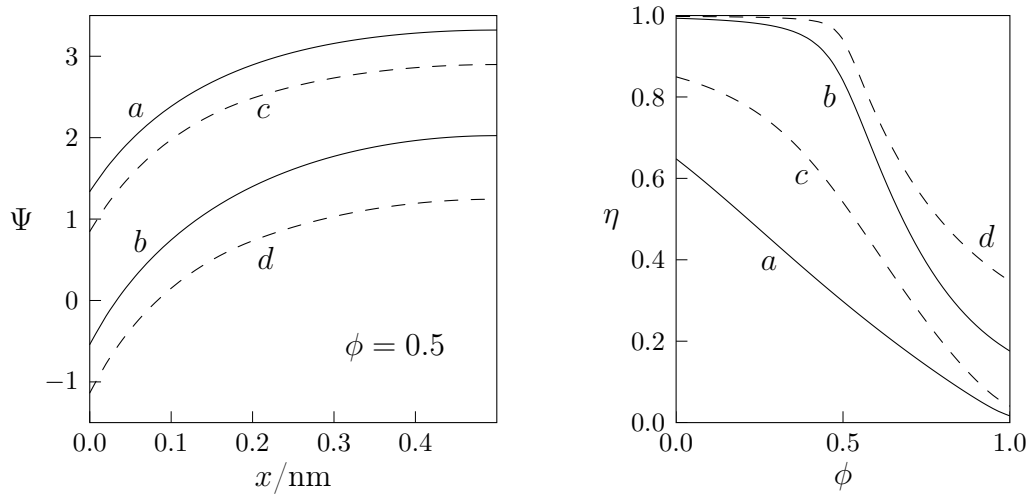


Figure 9.5. Left diagram: $\Psi(x)$ inside the headgroup region for the membrane-protein complex. The different curves refer to $\eta_0 = 0.1$ and $U_0 = 0$ (curve *a*), $\eta_0 = 0.9$ and $U_0 = 0$ (curve *b*), $\eta_0 = 0.1$ and $U_0 = 2$ (curve *c*), $\eta_0 = 0.9$ and $U_0 = 2$ (curve *d*). All curves are derived for $\phi = 0.5$ as indicated. Right diagram: The deprotonation fractions as function of $\phi$. Labeling of the four curves is as in the left diagram.

Once $\Psi(x)$ and $\eta$ are known, they can be used to calculate $n_\pm$, $P_l$, $P_p$ and thus the free energy $f_c$ in Eq. (9.10).

As an example for solving the modified Poisson-Boltzmann equation for a membrane-protein complex we show in Fig. 9.5 the potential $\Psi(x)$ for the specific choice $\phi = 0.5$ (left diagram) and the degree of protonation $\eta$ as function of $\phi$ (right diagram) for the four combinations of $U_0 = 0$ and $U_0 = 2$ as well as $\eta_0 = 0.1$ and $\eta_0 = 0.9$. The 50% mole fraction of PA in the left diagram of Fig. 9.5 may seem unreasonably high, but we point out that proteins are able to sequester lipids that they interact with favorably. That is, the *local* mole fraction of PA within the adsorption site of a protein may be significantly larger than the average value in the bulk membrane. Indeed, below (see Fig. 9.6) we find the present model to predict local PA mole fractions of 50% and even higher. Due to the presence of the positive protein charges, the potential becomes more positive as compared to the bare lipid layer (see Fig. 9.2). Larger $\eta_0$ implies a larger degree of deprotonation $\eta$ and thus a more negative potential. Increasing $U_0$ to $U_0 = 2$ (curves *c* and *d*) decreases $\Psi(x)$ because the more favorable

non-electrostatic interaction of the basic protein residues with $PA^{2-}$ further increases the degree of deprotonation $\eta$.

### 9.3. Results and discussion

In Section 9.2 we have presented our models for the free energies of the bare lipid layer $f_b$, the bare protein $f_p$, and the membrane-protein complex $f_c$. All these energies are measured with respect to the same lateral system extension $a$; i.e., with respect to a single lipid for $f_b$ and $f_c$ as well as a single basic protein residue for $f_p$. One lipid occupies a cross-sectional area $a = 0.65\,\mathrm{nm}^2$ and so does a single basic protein residue. Our objective is to calculate the adsorption free energy of the protein using $f_b$, $f_p$, and $f_c$. In a typical experimental situation the molar fraction $\phi$ of PA will be fixed in the bare membrane, we refer to that fixed value as $\phi_b$. The molar fraction of PA in a biomembrane is small, we only consider values with $\phi_b < 0.1$. More specifically, we first investigate the particular choice $\phi_b = 0.03$ (below in Fig. 9.6), and further on (in Fig. 9.7) we also derive results for two other choices, $\phi_b = 0.06$ and $\phi_b = 0.09$.

As already indicated above, when the protein adsorbs onto the lipid membrane, it can recruit additional PA within the adsorption region. Hence, PA's mole fraction $\phi$ within the membrane-protein complex (we refer to that mole fraction as $\phi_c$) may be larger than $\phi_b$. The quantity that is kept constant during the adsorption is the chemical potential

$$\mu = \left( \frac{\partial f_b(\phi)}{\partial \phi} \right)_{\phi_b} . \tag{9.13}$$

Here we have used the free energy of the bare lipid layer $f_b = f_b(\phi)$ as function of the mole fraction $\phi$ of PA. Taking the derivative with respect for $\phi$ (where the internal degrees of freedom $n_\pm$, $P_l$, and $\eta$ adjust) at fixed $\phi_b$ specifies the chemical potential $\mu$ of PA. At equilibrium, the chemical potential of PA residing in either the bulk lipid

layer or within the protein adsorption site must be equal. This implies equality of the derivatives

$$\left(\frac{\partial f_b(\phi)}{\partial \phi}\right)_{\phi_b} = \left(\frac{\partial f_c(\phi)}{\partial \phi}\right)_{\phi_c} , \tag{9.14}$$

taken at the coexisting mole fractions $\phi_b$ and $\phi_c$. Eq. (9.14) constitutes a relation to compute $\phi_c$. Once $\phi_c$ is known we can calculate the adsorption free energy (measured per lipid with cross-sectional area $a$) of the protein through

$$\Delta f_{ads} = f_c(\phi_c) - f_b(\phi_b) - f_p - \mu(\phi_c - \phi_b) . \tag{9.15}$$

Here, we have also expressed $f_c = f_c(\phi_c)$ as function of the mole fraction of PA at the protein adsorption site. (Note that $f_p$ does not depend on $\phi$). To provide a straightforward physical interpretation of Eq. (9.15), we simply write the adsorption as a two-step process. The first is the demixing of the membrane adsorption site from $\phi_b$ to $\phi_c$ without the protein yet adsorbed. This can be written as $f_b(\phi_c) - f_b(\phi_b) - \mu(\phi_c - \phi_b)$. The second is the adsorption of the protein onto a lipid layer of pre-formed composition $\phi_c$. This part is $f_c(\phi_c) - f_b(\phi_c) - f_p$. Adding the two contributions together indeed yields $\Delta f_{ads}$ in Eq. (9.15).

To illustrate the calculation of $\Delta f_{ads}$, we show in Fig. 9.6 the different free energy contributions, $f_b(\phi)$ and $f_c(\phi)$ as function of $\phi$ (as well as $f_p$, which is a constant). Left and right diagrams in Fig. 9.6 refer to $\eta_0 = 0.1$ and $\eta_0 = 0.9$ as indicated. The curve for $f_b(\phi)$ is marked by the symbol $\circ$ at $\phi_b = 0.03$, and the corresponding derivative (i.e., the chemical potential) is indicated. For the three different curves of $f_c(\phi)$ (which refer to $U_0 = 0$ in curve $a$, $U_0 = 2$ in curve $b$, and $U_0 = 4$ in curve $c$), the positions with the same chemical potential are indicated (again by the symbol $\circ$ for each curve and the corresponding slopes). We emphasize that the coexisting mole fractions marked in Fig. 9.6 refer to $\phi_b = 0.03$ (where 3% of the lipids

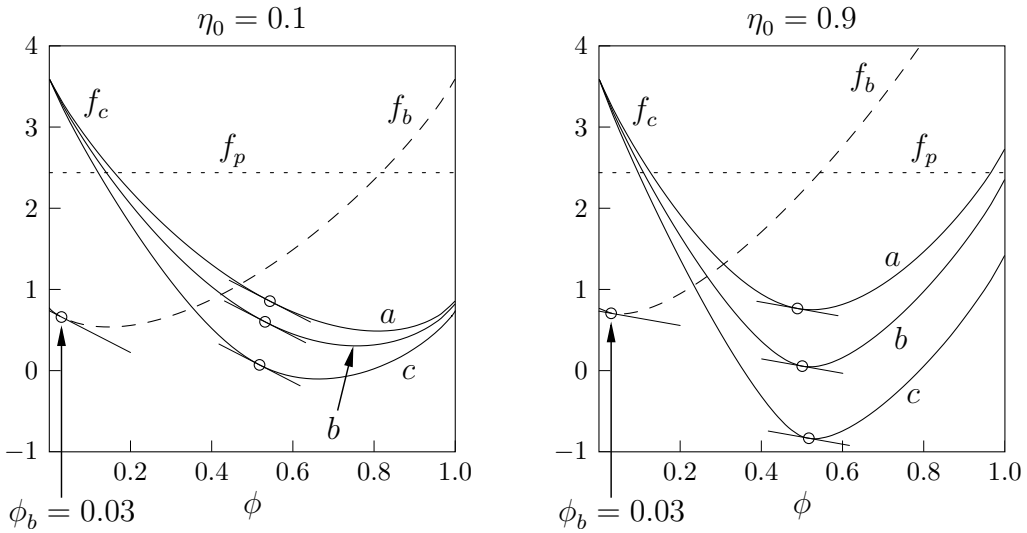


Figure 9.6. The different free energy contributions as function of the mole fraction $\phi$ of PA. The dashed line shows $f_b$, the dotted line shows $f_p$ (which is a constant), and the three solid lines show $f_c$, where curves $a$, $b$, $c$ correspond to $U_0 = 0$, $U_0 = 2$, $U_0 = 4$, respectively. The position $f_b(\phi = \phi_b)$ with $\phi_b = 0.03$ is marked by the symbol $\circ$; the corresponding slope (indicated by a short solid line) signifies the chemical potential $\mu$. For each of the three functions $f_c(\phi)$, the corresponding coexisting composition $\phi_c$ within the protein's adsorption site (i.e., with the same chemical potential) is also indicated (and marked by the symbol $\circ$ with the corresponding slope). All energies are plotted in units of $k_{\mathrm{B}}T$. Left and right diagrams refer to $\eta_0 = 0.1$ and $\eta_0 = 0.9$ as indicated.

in the bulk lipid layer are PA); other choices can be analyzed analogously using the same functions for the free energies. A few observations regarding Fig. 9.6 are worth mentioning:

- The mole fraction of PA within the protein's adsorption region ($\phi_c \approx 0.5$) is much larger than that in the bulk ($\phi_b = 0.03$). This is a result of the favorable interaction of PA with the basic protein residues. For vanishing $U_0$ this interaction is only electrostatic, whereas for $U_0 > 0$ there is an additional non-electrostatic contribution.

- With growing $U_0$ the free energy $f_c$ becomes more negative. This is strictly implied by the negative contribution of the non-electrostatic interaction term in Eq. (9.10). Also, for growing $U_0$ the degree of deprotonation $\eta$ grows because

the non-electrostatic attraction takes place selectively with $PA^{2-}$ and thus favors the deprotonated state.

- All free energies ($f_c$ and similarly for $f_b$) converge to the same value at $\phi = 0$, irrespective of $\eta_0$ and $U_0$. This is because the choice $\phi = 0$ corresponds to a pure zwitterionic lipid layer where $\eta_0$ and $U_0$ are irrelevant. The properties of a pure zwitterionic lipid layer have been analyzed in previous work [182, 183].

We finally note that Fig. 9.6 provides all information to calculate the adsorption free energy $\Delta f_{ads}$ according to Eq. (9.15). We have performed this calculation as function of $U_0$ for three different values of $\phi_b$ (namely $\phi_b = 0.03$, $\phi_b = 0.06$, and $\phi_b = 0.09$). The results are displayed in Fig. 9.7.

Here the left diagram shows the adsorption free energy $\Delta f_{ads}$ and the right two diagrams display the corresponding degree of protonation $\eta$ and mole fraction $\phi_c$ of PA within the adsorption region. All diagrams show two sets of three curves. The three curves refer to $\phi_b = 0.03$ (solid), $\phi_b = 0.06$ (dashed), and $\phi_b = 0.09$ (dotted), and the two sets to $\eta_0 = 0.1$ and $\eta_0 = 0.9$. The three points marked by the symbol $\circ$ correspond to the system in Fig. 9.6 (i.e., $\phi_b = 0.03$ and the three choices $U_0 = 0$, $U_0 = 2$, $U_0 = 4$).

Fig. 9.7 is the main result of this work. It shows how the adsorption free energy (measured per lipid within the adsorption region of the protein) is affected by a change of two units in the pH (as expressed by changing $\eta_0$ from 0.1 to 0.9). Generally, $\Delta f_{ads}$ is on the order of a few $k_{\mathrm{B}}T$. It is always negative; i.e., the adsorption process is energetically favorable. For example, for $\phi_b = 0.03$ and $U_0 = 0$, where all interactions are electrostatic in nature, the adsorption free energy decreases from $\Delta f_{ads} = -0.92 k_{\mathrm{B}}T$ for $\eta_0 = 0.1$ to $\Delta f_{ads} = -1.97 k_{\mathrm{B}}T$ for $\eta_0 = 0.9$. Already this can be a significant decrease that a real system could exploit to regulate the adsorption process. Say, a peripheral protein has a total lateral contact area of 4 $\mathrm{nm}^2$ with a membrane,

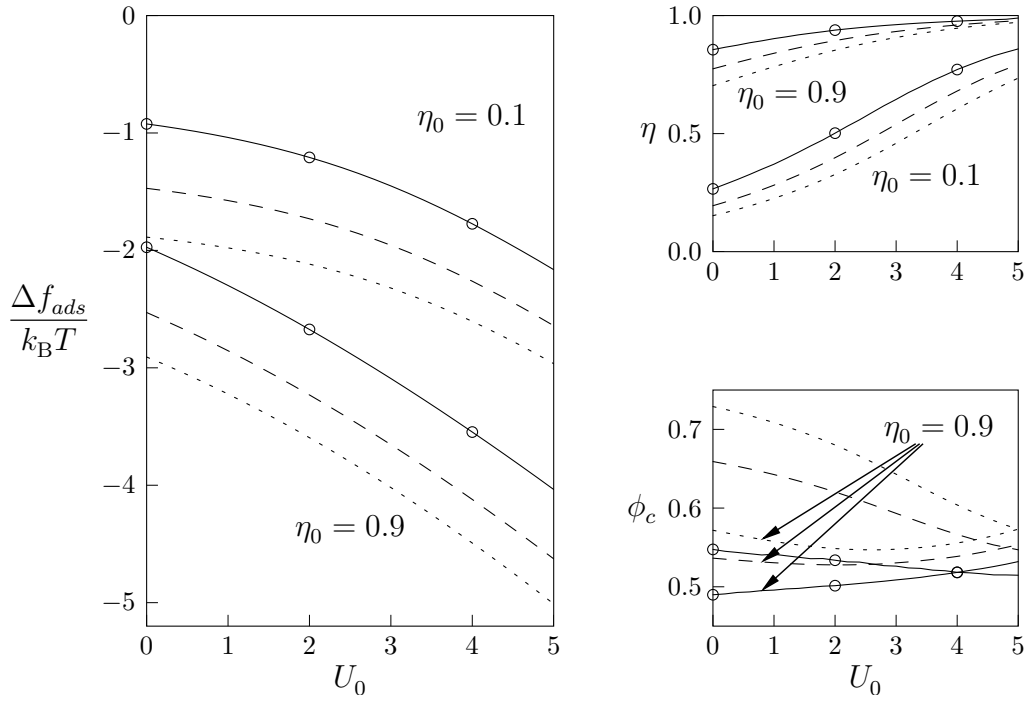


Figure 9.7. Protein adsorption free energy per lipid $\Delta f_{ads}$ (left diagram) and corresponding degree of protonation $\eta$ (right top diagram) and mole fraction $\phi_c$ (right bottom diagram) of PA within the adsorption region, all plotted as function of the strength $U_0$ of the non-electrostatic interaction. Each of the diagrams shows two sets of three curves. The three curves refer to $\phi_b = 0.03$ (solid), $\phi_b = 0.06$ (dashed), and $\phi_b = 0.09$ (dotted), and the two sets to $\eta_0 = 0.1$ and $\eta_0 = 0.9$ as indicated. The symbols $\circ$ mark the values for $\phi_b = 0.03$ to which the specific examples in Fig. 9.6 refers. Recall that $\eta_0 = 0.9$ and $\eta_0 = 0.1$ correspond to pH=7 and pH=5, respectively.

corresponding to about $6 \approx 4/0.65$ lipids within the protein adsorption region. The total adsorption free energy would then amount to $-0.92 \times 6\ k_B T = -5.52\ k_B T$ for $\eta_0 = 0.1$, and $-1.97 \times 6\ k_B T = -11.8\ k_B T$ for $\eta_0 = 0.9$. For small protein coverage the binding constant $K \sim \exp(-\Delta f_{ads}/k_B T)$ is exponentially related to the adsorption free energy. Hence, the binding constant would grow by a factor of $\exp(11.2)/\exp(5.2) = 730$ upon a two-unit increase of the pH. In the presence of non-electrostatic interactions this increase becomes substantially larger. For example, for $U_0 = 4$ we would obtain for the same system (i.e., 3% PA in the bulk membrane and 6 lipid within the protein adsorption site) $\exp(3.5 \times 6)/\exp(1.77 \times 6) = 32,000$. Similar increases are found for different $\phi_b$.

The question asked in the present work is to what extent the addition of a non-electrostatic interaction energy ($U_0$ in our case) affects the pH-sensitivity of the adsorption process. *A priory* it is not evident that a non-electrostatic interaction has any influence on pH-regulation, which is an electrostatic effect. However, Fig. 9.7 reveals that upon increasing $U_0$ the adsorption free energy $\Delta f_{ads}$ decreases more for $\eta_0 = 0.9$ than for $\eta_0 = 0.1$. For example, with 3mol% PA in the membrane (the solid lines in Fig. 9.7) the loss in adsorption free energy (per lipid and in units of $k_{\mathrm{B}}T$) upon a 2-unit decrease of the pH value (i.e., from pH=7 down to pH=5) is $1.97 - 0.92 = 1.05$ for $U_0 = 0$ whereas it is $3.55 - 0.92 = 2.63$ for $U_0 = 4$. Hence, using a pH decrease to release a protein from the membrane is much easier in presence of non-electrostatic interactions ($U_0 > 0$) as compared to their absence ($U_0 = 0$). This statement is qualitatively correct for any particular choices of $U_0$ and $\phi_b$. Hence, our model predicts generally that the interplay of electrostatic and non-electrostatic interactions increases the pH-sensitivity. The key for the physical mechanisms to work is that the non-electrostatic interactions are sensitive with regards to the two protonation states, $\mathrm{PA}^-$ and $\mathrm{PA}^{2-}$, and thus can be regulated by pH-changes.

## 9.4. Conclusion

The present theoretical work has focused on the pH regulation of the membrane affinity of PA binding proteins. We have specifically investigated whether the electrostatic hydrogen bond switch mechanism increases the affinity of PA binding proteins for PA through non-electrostatic interactions, and how this depends on pH. Figure 7 clearly shows that as the hydrogen bond strength is increased, the adsorption free energy becomes more negative (i.e. more favorable), and this effect is significantly larger at higher pH (i.e. the slope of $\Delta f_{ads}$ is significantly steeper for $\eta_0 = 0.9$ than for $\eta_0 = 0.1$). The electrostatic-hydrogen bond switch mechanism thus facilitates PA

binding proteins to bind to PA in pH dependent way. It is likely that the electrostatic-hydrogen bond switch also helps proteins to distinguish PA from more abundant acidic lipid species such as phosphatidylserine (PS). To include PS into our present model would be an interesting extension.

It is evident that the protonation/deprotonation equilibrium of an acidic lipid that binds a basic protein entails a pH-dependence of the protein's binding constant. Such a dependence would already exist based on electrostatic interactions alone. Yet, much less evident is the role that additional non-electrostatic interactions play in this pH-dependence. Our work demonstrates that the presence of an additional non-electrostatic contribution to the binding *increases the sensitivity* of this pH-dependence. Hence, a physiological decrease in pH can cause a larger drop in the affinity of PA-binding proteins for the membrane.

Given the approximative nature of our model, how reliable are our conclusions? Recall that we employ an array of assumptions, ranging from the mean-field nature of the Poisson-Boltzmann model to a number of drastic structural simplifications. However, none of these appears likely to qualitatively change the model predictions. For example, allowing the lateral cross-sectional area $a$ of PA to depend on its protonation state and to be significantly smaller from that of the zwitterionic lipid (instead of assuming they are all the same) will render the present theoretical model considerably more involved but is expected to affect the results only in a minor way. This is because the number of PA that migrates to the protein binding site is dominated by the tendency of *charge matching* between membrane and protein rather than the cross-sectional area per lipid. A different cross-sectional area for PA would thus not affect the number of PA molecules that migrate into the protein binding site. In fact, if – as we propose – the electrostatic hydrogen bond switch mechanism constitutes a general mechanism to regulate protein adsorption, it should depend on structural motifs rather than structural details. This is what the present work has focused on.

The pH-regulation of membrane affinity is illustrated by the transcription factor Opi1 [302]. At acidic pH (e.g. upon starvation which leads to a drop in cytosolic pH) Opi1 is released from the ER membrane to turn off membrane biogenesis. Conversely, at neutral pH, which is maintained when yeast is metabolizing glucose; e.g., Opi1 is kept bound to the ER membrane and subsequently membrane biogenesis takes place. Thus when the yeast cell has a sufficient energy supply it is able to grow, and when it is starved of nutrients it effectively shuts down growth. Our model thus shows how PA is able to act as a pH sensor. Opi1 is likely not unique in this pH sensitivity and other instances have been noted in the literature [250]. It will be important to investigate the role of pH modulation for other pathways in which PA functions. Aside from PA there are other signaling lipids that contain a phosphomonoester group (e.g. ceramide-1-phosphate (cer-1-p) and polyphosphoinositides) and the electrostatic hydrogen bond switch mechanism might act in those circumstances as well to make the signaling process pH-dependent. Since our formalism is general it can be adjusted to investigate these additional cases where a lipid phosphomonoester is responsible for binding to basic amino acid residues. In the case of cer-1-p it was recently found that the free OH group in the headgroup creates specificity for the binding of cPLA2$\alpha$ to cer-1-p over PA which is structurally similar but which lacks the OH group (personal communication, Robert Stahelin). The interaction of the polyphosphoinositides to proteins also poses an interesting case where multiple phosphomonoesters coordinate to bind protein partners. We are currently investigating the possibility of adopting our model to treat these considerably more complicated cases.

## 9.5. Acknowledgments

EEK is grateful for funding from I2CAM and NSF grant CHE 1058719.

# REFERENCES


[1] Akimov, S. A., Frolov, V. A. J., Kuzmin, P. I., Zimmerberg, J., Chizmadzhev, Y. A., and Cohen, F. S., *Domain formation in membranes caused by lipid wetting of protein*, Phys. Rev. E **77** (2008), no. 5, 051901.

[2] Alberts, B., Johnson, A., Lewis, J., Raff, M., Roberts, K., and Walter, P., *Molecular biology of the cell*, Garland Science, New York, 2002.

[3] Allender, D. W. and Schick, M., *Phase separation in bilayer lipid membranes: Effects on the inner leaf due to coupling to the outer leaf*, Biophys. J. **91** (2006), no. 8, 2928–2935.

[4] Almeida, P. F. F., *Lipid transfer between vesicles: Effect of high vesicle concentration*, Biophys. J. **76** (1999), no. 4, 1922–1928.

[5] Almeida, P. F. F., Pokorny, A., and Hinderliter, A., *Thermodynamics of membrane domains*, Biochim. Biophys. Acta – Biomembr. **1720** (2005), no. 1-2, 1–13.

[6] Andelman, D., *Electrostatic properties of membranes: The Poisson-Boltzmann theory*, Structure and Dynamics of Membranes (Lipowsky, R. and Sackmann, E., eds.), vol. 1, Elsevier, Amsterdam, second ed., 1995, pp. 603–642.

[7] Andersen, O. S. and Koeppe, R. E., *Bilayer thickness and membrane protein function: An energetic perspective*, Annu. Rev. Biophys. Biomol. Struct. **36** (2007), no. 1, 107–130.

[8] Andresen, T. L., Jensen, S. S., and Jorgensen, K., *Advanced strategies in liposomal cancer therapy: Problems and prospects of active and tumor specific drug release*, Prog. Lipid Res. **44** (2005), no. 1, 68–97.

[9] Aranda-Espinoza, H., Berman, A., Dan, N., Pincus, P. A., and Safran, S. A., *Interaction between inclusions embedded in membranes*, Biophys. J. **71** (1996), no. 2, 648–656.

[10] Athenstaedt, K. and Daum, G., *Phosphatidic acid, a key intermediate in lipid metabolism*, Eur. J. Biochem. **266** (1999), no. 1, 1–16.

[11] Atkins, P. and de Paula, J., *Physical chemistry*, eighth ed., W. H. Freeman, New York, 2007.

[12] Baird, B. A., Sheets, E. D., and Holowka, D. A., *How does the plasma membrane participate in cellular signaling by receptors for immunoglobulin E?*, Biophys. Chem. **82** (1999), no. 2-3, 109–119.

[13] Balaz, S., *Lipophilicity in trans-bilayer transport and subcellular pharmacokinetics*, Perspect. Drug Discov. Des. **19** (2000), no. 1, 157–177.

[14] Baumgart, T., Hess, S. T., and Webb, W. W., *Imaging coexisting fluid domains in biomembrane models coupling curvature and line tension*, Nature **425** (2003), no. 6960, 821–824.

[15] Baumgart, T., Hammond, A. T., Sengupta, P., Hess, S. T., Holowka, D. A., Baird, B. A., and Webb, W. W., *Large-scale fluid/fluid phase separation of proteins and lipids in giant plasma membrane vesicles*, Proc. Natl. Acad. Sci. USA **104** (2007), no. 9, 3165–3170.

[16] Ben-Shaul, A. and Gelbart, W. M., *Statistical thermodynamics of amphiphile self-assembly: Structure and phase transitions in micellar solutions*, Micelles, Membranes, Microemulsions, and Monolayers (Gelbart, W. M., Ben-Shaul, A., and Roux, D., eds.), Springer, New York, first ed., 1994, pp. 1–104.

[17] Ben-Shaul, A., *Molecular theory of chain packing, elasticity and lipid protein interaction in lipid bilayers*, Structure and Dynamics of Membranes (Lipowsky, R. and Sackmann, E., eds.), vol. 1, Elsevier, Amsterdam, second ed., 1995, pp. 359–401.

[18] Ben-Tal, N., Honig, B., Miller, C., and McLaughlin, S., *Electrostatic binding of proteins to membranes. Theoretical predictions and experimental results with charybdotoxin and phospholipid vesicles*, Biophys. J. **73** (1997), no. 4, 1717–1727.

[19] Bergethon, P. R., *The physical basis of biochemistry: The foundations of molecular biophysics*, Springer, New York, 1998.

[20] Bickel, T. and Marques, C. M., *Entropic interactions in soft nanomaterials*, J. Nanosci. Nanotechnol. **6** (2006), no. 8, 2386–2395.

[21] Biesheuvel, P. M., *Electrostatic free energy of interacting ionizable double layers*, J. Coll. Interf. Sci. **275** (2004), no. 2, 514–522.

[22] Bohinc, K., Kralj-Iglič, V., and May, S., *Interaction between two cylindrical inclusions in a symmetric lipid bilayer*, J. Chem. Phys. **119** (2003), no. 14, 7435–7444.

[23] Bombelli, C., Caracciolo, G., Di Profio, P., Diociaiuti, M., Luciani, P., Mancini, G., Mazzuca, C., Marra, M., Molinari, A., Monti, D., Toccacieli, L., and Venanzi, M., *Inclusion of a photosensitizer in liposomes formed by DMPC/Gemini surfactant: Correlation between physicochemical and biological features of the complexes*, J. Med. Chem. **48** (2005), no. 15, 4882–4891.

[24] Bonnett, R., White, R. D., Winfield, U. J., and Berenbaum, M. C., *Hydroporphyrins of the meso-tetra(hydroxyphenyl)porphyrin series as tumour photosensitizers*, Biochem. J. **261** (1989), no. 1, 277–280.

[25] Boroudjerdi, H., Kim, Y. W., Naji, A., Netz, R. R., Schlagberger, X., and Serr, A., *Statics and dynamics of strongly charged soft matter*, Phys. Rep. **416** (2005), no. 3, 129–199.

[26] Bowick, M. J. and Travesset, A., *The statistical mechanics of membranes*, Phys. Rep. **344** (2001), no. 4-6, 255–308.

[27] Brannigan, G. and Brown, F. L. H., *Solvent-free simulations of fluid membrane bilayers*, J. Chem. Phys. **120** (2004), no. 2, 1059–1071.

[28] Brewster, R., Pincus, P. A., and Safran, S. A., *Hybrid lipids as a biological surface-active component*, Biophys. J. **97** (2009), no. 4, 1087–1094.

[29] Byk, G., Dubertret, C., Escriou, V., Frederic, M., Jaslin, G., Rangara, R., Pitard, B., Crouzet, J., Wils, P., Schwartz, B., and Scherman, D., *Synthesis, activity, and structure–activity relationship studies of novel cationic lipids for DNA transfer*, J. Med. Chem. **41** (1998), no. 2, 224–235.

[30] Caffrey, M., *Crystallizing membrane proteins for structure determination: Use of lipidic mesophases*, Annu. Rev. Biophys. **38** (2009), 29–51.

[31] Cahn, J. W. and Hilliard, J. E., *Free energy of a nonuniform system. i. interfacial free energy*, J. Chem. Phys. **28** (1958), no. 2, 258–267.

[32] Cai, Z., Wang, Y., Zhu, L. J., and Liu, Z. Q., *Nanocarriers: A general strategy for enhancement of oral bioavailability of poorly absorbed or pre-systemically metabolized drugs*, Curr. Drug Metab. **11** (2010), no. 2, 197–207.

[33] Callen, H. B., *Thermodynamics and an introduction to thermostatistics*, second ed., Wiley, New York, 1985.

[34] Camenisch, G., Folkers, G., and van de Waterbeemd, H., *Shapes of membrane permeability-lipophilicity curves: Extension of theoretical models with an aqueous pore pathway*, Eur. J. Pharm. Sci. **6** (1998), no. 4, 321–329.

[35] Castellana, E. T. and Cremer, P. S., *Solid supported lipid bilayers: From biophysical studies to sensor design*, Surf. Sci. Rep. **61** (2006), no. 10, 429–444.

[36] Chandler, D., *Interfaces and the driving force of hydrophobic assembly*, Nature **437** (2005), no. 7059, 640–647.

[37] Chang, H. I. and Yeh, M. K., *Clinical development of liposome-based drugs: Formulation, characterization, and therapeutic efficacy*, Int. J. Nanomed. **7** (2012), 49–60.

[38] Chatelier, R. C. and Minton, A. P., *Adsorption of globular proteins on locally planar surfaces: Models for the effect of excluded surface area and aggregation of adsorbed protein on adsorption equilibria*, Biophys. J. **71** (1996), no. 5, 2367–2374.

[39] Chou, T., Kim, K. S., and Oster, G., *Statistical thermodynamics of membrane bending-mediated protein–protein attractions*, Biophys. J. **80** (2001), no. 3, 1075–1087.

[40] Cockcroft, S., *Phosphatidic acid regulation of phosphatidylinositol 4-phosphate 5-kinases*, Biochim. Biophys. Acta – Mol. Cell Biol. Lipids **1791** (2009), no. 9, 905–912.

[41] Cooke, I. R., Kremer, K., and Deserno, M., *Tunable generic model for fluid bilayer membranes*, Phys. Rev. E **72** (2005), no. 1, 011506.

[42] Corbin, J. A., Evans, J. H., Landgraf, K. E., and Falke, J. J., *Mechanism of specific membrane targeting by C2 domains: Localized pools of target lipids enhance ca2+ affinity*, Biochem. **46** (2007), no. 14, 4322–4336.

[43] Cozzani, I., Jori, G., Bertoloni, G., Milanesi, C., Carlini, P., Sicuro, T., and Ruschi, A., *Efficient photosensitization of malignant human cells in vitro by liposome-bound porphyrins*, Chem.-Biol. Interact. **53** (1985), no. 1-2, 131–143.

[44] Crane, J. M., Kiessling, V., and Tamm, L. K., *Measuring lipid asymmetry in planar supported bilayers by fluorescence interference contrast microscopy*, Langmuir **21** (2005), no. 4, 1377–1388.

[45] Cronan, J. E., *Bacterial membrane lipids: Where do we stand?*, Annu. Rev. Microbiol. **57** (2003), no. 1, 203–224.

[46] Daniel, R. M. and Cowan, D. A., *Biomolecular stability and life at high temperatures*, Cell. Mol. Life Sci. **57** (2000), no. 2, 250–264.

[47] Davis, H. T., *Statistical mechanics of phases, interfaces, and thin films*, VCH, New York, 1996.

[48] de Planque, M. R. R. and Killian, J. A., *Protein-lipid interactions studied with designed transmembrane peptides: Role of hydrophobic matching and interfacial anchoring (review)*, Mol. Membr. Biol. **20** (2003), no. 4, 271–284.

[49] Decker, D. E., Vroegop, S. M., Goodman, T. G., Peterson, T., and Buxser, S. E., *Kinetics and thermodynamics of emulsion delivery of lipophilic antioxidants to cells in culture*, Chem. Phys. Lipids **76** (1995), no. 1, 7–25.

[50] Devaux, P. F. and Morris, R., *Transmembrane asymmetry and lateral domains in biological membranes*, Traffic **5** (2004), no. 4, 241–246.

[51] Dietrich, C., Bagatolli, L. A., Volovyk, Z. N., Thompson, N. L., Levi, M., Jacobson, K., and Gratton, E., *Lipid rafts reconstituted in model membranes*, Biophys. J. **80** (2001), no. 3, 1417–1428.

[52] Dill, K. A. and Stigter, D., *Lateral interactions among phosphatidylcholine and phosphatidylethanolamine head groups in phospholipid monolayers and bilayers*, Biochem. **27** (1988), no. 9, 3446–3453.

[53] Döbereiner, H.-G., Evans, E., Kraus, M., Seifert, U., and Wortis, M., *Mapping vesicle shapes into the phase diagram: A comparison of experiment and theory*, Phys. Rev. E **55** (1997), no. 4, 4458–4474.

[54] Doisy, A., Proust, J. E., Ivanova, T., Panaiotov, I., and Dubois, J. L., *Phospholipid/drug interactions in liposomes studied by rheological properties of monolayers*, Langmuir **12** (1996), no. 25, 6098–6103.

[55] Dommersnes, P. G. and Fournier, J. B., *Casimir and mean-field interactions between membrane inclusions subject to external torques*, Europhys. Lett. **46** (1999), no. 2, 256–261.

[56] Dowhan, W., *Molecular basis for membrane phospholipid diversity: Why are there so many lipids?*, Ann. Rev. Biochem. **66** (1997), no. 1, 199–232.

[57] Edidin, M., *The state of lipid rafts: From model membranes to cells*, Annu. Rev. Biophys. Biomol. Struct. **32** (2003), no. 1, 257–283.

[58] Epand, R. M., *Do proteins facilitate the formation of cholesterol-rich domains?*, Biochim. Biophys. Acta – Biomembr. **1666** (2004), no. 1, 227–238.

[59] Epand, R. M., *Proteins and cholesterol-rich domains*, Biochim. Biophys. Acta – Biomembr. **1778** (2008), no. 7-8, 1576–1582.

[60] Evans, D. F. and Wennerström, H., *The colloidal domain: Where physics, chemistry, and biology meet*, second ed., VCH, New York, 1994.

[61] Fahr, A., Holz, M., and Fricker, G., *Liposomal formulations of cyclosporin A: Influence of lipid type and dose on pharmacokinetics*, Pharm. Res. **12** (1995), no. 8, 1189–1198.

[62] Fahr, A. and Reiter, G., *Biophysical characterisation of liposomal delivery systems for lipophilic drugs: Cyclosporin A as an example*, Cell. Mol. Biol. Lett. **4** (1999), no. 4, 611–624.

[63] Fahr, A. and Seelig, J., *Liposomal formulations of cyclosporin A: A biophysical approach to pharmacokinetics and pharmacodynamics*, Crit. Rev. Ther. Drug Carrier Syst. **18** (2001), no. 2, 141–172.

[64] Fahr, A., van Hoogevest, P., May, S., Bergstrand, N., and Leigh, M. L. S., *Transfer of lipophilic drugs between liposomal membranes and biological interfaces: Consequences for drug delivery*, Eur. J. Pharm. Sci. **26** (2005), no. 3-4, 251–265.

[65] Fahr, A., van Hoogevest, P., Kuntsche, J., and Leigh, M. L. S., *Lipophilic drug transfer between liposomal and biological membranes: What does it mean for parenteral and oral drug delivery?*, J. Liposome Res. **16** (2006), no. 3, 281–301.

[66] Fahr, A. and Liu, X., *Drug delivery strategies for poorly water-soluble drugs*, Expert Opin. Drug Delivery **4** (2007), no. 4, 403–416.

[67] Fahr, A. and Liu, X., *Utilization of liposomes for studying drug transfer and uptake*, Methods Mol. Biol. **606** (2010), 1–10.

[68] Fan, J., Sammalkorpi, M., and Haataja, M., *Domain formation in the plasma membrane: Roles of nonequilibrium lipid transport and membrane proteins*, Phys. Rev. Lett. **100** (2008), no. 17, 178102.

[69] Fan, J., Sammalkorpi, M., and Haataja, M., *Influence of nonequilibrium lipid transport, membrane compartmentalization, and membrane proteins on the lateral organization of the plasma membrane*, Phys. Rev. E **81** (2010), no. 1, 011908.

[70] Farago, O., *"Water-free" computer model for fluid bilayer membranes*, J. Chem. Phys. **119** (2003), no. 1, 596–605.

[71] Faraudo, J. and Travesset, A., *Phosphatidic acid domains in membranes: Effect of divalent counterions*, Biophys. J. **92** (2007), no. 8, 2806–2818.

[72] Flory, P. J. and Volkenstein, M., *Statistical mechanics of chain molecules*, vol. 8, Wiley, New York, 1969.

[73] Fogolari, F., Brigo, A., and Molinari, H., *The Poisson-Boltzmann equation for biomolecular electrostatics: A tool for structural biology*, J. Mol. Recognit. **15** (2002), no. 6, 377–392.

[74] Frolov, V. A. J., Chizmadzhev, Y. A., Cohen, F. S., and Zimmerberg, J., *"Entropic traps" in the kinetics of phase separation in multicomponent membranes stabilize nanodomains*, Biophys. J. **91** (2006), no. 1, 189–205.

[75] Futerman, A. H. and Hannun, Y. A., *The complex life of simple sphingolipids*, Embo Reports **5** (2004), no. 8, 777–782.

[76] Gabizon, A. A., Shmeeda, H., and Zalipsky, S., *Pros and cons of the liposome platform in cancer drug targeting*, J. Liposome Res. **16** (2006), no. 3, 175–183.

[77] Gambhir, A., Hangyas-Mihalyne, G., Zaitseva, I., Cafiso, D. S., Wang, J. Y., Murray, D., Pentyala, S. N., Smith, S. O., and McLaughlin, S., *Electrostatic sequestration of PIP2 on phospholipid membranes by basic/aromatic regions of proteins*, Biophys. J. **86** (2004), no. 4, 2188–2207.

[78] Garbès Putzel, G. and Schick, M., *Phenomenological model and phase behavior of saturated and unsaturated lipids and cholesterol*, Biophys. J. **95** (2008), no. 10, 4756–4762.

[79] Garg, S., Rühe, J., Lüdtke, K., Jordan, R., and Naumann, C. A., *Domain registration in raft-mimicking lipid mixtures studied using polymer-tethered lipid bilayers*, Biophys. J. **92** (2007), no. 4, 1263–1270.

[80] Garidel, P., Johann, C., and Blume, A., *Nonideal mixing and phase separation in phosphatidylcholine phosphatidic acid mixtures as a function of acyl chain length and pH*, Biophys. J. **72** (1997), no. 5, 2196–2210.

[81] Gil, T., Sabra, M. C., Ipsen, J. H., and Mouritsen, O. G., *Wetting and capillary condensation as means of protein organization in membranes*, Biophys. J. **73** (1997), no. 4, 1728–1741.

[82] Golebiewska, U., Gambhir, A., Hangyas-Mihalyne, G., Zaitseva, I., Rädler, L., and McLaughlin, S., *Membrane-bound basic peptides sequester multivalent (PIP2), but not monovalent (PS), acidic lipids*, Biophys. J. **91** (2006), no. 2, 588–599.

[83] Gompper, G. and Kroll, D. M., *Network models of fluid, hexatic and polymerized membranes*, J. Phys.-Condens. Mat. **9** (1997), no. 42, 8795–8834.

[84] Goñi, F. M., Alonso, A., Bagatolli, L. A., Brown, R. E., Marsh, D., Prieto, M., and Thewalt, J. L., *Phase diagrams of lipid mixtures relevant to the study of membrane rafts*, Biochim. Biophys. Acta – Mol. Cell Biol. Lipids **1781** (2008), no. 11, 665–684.

[85] Gorbenko, G. P., Ioffe, V. M., and Kinnunen, P. K. J., *Binding of lysozyme to phospholipid bilayers: Evidence for protein aggregation upon membrane association*, Biophys. J. **93** (2007), no. 1, 140–153.

[86] Goulian, M., Bruinsma, R., and Pincus, P. A., *Long-range forces in heterogeneous fluid membranes*, Europhys. Lett. **22** (1993), no. 2, 145–150.

[87] Goulian, M., *Inclusions in membranes*, Curr. Opin. Coll. Interf. Sci. **1** (1996), no. 3, 358–361.

[88] Grassi, M., Grassi, G., Lapasin, R., and Colombo, I., *Understanding drug release and absorption mechanisms: A physical and mathematical approach*, CRC Press, Boca Raton, 2006.

[89] Grosberg, A. Y., Nguyen, T. T., and Shklovskii, B. I., *Colloquium: The physics of charge inversion in chemical and biological systems*, Rev. Mod. Phys. **74** (2002), no. 2, 329–345.

[90] Gurtovenko, A. A., Patra, M., Karttunen, M., and Vattulainen, I., *Cationic DMPC/DMTAP lipid bilayers: Molecular dynamics study*, Biophys. J. **86** (2004), no. 6, 3461–3472.

[91] Haleva, E., Ben-Tal, N., and Diamant, H., *Increased concentration of polyvalent phospholipids in the adsorption domain of a charged protein*, Biophys. J. **86** (2004), no. 4, 2165–2178.

[92] Hamilton, J. A., *Fast flip-flop of cholesterol and fatty acids in membranes: Implications for membrane transport proteins*, Curr. Opin. Lipidol. **14** (2003), no. 3, 263–271.

[93] Hammond, A. T., Heberle, F. A., Baumgart, T., Holowka, D. A., Baird, B. A., and Feigenson, G. W., *Crosslinking a lipid raft component triggers liquid ordered–liquid disordered phase separation in model plasma membranes*, Proc. Natl. Acad. Sci. USA **102** (2005), no. 18, 6320–6325.

[94] Hansen, J. P. and Lowen, H., *Effective interactions between electric double-layers*, Annu. Rev. Phys. Chem. **51** (2000), no. 1, 209–242.

[95] Hansen, J. P. and McDonald, I. R., *Theory of simple liquids*, third ed., Academic Press, London, 2006.

[96] Hansen, P. L., Miao, L., and Ipsen, J. H., *Fluid lipid bilayers: Intermonolayer coupling and its thermodynamic manifestations*, Phys. Rev. E **58** (1998), no. 2, 2311–2324.

[97] Hartvig, R. A., van de Weert, M., Ostergaard, J., Jorgensen, L., and Jensen, H., *Protein adsorption at charged surfaces: The role of electrostatic interactions and interfacial charge regulation*, Langmuir **27** (2011), no. 6, 2634–2643.

[98] Hefesha, H., Loew, S., Liu, X., May, S., and Fahr, A., *Transfer mechanism of temoporfin between liposomal membranes*, J. Controlled Release **150** (2011), no. 3, 279–286.

[99] Heimburg, T., Angerstein, B., and Marsh, D., *Binding of peripheral proteins to mixed lipid membranes: Effect of lipid demixing upon binding*, Biophys. J. **76** (1999), no. 5, 2575–2586.

[100] Heimburg, T., *Monte Carlo simulations of lipid bilayers and lipid protein interactions in the light of recent experiments*, Curr. Opin. Coll. Interf. Sci. **5** (2000), no. 3-4, 224–231.

[101] Helfrich, W., *Elastic properties of lipid bilayers: Theory and possible experiments*, Z. Naturforsch. **28** (1973), no. 11, 693–703.

[102] Herrig, A., Janke, M., Austermann, J., Gerke, V., Janshoff, A., and Steinem, C., *Cooperative adsorption of ezrin on PIP2-containing membranes*, Biochem. **45** (2006), no. 43, 13025–13034.

[103] Hinderliter, A., Almeida, P. F. F., Creutz, C. E., and Biltonen, R. L., *Domain formation in a fluid mixed lipid bilayer modulated through binding of the C2 protein motif*, Biochem. **40** (2001), no. 13, 4181–4191.

[104] Hinderliter, A., Biltonen, R. L., and Almeida, P. F. F., *Lipid modulation of protein-induced membrane domains as a mechanism for controlling signal transduction*, Biochem. **43** (2004), no. 22, 7102–7110.

[105] Honerkamp-Smith, A. R., Veatch, S. L., and Keller, S. L., *An introduction to critical points for biophysicists; observations of compositional heterogeneity in lipid membranes*, Biochim. Biophys. Acta – Biomembr. **1788** (2009), no. 1, 53–63.

[106] Horton, M. R., Rädler, J., and Gast, A. P., *Phase behavior and the partitioning of caveolin-1 scaffolding domain peptides in model lipid bilayers*, J. Coll. Interf. Sci. **304** (2006), no. 1, 67–76.

[107] Hu, M. Y., Diggins, IV, P., and Deserno, M., *Determining the bending modulus of a lipid membrane by simulating buckling*, J. Chem. Phys. **138** (2013), no. 21, 214110.

[108] Hu, M. Y., de Jong, D. H., Marrink, S. J., and Deserno, M., *Gaussian curvature elasticity determined from global shape transformations and local stress distributions: A comparative study using the MARTINI model*, Faraday Discuss. **161** (2013), 365–382.

[109] Huang, J. and Feigenson, G. W., *A microscopic interaction model of maximum solubility of cholesterol in lipid bilayers*, Biophys. J. **76** (1999), no. 4, 2142–2157.

[110] Humberstone, A. J. and Charman, W. N., *Lipid-based vehicles for the oral delivery of poorly water soluble drugs*, Adv. Drug Delivery Rev. **25** (1997), no. 1, 103–128.

[111] Immordino, M. L., Dosio, F., and Cattel, L., *Stealth liposomes: Review of the basic science, rationale, and clinical applications, existing and potential*, Int. J. Nanomed. **1** (2006), no. 3, 297–315.

[112] Israelachvili, J. N., Mitchell, J., and Ninham, B. W., *Theory of self-assembly of lipid bilayers and vesicles*, Biochim. Biophys. Acta – Biomembr. **470** (1977), no. 2, 185–201.

[113] Israelachvili, J. N., *Intermolecular and surface forces*, second ed., Academic Press, London, 1992.

[114] Jackson, J. D., *Classical electrodynamics*, third ed., Wiley, New York, 1998.

[115] Jenning, V., Schäfer-Korting, M., and Gohla, S., *Vitamin A–loaded solid lipid nanoparticles for topical use: Drug release properties*, J. Controlled Release **66** (2000), no. 2-3, 115–126.

[116] Jones, J. A., Rawles, R., and Hannun, Y. A., *Identification of a novel phosphatidic acid binding domain in protein phosphatase-1*, Biochem. **44** (2005), no. 40, 13235–13245.

[117] Jones, J. D. and Thompson, T. E., *Spontaneous phosphatidylcholine transfer by collision between vesicles at high lipid concentration*, Biochem. **28** (1989), no. 1, 129–134.

[118] Jones, J. D., Almeida, P. F. F., and Thompson, T. E., *Spontaneous interbilayer transfer of hexosyl ceramides between phospholipid bilayers*, Biochem. **29** (1990), no. 16, 3892–3897.

[119] Jores, K., Mehnert, W., and Mäder, K., *Physicochemical investigations on solid lipid nanoparticles and on oil-loaded solid lipid nanoparticles: A nuclear magnetic resonance and electron spin resonance study*, Pharm. Res. **20** (2003), no. 8, 1274–83.

[120] Jori, G., Tomio, L., Reddi, E., Rossi, E., Corti, L., Zorat, P. L., and Calzavara, F., *Preferential delivery of liposome-incorporated porphyrins to neoplastic cells in tumour-bearing rats*, Br. J. Cancer **48** (1983), no. 2, 307–309.

[121] Jurkiewicz, P., Olzynska, A., Langner, M., and Hof, M., *Headgroup hydration and mobility of DOTAP/DOPC bilayers: A fluorescence solvent relaxation study*, Langmuir **22** (2006), no. 21, 8741–8749.

[122] Kaganer, V. M., Mohwald, H., and Dutta, P., *Structure and phase transitions in Langmuir monolayers*, Rev. Mod. Phys. **71** (1999), no. 3, 779–819.

[123] Kahya, N. and Schwille, P., *Fluorescence correlation studies of lipid domains in model membranes (review)*, Mol. Membr. Biol. **23** (2006), no. 1, 29–39.

[124] Kardar, M. and Golestanian, R., *The "friction" of vacuum, and other fluctuation-induced forces*, Rev. Mod. Phys. **71** (1999), no. 4, 1233–1245.

[125] Kiessling, V., Crane, J. M., and Tamm, L. K., *Transbilayer effects of raft-like lipid domains in asymmetric planar bilayers measured by single molecule tracking*, Biophys. J. **91** (2006), no. 9, 3313–3326.

[126] Killian, J. A., Salemink, I., de Planque, M. R. R., Lindblom, G., Koeppe, R. E., and Greathouse, D. V., *Induction of nonbilayer structures in diacylphosphatidylcholine model membranes by transmembrane alpha-helical peptides: Importance of hydrophobic mismatch and proposed role of tryptophans*, Biochem. **35** (1996), no. 3, 1037–1045.

[127] Killian, J. A., *Hydrophobic mismatch between proteins and lipids in membranes*, Biochim. Biophys. Acta – Rev Biomembranes **1376** (1998), no. 3, 401–416.

[128] Kim, K. H., Kim, D. H., Jang, H. H., Kim, M., Kim, D. H., Kim, J. S., Kim, J. I., Chae, H. Z., Ahn, T., and Yun, C. H., *Lateral segregation of anionic phospholipids in model membranes induced by cytochrome P450 2B1: Bi-directional coupling between CYP2B1 and anionic phospholipid*, Arch. Biochem. Biophys. **468** (2007), no. 2, 226–233.

[129] Kim, K. S., Neu, J., and Oster, G., *Many-body forces between membrane inclusions: A new pattern-formation mechanism*, Europhys. Lett. **48** (1999), no. 1, 99–105.

[130] Komura, S., Shirotori, H., Olmsted, P. D., and Andelman, D., *Lateral phase separation in mixtures of lipids and cholesterol*, Europhys. Lett. **67** (2004), no. 2, 321–327.

[131] Kooijman, E. E., Carter, K. M., van Laar, E. G., Chupin, V., Burger, K. N. J., and de Kruijff, B., *What makes the bioactive lipids phosphatidic acid and lysophosphatidic acid so special?*, Biochem. **44** (2005), no. 51, 17007–17015.

[132] Kooijman, E. E., Tieleman, D. P., Testerink, C., Munnik, T., Rijkers, D. T. S., Burger, K. N. J., and de Kruijff, B., *An electrostatic/hydrogen bond switch as the basis for the specific interaction of phosphatidic acid with proteins*, J. Biol. Chem. **282** (2007), no. 15, 11356–11364.

[133] Kooijman, E. E., Sot, J., Montes, L. R., Alonso, A., Gericke, A., de Kruijff, B., Kumar, S., and Goñi, F. M., *Membrane organization and ionization behavior of the minor but crucial lipid ceramide-1-phosphate*, Biophys. J. **94** (2008), no. 11, 4320–4330.

[134] Kooijman, E. E. and Burger, K. N. J., *Biophysics and function of phosphatidic acid: A molecular perspective*, Biochim. Biophys. Acta – Mol. Cell Biol. Lipids **1791** (2009), no. 9, 881–888.

[135] Kooijman, E. E., King, K. E., Gangoda, M., and Gericke, A., *Ionization properties of phosphatidylinositol polyphosphates in mixed model membranes*, Biochem. **48** (2009), no. 40, 9360–9371.

[136] Korlach, J., Schwille, P., Webb, W. W., and Feigenson, G. W., *Characterization of lipid bilayer phases by confocal microscopy and fluorescence correlation spectroscopy*, Proc. Natl. Acad. Sci. USA **96** (1999), no. 15, 8461–8466.

[137] Koynova, R. and Caffrey, M., *Phases and phase transitions of the hydrated phosphatidylethanolamines*, Chem. Phys. Lipids **69** (1994), no. 1, 1–34.

[138] Koynova, R. and Caffrey, M., *Phases and phase transitions of the phosphatidylcholines*, Biochim. Biophys. Acta – Rev Biomembranes **1376** (1998), no. 1, 91–145.

[139] Kuntsche, J., Freisleben, I., Steiniger, F., and Fahr, A., *Temoporfin-loaded liposomes: Physicochemical characterization*, Eur. J. Pharm. Sci. **40** (2010), no. 4, 305–315.

[140] Kutateladze, T. G., *Mechanistic similarities in docking of the FYVE and PX domains to phosphatidylinositol 3-phosphate containing membranes*, Prog. Lipid Res. **46** (2007), no. 6, 315–327.

[141] Kuzmin, P. I., Akimov, S. A., Chizmadzhev, Y. A., Zimmerberg, J., and Cohen, F. S., *Line tension and interaction energies of membrane rafts calculated from lipid splay and tilt*, Biophys. J. **88** (2005), no. 2, 1120–1133.

[142] Lange, Y., Molinaro, A. L., Chauncey, T. R., and Steck, T. L., *On the mechanism of transfer of cholesterol between human erythrocytes and plasma*, J. Biol. Chem. **258** (1983), no. 11, 6920–6926.

[143] Langner, M. and Kubica, K., *The electrostatics of lipid surfaces*, Chem. Phys. Lipids **101** (1999), no. 1, 3–35.

[144] Laradji, M. and Kumar, P. B. S., *Anomalously slow domain growth in fluid membranes with asymmetric transbilayer lipid distribution*, Phys. Rev. E **73** (2006), no. 4, 040901.

[145] Lasic, D. D., *Novel applications of liposomes*, Trends Biotechnol. **16** (1998), no. 7, 307–321.

[146] Lehtonen, J. Y. A., Holopainen, J. M., and Kinnunen, P. K. J., *Evidence for the formation of microdomains in liquid crystalline large unilamellar vesicles caused by hydrophobic mismatch of the constituent phospholipids*, Biophys. J. **70** (1996), no. 4, 1753–1760.

[147] Leidy, C., Linderoth, L., Andresen, T. L., Mouritsen, O. G., Jorgensen, K., and Peters, G. H., *Domain-induced activation of human phospholipase A2 type IIA: Local versus global lipid composition*, Biophys. J. **90** (2006), no. 9, 3165–3175.

[148] Lemmon, M. A., *Pleckstrin homology (ph) domains and phosphoinositides*, Biochem. Soc. Symp. **93** (2007), no. 74, 81–93.

[149] Lichtenberg, D., Goñi, F. M., and Heerklotz, H., *Detergent-resistant membranes should not be identified with membrane rafts*, Trends Biochem Sci. **30** (2005), no. 8, 430–436.

[150] Lindner, L. H. and Hossann, M., *Factors affecting drug release from liposomes*, Current Opinion In Drug Discovery & Development **13** (2010), no. 1, 111–123.

[151] Lingwood, D., Ries, J., Schwille, P., and Simons, K., *Plasma membranes are poised for activation of raft phase coalescence at physiological temperature*, Proc. Natl. Acad. Sci. USA **105** (2008), no. 29, 10005–10010.

[152] Lingwood, D. and Simons, K., *Lipid rafts as a membrane-organizing principle*, Science **327** (2010), no. 5961, 46–50.

[153] Lipinski, C. A., *Drug-like properties and the causes of poor solubility and poor permeability*, J. Pharmacol. Toxicol. Methods **44** (2000), no. 1, 235–249.

[154] Lipowsky, R., *Statistical physics of flexible membranes*, Physica A **194** (1993), no. 1-4, 114–127.

[155] Liu, J. B., Lee, H., Huesca, M., Young, A. P., and Allen, C., *Liposome formulation of a novel hydrophobic aryl-imidazole compound for anti-cancer therapy*, Cancer Chemother. Pharmacol. **58** (2006), no. 3, 306–318.

[156] Liu, N. and Park, H. J., *Factors effect on the loading efficiency of Vitamin C loaded chitosan-coated nanoliposomes*, Colloids Surf. B **76** (2010), no. 1, 16–19.

[157] Loew, S., Hinderliter, A., and May, S., *Stability of protein-decorated mixed lipid membranes: The interplay of lipid-lipid, lipid-protein, and protein-protein interactions*, J. Chem. Phys. **130** (2009), no. 4, 045102.

[158] Loew, S., Fahr, A., and May, S., *Modeling the release kinetics of poorly water-soluble drug molecules from liposomal nanocarriers*, J. Drug Delivery **2011** (2011), 376548.

[159] Loew, S., Kooijman, E. E., and May, S., *Increased pH-sensitivity of protein binding to lipid membranes through the electrostatic-hydrogen bond switch*, Chem. Phys. Lipids **169** (2013), 9–18.

[160] Lorenz, C. D., Faraudo, J., and Travesset, A., *Hydrogen bonding and binding of polybasic residues with negatively charged mixed lipid monolayers*, Langmuir **24** (2008), no. 5, 1654–1658.

[161] Lund, M., Akesson, T., and Jonsson, B., *Enhanced protein adsorption due to charge regulation*, Langmuir **21** (2005), no. 18, 8385–8388.

[162] Lundbaek, J. A., Birn, P., Girshman, J., Hansen, A. J., and Andersen, O. S., *Membrane stiffness and channel function*, Biochem. **35** (1996), no. 12, 3825–3830.

[163] Lundbaek, J. A. and Andersen, O. S., *Spring constants for channel-induced lipid bilayer deformations estimates using gramicidin channels*, Biophys. J. **76** (1999), no. 2, 889–895.

[164] MacDonald, R. C., MacDonald, R. I., Menco, B. P., Takeshita, K., Subbarao, N. K., and Hu, L. R., *Small-volume extrusion apparatus for preparation of large, unilamellar vesicles*, Biochim. Biophys. Acta **1061** (1991), no. 2, 297–303.

[165] Machta, B. B., Veatch, S. L., and Sethna, J. P., *Critical Casimir forces in cellular membranes*, Phys. Rev. Lett. **109** (2012), no. 13, 138101.

[166] Maman, N. and Brault, D., *Kinetics of the interactions of a dicarboxylic porphyrin with unilamellar lipidic vesicles: Interplay between bilayer thickness and pH in rate control*, Biochim. Biophys. Acta **1414** (1998), no. 1-2, 31–42.

[167] Manley, S., Horton, M. R., Lecszynski, S., and Gast, A. P., *Sorting of streptavidin protein coats on phase-separating model membranes*, Biophys. J. **95** (2008), no. 5, 2301–2307.

[168] Margalit, R., Alon, R., Linenberg, M., Rubin, I., Roseman, T. J., and Wood, R. W., *Liposomal drug delivery: Thermodynamic and chemical kinetic considerations*, J. Controlled Release **17** (1991), no. 3, 285–296.

[169] Marrink, S. J., de Vries, A. H., and Mark, A. E., *Coarse grained model for semiquantitative lipid simulations*, J. Phys. Chem. B **108** (2004), no. 2, 750–760.

[170] Marrink, S. J., Risselada, H. J., Yefimov, S., Tieleman, D. P., and de Vries, A. H., *The MARTINI force field: Coarse grained model for biomolecular simulations*, J. Phys. Chem. B **111** (2007), no. 27, 7812–7824.

[171] Marrink, S. J., de Vries, A. H., and Tieleman, D. P., *Lipids on the move: Simulations of membrane pores, domains, stalks and curves*, Biochim. Biophys. Acta – Biomembr. **1788** (2009), no. 1, 149–168.

[172] Matsuzaki, K., *Magainins as paradigm for the mode of action of pore forming polypeptides*, Biochim. Biophys. Acta – Rev Biomembranes **1376** (1998), no. 3, 391–400.

[173] May, S., Harries, D., and Ben-Shaul, A., *Lipid demixing and protein-protein interactions in the adsorption of charged proteins on mixed membranes*, Biophys. J. **79** (2000), no. 4, 1747–1760.

[174] May, S., Harries, D., and Ben-Shaul, A., *Macroion-induced compositional instability of binary fluid membranes*, Phys. Rev. Lett. **89** (2002), no. 26, 268102.

[175] May, S. and Ben-Shaul, A., *Membrane-macromolecule interactions and their structural consequences*, Membrane Science and Technology (Tien, H. T. and Ottova-Leitmannova, A., eds.), vol. 7, Elsevier, Amsterdam, 2003, pp. 315–346.

[176] May, S., *Mean-field continuum electrostatics of lipid membranes*, Encyclopedia of Surface and Colloid Science (Somasundaran, P., ed.), Taylor and Francis, New York, second ed., 2012, pp. 1–15.

[177] Mbamala, E. C., Ben-Shaul, A., and May, S., *Domain formation induced by the adsorption of charged proteins on mixed lipid membranes*, Biophys. J. **88** (2005), no. 3, 1702–1714.

[178] Mbamala, E. C., Fahr, A., and May, S., *Electrostatic model for mixed cationic-zwitterionic lipid bilayers*, Langmuir **22** (2006), no. 11, 5129–5136.

[179] McConnell, H. M., *Complexes in ternary cholesterol-phospholipid mixtures*, Biophys. J. **88** (2005), no. 4, L23–L25.

[180] McLean, L. R. and Phillips, M. C., *Mechanism of cholesterol and phosphatidylcholine exchange or transfer between unilamellar vesicles*, Biochem. **20** (1981), no. 10, 2893–2900.

[181] McMullen, T. P. W., Lewis, R. N. A. H., and McElhaney, R. N., *Cholesterol-phospholipid interactions, the liquid-ordered phase and lipid rafts in model and biological membranes*, Curr. Opin. Coll. Interf. Sci. **8** (2004), no. 6, 459–468.

[182] Mengistu, D. H. and May, S., *Debye-Hückel theory of mixed charged-zwitterionic lipid layers*, Eur. Phys. J. E **26** (2008), no. 3, 251–260.

[183] Mengistu, D. H. and May, S., *Nonlinear Poisson-Boltzmann model of charged lipid membranes: Accounting for the presence of zwitterionic lipids*, J. Chem. Phys. **129** (2008), no. 12, 121105.

[184] Mengistu, D. H., Kooijman, E. E., and May, S., *Ionization properties of mixed lipid membranes: A Gouy-Chapman model of the electrostatic-hydrogen bond switch*, Biochim. Biophys. Acta – Biomembr. **1808** (2011), no. 8, 1985–1992.

[185] Menke, M., Gerke, V., and Steinem, C., *Phosphatidylserine membrane domain clustering induced by annexin A2/S100A10 heterotetramer*, Biochem. **44** (2005), no. 46, 15296–15303.

[186] Mishra, B., Patel, B. B., and Tiwari, S., *Colloidal nanocarriers: A review on formulation technology, types and applications toward targeted drug delivery*, Nanomedicine: NBM **6** (2010), no. 1, 9–24.

[187] Moghimi, S. M. and Szebeni, J., *Stealth liposomes and long circulating nanoparticles: Critical issues in pharmacokinetics, opsonization and protein-binding properties*, Prog. Lipid Res. **42** (2003), no. 6, 463–478.

[188] Mohammed, A. R., Weston, N., Coombes, A. G. A., Fitzgerald, M., and Perrie, Y., *Liposome formulation of poorly water soluble drugs: Optimisation of drug loading and ESEM analysis of stability*, Int. J. Pharmaceutics **285** (2004), no. 1-2, 23–34.

[189] Mojzisova, H., Bonneau, S., and Brault, D., *Structural and physico-chemical determinants of the interactions of macrocyclic photosensitizers with cells*, Eur. Biophys. J. **36** (2007), no. 8, 943–953.

[190] Monette, M. and Lafleur, M., *Modulation of melittin-induced lysis by surface charge density of membranes*, Biophys. J. **68** (1995), no. 1, 187–195.

[191] Moritz, A., De Graan, P. N. E., Gispen, W. H., and Wirtz, K. W. A., *Phosphatidic-acid is a specific activator of phosphatidylinositol-4-phosphate kinase*, J. Biol. Chem. **267** (1992), no. 11, 7207–7210.

[192] Mouritsen, O. G. and Bloom, M., *Mattress model of lipid-protein interactions in membranes*, Biophys. J. **46** (1984), no. 2, 141–153.

[193] Mouritsen, O. G., *Life – as a matter of fat*, Springer, New York, 2005.

[194] Munro, S., *Lipid rafts: Elusive or illusive?*, Cell **115** (2003), no. 4, 377–388.

[195] Murray, D., Arbuzova, A., Hangyas-Mihalyne, G., Gambhir, A., Ben-Tal, N., Honig, B., and McLaughlin, S., *Electrostatic properties of membranes containing acidic lipids and adsorbed basic peptides: Theory and experiment*, Biophys. J. **77** (1999), no. 6, 3176–3188.

[196] Murray, D., McLaughlin, S., and Honig, B., *The role of electrostatic interactions in the regulation of the membrane association of G protein beta gamma heterodimers*, J. Biol. Chem. **276** (2001), no. 48, 45153–45159.

[197] Nakanishi, H., Morishita, M., Schwartz, C. L., Coluccio, A., Engebrecht, J., and Neiman, A. M., *Phospholipase D and the SNARE Sso1p are necessary for vesicle fusion during sporulation in yeast*, J. Cell Sci. **119** (2006), no. 7, 1406–1415.

[198] Netz, R. R. and Andelman, D., *Neutral and charged polymers at interfaces*, Phys. Rep. **380** (2003), no. 1-2, 1–95.

[199] Neville, F., Cahuzac, M., Konovalov, O., Ishitsuka, Y., Lee, K. Y. C., Kuzmenko, I., Kale, G. M., and Gidalevitz, D., *Lipid headgroup discrimination by antimicrobial peptide LL-37: Insight into mechanism of action*, Biophys. J. **90** (2006), no. 4, 1275–1287.

[200] Newmeyer, D. D. and Ferguson-Miller, S., *Mitochondria: Releasing power for life and unleashing the machineries of death*, Cell **112** (2003), no. 4, 481–490.

[201] Nicolini, C., Baranski, J., Schlummer, S., Palomo, J., Lumbierres-Burgues, M., Kahms, M., Kuhlmann, J., Sanchez, S., Gratton, E., Waldmann, H., and Winter, R., *Visualizing association of N-Ras in lipid microdomains: Influence of domain structure and interfacial adsorption*, J. Am. Chem. Soc. **128** (2006), no. 1, 192–201.

[202] Nielsen, S. O., Lopez, C. F., Srinivas, G., and Klein, M. L., *Coarse grain models and the computer simulation of soft materials*, J. Phys.-Condens. Mat. **16** (2004), no. 15, R481–R512.

[203] Niggli, V., *Lipid interactions of cytoskeletal proteins*, Adv. Mol. Cell Biol. **37** (2006), 221–250.

[204] Nii, T. and Ishii, F., *Encapsulation efficiency of water-soluble and insoluble drugs in liposomes prepared by the microencapsulation vesicle method*, Int. J. Pharmaceutics **298** (2005), no. 1, 198–205.

[205] Ninham, B. W. and Parsegian, V. A., *Electrostatic potential between sufraces bearing ionizable groups in ionic equilibrium with physiologic saline solution*, J. Theor. Biol. **31** (1971), no. 3, 405–428.

[206] Norman, K. E. and Nymeyer, H., *Indole localization in lipid membranes revealed by molecular simulation*, Biophys. J. **91** (2006), no. 6, 2046–2054.

[207] Osborn, W. R., Orlandini, E., Swift, M. R., Yeomans, J. M., and Banavar, J. R., *Lattice boltzmann study of hydrodynamic spinodal decomposition*, Phys. Rev. Lett. **75** (1995), no. 22, 4031–4034.

[208] Pandey, A. P., Haque, F., Rochet, J., and Hovis, J. S., *Clustering of alpha-synuclein on supported lipid bilayers: Role of anionic lipid, protein, and divalent ion concentration*, Biophys. J. **96** (2009), no. 2, 540–551.

[209] Pandit, S. A., Bostick, D., and Berkowitz, M. L., *Complexation of phosphatidylcholine lipids with cholesterol*, Biophys. J. **86** (2004), no. 3, 1345–1356.

[210] Petersen, F. N. R., Jensen, M. O., and Nielsen, C. H., *Interfacial tryptophan residues: A role for the cation-pi effect?*, Biophys. J. **89** (2005), no. 6, 3985–3996.

[211] Pike, L. J., *Lipid rafts: Bringing order to chaos*, J. Lipid Res. **44** (2003), no. 4, 655–667.

[212] Pokorny, A., Yandek, L. E., Elegbede, A. I., Hinderliter, A., and Almeida, P. F. F., *Temperature and composition dependence of the interaction of delta-lysin with ternary mixtures of sphingomyelin/cholesterol/POPC*, Biophys. J. **91** (2006), no. 6, 2184–2197.

[213] Poste, G. and Papahadjopoulos, D., *Lipid vesicles as carriers for introducing materials into cultured cells: Influence of vesicle lipid composition on mechanism(s) of vesicle incorporation into cells*, Proc. Natl. Acad. Sci. USA **73** (1976), no. 5, 1603–1607.

[214] Pratt, L. R., *Molecular theory of hydrophobic effects: "She is too mean to have her name repeated."*, Annu. Rev. Phys. Chem. **53** (2002), 409–436.

[215] Pyenta, P. S., Holowka, D. A., and Baird, B. A., *Cross-correlation analysis of inner-leaflet–anchored green fluorescent protein co-redistributed with IgE receptors and outer leaflet lipid raft components*, Biophys. J. **80** (2001), no. 5, 2120–2132.

[216] Radhakrishnan, A. and McConnell, H. M., *Cholesterol-phospholipid complexes in membranes*, J. Am. Chem. Soc. **121** (1999), no. 2, 486–487.

[217] Radhakrishnan, A. and McConnell, H. M., *Condensed complexes in vesicles containing cholesterol and phospholipids*, Proc. Natl. Acad. Sci. USA **102** (2005), no. 36, 12662–12666.

[218] Raghu, P., Manifava, M., Coadwell, J., and Ktistakis, N. T., *Emerging findings from studies of phospholipase D in model organisms (and a short update on phosphatidic acid effectors)*, Biochim. Biophys. Acta – Mol. Cell Biol. Lipids **1791** (2009), no. 9, 889–897.

[219] Raja, M., Spelbrink, R. E. J., de Kruijff, B., and Killian, J. A., *Phosphatidic acid plays a special role in stabilizing and folding of the tetrameric potassium channel KcsA*, FEBS Lett. **581** (2007), no. 29, 5715–5722.

[220] Reddy, K. V. R., Yedery, R. D., and Aranha, C., *Antimicrobial peptides: Premises and promises*, Int. J. Antimicrob. Ag. **24** (2004), no. 6, 536–547.

[221] Redfern, D. A. and Gericke, A., *pH-dependent domain formation in phosphatidylinositol polyphosphate/phosphatidylcholine mixed vesicles*, J. Lipid Res. **46** (2005), no. 3, 504–515.

[222] Ricchelli, F., Gobbo, S., Moreno, G., Salet, C., Brancaleon, L., and Mazzini, A., *Photophysical properties of porphyrin planar aggregates in liposomes*, Eur. J. Biochem. **253** (1998), no. 3, 760–765.

[223] Rogerson, A., Cummings, J., and Florence, A. T., *Adriamycin-loaded niosomes: Drug entrapment, stability and release*, J. Microencaps. **4** (1987), no. 4, 321–328.

[224] Rosetti, C. M., Maggio, B., and Oliveira, R. G., *The self-organization of lipids and proteins of myelin at the membrane interface. Molecular factors underlying the microheterogeneity of domain segregation*, Biochim. Biophys. Acta – Biomembr. **1778** (2008), no. 7-8, 1665–1675.

[225] Roth, C. M., Sader, J. E., and Lenhoff, A. M., *Electrostatic contribution to the energy and entropy of protein adsorption*, J. Coll. Interf. Sci. **203** (1998), no. 1, 218–221.

[226] Roth, M. G., *Molecular mechanisms of PLD function in membrane traffic*, Traffic **9** (2008), no. 8, 1233–1239.

[227] Saarinen-Savolainen, P., Jarvinen, T., Taipale, H., and Urtti, A., *Method for evaluating drug release from liposomes in sink conditions*, Int. J. Pharmaceutics **159** (1997), no. 1, 27–33.

[228] Safran, S. A., *Statistical thermodynamics of surfaces, interfaces, and membranes*, Addison-Wesley, Reading, MA, 1994.

[229] Safran, S. A., *Curvature elasticity of thin films*, Adv. Phys. **48** (1999), no. 4, 395–448.

[230] Sapra, P. and Allen, T. M., *Ligand-targeted liposomal anticancer drugs*, Prog. Lipid Res. **42** (2003), no. 5, 439–462.

[231] Sasnouski, S., Kachatkou, D., Zorin, V., Guillemin, F., and Bezdetnaya, L., *Redistribution of Foscan(R) from plasma proteins to model membranes*, Photochem. Photobiol. Sci. **5** (2006), no. 8, 770–777.

[232] Sawant, R. R. and Torchilin, V. P., *Liposomes as 'smart' pharmaceutical nanocarriers*, Soft Matter **6** (2010), no. 17, 4026–4044.

[233] Schäffer, E. and Thiele, U., *Dynamic domain formation in membranes: Thickness-modulation-induced phase separation*, Eur. Phys. J. E **14** (2004), no. 2, 169–175.

[234] Scherer, P. G. and Seelig, J., *Electric charge effects on phospholipid headgroups. Phosphatidylcholine in mixtures with cationic and anionic amphiphiles*, Biochem. **28** (1989), no. 19, 7720–7728.

[235] Schiller, P., Mogel, H. J., Wahab, M., and Reimer, U., *Cooperative effects induced by adsorbed polypeptides in mixed membranes*, J. Phys. Chem. B **106** (2002), no. 47, 12323–12330.

[236] Schiller, P., Wahab, M., and Mogel, H. J., *Forces between colloidal particles adsorbed on fluid membranes*, J. Non-Newtonian Fluid Mech. **119** (2004), no. 1-3, 145–153.

[237] Schote, U., Ganz, P., Fahr, A., and Seelig, J., *Interactions of cyclosporines with lipid membranes as studied by solid-state nuclear magnetic resonance spectroscopy and high-sensitivity titration calorimetry*, J. Pharm. Sci. **91** (2002), no. 3, 856–867.

[238] Schreier, S., Malheiros, S. V. P., and de Paula, E., *Surface active drugs: Self-association and interaction with membranes and surfactants. Physicochemical and biological aspects*, Biochim. Biophys. Acta – Biomembr. **1508** (2000), no. 1-2, 210–234.

[239] Schulthess, G., Lipka, G., Compassi, S., Boffelli, D., Weber, F. E., Paltauf, F., and Hauser, H., *Absorption of monoacylglycerols by small intestinal brush border membrane*, Biochem. **33** (1994), no. 15, 4500–4508.

[240] Seddon, A. M., Curnow, P., and Booth, P. J., *Membrane proteins, lipids and detergents: Not just a soap opera*, Biochim. Biophys. Acta – Biomembr. **1666** (2004), no. 1-2, 105–117.

[241] Seddon, J. M. and Templer, R. H., *Polymorphism of lipid-water systems*, Structure and Dynamics of Membranes (Lipowsky, R. and Sackmann, E., eds.), vol. 1, Elsevier, Amsterdam, second ed., 1995, pp. 97–160.

[242] Seifert, U., *Configurations of fluid membranes and vesicles*, Adv. Phys. **46** (1997), no. 1, 13–137.

[243] Sengupta, D., Smith, J. C., and Ullmann, G. M., *Partitioning of amino-acid analogues in a five-slab membrane model*, Biochim. Biophys. Acta – Biomembr. **1778** (2008), no. 10, 2234–2243.

[244] Sengupta, P., Hammond, A. T., Holowka, D. A., and Baird, B. A., *Structural determinants for partitioning of lipids and proteins between coexisting fluid phases in giant plasma membrane vesicles*, Biochim. Biophys. Acta – Biomembr. **1778** (2008), no. 1, 20–32.

[245] Sens, P. and Safran, S. A., *Inclusions induced phase separation in mixed lipid film*, Eur. Phys. J. E **1** (2000), no. 2-3, 237–248.

[246] Sens, P., Johannes, L., and Bassereau, P., *Biophysical approaches to protein-induced membrane deformations in trafficking*, Curr. Opin. Cell Biol. **20** (2008), no. 4, 476–482.

[247] Sharma, A. and Sharma, U. S., *Liposomes in drug delivery: Progress and limitations*, Int. J. Pharmaceutics **154** (1997), no. 2, 123–140.

[248] Shearman, G. C., Tyler, A. I. I., Brooks, N. J., Templer, R. H., Ces, O., Law, R. V., and Seddon, J. M., *Ordered micellar and inverse micellar lyotropic phases*, Liq. Cryst. **37** (2010), no. 6-7, 679–694.

[249] Shenoy, S., Shekhar, P., Heinrich, F., Daou, M. C., Gericke, A., Ross, A. H., and Lösche, M., *Membrane association of the PTEN tumor suppressor: Molecular details of the protein-membrane complex from SPR binding studies and neutron reflection*, PLoS One **7** (2012), no. 4, e32591.

[250] Shin, J. J. H. and Loewen, C. J. R., *Putting the pH into phosphatidic acid signaling*, BMC Biol. **9** (2011), no. 1, 85.

[251] Simons, K. and Ikonen, E., *Functional rafts in cell membranes*, Nature **387** (1997), no. 6633, 569–572.

[252] Simons, K. and Vaz, W. L. C., *Model systems, lipid rafts, and cell membranes*, Annu. Rev. Biophys. Biomol. Struct. **33** (2004), 269–295.

[253] Simons, K. and Gerl, M. J., *Revitalizing membrane rafts: New tools and insights*, Nat. Rev. Mol. Cell Biol. **11** (2010), no. 10, 688–699.

[254] Singer, S. J. and Nicolson, G. L., *The fluid mosaic model of the structure of cell membranes*, Science **175** (1972), no. 23, 720–731.

[255] Sinner, E. K. and Knoll, W., *Functional tethered membranes*, Curr. Opin. Chem. Biol. **5** (2001), no. 6, 705–711.

[256] Southall, N. T. and Dill, K. A., *Potential of mean force between two hydrophobic solutes in water*, Biophys. Chem. **101** (2002), no. 102, 295–307.

[257] Spagnou, S., Miller, A. D., and Keller, M., *Lipidic carriers of siRNA: Differences in the formulation, cellular uptake, and delivery with plasmid DNA*, Biochem. **43** (2004), no. 42, 13348–13356.

[258] Sperotto, M. M., *A theoretical model for the association of amphiphilic transmembrane peptides in lipid bilayers*, Eur. Biophys. J. **26** (1997), no. 5, 405–416.

[259] Stace, C. L. and Ktistakis, N. T., *Phosphatidic acid- and phosphatidylserine-binding proteins*, Biochim. Biophys. Acta – Mol. Cell Biol. Lipids **1761** (2006), no. 8, 913–926.

[260] Steck, T. L., Kezdy, F. J., and Lange, Y., *An activation-collision mechanism for cholesterol transfer between membranes*, J. Biol. Chem. **263** (1988), no. 26, 13023–13031.

[261] Stockl, M., Fischer, P., Wanker, E., and Herrmann, A., *alpha-synuclein selectively binds to anionic phospholipids embedded in liquid-disordered domains*, J. Mol. Biol. **375** (2008), no. 5, 1394–1404.

[262] Stottrup, B. L., Veatch, S. L., and Keller, S. L., *Nonequilibrium behavior in supported lipid membranes containing cholesterol*, Biophys. J. **86** (2004), no. 5, 2942–2950.

[263] Strandberg, E. and Killian, J. A., *Snorkeling of lysine side chains in transmembrane helices: How easy can it get?*, FEBS Lett. **544** (2003), no. 1-3, 69–73.

[264] Strawn, L., Babb, A., Testerink, C., and Kooijman, E. E., *The physical chemistry of the enigmatic phospholipid diacylglycerol pyrophosphate*, Front. Plant. Sci. **3** (2012), no. 40, 40.

[265] Swift, M. R., Orlandini, E., Osborn, W. R., and Yeomans, J. M., *Lattice boltzmann simulations of liquid-gas and binary fluid systems*, Phys. Rev. E **54** (1996), no. 5, 5041–5052.

[266] Tanford, C., *The hydrophobic effect*, second ed., Wiley, New York, 1980.

[267] Testerink, C. and Munnik, T., *Phosphatidic acid: A multifunctional stress signaling lipid in plants*, Trends Plant Sci. **10** (2005), no. 8, 368–375.

[268] Testerink, C. and Munnik, T., *Molecular, cellular, and physiological responses to phosphatidic acid formation in plants*, J. Exp. Bot. **62** (2011), no. 7, 2349–2361.

[269] Thilo, L., *Kinetics of phospholipid exchange between bilayer membranes*, Biochim. Biophys. Acta **469** (1977), no. 3, 326–334.

[270] Tian, A. W., Johnson, C., Wang, W., and Baumgart, T., *Line tension at fluid membrane domain boundaries measured by micropipette aspiration*, Phys. Rev. Lett. **98** (2007), no. 20, 208102.

[271] Tieleman, D. P., Marrink, S. J., and Berendsen, H. J. C., *A computer perspective of membranes: Molecular dynamics studies of lipid bilayer systems*, Biochim. Biophys. Acta – Rev Biomembranes **1331** (1997), no. 3, 235–270.

[272] Torchilin, V. P., *Micellar nanocarriers: Pharmaceutical perspectives*, Pharm. Res. **24** (2007), no. 1, 1–16.

[273] Towles, K. B. and Dan, N., *Coupling between line tension and domain contact angle in heterogeneous membranes*, Biochim. Biophys. Acta – Biomembr. **1778** (2008), no. 4, 1190–1195.

[274] Tzlil, S. and Ben-Shaul, A., *Flexible charged macromolecules on mixed fluid lipid membranes: Theory and Monte Carlo simulations*, Biophys. J. **89** (2005), no. 5, 2972–2987.

[275] Tzlil, S., Murray, D., and Ben-Shaul, A., *The "Electrostatic-Switch" mechanism: Monte Carlo study of MARCKS-membrane interaction*, Biophys. J. **95** (2008), no. 4, 1745–1757.

[276] Urbic, T., Vlachy, V., Kalyuzhnyi, Y. V., Southall, N. T., and Dill, K. A., *A two-dimensional model of water: Theory and computer simulations*, J. Chem. Phys. **112** (2000), no. 6, 2843–2848.

[277] van den Besselaar, A. M., Helmkamp, Jr, G. M., and Wirtz, K. W. A., *Kinetic model of the protein-mediated phosphatidylcholine exchange between single bilayer liposomes*, Biochem. **14** (1975), no. 9, 1852–1858.

[278] van Meer, G., Voelker, D. R., and Feigenson, G. W., *Membrane lipids: Where they are and how they behave*, Nat. Rev. Mol. Cell Biol. **9** (2008), no. 2, 112–124.

[279] Veatch, S. L. and Keller, S. L., *Organization in lipid membranes containing cholesterol*, Phys. Rev. Lett. **89** (2002), no. 26, 268101.

[280] Veatch, S. L. and Keller, S. L., *Seeing spots: Complex phase behavior in simple membranes*, Biochim. Biophys. Acta – Mol. Cell Res. **1746** (2005), no. 3, 172–185.

[281] Veatch, S. L., Gawrisch, K., and Keller, S. L., *Closed-loop miscibility gap and quantitative tie-lines in ternary membranes containing diphytanoyl PC*, Biophys. J. **90** (2006), no. 12, 4428–4436.

[282] Venturoli, M., Smit, B., and Sperotto, M. M., *Simulation studies of protein-induced bilayer deformations, and lipid-induced protein tilting, on a mesoscopic model for lipid bilayers with embedded proteins*, Biophys. J. **88** (2005), no. 3, 1778–1798.

[283] Venturoli, M., Sperotto, M. M., Kranenburg, M., and Smit, B., *Mesoscopic models of biological membranes*, Phys. Rep. **437** (2006), no. 1-2, 1–54.

[284] Venugopalan, P., Jain, S., Sankar, S., Singh, P., Rawat, A., and Vyas, S. P., *pH-sensitive liposomes: Mechanism of triggered release to drug and gene delivery prospects*, Pharmazie **57** (2002), no. 10, 659–671.

[285] Wagner, A. J., *Theory and application of the lattice boltzmann method*, Ph.D. thesis, Oxford University, Cambridge, UK, 1997.

[286] Wagner, A. J., Loew, S., and May, S., *Influence of monolayer-monolayer coupling on the phase behavior of a fluid lipid bilayer*, Biophys. J. **93** (2007), no. 12, 4268–4277.

[287] Wallace, E. J., Hooper, N. M., and Olmsted, P. D., *The kinetics of phase separation in asymmetric membranes*, Biophys. J. **88** (2005), no. 6, 4072–4083.

[288] Wallace, E. J., Hooper, N. M., and Olmsted, P. D., *Effect of hydrophobic mismatch on phase behavior of lipid membranes*, Biophys. J. **90** (2006), no. 11, 4104–4118.

[289] Wang, J. Y., Gambhir, A., McLaughlin, S., and Murray, D., *A computational model for the electrostatic sequestration of PI(4,5)P2 by membrane-adsorbed basic peptides*, Biophys. J. **86** (2004), no. 4, 1969–1986.

[290] Wang, T.-Y. and Silvius, J. R., *Cholesterol does not induce segregation of liquid-ordered domains in bilayers modeling the inner leaflet of the plasma membrane*, Biophys. J. **81** (2001), no. 5, 2762–2773.

[291] Wang, W. J., Anderson, N. A., Travesset, A., and Vaknin, D., *Regulation of the electric charge in phosphatidic acid domains*, J. Phys. Chem. B **116** (2012), no. 24, 7213–7220.

[292] Watson, M. C., Brandt, E. G., Welch, P. M., and Brown, F. L. H., *Determining biomembrane bending rigidities from simulations of modest size*, Phys. Rev. Lett. **109** (2012), no. 2, 028102.

[293] Wenk, M. R., Fahr, A., Reszka, R., and Seelig, J., *Paclitaxel partitioning into lipid bilayers*, J. Pharm. Sci. **85** (1996), no. 2, 228–231.

[294] West, B., Brown, F. L. H., and Schmid, F., *Membrane-protein interactions in a generic coarse-grained model for lipid bilayers*, Biophys. J. **96** (2009), no. 1, 101–115.

[295] Winget, J. M., Pan, Y. H., and Bahnson, B. J., *The interfacial binding surface of phospholipase A2s*, Biochim. Biophys. Acta – Mol. Cell Biol. Lipids **1761** (2006), no. 11, 1260–1269.

[296] Wootan, M. G., Bernlohr, D. A., and Storch, J., *Mechanism of fluorescent fatty acid transfer from adipocyte fatty acid binding protein to membranes*, Biochem. **32** (1993), no. 33, 8622–8627.

[297] Wright, S. E., White, J. C., and Huang, L., *Partitioning of teniposide into membranes and the role of lipid composition*, Biochim. Biophys. Acta **1021** (1990), no. 2, 105–113.

[298] Yang, E. Y. and Huestis, W. H., *Mechanism of intermembrane phosphatidylcholine transfer: Effects of pH and membrane configuration*, Biochem. **32** (1993), no. 45, 12218–12228.

[299] Yang, J. S., Gad, H., Lee, S. Y., Mironov, A., Zhang, L. L., Beznoussenko, G. V., Valente, C., Turacchio, G., Bonsra, A. N., Du, G. W., Baldanzi, G., Graziani, A., Bourgoin, S., Frohman, M. A., Luini, A., and Hsu, V. W., *A role for phosphatidic acid in COPI vesicle fission yields insights into Golgi maintenance*, Nat. Cell Biol. **10** (2008), no. 10, 1146–1153.

[300] Yethiraj, A. and Weisshaar, J. C., *Why are lipid rafts not observed in vivo?*, Biophys. J. **93** (2007), no. 9, 3113–3119.

[301] Yim, H., Kent, M. S., Sasaki, D. Y., Polizzotti, B. D., Kiick, K. L., Majewski, J., and Satija, S., *Rearrangement of lipid ordered phases upon protein adsorption due to multiple site binding*, Phys. Rev. Lett. **96** (2006), no. 19, 198101.

[302] Young, B. P., Shin, J. J. H., Orij, R., Chao, J. T., Li, S. C., Guan, X. L., Khong, A., Jan, E., Wenk, M. R., Prinz, W. A., Smits, G. J., and Loewen, C. J. R., *Phosphatidic acid is a pH biosensor that links membrane biogenesis to metabolism*, Science **329** (2010), no. 5995, 1085–1088.

[303] Zantl, R., Baicu, L., Artzner, F., Sprenger, I., Rapp, G., and Rädler, J. O., *Thermotropic phase behavior of cationic lipid-DNA complexes compared to binary lipid mixtures*, J. Phys. Chem. B **103** (1999), no. 46, 10300–10310.

[304] Zemel, A., Ben-Shaul, A., and May, S., *Membrane perturbation induced by interfacially adsorbed peptides*, Biophys. J. **86** (2004), no. 6, 3607–3619.

[305] Zhang, S. B., Xu, Y. M., Wang, B., Qiao, W. H., Liu, D. L., and Li, Z. S., *Cationic compounds used in lipoplexes and polyplexes for gene delivery*, J. Controlled Release **100** (2004), no. 2, 165–180.

[306] Zhdanov, V. P. and Kasemo, B., *Adsorption of proteins on a lipid bilayer*, Eur. Biophys. J. **39** (2010), no. 11, 1477–1482.